1.0 SAFETY LIMITS AND LIMITING SAFETY SYSTEM SETTINGS

1.1 Safety Limits - Reactor Core

Applicability

This specification applies to the limiting combinations of reactor power and reactor coolant system flow, temperature and pressure during operation.

Objective

To maintain the integrity of the fuel cladding and prevent the release of significant amounts of fission products to the reactor coolant.

Specifications

The reactor power level shall not exceed the allowable limit for the pressurizer pressure and the cold leg temperatures as shown in Figure 1-1 for 4-pump operation. The safety limit is exceeded if the point defined by the combination of reactor coolant cold leg temperature and power level is at any time above the appropriate pressurizer pressure line.

Basis

To maintain the integrity of the fuel cladding and prevent the release of significant amounts of fission products to the reactor coolant, it is necessary to prevent overheating of the cladding under normal operating conditions. This is accomplished by operating within the nucleate boiling regime of heat transfer, wherein the heat transfer coefficient is large enough so that the clad surface temperature is only slightly greater than the coolant saturation temperature. The upper boundary of the nucleate boiling regime is termed "departure from nucleate boiling" (DNB).

At this point there is a sharp reduction of the heat transfer coefficient, which would result in high clad temperature and the possibility of clad failure. Although DNB is not an observable parameter during reactor operation, the observable parameters of reactor thermal power and reactor coolant flow, temperature and pressure can be related to DNB through the CE-1 correlation. (1) The CE-1 DNB correlation has been developed to predict DNB and the location of DNB for axially uniform and non-uniform heat flux distributions. The local DNB ratio (DNBR), defined as the ratio of the heat flux that

would cause DNB at a particular core location to the actual heat flux at that location, is indicative of the margin to DNB. The minimum value of the DNBR during steady state operation, normal operational transients, and anticipated transients is limited to 1.19. A DNBR of 1.19 corresponds to a 95% probability at a 95% confidence level that DNB will not occur, which is considered an appropriate margin to DNB for all operating conditions. (1)

The curves of Figure 1-1 represent the loci of points of reactor thermal power (either neutron flux instruments of ΔT instruments), reactor coolant system pressure, and cold leg temperature for which the DNBR is 1.19. The area of safe operation is below these lines.

The reactor core safety limits are based on radial peaks limited by the CEA insertion limits in Section 2-10 and axial shapes within the axial power distribution trip limits in Figure 1-2 and a total unrodded planar radial peak of 1.70. The LSSS in Figure 1-3 is based on the assumption that the unrodded integrated total radial peak (F_R^T) is 1.62. This peaking factor is slightly higher (more conservative) than the maximum predicted unrodded total radial peak during core life, excluding measurement uncertainty.

Flow maldistribution effects for operation under less than full reactor coolant flow have been evaluated via model tests.(2) The flow model data established the maldistribution factors and hot channel inlet temperature for the thermal analyses that were used to establish the safe operating envelopes presented in Figure 1-1. The reactor protective system is designed to prevent any anticipated conbination of transient conditions for reactor coolant system temperature, pressure and thermal power level that would result in a DNBR of less than 1.19.(3)

References

(1) USAR, Section 3.6.7
(2) USAR, Section 1.4.6
(3) USAR, Section 3.6.2

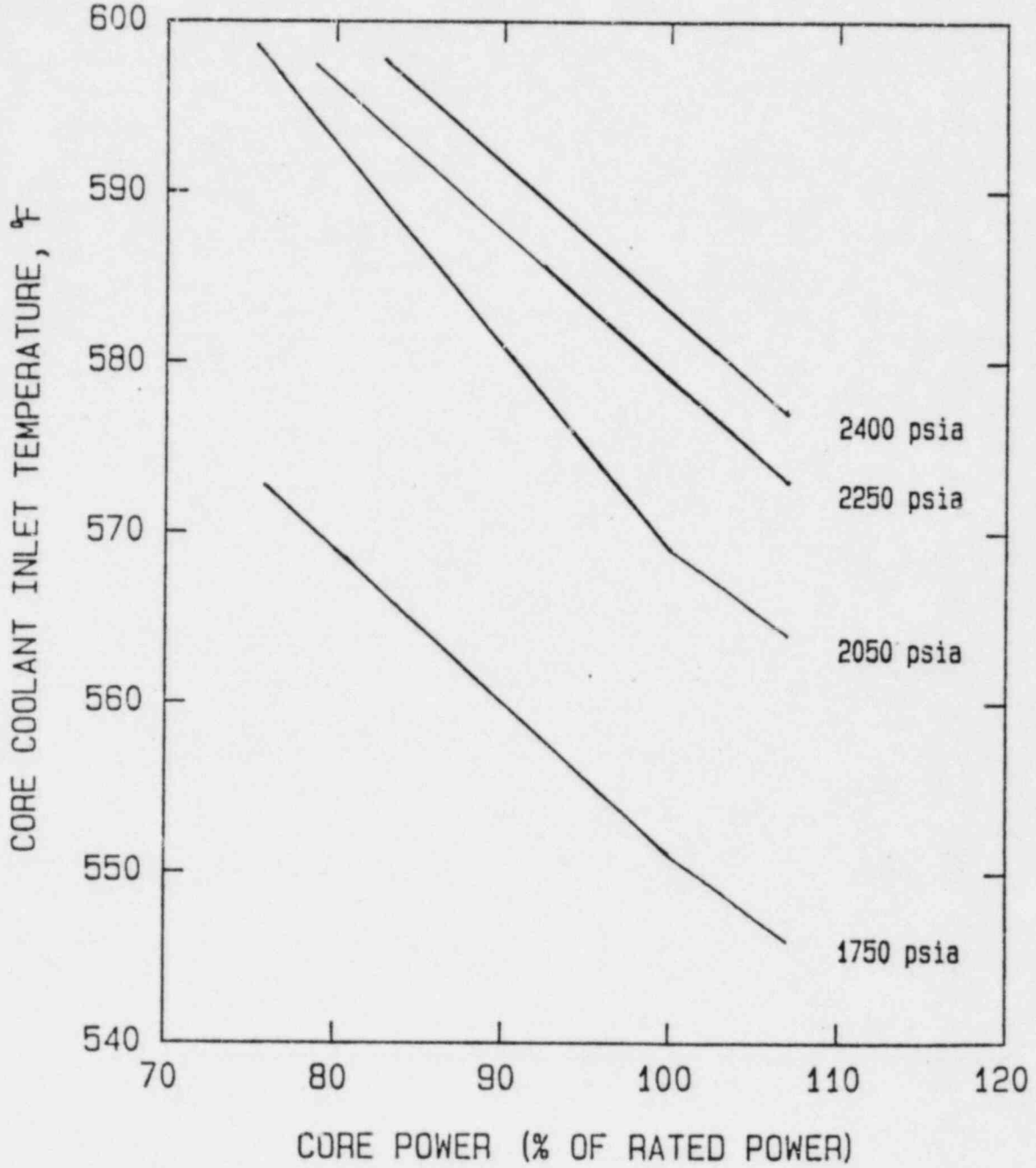

Thermal Margin/Low Pressure Safety Limits 4 Pump Operation	Omaha Public Power District Fort Calhoun Station-Unit No. 1	Figure 1-1

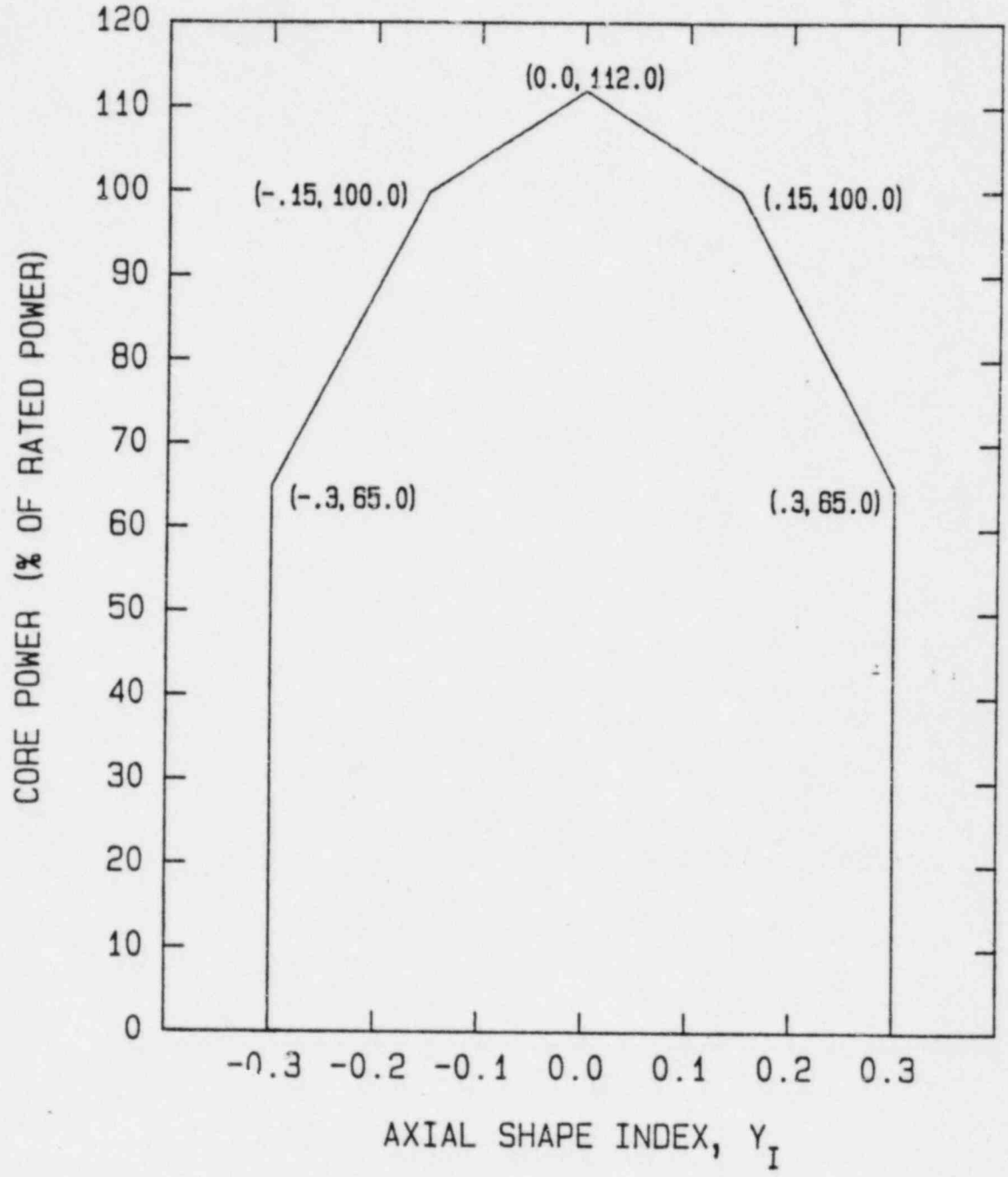

Axial Power Distribution LSSS for 4 Pump Operation	Omaha Public Power District Fort Calhoun Station-Unit No. 1	Figure 1-2

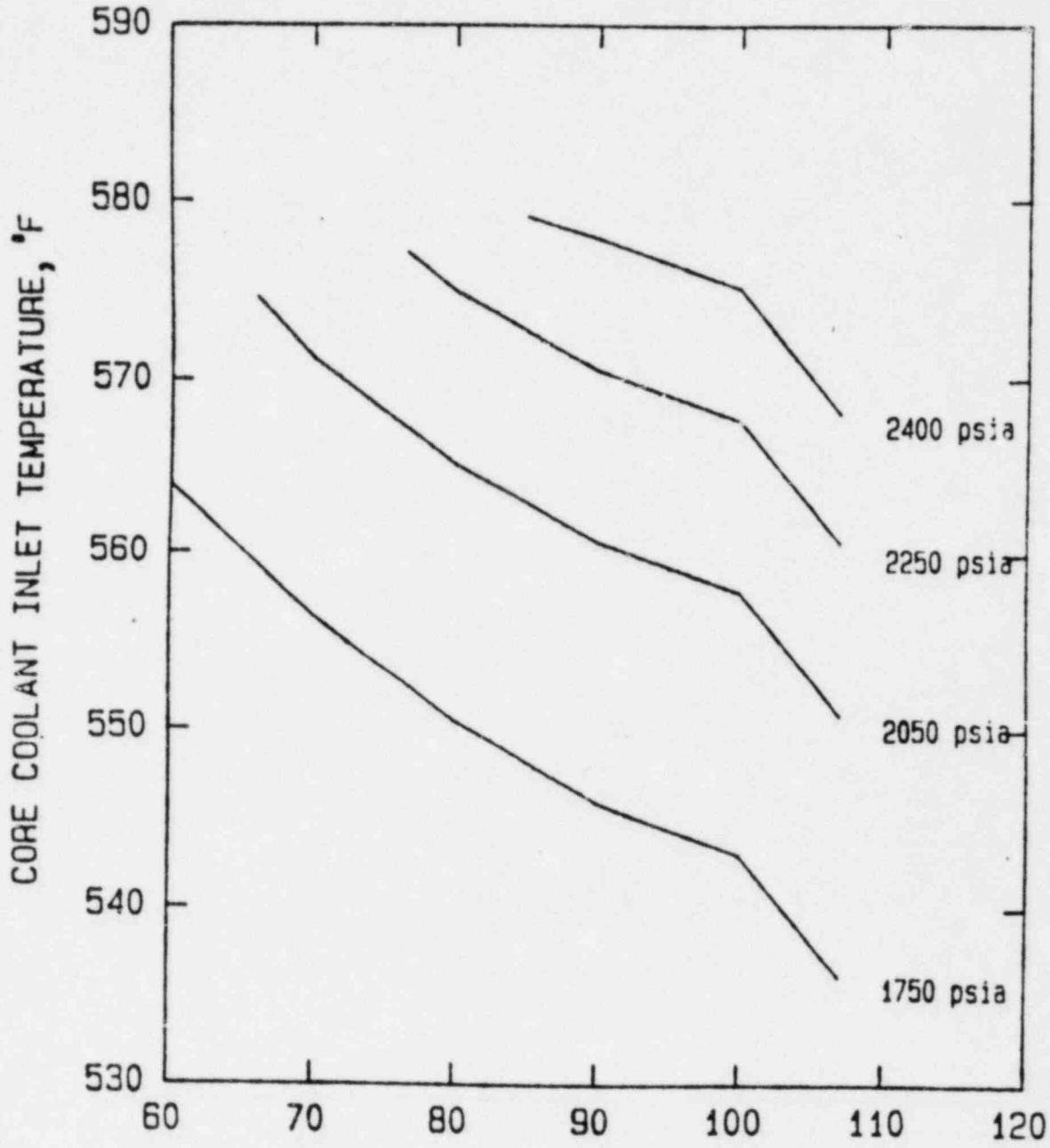

$$P_{VAR} = 20.3\ PF(B)\ B + 20.3\ T_{IN} - 11,283$$

$$PF(B) = 1.0 \quad B \geq 100\%$$
$$= -.008\ B + 1.8 \quad 50\% \leq B \leq 100\%$$
$$= 1.4 \quad B \leq 50\%$$

Thermal Margin/Low Pressure LSSS 4 Pump Operation	Omaha Public Power District Fort Calhoun Station-Unit No. 1	Figure 1-3

During reactor operation at power levels below 19.1% rated power, a reactor trip will occur in the event of a reactivity excursion that results in a power increase up to the lower fixed set point of the VHPT circuit of 19.1% of rated power. During normal power increases below 19.1% reactor trip would be initiated at 19.1% of rated power unless the set point is manually adjusted.

(2) Low Reactor Coolant Flow - A reactor trip is provided to protect the core against DNB should the coolant flow suddenly decrease significantly. Provisions are made in the reactor protective system to permit operation of the reactor at reduced power if one or two coolant pumps are taken out of service. These low-flow and high-flux settings have been derived in consideration of instrument errors and response times of equipment involved to maintain the DNB ratio above 1.19 under normal operation (4) and expected transients.(5) For reactor operation with one or two coolant pumps inoperative, the low-flow trip points, the overpower trip points, and the thermal margin/low pressure trip points and the axial power distribution trip points are simultaneously changed when the pump condition selector switches (one per safety channel for a total of four switches) are set to the desired 2 or 3 pump position.(2)

Flow in each of the four coolant loops is determined from a measurement of pressure drop from inlet to outlet of the steam generators. The total flow through the reactor core is measured by summing the loop pressure drops across the steam generators and correlating this pressure sum with the pump calibration flow curves.

The percent of normal core flow is shown in the following table:(6)

4 Pumps	100%
3 Pumps	73.3%
2 Pumps (each on a different steam generator)	49.6%
2 Pumps (both on same steam generator)	48.8%

During four-pump operation, the low flow trip setting of 85% insures that the reactor cannot operate when the flow rate is less than 93% of the nominal value considering instrument errors. The high-power level trip, the thermal margin/low pressure trip, the low reactor coolant flow trip, and the axial power distribution trip are reduced to compensate for the corresponding core flow reduction experienced with fewer than four pumps in operation. The limits of trip points are shown in Table 1-1.

(3) High Pressurizer Pressure - A reactor trip for high pressurizer pressure is provided in conjunction with the reactor and steam system safety valves to prevent reactor coolant system overpressure (Specification 2.1.6) In the event of loss of load without reactor trip, the temperature and pressure of the reactor coolant system would increase due to the reduction in the heat removed from the coolant via the steam generators. The power-operated relief valves are set to operate concurrently with the high pressurizer pressure reactor trip. This setting is 100 psi below the nominal safety valve setting (2500 psia) to avoid unnecessary operation of the safety valves. This setting is consistent with the trip point assumed in the accident analysis.(1)

(4) Thermal Margin/Low Pressure Trip - The thermal margin/low pressure trip is provided to prevent operation when the DNBR is less than 1.19, including allowance for measurement error. The thermal and hydraulic limits shown on Figure 1-3 define the limiting values of reactor coolant pressure, reactor inlet temperature, and reactor power level which ensure that the thermal criteria (8) are not exceeded. The low set point of 1750 psia trips the reactor in the unlikely event of a loss-of-coolant accident. The thermal margin/low pressure trip set points shall be set according to the formula given on Figure 1-3. The variables in the formula are defined as:

B = High auctioneered thermal (T) or nuclear power in % of rated power.
T_{IN} = Core inlet temperature, °F.
P_{VAR} = Reactor pressure, psia.

(7) Containment High Pressure - A reactor trip on containment high pressure is provided to assure that the reactor is shut down simultaneously with the initiation of the safety injection system. The setting of this trip is identical to that of the containment high pressure signal which indicates safety injection system operation.

(8) Axial Power Distribution - The axial power trip is provided to ensure that excessive axial peaking will not cause fuel damage. The Axial Shape Index is determined from the axially split excore detectors. The set point functions, shown in Figure 1-2 ensure that neither a DNBR of less than 1.19 nor a maximum linear heat rate of more than 21 kW/ft (deposited in the fuel) will exist as a consequence of axial power maldistributions. Allowances have been made for instrumentation inaccuracies and uncertainties associated with the excore symmetric offset - incore axial peaking relationship.

(9) Physics Testing at Low Power - During physics testing at power levels less than 10^{-1}% of rated power, the tests may require that the reactor be critical. For these tests only the low reactor coolant flow and thermal margin/low pressure trips may be bypassed below 10^{-1}% of rated power. Written test procedures which are approved by the Plant Review Committee, will be in effect during these tests. At reactor power levels less than 10^{-1}% of rated power the low reactor coolant flow and the thermal margin/low pressure trips are not required to prevent fuel element thermal limits being exceeded. Both of these trips are bypassed using the same bypass switch. The low steam generator pressure trip is not required because the low steam generator pressure will not allow a severe reactor cooldown if a steam line break were to occur during the tests.

References

(1) USAR, Section 14.1

(2) USAR, Section 7.2.3.3

(3) USAR, Section 7.2.3.2

(4) USAR, Section 3.6.6

(5) USAR, Section 14.6.2.2, 14.6.4

(6) USAR, Section 14.7

(7) USAR, Section 7.2.3.1

(8) USAR, Section 3.6

(9) USAR, Section 14.10

2.0 LIMITING CONDITIONS FOR OPERATION

2.1 Reactor Coolant System (Continued)

2.1.1 Operable Components (Continued)

(a) A pressurizer steam space of 60% by volume or greater exists, or

(b) The steam generator secondary side temperature is less than 50°F above that of the reactor coolant system cold leg.

(12) Reactor Coolant System Pressure Isolation Valves

(a) The integrity of all pressure isolation valves listed in Table 2-9 shall be demonstrated, except as specified in (b). Valve leakage shall not exceed the amounts indicated.

(b) In the event that the integrity of any pressure isolation valve specified in Table 2-9 cannot be demonstrated, reactor operation may continue, provided that at least two valves in each high pressure line having a non-functional valve are in and remain in, the mode corresponding to the isolated condition.*

(c) If Specifications (a) and (b) above cannot be met, an orderly shutdown shall be initiated and the reactor shall be in the cold shutdwn condition within 24 hours.

Basis

The plant is designed to operate with both reactor coolant loops and associated reactor coolant pumps in operation and maintain DNBR above 1.19 during all normal operations and anticipated transients.

In the hot shutdown mode, a single reactor coolant loop provides sufficient heat removal capability for removing decay heat; however, single failure considerations require that two loops be operable.

In the cold shutdown mode, a single reactor coolant loop or shutdown cooling loop provides sufficient heat removal capability for removing decay heat, but single failure considerations require that at least two loops be operable. Thus, if the reactor coolant loops are not operable, this specification requires two shutdown cooling pumps to be operable.

The requirement that at least one shutdown cooling loop be in operation during refueling ensures that: (1) sufficient cooling capacity is available to remove decay heat and maintain the water in the reactor pressure vessel below 210°F as required during the refueling mode, and (2) the effects of a boron dilution incident is minimized and prevents boron stratification.

* Manual valves shall be locked in the closed position; motor operated valves shall be placed in the closed position and power supplies deenergized.

Amendment No. 36, Order dated 4/20/81

2.0 LIMITING CONDITIONS FOR OPERATION
2.10 Reactor Core (Continued)

2.10.2 Reactivity Control Systems and Core Physics Parameters Limits

Applicability

Applies to operation of control element assemblies and monitoring of selected core parameters whenever the reactor is in cold or hot shutdown, hot standby, or power operation conditions.

Objective

To ensure (1) adequate shutdown margin following a reactor trip, (2) the MTC is within the limits of the safety analysis, and (3) control element assembly operation is within the limits of the setpoint and safety analysis.

Specification

(1) Shutdown Margin With T_{cold} >210°F

Whenever the reactor is in hot shutdown, hot standby or power operation conditions, the shutdown margin shall be $\geq$4.0% $\Delta k/k$. With the shutdown margin <4.0% $\Delta k/k$, initiate and continue boration until the required shutdown margin is achieved.

(2) Shutdown Margin With $T_{cold} \leq$210°F

Whenever the reactor is in cold shutdown conditions, the shutdown margin shall be $\geq$3.0% $\Delta k/k$. With the shutdown margin <3.0% $\Delta k/k$, initiate and continue boration until the required shutdown margin is achieved.

(3) Moderator Temperature Coefficient

The moderator temperature coefficient (MTC) shall be:

a. Less positive than $+0.2 \times 10^{-4}$ $\Delta\rho/°F$ including uncertainties for power levels at or above 80% of rated power.

b. Less positive than $+0.5 \times 10^{-4}$ $\Delta\rho/°F$ including uncertainties for power levels below 80% of rated power.

c. More positive than -2.5×10^{-4} $\Delta\rho/°F$ including uncertainties at rated power.

With the moderator temperature coefficient confirmed outside any one of the above limits, change reactivity control parameters to bring the extrapolated MTC value within the above limits within 3 hours or be in at least hot shutdown within 6 hours.

1. The total available shutdown margin may be reduced to 2% Δk/k during the measurement of the shutdown CEA group reactivities, or

2. The total available shutdown margin may be reduced to the worth of the worst stuck CEA's during the measurement of the stuck CEA reactivity.

(ii) If the shutdown margin specified in part (i) above is not available immediately, initiate and continue boration until the requirements of 2.10.2(1) are met.

(iii) The shutdown margin specified in part (i) above shall be verified every 8 hour shift.

c. Moderator Temperature Coefficient

(i) The moderator temperature coefficient (MTC) requirements of 2.10.2(3) may be suspended during physics tests at less than 10^{-1}% of rated power.

(ii) If power exceeds 10^{-1}% of rated power, either:

1. Reduce power to less than 10^{-1}% of rated power within 15 minutes, or

2. Be in hot shutdown in 2 hours.

Basis

Shutdown Margin

A sufficient shutdown margin ensures that (1) the reactor can be made subcritical from all operating conditions, (2) the reactivity transients associated with postulated accident conditions are controllable within acceptable limits, and (3) the reactor will be maintained sufficiently subcritical to preclude inadvertent criticality in the shutdown condition.

Shutdown margin requirements vary throughout core life as a function of fuel depletion, RCS boron concentration, and RCS T_{avg}. The most restrictive condition occurs at EOL, with T_{avg} at no load operating temperature, and is associated with a postulated steam line break accident and resulting uncontrolled RCS cooldown. In the analysis of this accident, a minimum shutdown margin of 4.0% Δk/k is initially adequate to control the reactivity transient. Accordingly,

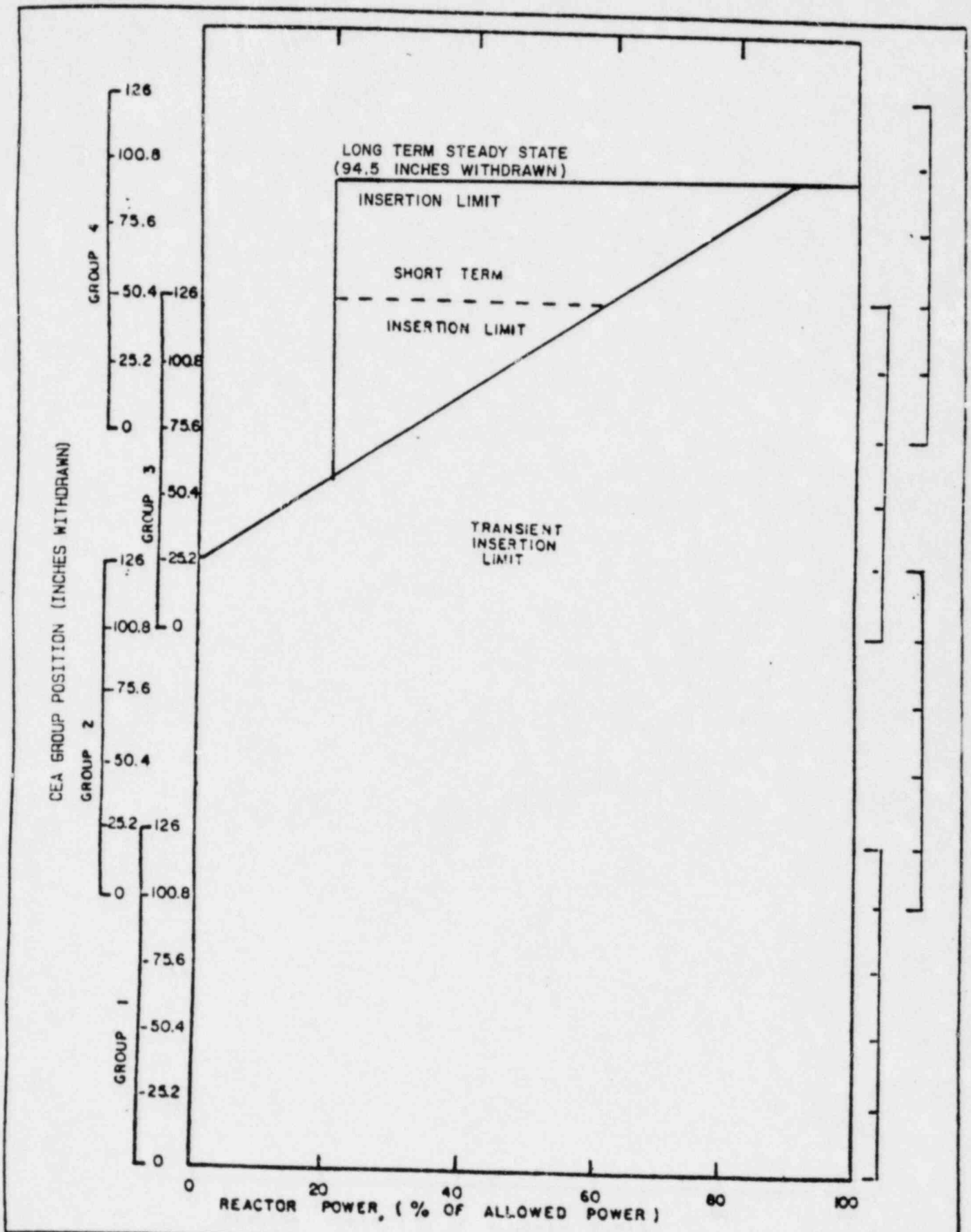

POWER DEPENDENT INSERTION LIMIT	OMAHA PUBLIC POWER DISTRICT FORT CALHOUN STATION UNIT NO. 1	FIGURE 2-4

Amendment No. 5, 20, 32

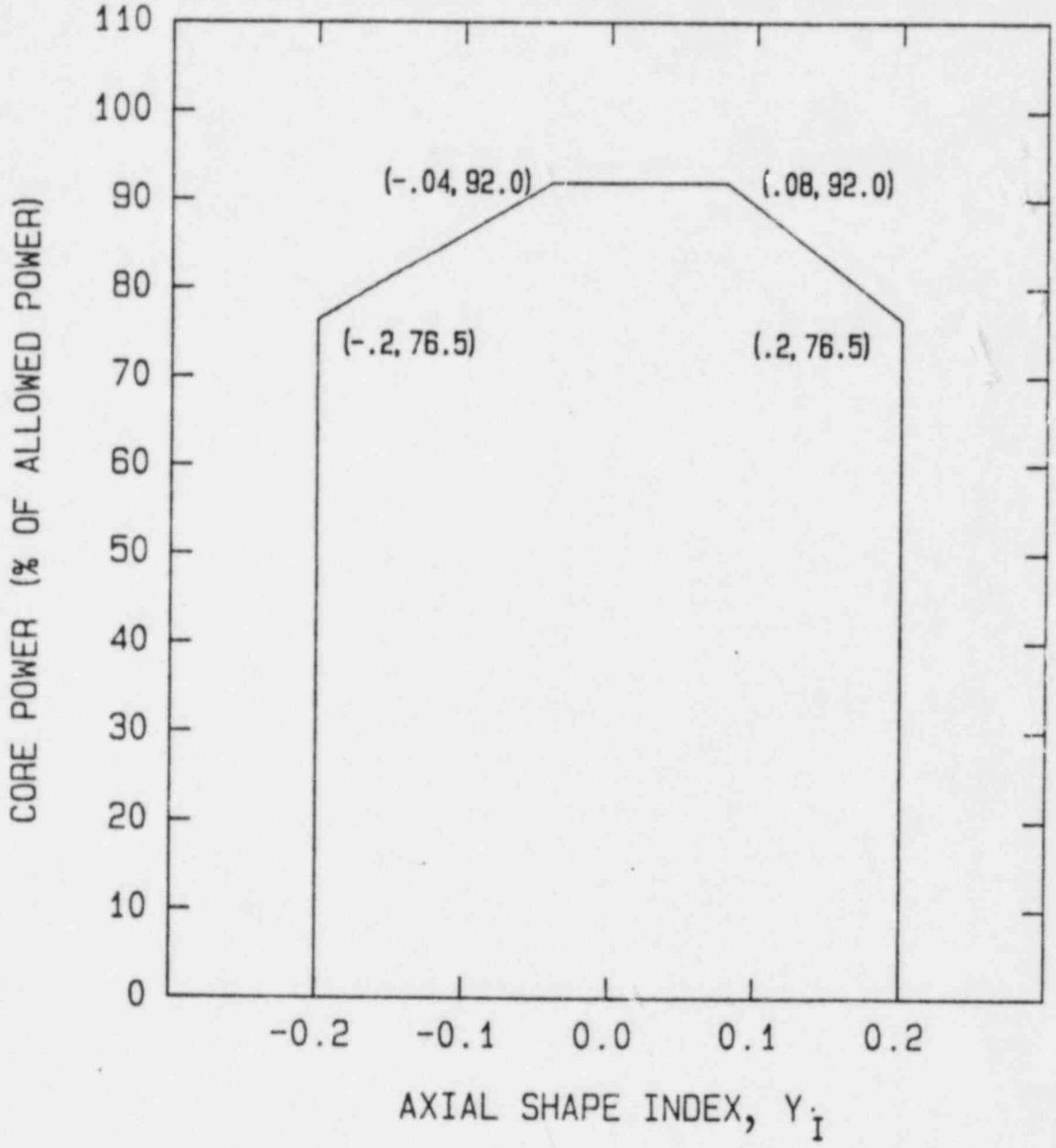

Limiting Condition for Operation for Excore Monitoring of LHR	Omaha Public Power District Fort Calhoun Station-Unit No. 1	Figure 2-6

Amendment No. 8, 20, 32, 42, 47

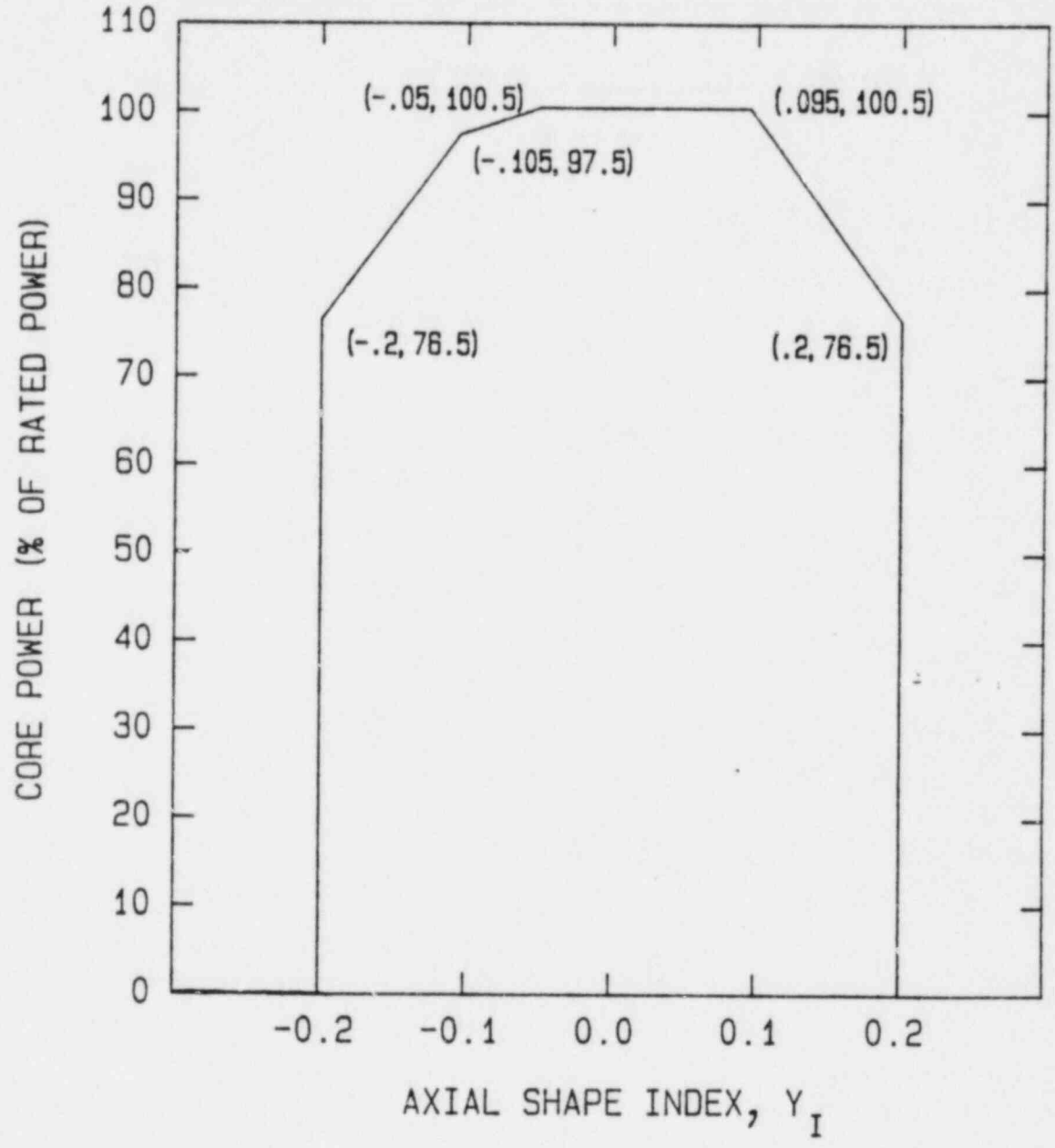

Limiting Condition for Operation for DNB Monitoring	Omaha Public Power District Fort Calhoun Station-Unit No. 1	Figure 2-7

Amendment No. 8, 20, 32, 47

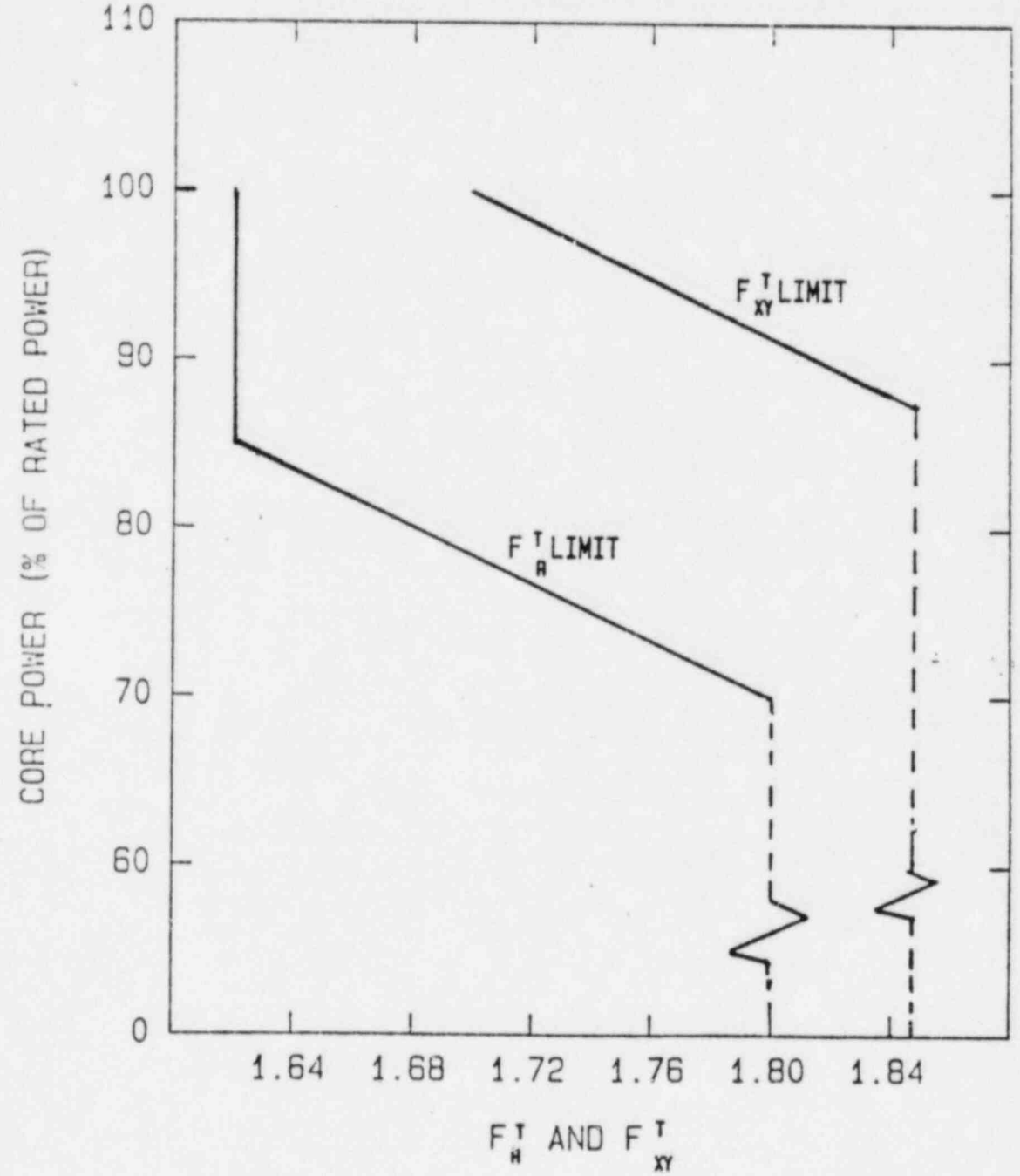

F^T_R, F^T_{XY} and Core Power Limitations	Omaha Public Power District Fort Calhoun Station-Unit No. 1	Figure 2-9

(ii) Be in at least hot standby within the next 6 hours.

(2) Total Integrated Radial Peaking Factor

The calculated value of F_R^T defined by $F_R^T = F_R (1+T_q)$ shall be limited to ≤ 1.62. F_R is determined from a power distribution map with no part length CEA's inserted and with all full length CEA's at or above the Long Term Steady State Insertion Limit for the existing Reactor Coolant Pump combination. The azimuthal tilt, T_q, is the measured value of T_q at the time F_R is determined.

With $F_R^T > 1.62$ within 6 hours:

(a) Reduce power to bring power and F_R^T within the limits of Figure 2-9, withdraw the full length CEA's to or beyond the Long Term Steady State Insertion Limits of Specification 2.10.2(7), and fully withdraw the PLCEA's, or

(b) Be in at least hot standby.

(3) Total Planar Radial Peaking Factor

The calculated value of F_{xy}^T defined as $F_{xy}^T = F_{xy} (1+T_q)$ shall be limited to ≤ 1.70. F_{xy} is determined from a power distribution map with no part length CEA's inserted and with all full length CEA's at or above the Long Term Steady State Insertion Limit for the existing Reactor Coolant Pump conbination. The azimuthal tilt, T_q, is the measured value of T_q at the time F_{xy} is determined.

With $F_{xy}^T > 1.70$ within 6 hours:

(a) Reduce power to bring power and F_{xy}^T within the limits of Figure 2-9, withdraw the full length CEA's to or beyond the Long Term Steady State Insertion Limits of Specification 2.10.2(7), and fully withdraw the PLCEA's, or

(b) Be in at least hot standby.

(5) DNBR Margin During Power Operation Above 15% of Rated Power

(a) The following DNB related parameters shall be maintained within the limits shown:

(i)	Cold Leg Temperature	$\leq$545°F *
(ii)	Pressurizer Pressure	$\geq$2075 psia*
(iii)	Reactor Coolant Flow	$\geq$197,000**
(iv)	Axial Shape Index, Y_I	$\leq$ Figure 2-7

(b) With any of the above parameters exceeding the limit, restore the parameter to within its limit within 2 hours or reduce power to less than 15% of rated power within the next 8 hours.

Basis

Linear Heat Rate

The limitation on linear heat rate ensures that in the event of a LOCA, the peak temperature of the fuel cladding will not exceed 2200°F.

Either of the two core power distribution monitoring systems, the Excore Detector Monitoring System, or the Incore Detector Monitoring System, provide adequate monitoring of the core power distribution and are capable of verifying that the linear heat rate does not exceed its limits. The Excore Detector Monitoring System performs this function by continuously monitoring the axial shape index with the operable quadrant symmetric excore neutron flux detectors and verifying that the axial shape index is maintained within the allowable limits of Specification 2.10.4.(5)(a) as adjusted by Specification 2.10.4.(1).(c) for the allowed linear heat rate of Figure 2-5, RC Pump configuration, and F_{xy}^T of Figure 2-9. In conjunction with the use of the excore monitoring system and in establishing the axial shape index limits, the following assumptions are made: (1) the CEA insertion limits of Specification 2.10.2.(6) and long term insertion limits of Specification 2.10.2.(7) are satisfied, (2) the flux peaking augmentation factors are as shown in Figure 2-8, (3) the azimuthal power tilt restrictions of Specification 2.10.4.(4) are satisfied, and (4) the total planar radial peaking factor does not exceed the limits of Specification 2.10.4.(3).

*Limit not applicable during either a thermal power ramp in excess of 5% of rated thermal power per minute or a thermal power step of greater than 10% of rated thermal power.

**This number is an actual limit (not including uncertainties). All other values in this listing are indicated values and include an allowance for measurement uncertainty (e.g., 545°F, indicated, allows for an actual T_c 547°F).

TABLE 2.6

DELETED

DISCUSSION

The proposed Technical Specification changes concern the upcoming reactor core reload and are required for Cycle 8 operation of the Fort Calhoun Station, which is currently scheduled to commence in April, 1983. The Cycle 8 core design incorporates a low radial leakage fuel loading pattern which will reduce neutron flux to critical reactor vessel longitudinal welds. This new fuel management scheme is being implemented to reduce the rate of reactor vessel embrittlement due to neutron irradiation. The District estimates that embrittlement rate will be reduced by a factor of two at the critical welds and thus will increase the time available prior to exceeding the proposed NRC pressurized thermal shock RT-NDT screening criteria.

The analysis supporting these Technical Specification changes is being submitted in the form of revisions to the Fort Calhoun Station Updated Safety Analysis Report (USAR). This method provides a convenient means to reference and compare previous cycles and to establish the USAR as the single source document for core reload analyses.

The utilization of a low radial leakage loading pattern has necessitated an increase in the F_R^I and F_{xy}^T limits in Section 2.10.4. In addition, the Moderator Temperature Coefficient (MTC) negative limit has been changed to -2.5×10^{-4} $\Delta\rho/°F$ to accommodate a more negative MTC at the end-of-cycle 8. The supporting physics analysis and methodology for these changes is provided in the attached revision to USAR Section 3.4. It should be noted that the physics methodology is the same as that used in the Fort Calhoun Station Cycle 5 reload analysis which was approved by the Commission in the referenced letter.

The increase in the peaking factor limits has been reviewed and justified utilizing Combustion Engineering setpoint and safety analysis methodology. This is the same methodology used in the Cycle 5 analysis and approved for use at the Fort Calhoun Station in the referenced letter, with the exception of the steady-state DNBR analysis. The District has utilized the TORC and CETOP computer codes and the CE-1 critical heat flux correlation for the Cycle 8 DNBR analysis. Details of the steady-state DNBR analysis are provided in a new Section 3.6 to the USAR. A revised USAR Section 3.5 is included to document the DNBR analysis of selected transients which have a high DNBR compared to the DNBR statistical limit and are not normally analyzed each cycle.

The proposed changes to Technical Specification Section 1.0, "Safety Limits and Limiting Safety Settings", incorporate the results of the revised DNBR analysis and the use of the CE setpoint methodology previously used in the Cycle 5 analysis. The "Basis" sections of TS Section 1.0 have been revised to incorporate the CE-1 critical heat flux correlation and its statistical limit of 1.19 for 14 by 14 fuel assemblies.

The Thermal Margin/Low Pressure LSSS, Figure 1-3, has been revised using the setpoint methodology approved in the Reference and the DNBR analysis techniques provided in attached USAR Section 3.6. The pressure bias term of the Thermal Margin/Low Pressure (TM/LP) equation was derived from the RCS depressurization analysis provided in the attached USAR Section 14.22. Previously, this term

had been derived from the CEA Withdrawal Incident analysis, but the Cycle 8 analysis contained in attached USAR Section 14.2 demonstrates that the TM/LP trip is not required for the CEA Withdrawal Incident. The Axial Power Distribution LSSS, Figure 1-2, was changed to require more restrictive limits on the Axial Shape Index (ASI) at 100% of rated power to provide additional DNBR overpower margin. In addition, the lower power ASI limits are now more restrictive to be consistent with the constant ASI operating mode employed at the Fort Calhoun Station. The Thermal Margin/Low Pressure Safety Limit, Figure 1-1, has been revised and is consistent with the changes to Figure 1-3.

The changes to Section 2.0, "Limiting Conditions of Operation" incorporate the expected physics characteristics of the Cycle 8 core, the revised DNBR analysis and the use of the CE setpoint methodology previously used in the Cycle 5 analysis.

The shutdown margin requirement with Tcold >210°F of Specification 2.10.2(1) has been increased to 4.0% $\Delta k/k$ as required by the revised Main Steam Line Break analysis detailed in attached USAR Section 14.12. In addition, the Power Dependent Insertion Limit, Figure 2-4, has been revised to provide for additional shutdown margin at zero power and to eliminate the Group 2 CEA's from consideration in the CEA Ejection Accident.

The analysis of the Boron Dilution Incident provided in the attached USAR Section 14.3 demonstrates that the revised Specifications maintain adequate shutdown margin.

The limits on F_R^T and F_{xy}^T of Specifications 2.10.4(2) and 2.10.4(3) have been revised to accommodate the increased peaking expected from the Cycle 8 core. The F_R^T, F_{xy}^T and Core Power Limitations, Figure 2-9, have also been revised utilizing the methodology used in the Cycle 5 analysis.

The DNBR Margin for operation above 15% of Rated Power, Specification 2.10.4(5), has been revised. Figure 2-7 has been changed at lower power levels to be consistent with the restrictions of Figure 1-2. The minimum reactor coolant flow has been increased to credit additional flow available from the Reactor Coolant Pumps.

Specification 2.10.4(5) limits those parameters which define the available overpower DNBR margin. The CEA Drop Incident continues to require the largest overpower DNBR margin. The CEA Drop Incident analysis, provided in attached USAR Section 14.4, demonstrates that sufficient DNBR overpower margin is maintained by Section 2.10.4(5).

The Limiting Conditions for Operation for Excore Monitoring of Linear Heat Rate (LHR) Figure 2-6, has been revised at lower power levels to be consistent with Figure 2-7.

The Loss of Coolant Flow Incident, USAR Section 14.6, and the Loss-of-Coolant Accident, USAR Section 14.15, analyses are presently being completed. These accident analyses will use the methodologies described in the current USAR sections with the exception that the CE-1 critical heat flux correlation is being used to determine the amount of failed fuel in the Loss-of-Coolant Flow Incident. These analyses are being performed because of the increases in F_R^T and F_{xy}^T. These analyses will be submitted in December, 1982.

Table 2-6 has been deleted since the subject DNB related operating parameters have previously been incorporated into the Limiting Conditions for Operation, Specification 2.10.4(5).

References

Letter, R.W. Reid (NRC) to T.E. Short dated December 5, 1978.

SECTION 3
REACTOR

CONTENTS

CONTENTS (cont'd)

CONTENTS (cont'd)

LIST OF TABLES

LIST OF FIGURES

SECTION 3
REACTOR

3.1 Summary of Description

The reactor is of the pressurized water type, using two reactor coolant loops. A vertical cross section of the reactor is shown in Figure 3.1-1. The reactor core is composed of 133 fuel assemblies and 49 control element assemblies (CEA's). The fuel assemblies are arranged to approximate a right circular cylinder with an equivalent diameter of 106.5 inches and an active fuel length of 128 inches. The fuel assembly, which provides for 176 fuel rod positions, (14 x 14 array) consists of 5 guide tubes attached to spacer grids and is closed at the top and bottom by end fittings. The fuel rods are retained in an open zircaloy and stainless steel framework, restrained laterally by zircaloy or inconel leaf spring spacer grids. The guide tubes each displace four fuel rod positions and provide channels which guide the CEA's over their entire length of travel. In-core instrumentation is routed into the fuel assemblies through the upper head of the reactor vessel. Figure 3.1-2 shows the reactor core cross section and dimensional relations between fuel assemblies, fuel rods and CEA guide tubes.

The fuel is low enrichment UO_2 in the form of ceramic pellets and is encapsulated in prepressurized helium filled zircaloy tubes which form a hermetic enclosure.

The reactor coolant enters the inlet nozzles of the reactor vessel, flows downward between the reactor vessel wall and the core barrel, and passes through the flow skirt and lower core barrel section, where the flow distribution is equalized, and into the lower plenum. The coolant then flows upward through the core removing heat from the fuel rods. The heated coolant enters the core outlet region where the coolant flows around the outside of control element assembly shroud tubes to the reactor vessel outlet nozzles. The control element assembly shroud tubes protect the individual neutron absorber elements of the CEA's from the effects of coolant cross flow above the core.

The reactor internals, which support and orient the fuel assemblies, control element assemblies, and in-core instrumentation, also guide the reactor coolant through the reactor vessel. The internals absorb the static and dynamic loads and transmit the loads to the reactor vessel flange, and they will safely perform their functions during normal operating, upset and emergency conditions. The internals are designed to safely withstand the forces due to the deadweight, handling, pressure differentials, flow impingement, temperature differentials, vibration and seismic acceleration. The design of the reactor internals limits deflection where such limits are required by function. The stress values of all structural members under normal operating and expected transient conditions are not greater than those established by Section III of the ASME Pressure Vessel Code. The effect of neutron irradiation on the materials utilized is included in the design evaluation. The effect of accident loadings on the internals is included in the design analysis.

Reactivity control is provided by two independent systems; namely, the Control Element Drive System and the Chemical and Volume Control System. The Control Element Drive System controls short term reactivity changes and is used for rapid shutdown. The Chemical and Volume Control System is used to compensate

for long-term reactivity changes and can make the reactor subcritical without the benefit of the Control Element Drive System. The design of the core and the Reactor Protective System prevents fuel damage limits from being exceeded for any single malfunction in either of the reactivity control systems.

The CEA's consist of five Inconel tubes, 0.948 inch in diameter, containing boron carbide pellets. Four tubes are assembled in a square array around the central fifth tube. The tubes are joined by a spider at the upper end. The hub of the spider couples the CEA to the drive assembly. The CEA's are actuated by rack and pinion control element drive mechanisms (CEDM's) mounted on the reactor vessel head. Four of the CEA's designated as partial length CEA's, have been provided with poison sections only in the lower portion of their length. These partial length CEA's were provided to control the axial power distribution during power level changes or during xenon redistributions. However, it was found that the part length CEA's could adversely affect reactor operations and the axial power distribution could be satisfactorily controlled by use of the full length CEA's. Therefore, these CEA's are required by the Technical Specifications to remain in an essentially fully withdrawn position during power operation.

Control element assemblies are moved in groups to satisfy the requirements of shutdown, power level changes and operational maneuvering. The maximum reactivity worth of the CEA's and the associated reactivity addition rate are limited by system design to prevent rapid large reactivity increases. The design restraints are such that reactivity increases will not result in the violation of the fuel damage limits, rupture of the reactor coolant pressure boundary, or physical disruption of the core or other internals in such a way as to impair the effectiveness of emergency core cooling.

Boric acid dissolved in the coolant is used as a neutron absorber to provide long term reactivity control. In the event it becomes necessary to reduce the boric acid concentration required at the beginning-of-cycle operating conditions in order to reduce the algebraic magnitude of the moderator temperature coefficient of the core, appropriate neutron absorber material (poison) will be provided in certain reload fuel assemblies.

The nuclear design of the core will assure that, in the power operating range, the combined response of all reactivity coefficients to an increase in reactor thermal power yields a net decrease in reactivity. Core monitoring and administrative controls on the plant will result in power distributions during normal operation such that the Reactor Protective System will limit both the fuel temperature and the departure from nucleate boiling ratio (DNBR) to acceptable values for postulated accidents and anticipated transients.

The details of the reactor and core design are discussed in the following subsections of this Section 3 of the USAR. The design bases are described in Section 3.2, and reactor core and fuel cycle considerations are discussed in Section 3.3. The design and evaluation of the nuclear, thermal hydraulic, and mechanical characteristics of the reactor are described in Sections 3.4, 3.5, and 3.6, respectively, and the corresponding summary lists of significant core parameters are presented in Tables 3.4-1, 3.5-1 and 3.6-1, respectively.

3.2 DESIGN BASES

3.2.1 Performance Objectives

The initial full-power thermal rating of the core was 1420 MWt, which corresponds to a gross electrical output of 481 MWe. Although the plant was designed for a full-power rating of 1500 MWt, the initial license application and the first five fuel cycles of operation were at this lower power rating of 1420 MWt. On August 5, 1980, Fort Calhoun Station was issued a license amendment to allow operation at a steady state full rated power level of 1500 MWt, and the safety analysis described in this FSAR was perfomed for a full rated power level of 1500 MWt.

3.2.2 Design Objectives

During normal operating conditions and anticipated transients, the reactor core, together with its control systems and the reactor protective system, is designed to function over its lifetime to prevent fuel damage based upon application of conservative limits for excessive fuel temperature, cladding strain, and cladding stress as specified in Section 3.2.3.

The combined response of all reactivity feedback mechanisms to an increase in reactor thermal power is a net decrease in reactivity. The combined effect of all reactivity coefficients in conjunction with the reactor control system provides stable reactor operation. If power oscillations do occur, their magnitude will be such that the fuel damage limits are not exceeded.

The maximum reactivity worth of the CEA's and the associated reactivity addition rate are limited by core, CEA and control element drive system designs to prevent rapid, large reactivity increases. Such reactivity increases are precluded in order to avoid violation of the fuel damage limits, rupture of the reactor coolant pressure boundary, or disruption of the core or other internals sufficient to impair the effectiveness of emergency cooling.

3.2.3 Design Criteria and Limits

3.2.3.1 Nuclear Criteria and Limits

The design of the core is based upon the following nuclear criteria and limitations:

a. The local fuel pellet burnup limit is determined by material and mechanical design rather than nuclear considerations. The conservatism of the resulting limit is confirmed by actual irradiation of demonstration fuel assemblies to the corresponding limit specified for that particular fuel design.

b. The combined response of all reactivity coefficients to an increase in reactor thermal power yields a net decrease in reactivity.

c. As noted in Section 3.1, CEA's are moved in groups to satisfy the requirements of shutdown, power level changes and operational maneuvering. The control systems are designed to produce power distributions that are within the acceptable limits on the overall nuclear heat

flux factor (F_Q^N) and departure from nucleate boiling ratio (DNBR) limits. The reactor protective system and the limiting conditions for operation assure that these limits are not exceeded.

d. Axial power distributions are manually controlled by full length CEA's, using information provided by the out-of-core detectors.

e. The melting point of the UO_2 fuel shall not be reached during normal operation and anticipated transients.

3.2.3.2 Reactivity Control Criteria and Limits

The control system and operating procedures provide for adequate control of the core reactivity and power distributions such that the following are met:

a. Sufficient CEA's are withdrawn to provide an adequate shutdown reactivity margin following a reactor trip;

b. The shutdown margin is maintained with the highest worth CEA assumed stuck in its fully withdrawn position;

c. The chemical and volume control system is capable of adding boric acid to the reactor coolant at a rate sufficient to maintain the shutdown margin during a reactor coolant system cooldown at the design rate following a reactor trip.

3.2.3.3 Thermal and Hydraulic Criteria and Limits

The principal criterion for the thermal and hydraulic design is to avoid thermally induced fuel damage during normal operation and anticipated transients. It is recognized that there is a small probability of limited fuel damage in certain postulated events as discussed in Section 14.

The following corollary thermal and hydraulic design bases are established, but violation of either does not necessarily result in fuel damage:

a. There shall be a high confidence level that DNB is avoided during normal operation and anticipated transients.

b. For LSS's, LOC's and certain transients (Section 3.6) a design lower limit of 1.19 on minimum DNBR as calculated according to the CE-1 correlation (References 63, 64 & 65) was used.

c. For transients which have a large margin to the DNBR design lower limit (Section 3.5) a design lower limit of 1.30 on the minimum DNBR calculated according to the W-3 correlation (Reference 1) was used in the analysis.

The reactor protective system and the reactor control system provide for automatic reactor trip or corrective actions before these design limits are violated.

Reactor internal flow passages and fuel coolant channels are designed to prevent hydraulic instabilities. Flow maldistributions are limited by design to be compatible with the specified thermal design criteria.

3.2.3.4 Mechanical Design Criteria and Limits

The reactor internals are designed to safely perform their functions during steady state conditions and normal operating transients. The internals can safely withstand the forces due to deadweight, handling, system pressure, flow-inducted pressure drop, flow impingement, temperature differential, shock, and vibration. The structural components satisfy stress values given in Section III of the ASME Boiler and Pressure Vessel Code.

The following limitations on stresses or deformations are employed to assure the capability exists for a safe and orderly shutdown in the event of earthquake and major loss-of-coolant accident loading conditions. For reactor vessel internal structures, the stress criteria are given in Table 3.2-1. The intents of the limits in this table are as follows:

a. Under design loadings plus design earthquake forces, (see Appendix F) the critical reactor vessel internal structures are designed in accordance with the stress criteria established in Section III of the ASME Boiler and Pressure Vessel Code, Article 4;

b. Under normal operating loadings plus maximum hypothetical earthquake forces, the design criteria permit a small amount of local yielding;

c. Under normal operating loadings plus coolant pipe rupture loadings plus maximum hypothetical earthquake forces, permanent deformations are permitted by the design criteria.

In the loading combinations listed in Table 3.2-1, the earthquake forces include both horizontal and vertical seismic excitations acting simultaneously.

To properly perform their functions, the critical reactor internal structures are designed to satisfy the additional deflection limits described below, in addition to the stress limits given in Table 3.2-1.

Under loading combinations (a) and (b) of Table 3.2-1, deflections are limited, so that the CEA's can function and adequate core cooling is maintained. Under loading combination (c) of Table 3.2-1, the deflection design criteria depend on the size of the piping break. If the equivalent diameter of the pipe break is no larger than the largest line connected to the main reactor coolant lines, deflections are limited, so that the core is held in place, the CEA's function normally, and adequate core cooling is maintained. Those deflections which would influence CEA movement are limited to less than two-thirds of the deflection required to prevent CEA function. For pipe breaks larger than the above, the criteria are that the fuel is held in place in a manner permitting core cooling and that adequate coolant flow passages are maintained. Further, although not required for shutdown, all CEA's will be insertable. For the larger break sizes, critical components which meet the stress criteria of Table 3.2-1 are also restrained from buckling by further limiting the stress levels to two-thirds of the stress level calculated to produce buckling.

TABLE 3.2-1

PRIMARY STRESS LIMITS FOR
CRITICAL REACTOR VESSEL INTERNAL STRUCTURES

a.	Design Loadings Plus Design Earthquake Forces	$P_m - S_m$
		$P_B + P_L - 1.5\ S_m$
b.	Normal Operating Loadings Plus Maximum Hypothetical Earthquake Forces	$P_m - S_D$
		$P_B - 1.5\ \left(1 - \frac{P_m}{S_D}^2\right) S_D$
c.	Normal Operating Loadings Plus Maximum Hypothetical Earthquake Forces Plus Pipe Rupture Loadings	$P_m - S_L$
		$P_B - 1.5\ \left(1 - \frac{P_m}{S_L}^2\right) S_L$

where:

P_L, P_m, P_B, S_m, S_y are defined in the ASME Boiler and Pressure Vessel Code, Section III, Article 4

S_u = Minimum tensile strength of material at temperature

$S_L = S_y + (1/3)\ (S_u - S_y)$

S_D = Design Stresses = $1.2\ S_m$

Fuel Assemblies

The fuel assemblies are designed to maintain their structural integrity under steady state and transient operating conditions, as well as under normal handling, shipping, and refueling loads. The design takes into account differential thermal expansion of fuel rods, thermal bowing of fuel rods and CEA guide tubes, irradiation effects, and wear of all components. Mechanical tolerances and clearances have been established on the basis of the functional requirements of the components. All components including welds are highly resistant to the corrosive action of the reactor environment.

The fuel rod design takes into account external pressure, differential expansion of the fuel and clad, fuel swelling, clad creep, fission and other gas releases, thermal stress, pressure and temperature cycling and flow-induced vibrations. The structural criteria are based on the following:

a. The maximum tensile stress during steady state operation, expected transients, and depressurization is limited to two-thirds of the minimum yield strength of the material at temperature;

b. The net unrecoverable circumferential strain shall not exceed one percent as predicted by computations considering clad creep and fuel-clad interaction effects.

Control Element Assemblies (CEA's)

The CEA's are designed to maintain their structural integrity both under all steady state and transient operating conditions, and under handling, shipping and refueling loads. Thermal distortion, mechanical tolerances, vibration and wear are all taken into account in the design. Clearances and corresponding fuel assembly alignment are established so that the possible stackup of mechanical tolerances and thermal distortion would not result in frictional forces that could prevent reliable operation of the system. The structural criteria are based on limiting the maximum stress intensity to those values specified in Section III of the ASME Boiler and Pressure Vessel Code.

The control element drive mechanisms (CEDM's) are capable of actuating the CEA's under steady state and transient operating conditions and during hypothetical seismic occurrences. For pipe rupture accident loads, the CEDM's are designed to support and maintain the position of the CEA's in the core and to be capable of actuating them when these loads have diminished.

The speed at which the CEA's are inserted or withdrawn from the core is consistent with the reactivity change requirements during reactor operation. For conditions that require a rapid shutdown of the reactor, the CEDM clutches release to allow the CEA's and the connecting CEDM components to drop by gravity into the core. The reactivity is reduced during such a CEA drop at a rate sufficient to prevent violation of fuel damage limits.

The CEDM pressure housings are an extension of the reactor vessel, providing a part of the reactor coolant boundary, and are therefore, designed to meet the requirements of the ASME Boiler and Pressure Vessel Code, Section III, Nuclear Vessels. Pressure and thermal transients as well as steady state loadings were considered in the design analysis.

3.3 REACTOR AND CORE FUEL CYCLE CONSIDERATIONS

The Fort Calhoun Station initial core and the subsequent four reloads utilized fuel assemblies designed and manufactured by Combustion Engineering, Inc. Starting with Cycle 6, Exxon Nuclear Company has designed and supplied the subsequent reloads. Future reloads may be obtained from either of these two suppliers or any other qualified reload fuel vendor.

Such diversity of supply is possible because the characteristics of any new reload fuel designs are required to be compatible with the existing fuel assemblies with which they will reside in the core. The designs and analyses described in this FSAR are intended to remain valid for a wide range of reload fuel design parameters. When there is uncertainty regarding the validity of existing FSAR analyses for new reload fuel designs, such analyses will be redone to demonstrate the suitability of such new designs for use in Fort Calhoun reload cores.

In general, the parameters used in the safety analyses (see Section 14.1) cover a range rather than a single value. It is anticipated that for most reload core designs, a significant portion of the core parameters will fall within the range of values used for the existing accident analyses. For those parameters that fall outside the range of values used for the analyses, re-analysis of the appropriate accidents will be conducted and the results evaluated accordingly. Changes in Technical Specifications will be requested if necessary. The design of reload fuel has been and will continue to be done on a timely basis consistent with the refueling schedule, normally 9 to 18 months in advance of the scheduled refueling date.

3.4 NUCLEAR DESIGN AND EVALUATION

This section summarizes the nuclear characteristics of the design and discusses the design parameters which are of significance to the performance of the core in normal transient and steady state operational conditions. A discussion of the nuclear design methods employed and comparisons with experiments which support the use of these methods is included.

The numerical values presented are based on the Cycle 8 core. The anaylsis performed for this fuel cycle shows that all necessary requirements for safe operation have been met. Table 3.4-1 shows a summary of the nuclear design parameters for the fuel cycle. Figures 3.4-1 and 3.4-2 show the assembly average burnup distributions for both the beginning and end of Cycle 8, respectively.

TABLE 3.4-1

NUCLEAR DESIGN PARAMETERS

Performance Characteristics	
Fuel Management	4-Batch, Mixed Central Zone
Average Cycle Burnup, MWD/MTU	9,000
U-235 Enrichment, w/o (initial)	
Type G (29 assemblies)*	3.03
Type H (40 assemblies)	3.50
Type I (32 assemblies)	3.50
Type J (28 assemblies)	3.50
H_2O/UO_2 Volume Ratio, Unit Cell (Cold)	1.66
*High burnup demonstration assemblies	21
Control Characteristics	
k_{eff}, Beginning-of-Cycle, No Control Element Assemblies	
Cold (68°F)	1.20
Hot (532°F), Zero Power	1.15
Hot, Equilibrium Xe, Full Power	1.10
Number of Control Element Assemblies (CEA's)	
Full Length	45
Part Length	4

(continued)

TABLE 3.4-1 (cont'd)

Total CEA Worth, %Δρ	
Beginning-of-Cycle	
Hot Zero Power (532°F)	9.12
End-of-Cycle	
Hot Zero Power (532°F)	9.41
Dissolved Boron	
Dissolved Boron Content for Criticality, ppm, (CEA's withdrawn, BOC))	
Cold (68°F) ARI	916
Hot (532°F), Zero Power, ARO	1256
Hot (572°F), Equilibrium Xe, Full Power, ARO	855
Dissolved Boron Content for Refueling, ppm	1700
Boron Worth, ppm/%Δρ	
Hot (572°F)	97.8
Cold (68°F)	55
Reactivity Coefficients (CEA's Withdrawn)	
Moderator Temperature Coefficient, α_{mod}, Δρ/°F	
Hot, Full Power (572°F)	
Beginning-of-Cycle	-0.85×10^{-4}
End-of-Cycle	-2.40×10^{-4}
Hot Zero Power (532°F)	
Beginning-of-Cycle	$+0.16 \times 10^{-4}$
Fuel Temperature Coefficient, α_{fuel}, Δρ/°F	
Hot, Zero Power (532°F, BOC)	-1.9×10^{-5}
Full Power (1850°F, BOC)	-1.4×10^{-5}
Moderator Void Coefficient, α_{void}, Δρ/% Void	
Hot, Operating (572°F)	
Beginning-of-Cycle	-0.18×10^{-3}
End-of-Cycle	-1.46×10^{-3}
Moderator Pressure Coefficient, α_{ρ}, Δρ/psi	
Hot, Operating, (572°F)	
Beginning-of-Cycle	$+0.4 \times 10^{-6}$
End-of-Cycle	-2.1×10^{-6}

3.4.1 Reactivity and Control Requirements

Tables 3.4-2 lists the effective multiplication factors (k_{eff}) and reactivity (ρ) under various conditions.

TABLE 3.4-2

EFFECTIVE MULTIPLICATION FACTORS AND REACTIVITY UNDER VARIOUS CONDITIONS (NO CONTROL ELEMENT ASSEMBLIES OR DISSOLVED BORON, BEGINNING-OF-CYCLE CYCLE 8 CORE)

	k_{eff}	ρ
Cold (68°F), ARI	1.20	0.167
Hot (532°F), Zero Power	1.15	0.133
Hot, Full Power, Equilibrium Xe, ARO	1.10	0.087

The maximum excess reactivity ρ is 16.7 percent for the cold, unborated core at beginning of cycle. The reactivity decrease from zero to full power is due to the change in fuel temperature which causes Doppler broadening of the U-238 resonances and the change in moderator temperature coefficient which becomes more negative (due to a lower reactor coolant system boron concentration).

Reactivity control in the reactor is accomplished by adjusting both the position of the CEA's and the concentration of boric acid dissolved in the reactor coolant system. The CEA's permit rapid changes in reactivity, as required for reactor trip and to compensate for changes in moderator and fuel temperature and void formation associated with changes in power level. There are 45 standard and four part length CEA's. The standard CEA's are used for shutdown and for regulation. The CEA's designated as shutdown CEA's are divided into two separately controlled groups; those designated as regulating CEA's are divided into four groups. During power operation, the shutdown groups are fully withdrawn while the position of the regulating groups is adjusted to meet reactivity and power distribution requirements. All CEA's except the part length CEA's drop to a fully inserted position upon reactor trip.

Adjustment of the boric acid concentration is used to control the relatively slow reactivity changes associated with plant heatup and cooldown, fuel burnup, and certain xenon variations. Also, additional boric acid is used to provide a large shutdown margin for refueling. The use of boric acid dissolved in the reactor coolant makes it possible to maintain most of the CEA's in a withdrawn position during full power operation, thus minimizing the distortions in power distribution. Table 3.4-3 lists the concentrations of natural boron required to maintain the core critical under various conditions, assuming all control element assemblies are fully withdrawn.

TABLE 3.4-3

DISSOLVED BORON REQUIREMENTS FOR CRITICALITY
(CONTROL ELEMENT ASSEMBLIES FULLY WITHDRAWN, BEGINNING-OF-CYCLE)

	Natural Boron, ppm
Cold (68°F), ARI	916
Hot (532°F), Zero Power, ARO	1256
Hot, Full Power, Equilibrium Xe, ARO	855
Refueling (0.88 k_{eff}), ARI	1700

The boron concentration established for refueling is 1700 ppm. This concentration plus CEA's provides a reactivity shutdown of approximately 15 percent for the cold condition. The refueling concentration is equivalent to 1.0 weight percent boric acid (H_3BO_3) in the coolant which is approximately 10 percent of the solubility limit at refueling temperatures. After a normal shutdown or reactor trip, boric acid may be injected into the reactor coolant system to compensate for reactivity increases due to normal cooldown and xenon decay. Although the boric acid system reduces reactivity relatively slowly, the rate of reduction is more than sufficient to maintain the shutdown margin against the effects of normal cooldown and xenon decay.

Sufficient worth is available in the regulating CEA's to compensate for the rapid changes in reactivity associated with power level changes. In addition, these CEA's may be used for partial control of xenon transients and minor variations in moderator temperature and boron concentration. These requirements are tabulated on Table 3.4-4 for beginning and end-of-cycle conditions and are discussed below. The total worth of all CEA's including shutdown CEA's, covers these requirements and provides adequate shutdown with the most reactive CEA stuck in the fully withdrawn position. Margin is provided between the calculated CEA worth and the total reactivity allowances to account for uncertainties in the calculations; only the 45 full length CEA's are considered in this table.

TABLE 3.4-4

CEA REACTIVITY ALLOWANCES, %Δρ

	BOC		EOC (10,000 MWD/MT)	
Control Rod Worth (% Δρ)	HZP	HFP	HZP	HFP
Total Full Length Rod Worth	9.12	9.12	9.41	9.41
Stuck Rod Worth	2.06	2.06	2.01	2.01
Total Minus Stuck Rod	7.06	7.06	7.40	7.40
Uncertainty (10%)	.71	.71	.74	.74
Net Shutdown Rod Worth (1)	6.35	6.35	6.66	6.66

TABLE 3.4-4 (continued)

CEA REACTIVITY ALLOWANCES, %Δρ

	BOC		EOC (10,000 MWD/MT)	
	HZP	HFP	HZP	HFP
Reactivity Insertion (% Δρ)				
Doppler Defect plus Moderator Temperature Defect	0	1.4	0	2.0
Moderator Void Defect	0	0.1	0	0.1
Axial Flux Redistribution	0	.2	0	.2
Required Shutdown Margin	4.0	4.0	4.0	4.0
Total Reactivity Allowance (2)	4.0	5.7	4.0	6.3
Available for Maneuvering (1)-(2)	2.35	0.65	2.66	.36
PDIL Rod Insertion	1.21	0.19	1.19	0.27
Excess Margin (% Δρ)	1.14	0.46	1.47	.09

3.4.1.1 Doppler Defect and Moderator Temperature Defect

The increase in reactivity associated with the change from full to zero power from both the Doppler effect in U-238 and the moderator temperature effect is 1.4%Δρ at beginning-of-cycle and 2.0%Δρ at end-of-cycle. This change in reactivity is compensated by CEA movement.

3.4.1.2 Axial Flux Redistribution

A change in reactivity occurs due to axial flux redistribution over a cycle as a result of the localized burn-out and redistribution of Xenon. This is conservatively estimated to be 0.2%Δρ.

3.4.1.3 Moderator Voids

A change in reactivity results from the formation of voids due to local boiling. The average void content in this core is very small and is estimated to be one-fourth of 1 percent at full power. As with the moderator temperature effect, the maximum increase in reactivity from full to zero power occurs at end-of-cycle when the least amount of dissolved boron is present. The maximum reactivity variation due to one-fourth of 1 percent voids is conservatively estimated to be 0.1 percent Δρ.

3.4.1.4 CEA Power Dependent Insertion Limit (PDIL)

The PDIL rod insertion is a measure of the rod worth associated with the permissable CEA configurations (see Figure 3.4-3 or Technical Specification Figure 2-4) for both hot zero power and hot full power.

3.4.1.5 Maneuvering Band

An allowance is made in the reactivity worth of the CEA's to compensate for variations in xenon, dissolved boron concentration, and moderator temperature. When the CEA's reach the limits imposed on CEA motion, additional reactivity changes will be made by changing the boron concentration. The allowance made for the maneuvering band is 0.60 percent $\Delta\rho$ at BOC.

3.4.1.6 Shutdown Margin and Safeguards Allowance

An allowance of 4.0 percent $\Delta\rho$ at both the beginning-of-cycle (BOC) and at the end-of-cycle (EOC), respectively, has been made for the shutdown margin and safeguards allowances at hot, zero power conditions with the most reactive CEA stuck in the withdrawn position.

3.4.2 Reactivity Coefficients

The factors which contribute to the reactivity of a reactor, such as the thermal utilization, resonance escape probability, and nonleakage probabilities, are dependent upon certain parameters, such as moderator temperature and pressure and fuel temperature. Reactivity coefficients, denoted by α, relate changes in the core reactivity to variations in these parameters.

3.4.2.1 Moderator Temperature Coefficient

The reactivity worth of 855 ppm of boron (the amount of reactivity needed to maintain the reactor just critical at BOC full power conditions) increases from 8.7%$\Delta\rho$ to 13.3%$\Delta\rho$ as the moderator temperature decreases from operating to zero power temperature. The interaction of these temperature effects (along with the temperature coefficient of the unborated core) results in a net moderator temperature coefficient of reactivity, α_{mod}, at operating temperature which ranges from strongly negative to slightly positive, depending on the moderator temperature, the soluble boron content, and the fuel burnup.

In a core which is controlled by chemical shim dissolved in the moderator, there are two factors which cause the moderator temperature coefficient to become less negative as the fraction of reactivity controlled by the dissolved boron increases (i.e., at higher boron concentrations). First, an increase in moderator temperature reduces the effective density of the chemical poison and hardens the thermal neutron spectrum, thereby decreasing neutron absorption in the boron. Secondly, the effective reactivity worth of a solid poison such as the CEA's increases as the moderator temperature increases; thus, since there are fewer solid poison control elements than would be required in a reactor without chemical shim, the magnitude of this effect is reduced.

The calculated moderator temperature coefficient for various core conditions is given in Table 3.4-5. As shown in the table, the most positive value occurs at the beginning of cycle (HZP) when the dissolved Boron content is at its maximum.

TABLE 3.4-5

MODERATOR TEMPERATURE COEFFICIENTS

Conditions	α_{mod}, $\Delta\rho/°F$
Beginning of Cycle	
Hot, Full Power, CEA's Out	-0.85×10^{-4}
Hot, Zero Power, CEA's Out	-0.16×10^{-4}
End of Cycle	
Hot, Full Power, CEA's Out, Zero ppm	-2.46×10^{-4}

The moderator coefficient becomes more negative with burnup, due mainly to the reduction in the dissolved boron content with burnup. The effects of plutonium and fission products are small when compared to the above; however, the buildup of xenon supplies a positive contribution to the coefficient for a constant boron concentration. Equilibrium xenon raises α_{mod} by $0.05 \times 10^{-4}\rho/°F$. However, when the dissolved boron concentration is reduced by the reactivity equivalent of xenon, the α_{mod} becomes more negative by $0.3 \times 10^{-4}\rho/°F$.

The change in moderator temperature coefficient as a function of boron concentration is linear, being $+0.20 \times 10^{-4}\rho/°F$ per 100 ppm soluble boron.

3.4.2.2 Moderator Pressure Coefficient

The moderator pressure coefficient, $\alpha\rho$, is the change in reactivity per unit change in reactor coolant system pressure. Since an increase in pressure increases the water density, the pressure coefficient is opposite in sign to the temperature coefficient. The reactivity effect of increasing the pressure is reduced in the presence of dissolved boron because an increase in water density adds boron to the core. The calculated pressure coefficients for the beginning and end of the first cycle at full power were $+0.4 \times 10^{-6}$ $\Delta\rho$/psi and $+2.1 \times 10^{-6}$ $\Delta\rho$/psi, respectively.

3.4.2.3 Moderator Void Coefficient

During full power operation, some local boiling occurs resulting in a predicted average void fraction in the moderator of about one-fourth of 1 percent. Changes in reactivity are associated with the appearance of these voids in the moderator and are reflected in the void coefficient of reactivity, α_{void}. The presence of boron has a positive effect on the coefficient since an increase in voids results in a reduction in the boron content in the core. The calculated values at BOC and EOC are -0.18×10^{-3} $\Delta\rho$/% void and -1.46×10^{-3} $\Delta\rho$/% void, respectively.

3.4.2.4 Fuel Temperature Coefficient

The fuel temperature coefficient, α_{fuel} (commonly called the Doppler coefficient), reflects the change of core reactivity with fuel temperature. The effect may be broken into two parts, the thermal and the epithermal (Doppler) contributions. The thermal contribution is due to hardening of the spectrum as

the temperature increases. The epithermal contribution is the temperature dependence of the resonance escape probability, which in turn is physically due to Doppler broadening of the resonances in U-238.

The variation in fuel coefficient over the fuel cycle is small. The hot full power coefficient is -1.41×10^{-5} $\Delta\rho/°F$ at BOC and -1.46×10^{-5} $\Delta\rho/°F$ at EOC.

3.4.2.5 Power Coefficient

The power coefficient, α_{power}, is the change in core reactivity per unit change in core power level. All of the previously mentioned coefficients contribute to the α_{power}, but only the moderator temperature coefficient and the fuel temperature coefficient are significant due to the relative magnitudes. To determine the change in reactivity with power, it is necessary to know the change in the weighted average fuel temperature with power. However, the determination of average fuel pellet temperatures is extremely complex. An "effective fuel temperature" may be defined as that temperature which gives the correct fuel temperature and power coefficients when used in a standard design calculation. The method used is contained in Reference 2. This correlation which is a function of moderator temperature, fuel burnup and local power is incorporated into the standard design calculations.

3.4.3 Control Element Assembly Worths

Figure 3.4-4 is a schematic of one quadrant of the core cross section, showing the location and the groupings of the 45 full length and 4 part length CEA's. The total worth available from the full length CEA's and the worth with the highest worth CEA stuck out are given in Table 3.4-6 for beginning and end-of-cycle.

TABLE 3.4-6

CALCULATED CEA WORTHS, %Δρ (@ 572°F)

	Beginning-of-Cycle	End-of-Cycle
All 45 Standard CEA's Inserted	9.12	9.41
44 CEA's Inserted; Highest Worth CEA Stuck Out	7.06	7.40
Total Reactivity Allowance per Table 3.4-4 Shutdown Plus Uncertainty Plus Margin		

Table 3.4-7 gives the worth of each group of CEA's relative to the full power condition. These worths are from full out to full in. The CEA withdrawal procedure, meeting the minimum requirements of the PDIL as shown in Figure 3.4-3 (also Technical Specification Figure 2-4) is as follows:

a. With the reactor subcritical, Shutdown Group A is fully withdrawn and then Shutdown Group B is withdrawn;

b. Regulating Group 1 is fully withdrawn and Group 2 is withdrawn to at least 34% to take the core critical. Adjustments in dissolved boron concentration are made to maintain Group 2 above the PDIL;

c. Withdrawal of Groups 2 through 4 is made sequentially with the prescribed overlaps and within the specified range until the desired power level and power distribution is achieved.

TABLE 3.4-7

WORTH OF CEA GROUPS, %Δρ (@ 572°F)

When Sequenced as Listed Above	Beginning-of-Cycle*
Shutdown CEA's	
Group A	
Group B	
Regulating CEA's	
Group 1	
Group 2	
Group 3	
Group 4	

* These values will be calculated prior to Cycle 8 startup when all necessary information is available. Omission of these values does not impact this Technical Specification amendment application.

Adherence to the relationship of power to CEA insertion ensures that acceptable peaking factors are maintained within the bounds assumed for the LSSS and LCO shutdown margin is maintained, and that the potential consequences of a CEA ejection accident are limited to acceptable levels. Operation with the CEA's inserted beyond the PDIL is prevented by the rod block system.

3.4.4 Reactivity Insertion Rates

The maximum rate of reactivity insertion of the regulating groups at full power is 0.01%Δρ/sec. Analyses of CEA withdrawal incidents (Section 14.2) show that no core thermal limits would be exceeded for rates considerably in excess of the above values.

The maximum rate of reactivity insertion due to boron removal by operation of the chemical and volume control system is covered by the low end of the CEA insertion rate spectrum. Adequate time is available to take corrective measures as described in the analysis of the boron dilution incident in Section 14.3.

3.4.5 Power Distribution

The power distribution in the core, and in particular the peak heat flux and enthalpy rise, is of major importance in determining core thermal margin. The maximum expected peaking factors for Cycle 8 are 1.53 for F_r and 1.62 for F_{xy}. The corresponding Technical Specification limits for the untilted

values are 1.57 and 1.65. The maximum expected total peaking factor F_Q^T, is 2.17 including uncertainties.

Flux reduction to the vessel was one of the primary goals of the Fuel Management Design. A reduced radial leakage pattern was achieved as shown in Figure 3.4-2. Flux reduction was achieved by placing twice and thrice burned assemblies in quarter core locations 2 and 33 and 3 and 8, respectively. Power flattening was achieved by selective placement of once, twice, and thrice burned assemblies over the inner two-thirds of the core, and by placing the fresh assemblies, with the highest enrichment, in the remaining peripheral locations.

The behavior of the gross radial power distribution in the unrodded core through the eighth burnup cycle is shown in Figures 3.4-5, 3.4-6, and 3.4-7. It is seen that there is a slight trend in which the overall radial power distribution shifts towards the periphery of the core with depletion, reaching a maximum peak around 1000 MWD/MTU and then decreasing with burnup to the end-of-cycle.

CEA's are used to a minimum extent and in configurations that will result in a combined radial and axial peaking factor which is within the design limits stated above.

3.4.5.1 Malpositioned CEA's

The two worst cases of a malpositioned CEA were evaluated with respect to permissible operating modes and current administrative guidelines. The two cases evaluted are:

a. The worst case of a CEA left in the core and

b. Insertion of the CEA bank permissible at full power with one CEA left out.

Worst Case of a CEA Left in the Core

Startup or operation with the most reactive CEA left in the core would result in a large distortion in the radial power distribution and consequently excessive peaking. It is not necessary to analyze this event, because the rod block system will prevent its occurrence. This system prevents rod group motion with one CEA position deviating from the groups position by more than 12 inches. Group motion will stop before the 12 inch deviation limit is reached, preventing leaving one rod in and the rest of the group withdrawn. This limit is referenced in Technical Specification 2.10.2(4). In addition, the CEA position sensing system provides alarms from the synchros for deviations of four and eight inches.

If a CEA was not coupled to the rack and pinion drive system, which could occur after refueling, rack movement could indicate no deviation. This condition is assured not to exist by performing CEA coupling and symmetry checks during startup testing after each refueling outage. This test consists of withdrawing or inserting the CEA and determining its reactivity worth. An uncoupled CEA will have no worth. The adminstrative requirement for performing this test ensures that the CEA's are coupled, eliminating this concern.

Even if a rod was totally inserted with all others withdrawn, the inserted rod would be detected by the incore monitoring system which would cause alarms due to excessive flux peaking in detector locations across the core from the rodded and depressed neutron flux area. A detectable change in flux tilt would also be detected by both the incore and excore detector systems.

Insertion of the CEA Bank Permissible at Full Power With One CEA Left Out

Insertion of Regulating Group 4 with one of the CEA's left out is prevented from occurring by the rod block circuitry. As in the case of leaving one CEA inserted group motion will automatically be stopped and prevented prior to the rod-group deviation exceeding 12 inches. In addition, deviation alarms at four and eight inches provides warning of the asymmetry. Therefore, due to the rod block circuitry preventing the occurrence of this condition, no further analysis is required.

3.4.6 Pressure Vessel Fluence

The design of the reactor internals and of the water annulus between the active core and vessel wall is such that for NSSS operations at 1500 MWt and an 80 percent plant capacity factor, the integrated fast neutron fluence (E>1 MeV) is 4.4×10^{19} nvt over the 40-year design life of the vessel. The fluence was determined using the threshold detector analysis for the surveillance capsule removed at the end of Cycle 3 (Reference 3). The SAND-II and ANISIN computer codes were used to calculate the fast fluence at the reactor vessel clad interface.

The SAND-II computer code is used to calculate a neutron flux spectrum from the measured activities of the flux monitors. SAND-II requires an initial flux spectrum estimate; this is calculated using ANISN. The measured activities must be adjusted before they can be put into SAND-II. The various steps of the procedure are described below.

The measured activities must be decay corrected to reactor shutdown. Before being used by SAND-II, the foil activities must be converted to saturated activity with units of disintegrations per second per target atom (dps/a).

For U^{238} fission product activities, the required SAND input has dimensions of fissions per second per U^{238} atom (fps/a). This is obtained by dividing the saturated activity by the fractional fission yield of the fission product whose activity was measured.

The uranium foil is shielded with cadmium to prevent thermal fissioning in any U-235 impurities. However, the cadmium cover does not prevent fast fissioning in U-235. Therefore, an unshielded uranium foil is included in the flux monitor set. The activity of the unshielded foil can be used to determine the amount of fissioning in the shielded uranium foil casued by U-235. As a result of this calculation, the U-238 fission rate was determined to be 75% of the shielded uranium foil activity.

SAND-II requires an initial estimate of the neutron flux spectrum. This inital estimate was calculated using ANISN, a one-dimensional discrete ordinate code.

The calculated fluence at end of Cycle 3 was 3.4×10^{18} nvt. This fluence was linearly extrapolated to 32 EPFY at 1500 Mwt which gives a fluence of 4.4×10^{19} at end of vessel life.

The SAND-II code will give fluxes that are accurate to within ±10% to ±30% if the errors in the measured activities are within similar limits. The 2-sigma uncertainties in the measured activities were less than ±12%. Therefore, it is estimated that the uncertainty in the measured fluence at the surveillance capsule location is ±20% to ±30%. The extrapolated fluence in the vessel will be slightly higher and is estimated to be ±30%.

3.4.7 Nuclear Evaluation

3.4.7.1 Nuclear Design Methods

The nuclear analysis design package developed for use in the design of low enrichment PWR cores is based on a combination of multigroup spectrum calculations, over which cross sections are appropriately averaged to obtain few group constants, and few group, one- two- and three-dimensional diffusion theory calculations of integral and differential reactivity effects and power distributions. The multigroup calculations include spatial effects in those portions of the neutron energy spectrum where volume homogenization is inappropriate, e.g., the thermal neutron energy range. The majority of the calculations are performed with the aid of computer programs embodying analytical procedures and fundamental nuclear data consistent with the current state-of-the-art.

Current design methods involve the use of Combustion Engineering's design methodology (as outlined in Reference 4).

The Combustion Engineering methodoloy uses the CEPAK code (Reference 6) in generating the cross-sections, PDQ-7 and HARMONY (Reference 7) for x-y power distribution and depletions, and ROCS (Reference 8) for reactivities and three dimensional analyses.

3.4.7.2 Comparisons With Experiments

Reactivity

The Combustion Engineering nuclear design package has been checked against a variety of critical and subcritical experiments. Table 3.4-8 summarizes the properties of the fuel rods employed in the lattices analyzed; Tables 3.4-9 and 3.4-10 summarize certain pertinent characteristics of the lattice and the eigenvalues calculated with the design package.

TABLE 3.4-8

FUEL ROD DESCRIPTION

Laboratory	Clad OD (in.)	Clad Thickness (in.)	Clad Mat.	Fuel Pellet OD (in.)	Fuel Density (gm/cc)	Fuel Enrichment w/o U-235	Fuel Enrichment w/o PuO_2
B&W	0.4755	0.016	SS 304	0.4440	9.46	4.020	0
B&W	0.4748	0.032	Al 6061	0.4054	10.24	2.459	0
Yankee	0.3383	0.0161	SS 304	0.3000	10.18	2.700	0
Winfrith	0.4301	0.01051	SS 304	0.3984	10.44	3.003	0
Brookhaven	0.499	0.02743	SS 304	0.4441	9.30	3.006	0
Bettis	0.453	0.028	Al	0.3830	10.53	1.311	0
Hanford	0.426	0.027	Zr-2	0.372	9.646*	0.22	1.50
Battelle N. W. Westinghouse	0.568	0.030	Zr-4	0.508	9.869*	0.72	2.20

* effective fuel density

TABLE 3.4-9

RESULTS OF ANALYSIS OF CRITICAL AND SUBCRITICAL UO_2 SYSTEMS

	Lattice	w/o U-235	Pitch (in.)	H_2O/UO_2	Boron (ppm)	K_{eff}	Ref
B&W-1273	1	4.020	0.595	1.137	0	0.9998	14
	2	4.020	0.595	1.137	3390	1.0018	14
	3	4.020	0.571	0.956	0	0.9963	14
	4	2.459	0.595	1.371	0	1.0009	14
	5	2.459	0.595	1.371	1675	1.0016	14
B&W-3467	6	2.459	0.644	1.846	0	1.0004	15
	7	2.459	0.644	1.846	864	1.0014	15
	8	2.459	0.644	1.846	1536	0.9997	15
Yankee	9	2.700	0.405	1.048	0	0.9965	16
	10	2.700	0.435	1.405	0	0.9979	16
	11	2.700	0.470	1.853	0	0.9990	16
	12	2.700	0.493	2.166	0	1.0004	17
Winfrith	13 (20°C)	3.003	0.520	1.001	0	0.9987	18
	14 (80°C)	3.003	0.520	1.001	0	0.9977	18
	15	3.003	0.735	3.164	0	1.0009	18
	16	3.003	0.492	0.779	0	0.9992	18
Bettis	17	1.311	0.6133≠	1.429	0	0.9963	19
	18	1.311	0.6133≠	1.429	0	0.9963	19
	19	1.311	0.6133≠	1.429	0	0.9970	19
	20	1.311	0.6504≠	1.781	0	0.9962	19
	21	1.311	0.6504≠	1.781	0	0.9975	19
	22	1.311	0.7110≠	2.401	0	0.9968	19
	23	1.311	0.7110≠	2.401	0	0.9975	19
BNL[(a)]	24	3.006	0.6767≠	1.319	0	0.9997	20
	25	3.006	0.6767≠	1.319	1363	0.9932	20
	26	3.006	0.7163≠	1.632	0	0.9964	20
	27	3.006	0.7163≠	1.632	470	0.9950	20
	28	3.006	0.7163≠	1.632	992	0.9931	20
	29	3.006	0.7163≠	1.632	1345	0.9940	20
	30	3.006	0.7706≠	2.091	0	0.9981	20
	31	3.006	0.7706≠	2.091	1141	0.9931	20
B&W[(a)]	32 (66°F)	4.020	0.595	1.137	0	1.0046	21
	33 (103°F)	4.020	0.595	1.137	0	1.0036	21
	34 (203°F)	4.020	0.595	1.137	0	1.0003	21
	35 (308°F)	4.020	0.595	1.137	0	0.9992	21
	36 (406°F)	4.020	0.595	1.137	0	1.0010	21

≠ Triangular Pitch
(a) Subcritical Measurements

TABLE 3.4-10

RESULTS OF ANALYSIS OF PuO_2-UO_2 FUELED LATTICES

Lattice	w/o U-235	w/o Pu-O_2	Pitch (in.)	H_2O/Fuel	Boron (ppm)	k_{eff}	Ref
Hanford	0.22	1.50	0.55≠	1.099	0	1.0027	22
			0.60≠	1.557	0	1.0056	22
			0.71≠	2.705	0	1.0108	22
			0.80≠	3.788	0	1.0094	22
BNWL	0.72	2.2(1)	0.85≠	1.837	0	1.0056	23
			0.93≠	2.445	0	1.0099	23
WCAP	0.72	2.2(1)	0.69	1.099	0	0.9994	24
			0.75	1.525	0	1.0058	24
			0.69	1.099	261	0.9998	24
			0.9758	3.448	261	1.0122	24
			0.69	1.099	526	1.0005	24
			0.9758	3.448	526	1.0099	24
BNWL	0.72	2.2(2)	0.93≠	2.445	0	1.0112	23
			1.05≠	3.461	0	1.0068	23
BNWL	0.72	2.2(3)	0.85≠	1.837	0	1.0113	23
			0.93≠	2.445	0	1.0123	23
WCAP	0.72	2.2(3)	0.9758	3.448	0	1.0206	23

≠ Triangular Pitch
(1) 7.654 w/o Pu-240 in Pu
(2) 16.54 w/o Pu-240 in Pu
(3) 23.503 w/o Pu-240 in Pu

The average eigenvalue for the critical uranium lattices in Table 3.4-9 (numbers 1 through 23) is 0.9987 ± 0.0019 and for the mixed oxide lattices of Table 3.4-10 the corresponding number is 1.00799 ± .0053. The UO_2 experiments cover a wide range of core dimensions, boron concentrations, temperature, enrichment, water-to-fuel ratios, and clad materials, thus giving confidence in the validity of the design package to predict beginning-of-life fuel properties with an acceptable accuracy. The analysis of the mixed oxided lattices exhibits larger deviations than for the UO_2 lattices; this result is not surprising in view of the limited amount of data compared with UO_2 systems, the relatively large experimental bucklings, and uncertainties in the same.

The rods-out, beginning-of-cycle, cold and hot zero power reactivities of the Obrigheim (Reference 20) and Connecticut Yankee (Reference 21) reactors were also calculated to demonstrate the validity of the model in large multiregion cores.

The results are summarized here:

	Reactor	Temperature	Boron (ppm)	k_{eff}
(a)	Obrigheim	cold	1727	0.9964
		hot	1962	0.9989
(b)	Connecticut Yankee	260°F	2040	1.0025
		560°F	2305	1.0002

Table 3.4-11 summarizes the predicted and measured values of the BOC hot zero power critical boron concentrations, with all-rods-out (ARO), for Cycles 1 through 7. This table shows excellent agreement between the two values for each cycle. In addition, Figure 3.4-8 shows a comparison between the measured and predicted values of the HFP critical boron concentration (ARO) versus fuel burnup. These curves show good agreement.

TABLE 3.4-11

BOC HZP CRITICAL BORON CONCENTRATION (ARO)

Cycle	Predicted C_B (ppm)	Measured C_B (ppm)
1	911	933
2	1248	1240
3	964	996
4	1023	1027
5	1235	1242
6	1230	1230
7	1240	1241

Depletion Calculation

Over 50 spent fuel samples from Yankee Core I were subjected to isotopic and radio-chemical analyses which were performed in the Tracerlab Laboratory at Richmond, California and by the Vallecitos Atomic Laboratory of the General Electric Company (Reference 22). Depletion calculations were performed on the Yankee core for comparison with the above measurements. Figure 3.4-9 compares measured and calculated values of the Pu/U mass ratio versus exposure, and Figure 3.4-10 shows a comparison for the relative isotopic composition of plutonium as a function of fractional U-235 depletion.

The inventory changes for the 74 fuel assemblies from Yankee Core I are compared with measured results (Reference 23) in Table 3.4-12; the calculations were carried out using both one-dimensional and three-dimensional (RZ) representations.

TABLE 3.4-12

INVENTORY CHANGE COMPARISON

	U-235 Dep. (kg)	Total Pu. (kg)	Fiss. Pu. (kg)	Fissile Consumption (g/MWd)
NFS Meas.	171.0±4.7	91.1±1.0	80.27±0.88	0.535±0.028
1-D	170.8	91.0	80.88	0.530
3-D (RZ)	169.0	89.9	79.48	0.528

Doppler and Power Coefficient

The Doppler coefficient of reactivity is due to Doppler broadening of the U-238 resonances with increasing fuel temperature. The power coefficient of reactivity is the change in reactivity associated with the Doppler and moderator coefficients as a function of power. The fuel temperature used to calculate the Doppler coefficient as a function of the core average power level and coolant temperature is determined on the basis of the Reference 2 model. Table 3.4-13 shows a comparison between the predicted and measured power coefficients for Cycles 2 through 7. All of the pairs of measured and predicted values show good agreement.

TABLE 3.4-13

COMPARISON OF PREDICTED AND MEASURED POWER COEFFICIENTS

Cycle	Burnup MWD/MTU	Percent of Rated Power	Critical Boron Concentration	Predicted Power Coefficient ($\Delta\rho$/% Power)	Measured Power Coefficient ($\Delta\rho$/% Power)
2	10877	46(1)	104	-1.70×10^{-4}	-1.95×10^{-4}
3	157	46(1)	720	-1.60×10^{-4}	-1.47×10^{-4}
3	1513	90(1)	535	-1.20×10^{-4}	-1.12×10^{-4}
3	4183	90(1)	309	-1.26×10^{-4}	-1.31×10^{-4}
3	7208	90(1)	62	-1.74×10^{-4}	-1.48×10^{-4}
4	267	92(1)	690	-1.06×10^{-4}	-1.04×10^{-4}
4	4690	94(1)	288	-1.31×10^{-4}	-1.12×10^{-4}
4	8027	95(1)	44	-1.52×10^{-4}	-1.10×10^{-4}
5	426	93(1)	876	-0.65×10^{-4}	-1.05×10^{-4}
5	6815	94(1)	296	-1.33×10^{-4}	-1.25×10^{-4}

TABLE 3.4-13 (continued)

COMPARISON OF PREDICTED AND MEASURED POWER COEFFICIENTS

Cycle	Burnup MWD/MTU	Percent of Rated Power	Critical Boron Concentration	Predicted Power Coefficient ($\Delta\rho$/% Power)	Measured Power Coefficient ($\Delta\rho$/% Power)
6	400	95(1)	848	-1.18×10^{-4}	-1.11×10^{-4}
6	6467	96(2)	307	-1.53×10^{-4}	-1.45×10^{-4}
7	450	96(2)	817	-1.20×10^{-4}	-0.98×10^{-4}
7	6900	95(2)	283	-1.45×10^{-4}	-1.30×10^{-4}
7	7800	95(2)	192	-1.52×10^{-4}	-1.57×10^{-4}

(1) Full Rated Power = 1420 MWt
(2) Full Rated Power = 1500 MWt

Moderator Temperature Coefficient

The moderator temperature coefficient (MTC) for Fort Calhoun has been measured at both BOC and EOC (approximate), for full power conditions, beginning with Cycle 1. Table 3.4-14 summarizes the measurements and predictions which show good agreement for all cycles.

Power Distributions

Comparisons between predicted and measured power distributions using the design methodology of Combustion Engineering are contained in Reference 24.

TABLE 3.4-14

COMPARISON OF PREDICTED AND MEASURED MODERATOR TEMPERATURE COEFFICIENTS

	BOC				EOC			
Cycle	Percent of Rated Power	Critical Boron Concentration (ppm)	Predicted MTC ($\Delta\rho/°F$)	Measured MTC ($\Delta\rho/°F$)	Percent of Rated Power	Critical Boron Concentration (ppm)	Predicted MTC ($\Delta\rho/°F$)	Measured MTC ($\Delta\rho/°F$)
1	-	-	-	-	75(1)	239	-1.02×10^{-4}	-0.98×10^{-4}
2	69(1)	927	-0.27×10^{-4}	-0.28×10^{-4}	46(1)	104	-1.66×10^{-4}	-1.62×10^{-4}
3	46(1)	720	-1.04×10^{-4}	-0.41×10^{-4}	90(1)	62	-2.04×10^{-4}	-1.65×10^{-4}
4	92(1)	690	-0.66×10^{-4}	-0.42×10^{-4}	95(1)	44	-2.16×10^{-4}	-1.41×10^{-4}
5	93(1)	876	-0.64×10^{-4}	-0.19×10^{-4}	94(1)	296	-1.33×10^{-4}	-0.97×10^{-4}
6	95(1)	848	-0.61×10^{-4}	-0.34×10^{-4}	96(2)	307	-1.79×10^{-4}	-1.38×10^{-4}
7	96(2)	817	-0.61×10^{-4}(3)	-0.40×10^{-4}	95(2)(3)	192	$-1-79\times10^{-4}$	-1.79×10^{-4}

(1) Full Rated Power = 1420 MWt
(2) Full Rated Power = 1500 MWt
(3) Predicted

3.4.8 Reactor Stability

Xenon stability analyses on the Fort Calhoun core indicate that any radial and azimuthal xenon oscillations induced in the core will be damped, but that the core could exhibit instabilities with respect to axial xenon oscillations during certain portions of the burnup cycle, in the absence of appropriate control action. Before discussing the methods of analysis employed to obtain these predictions, it is appropriate to reiterate several important aspects of the xenon oscillation problem.

a. The time scale on which the oscillations occur is long, and any induced oscillations typically exhibit a period of 30 to 50 hours;

b. Xenon oscillations are detectable as discussed below;

c. As long as the initial power peak associated with the perturbation initiating the oscillation is acceptable, the operator has time in the order of from hours to days to decide upon and to take appropriate remedial action prior to the time when allowable peaking factors would be exceeded.

3.4.8.1 Method of Analysis

The classic method for assessing spatial xenon oscillations is that developed by Randall and St. John (Reference 25) which consists of expanding small perturbations of the flux and xenon concentrations about equilibrium values in eigenfunctions of the system with equilibrium xenon present. While the Randall-St. John technique is correct only for a uniform unreflected system, its use of the separations between the eigenvalues of the various excited states of the system and the eigenvalue of the fundamental state is helpful in directing attention to which of the various excited states are the most likely to occur. As indicated in Figure 3.4-11, the first axial mode, which has the miniumum eigenvalue separation from fundamental mode, is the most likely to occur, and the higher modes would have, on the basis of this simple theory, the indicated relative likelihoods of occurrence.

However, it is necessary to extend this simpler linear analysis to treat cores which are non-uniform because of fuel zoning, depletion and CEA patterns, for example. Such extensions have been worked out and are reported in Reference 26 and 27. In this extension, the eigenvalue separations between the excited state of interest and the fundamental are computed numerically for symmetrical flux shapes. For nonsymmetrical flux shapes, the eigenvalue separation can usually be obtained indirectly from the dominance ratio $\lambda 1/\lambda 0$, computed during the iteration cycle of the machine spatial calculation.

In making the analysis, numerical space-time calculations are performed in the required number of spatial dimensions for the various modes as checkpoints for the predictions of the extended Randall-St. John treatment described above.

3.4.8.2 Radial Mode Oscillations

From the remote position of the first radial excited eigenvalue in Figure 3.4-11 (over 4 percent in λ), it is expected that such oscillations would be rapidly damped even in a core whose power was flattened for example, by enrichment zoning. To confirm that this mode is extremely stable, a space-time calculation was run for a reflected, zone core 11 feet in diameter without including the damping effects of the negative power coefficient. The initial perturbation was a poison worth 0.4 percent in reactivity placed in the central 20 percent of the core for 1 hour. Following removal of the perturbation, the resulting oscillation was followed in 4-hour time steps for a period of 80 hours. As shown in Figure 3.4-12, the resulting oscillation died out very rapidly with a damping factor of about -0.06 per hour. If this damping coefficient is corrected for a finite time mesh by the formula in Reference 28, it would become even more strongly convergent. On this basis, it is concluded that radial oscillations are highly unlikely.

This conclusion is of particular significance because it means that there is no type of oscillation where the inner portions of the core act independently of the peripheral portions of the core whose behavior is most closely followed by the out-of-core flux detectors. As will be noted later, primary reliance is placed on these for the detection of any xenon oscillations.

3.4.8.3 Azimuthal Mode Oscillations

Azimuthal oscillations in an unreflected uniform reactor are less likely than axial mode oscillations as indicated in Figure 3.4-10. The situation is quite different in a radially power-flattened reflected core even at beginning of cycle, as shown in Figure 3.4-13. Here, the eigenvalue separations for the actual core are predicted by the modified Randall-St. John treatment and include the effects of power flattening. On the basis of this information, it appears that the azimuthal mode is the most easily excited at beginning of life even though the axial mode become the most unstable later.

With reference to Figure 3.4-13, it is indicated that the eigenvalue separation between the first azimuthal harmonic and the fundamental is about 1.2 percent in λ. Although the axial oscillations were found to be relatively insensitive to the moderator temperature feedback because of the constant power condition, the azimuthal modes should be stabilized appreciably by the negative moderator coefficient. Furthermore, the Doppler coefficient applicable to the Fort Calhoun reactor is calculated to be approximately -1.35×10^{-3} $\Delta\rho/kW\text{-}ft^{-1}$, which is more than enough to ensure stability of all the azimuthal modes.

3.4.8.4 Axial Mode Oscillations

As checkpoints for the predictions of the modified Randall-St John approach, numerical spatial time calculations have been performed for the axial case at both beginning and end of cycle. The fuel and poison distributions were obtained by depletion with soluble boron control so that, although the power distribution was strongly flattened, it was still symmetric about the core midplane. Spatial Doppler feedback was included in these calculations. In Figure 3.4-14 the time variation of the thermal neutron flux is shown for two

points along the core axis near end of life with Doppler feedback. The initial perturbation used to excite the oscillations was a 20 percent insertion into the top of the reactor of a 1.5 percent reactivity CEA bank for 1 hour. As is indicated, the damping factor for this case was about +0.02 per hour. When corrected for finite time mesh by the methods of Reference 28, however, the damping factor is approximately +0.05. When this damping factor is plotted on Figure 3.4-13 at the appropriate eigenvalue separation for this mode at end of cycle, it is apparent that good agreement is obtained with the modified Randall-St. John prediction.

At beginning of cyle, the space-time calculations indicated a positive damping coefficient of about +0.04 per hour in the absence of spatial Doppler feedback, and a negative damping coefficient of -0.05 per hour results with a power coefficient of -1.35×10^{-3} $\Delta\rho/kW\text{-}ft^{-1}$. Again, these space-time results are in excellent agreement with the predictions of the modified Randall-St. John technique.

Calculations performed with both Doppler and moderator feedback have resulted in damping factors which were essentially the same as those obtained with Doppler feedback alone. This result suggests that the constant power condition which applies to the axial oscillations results in a very weak moderator feedback since the moderator density is fixed at the top and bottom of the core and only the density distribution in between can change.

For the estimated Doppler coefficient of -1.35×10^{-3} $\Delta\rho/kW\text{-}ft^{-1}$ (see Section 3.4.2.4) it can be seen from Figure 3.4-14 that the damping factor toward end of the cycle burnup is positive; thus within the uncertainties in predicting power coefficients and uncertainties in the analysis, there is a possibility of unstable axial xenon oscillations in the absence of any control action. These oscillations, however, are sufficiently slow, (doubling time of 14 hours with a damping factor of $+0.05\ hr^{-1}$, detected as outlined below), that there would be sufficient time to institute corrective action to damp the oscillations by the movement of the part length CEA's.

3.4.8.5 Detection of Xenon Oscillations

Primary reliance for the detection of any xenon oscillations is placed on the out-of-core flux monitoring instrumentation, one channel of which per quadrant is an axially split ionization detector. As indicated earlier, oscillations in modes such as the radial, which would allow the center of the core to behave independently from the peripheral portions of the core, are highly unlikely and this lends support to reliance on the out-of-core detectors for this purpose. Furthermore, as an example of the ability of the axially split out-of-core detectors to respond to flux tilts in the core. Figure 3.4-15 indicates the ratio of the lower half of the axially split detector signal to the signal from the upper half for two different power distributions; one is axially symmetric, the other contains a strong contribution from the first axial harmonic and has a peaking factor of about 1.8. In the latter case, the signal from the lower half of the detector is 50 percent higher than that from the upper half.

Considering that the primary response of these detectors will be to the power in the peripheral fuel assemblies, but noting that the lower modes of any induced oscillations will affect the power shapes in these peripheral assemblies, it has been concluded that any flux tilts can be observed and identified by the use of out-of-core instrumentation to provide data upon which appropriate remedial action can be based.

The incore or core average flux tilt, Y_I is related to the excore detector flux tilt, Y_E, by the Shape Annealing Factor (SAF) in the following equation.

$$Y_I = SAF * Y_E$$

The SAF is a function of excore detector geometry and was determined during the initial reactor physics testing. The incore detectors (see Section 3.6.1) were utilized to compute the core average flux tilt, the excore detector signals were used to calculate excore flux tilt and the equation was solved for the SAF during a controlled axial xenon oscillation. The core average flux tilt is computed by the incore detectors during normal operation. This value is compared to Y_I computed by the excore detectors on a periodic basis and if the difference between the two exceeds a prescribed limit the split excore detectors are calibrated to assure that the "correct" value of Y_I is calculated.

3.4.8.6 Control of Xenon Oscillations

The split detectors of the power range safety and control channels are used to calculate the Axial Shape Index, ASI, which is defined as the ratio of the difference and sum of the signals from the lower and upper detectors respectively. Three separate limits have been established for allowable ASI as a function of reactor power. These functions allow the axial peaks to increase as reactor power decreases. The first and most restrictive of these limits is the maintenance of the ASI around an Equilibrium Shape Index (ESI). The ESI is defined as the ASI when the core is at a constant power level with an equilibrium xenon concentration and all CEA's removed from the core. The operator is to maintain the ASI within a given band using the Bank 4 CEA's for fuel performance considerations.

The second limit is a Limiting Condition for Operation (LCO) based either on DNBR or peak linear heat generation rate. These limits are shown in Technical Specification Figures 2-6 and 2-7. Since the peak linear heat generation rate is usually monitored by the incore detectors the DNBR LCO, Technical Specification Figure 2-7, defines the ASI limit during normal operation. The Technical Specifications state that if the ASI exceeds the DNBR LCO, it is to be restored to within the limits in two hours or take the reactor to less than 15% of rated power in the next eight hours. The operator is to utilize the Bank 4 CEA's to maintain the ASI within limits.

The last and least restrictive limit on ASI as a function of power is the Reactor Protective System Axial Power Distribution protection channels. Each independent channel compares the observed ASI with the ASI limit. A trip is initiated on two out of four logic if the ASI exceeds the limit. The limit is given in Technical Specification Figure 1-2. The limit is derived through consideration of the DNBR and the peak linear heat generation rate for various ASI's.

3.4.8.7 Xenon Oscillation Operating Experience

Section 3.4.8.4 discusses the theoretical possibility of unstable axial xenon oscillations in the absence of any control action. During the operation of the Fort Calhoun Station from August, 1973 through December, 1981, no unstable axial xenon oscillations have been observed. Near end of cycle stable axial xenon oscillations with slightly positive damping factors have been observed. Half cycle damping techniques utilizing Bank 4 CEA's have been successfully utilized to control these oscillations.

3.5 THERMAL AND HYDRAULIC DESIGN AND EVALUATION OF SELECTED TRANSIENTS

The thermal and hydraulic design of the reactor has as its primary objective the assurance that the core can meet normal steady state and transient performance requirements without exceeding thermal and hydraulic design limits. This section shall discuss the thermal and hydraulic characteristics that relate those transients that were analyzed when the core power rating was changed from 1420 Mwth to 1500 Mwth. The transients included in this analysis can be found in Section 14 and are as follows:

14.6	Loss of Coolant Flow - 2 pump coastdown - 4 pump coastdown
14.9	Loss of Load
14.10	Malfunctions of the Feedwater System
14.11	Excess Load

The thermal and hydraulic design is based on a limiting minimum departure from nucleate boiling ratio of 1.3 as calculated using the W-3 correlation. To ensure that this limit is not exceeded, the reactor protective system is designed to trip the reactor before this condition can be achieved.

This section also discusses the fuel pellet performance characteristics that relate the reactor performance to the margin to design limits. The fuel pellet performance design limit ensures that fuel pellet centerline melt does not occur. The fuel centerline melt design criterion is based on maintaining the peak linear heat rate below a prescribed limit of 21 kw/ft. To ensure that this limit is not exceeded, the reactor protective system is designed to trip the reactor before this condition can be achieved.

A summary of thermal and hydraulic parameters is presented in Table 3.5-1.

TABLE 3.5-1

THERMAL AND HYDRAULIC PARAMETERS

General Characteristics at Full Power

Total Heat Output, MWt	1500
Btu/hr	5120×10^6
Heat Generated in Fuel, Fraction	0.975
Pressurizer Pressure	
Nominal, psia	2,100
Minimum in Steady State, psia	2,075
Maximum in Steady State, psia	2,150

TABLE 3.5-1- (Continued)

General Characteristics at Full Power (Continued)

Nominal Coolant Inlet Temperature, °F	545
Design Inlet Temperature, Steady State, °F	547
Nominal Vessel Outlet Temperature, °F	596.5
Nominal Core Bulk Outlet Temperature, °F	599.5
Total Reactor Coolant Flow, lb/hr	71.7×10^6
Coolant Flow Through Core, lb/hr	68.5×10^6
Hydraulic Diameter Nominal Channel, ft	0.0436
Average Mass Velocity, lb/hr-ft^2	2.16×10^6
Average Coolant Velocity In-Core, ft/sec	12.7
Core Average Heat Flux, Btu/hr-ft^2	177,530
Total Heat Transfer Area, ft^2	28,840
Average Linear Heat Rate of Rod, kW/ft	6.01
Design Overpower, %	112
Average Core Enthalpy Rise, 100% Power, Btu/lb	72.6

Limiting Assembly Peaking

Engineering Heat Flux Factor	1.03
Planar Radial Peaking Factor	1.60
Axial Peaking Factor	1.52
Total Nuclear Peaking Factor	2.50

Enthalpy Rise Factors, Nominal Coolant Conditions, Hot Channel

Heat Input Factors	
Engineering Factor on Hot Channel Heat Input	1.03
Flow Factors	
Inlet Plenum Maldistribution	1.05
Total Flow Factor	1.05

3.5.1 Plant Parameter Variations

Normal reactor operation includes both the nominal steady state design conditions and variations from these conditions during expected operating transients. Instrument and control errors are taken into account in the analysis of transients by setting the initial conditions at the most adverse values within the steady state operating envelope. Delays between parameter changes, trip signals and initiation of CEA movement are made a part of the transient calculations. Values of plant parameters are shown in Table 3.5-2 for the nominal, steady state design and reactor trip conditions.

TABLE 3.5-2

PLANT PARAMETERS FOR THERMAL AND HYDRAULIC DESIGN, STEADY STATE

	Nominal	Design (Steady State)	Reactor Trip Condition
Pressure, psia	2100	2150 Max 2075 Min	2400 Max 1750 Min
Vessel Inlet Temperature, F	545	547	--
Vessel Outlet Temperature, F	596.5	598.5	--
Flow Rate, lb/hr x 10^6	71.7	71.7	66.7 Min
Reactor Power, %	100	100	112 Max

The plant parameters for reactor trip conditions as shown in Table 3.5-2 are based on the automatic protection set point being at the adverse value while the other plant parameters are at the nominal value. The maximum overpressure trip setpoint is 2400 psia. The minimum pressure at which a thermal margin trip will be actuated is 1750 psia. The maximum vessel outlet temperature when an overpower trip occurs (at 112 percent power), is 605°F for an inlet temperature of 547°F. The minimum flow rate at which a low flow trip occurs is 93 percent and the maximum overpower trip setpoint is 112 percent. All of the above trip setpoints are discussed in more detail in Section 7.2.

3.5.2 Hot Channel Factors

3.5.2.1 Description of Hot Channel Factors

The heat flux hot channel factor is the ratio of maximum heat flux in the core to the average heat flux, and the enthalpy rise hot channel factor is the ratio of enthalpy rise in the hot channel to the core average enthalpy rise. Each of these factors is customarily divided into subfactors to account for specific physical effects. A subfactor is identified as a nuclear or as an engineering factor.

Engineering factors account for physical differences between the hot channel and a nominal channel, other than those differences due to nuclear effects. The engineering hot channel factors can be further classified as statistical or nonstatistical factors. Statistical factors are those that result from the effects of manufacturing tolerances on heat flux or enthalpy rise. They are termed statistical factors because manufacturing tolerances are randomly distributed about a mean value. It is assumed that the functional combination of tolerance data into a subfactor results in a normally distributed value for the subfactor. This assumption is reasonable for the small tolerance deviations in fuel assemblies. Nonstatistical engineering factors are those that are due to known physical effects that can be measured or calculated.

Nuclear Power Factor

The nuclear heat flux factor relates the peak heat flux in the core to the core average heat flux. It is the maximum value of the product of the nuclear enthalpy factor, the rod-to-channel factor and the axial peaking factor. A design value of 2.50 is established for this factor. The core average heat flux is reduced by 2-½ percent from that obtained from total core power and total core heat transfer area to account for heat generated in the moderator.

Engineering Heat Flux Factor

The effect on local heat flux of deviations from nominal design dimensions and specifications is accounted for by the engineering heat flux factor. Design variables that contribute to this factor are fuel density, fuel enrichment, pellet diameter, and clad outside diameter. These variables may be combined statistically to obtain the engineering heat flux factor. A design value of 1.03 is used for the engineering heat flux factor.

Engineering Enthalpy Rise Factor

The engineering enthalpy rise factor accounts for the effects of deviations in fuel fabrication from nominal dimensions or specifications on the enthalpy rise in the hot channel. Tolerance deviations (averaged over the length of the four fuel rods that enclose the hot channel) for fuel density, fuel enrichment, pellet diameter, and clad outside diameter, contribute to this factor.

The engineering enthalpy rise factor accounts for increased heat input resulting from higher-than-nominal U-235 content. Because of the difficulty in evaluating average pellet tolerance variations for groups of four fuel rods, the enthalpy rise factor is conservatively assumed to be equal to the engineering heat flux factor.

Inlet Flow Distribution Factor

The inlet flow distribution factor accounts for the effects of nonuniform flow at the core inlet on the hot channel enthalpy rise. The latest hydraulic analysis was based on a value of 1.05. This value is conservative with respect to the value of 1.03 which was derived from flow model tests using a one-fourth scale model of the reactor. Details of the flow model program are given in section 1.4.6.

The evaluation of the core thermal-hydraulic performances was based on the minimum flow to the highest powered assembly. This, in effect reduces the flow in the hot region of the core by 5% and increases the flow to the cold region of the core by 5%.

3.5.2.2 Summary of Hot Channel Factors

Table 3.5-3 presents a summary of the hot channel factors for nominal, design, and hot channel conditions.

TABLE 3.5-3

SUMMARY OF HOT CHANNEL FACTORS

Heat Flux Factors	Nominal	Design	Hot Channel
Nuclear Heat Flux Factor	2.43	2.50	2.50
Engineering Heat Flux Factor	1.0	1.0	1.03
Total Heat Flux Factor	2.43	2.50	2.58

TABLE 3.5-3 (Continued)

SUMMARY OF HOT CHANNEL FACTORS

	Nominal	Design	Hot Channel
Enthalpy Rise Factor			
Engineering Enthalpy Rise Factor	1.0	1.0	1.03
Inlet Flow Distribution Factor	1.05	1.05	1.05
Total Enthalpy Rise Factor at Nominal Conditions	1.05	1.05	1.08

3.5.3 Coolant Flow

3.5.3.1 Total Coolant Flow Rate and Bypass Flow

The minimum total coolant flow rate at full power is 71.7 x 10^6 lb/hr. The coolant flow path can be traced in Figure 3.1-1. Coolant enters the four inlet nozzles and flows into the annular plenum between the reactor vessel and the core support barrel. It then flows down on both sides of the thermal shield and through the flow skirt to the plenum below the core lower support structure. Pressure losses in the skirt and lower support structure help to even out the inlet flow distribution to the core. The coolant passes through the openings in the lower core plate and flows axially upward through the fuel assemblies. A portion flows through the lower core plate and into the guide tubes in the fuel assemblies. Flow limiting devices have been incorporated in the guide tubes of fuel assemblies without CEA's to limit bypass flow when these fuel assemblies are placed under spare CEA locations. After passing through the core, the coolant flows into the region outside the control element assembly shrouds. From this region the coolant flows across the control element assembly shrouds and passes out through the outlet sleeves on the core barrel to the outlet nozzles.

The principal core bypass routes are direct inlet-to-outlet coolant flow at the joint between the core support barrel sleeve and the outlet nozzle and the flow in the reflector region in excess of that required for cooling. The design limits the total guide tube flow and core bypass to a maximum of 3.2 x 10^6 lb/hr, yielding a core flow rate of 68.5 x 10^6 lb/hr. Some internal leakage occurs within the core and is included in the 68.5 x 10^6 lb/hr flow rate.

The coolant required to cool the control elements flows in the annulus between the control element and the guide tube and then into the region outside the control element assembly shrouds. A similar but smaller leakage will occur at the upper end of those guide tubes without control elements.

3.5.3.2 Pressure Drop

At the design flow rate of 71.7 x 10^6 lb per hour and an inlet temperature of 534.6°F, the best estimate of irrecoverable pressure loss from inlet to outlet nozzles is 23.4 psi. Table 3.5-4 is a tabulation of the pressure drops and velocities for various segments along the inlet-to-outlet nozzle flow path.

These individual pressure drops were obtained using measured loss coefficients from the one-fourth scale airflow model of the Fort Calhoun reactor with appropriate Reynolds number corrections where necessary (see Section 1.4.6). The upper limit overall pressure drop, considering experimental uncertainties and adverse tolerances in the as-built reactor, is 29.1 psi for design flow rate and design inlet temperature of 547°F.

TABLE 3.5-4

REACTOR PRESSURE DROPS

	Velocity (ft/sec)		Pressure Drop (psi)
Inlet Nozzle and 90° Turn	33.2		4.3
Thermal Shield	24.2		2.1
Lower Plenum	11.8		4.4
Core	12.7		7.0
Core Outlet to Outlet Nozzle	40.7		5.6
		Total	23.4

3.5.3.3 Partial Flow Loop Operations

There are two steam generators and four reactor coolant pumps which give rise to six possible configurations for operation. At present the Fort Calhoun Nuclear Power Station is only licensed for the normal four pump configuration. In the future, the unit may be licensed for part loop pump configurations.

3.5.4 Subchannel MDNBR Analysis

The basic aims of the subchannel analysis are to evaluate the enthalpy rise in the MDNBR limiting subchannel and to predict the available margin to conditioning which would result in a departure from nucleate boiling (DNB). The subchannel MDNBR analysis resembles the core flow analysis in considering the lateral mixing of coolant between subchannels which results from diversion cross-flow and turbulent mixing. Such flow mixing between adjacent subchannels reduces the radial enthalpy gradient across the assembly.

In addition to the flow penalties due to differences in assembly pressure loss coefficients, the subchannel thermal analysis considers the effects of hot channel factors for heat flux and enthalpy, factors which arise from nuclear effects and engineering uncertainties. The individual factors included in the subchannel analysis are:

- Fuel fabrication tolerance (on rod pitch, and rod diameter) which can result in reduced subchannel flow.

- Fuel fabrication tolerances on pellet diameter, density, and enrichment which account for the variation in the quantity of fissionable material in the fuel pellet.

- Inlet flow maldistribution which results in reduction in flow to the hot assembly.

- Flow mixing which accounts for momentum and enthalpy interchange between parallel and laterally open subchannels.

- Heat flux penalties resulting from fuel densification, i.e., increase in linear heat generation rate due to a decrease in active fuel rod length.

The W-3 DNB correlation, with correction factors for both unheated subchannel boundaries and a nonuniform axial heat flux profile (30), was used to predict the margin to DNB. Reference 36 provides a detailed justification for using the W-3 correlation. Local subchannel fluid conditions are predicted with the XCOBRA-IIIC (32) computer code.

3.5.5 Departure From Nucleate Boiling

3.5.5.1 Design Approach to Departure From Nucleate Boiling

The margin to departure from nucleate boiling (DNB) at any point in the core is expressed in terms of the departure from nucleate boiling ratio (DNBR). The DNBR is defined as the ratio of the heat flux required to produce departure from nucleate boiling at specific local coolant conditions to the actual local heat flux. At some point in the core the DNBR is a minimum and it is at this point that the margin to DNB for the core is evaluated. The following items are important in determining the core margin to DNB:

a. The coolant inlet conditions;

b. The power level;

c. The nuclear power distribution;

d. The analytical methods utilized to predict local coolant conditions;

e. The correlation used to predict DNB heat flux.

The conventional approach for evaluating the margin to DNB concentrates on the most limiting location in the core and does not consider the DNBR of the core taken as a whole. Alternatively, typical distributions of DNBR for a larger group of channels can be calculated to show the number of rods which may approach the DNB limit.

Because of the uncertainties associated with predicting DNB there is a finite probability that if a channel is operated at a specified DNB ratio greater than one based on a particular correlation, it will be at or above its DNB heat flux. Therefore, the proper interpretation of DNB ratio is that it is a measure of the probability that DNB would occur in the particular design situation to which the DNB correlation is applied. This interpretation assumes, of course, that all operating parameters are known precisely and that the probability being evaluated is only that associated with the correlation. It is customary to establish the relationship between DNB ratio and probability of DNB by statistically evaluating

the scatter between actual values of DNB heat flux, as measured experimentally for many test geometries and operating conditions, and the corresponding values that are predicted by the correlation. Uncertainties associated with prediction of the operating conditions in the channel are subject to separate statistical interpretation. The approach used in design is to select core operating conditions and analytical methods in such a way that there is a very small probability that the actual hot channel coolant conditions are more severe than the calculated conditions used as input to the DNB correlation.

The W-3 DNB correlation presented in Reference 1 is used for the Fort Calhoun design. The probability that the DNB heat flux has been exceeded for several values of the DNB ratio, according to Reference 33 is shown in Table 3.5-5.

TABLE 3.5-5

PROBABILITY DISTRIBUTION, DNB LIMITS

DNB Ratio	Probability That DNB Heat Flux Has Been Exceeded
2.5	0.0000085
2.0	0.00018
1.75	0.001
1.50	0.01
1.30	0.05

3.5.6 Thermal and Hydraulic Evaluation

3.5.6.1 Analytical Models

The XCOBRA-IIIC (Reference 32) computer program provides both steady state and transient calculation capabilities while including the effects of cross flow mixing between fuel assemblies. XCOBRA computes flow and enthalpy distributions on a subchannel basis. For subchannel analysis the "hot" channel and its nearest neighbors are modeled explicitly. The balance of the "hot" assembly is "lumped" as one channel, and the balance of the symmetric section of the core is represented by a single "lumped" channel. Each channel is then axially nodalized for more detail.

For core flow distribution analysis, the core is nodalized such that each radial node represents no more than one fuel assembly and each assembly is represented by multiple axial nodes. In this way the calculations of the core flow distribution include: (1) differences in assembly hydraulic resistance, (2) localized flow leakage in assemblies, and (3) crossflow between the hot assembly and its neighbors.

3.5.6.2 Statistical Analysis of Hot Channel Factors

Random variations from nominal values in enrichment, pellet density, pellet diameter, and clad diameter affect the hot channel factors for heat flux. Hot channel heat input and rod diameter contribute to the flow factor. Estimation of these factors is based on inspection data on "as-manufactured" fuel assemblies.

The factors contributing to the engineering heat flux factor are pellet density, pellet diameter, pellet enrichment and clad diameter. The design value is 1.03. For conservatism, the hot channel heat input factor is set equal to the same value.

3.6 THERMAL AND HYDRAULIC DESIGN EVALUATION FOR LIMITING TRANSIENTS AND SETPOINT ANALYSIS

3.6.1 General

The thermal and hydraulic design of the reactor has as its primary objective the assurance that the core can meet normal steady state and transient performance requirements without exceeding thermal and hydraulic design limits. This section, therefore, discusses the thermal and hydraulic characteristics that relate reactor performance to the margin to design limits.

Several transients were not re-analyzed for Cycle 8 because their present analyses bound the Cycle 8 core performance (Section 3.5). The criteria of this section was applied to the Cycle 8 setpoint analysis and the following transients:

14.2	CEA Withdrawal Incident
14.4	CEA Drop
14.6	Loss of Coolant Flow -Seized Rotor
14.22	RCS Depressurization

The thermal and hydraulic design is based on a limiting minimum departure from nucleate boiling ratio of 1.19 as calculated using the CE-1 correlation. To ensure that this limit is not exceeded the reactor protective system is designed to trip the reactor before this condition can be achieved.

This section also discusses the fuel pellet performance characteristics that relate the reactor performance to the margin to design limits. The fuel pellet performance design limit ensures that fuel pellet centerline melt does not occur. The fuel centerline melt design criterion is based on maintaining the peak linear heat rate below prescribed limit of 21 Kw/ft. To ensure that this limit is not exceeded, the reactor protective system is designed to trip the reactor before this condition can be achieved.

A summary of thermal and hydraulic parameters is presented in Table 3.6-1.

TABLE 3.6-1

THERMAL AND HYDRAULIC PARAMETERS

General Characteristics at Full Power

Total Heat Output, MWt	1500
Btu/hr	5120×10^6
Heat Generated in Fuel, Fraction	0.975
Pressurizer Pressure	
Nominal, psia	2,100
Minimum in Steady State, psia	2,075
Maximum in Steady State, psia	2,150
Nominal Coolant Inlet Temperature, °F	545
Design Inlet Temperature, Steady State, °F	547
Nominal Vessel Outlet Temperature, °F	596.5
Nominal Core Bulk Outlet Temperature, °F	599.5
Total Reactor Coolant Flow, lb/hr	74.4×10^6
Coolant Flow Through Core, lb/hr	71.1×10^6
Hydraulic Diameter Nominal Channel, ft	0.0439
Average Mass Velocity, lb/hr-ft^2	2.179×10^6
Average Coolant Velocity In-Core, ft/sec	13.3
Core Average Heat Flux, Btu/hr-ft^2	177,367
Total Heat Transfer Area, ft^2	28,863
Average Linear Heat Rate of Rod, kW/ft	6.01
Design Overpower, %	112
Average Core Enthalpy Rise, 100% Power, Btu/lb	72.01

3.6.2 Coolant Flow

3.6.2.1 Total Coolant Flow Rate and Bypass Flow

The minimum total coolant flow rate at full power is 74.4 10^6 lb/hr. The coolant flow path can be traced in Figure 3.1-1. Coolant enters the four inlet nozzles and flows into the annular plenum between the reactor vessel and the core support barrel. It then flows down on both sides of the thermal shield and through the flow skirt to the plenum below the core lower support structure. Pressure losses in the skirt and lower support structure help to even out the inlet flow distribution to the core. The coolant passes through the openings in the lower flow plate and flows axially upward through the fuel assemblies. A portion flows through the lower core plate and into the guide tubes in the fuel assemblies. Flow limiting devices have been placed in the guide tubes of fuel assemblies located under spare CEDM locations to prevent asymmetric bypass flows. After passing through the core, the coolant flows into the region outside the control element shrouds. From this region the coolant flows across the control element assembly shrouds and passes out through the outlet sleeves on the core barrel to the outlet nozzles.

The principal core bypass routes are direct inlet-to-outlet coolant flow at the joint between the core support barrel sleeve and the outlet nozzle and the flow in the reflector region in excess of that required for cooling. The design limits the total guide tube low and core bypass to a maximum of 3.3 10^6 lb/hr, yielding a core flow rate of 71.1 10^6 lb/hr. Some internal leakage occurs within the core and is included in the 71.1×10^6 lb/hr flow rate.

The coolant required to cool the control elements flows in the annulus between the control element and the guide tube and then into the region outside the control element assembly shrouds. A similar but smaller leakage will occur at the upper end of those guide tubes without control elements.

3.6.2.2 Inlet Flow Distribution

The inlet flow distribution in conjunction with the core exit pressure distribution accounts for the effects of non-uniform flow on the enthalphy rise. The inlet flow distribution was derived from a series of air flow tests on a .243 scale model of the Fort Calhoun Unit No. 1 reactor (Section 1.4.6). The results were modified to account for the density differences between air and water. Separate distributions were generated for four pump and several of the three pump distributions. These distributions are input directly into the hydraulics code used to model the core.

3.6.2.3 Exit Pressure Distribution

The exit pressure distributions were derived in conjunction with the inlet flow distribution. For each inlet flow distribution there is a corresponding exit pressure distribution. They are also input directly into the hydraulic code. The exit pressures allow the code to more accurately predict the delta pressure across each assembly. This in turn leads to more accurate modeling of the enthalphy rise in each assembly.

3.6.2.4 Partial Flow Loop Operations

There are two steam generators and four reactor coolant pumps which give rise to six possible configurations of operation. At present the Fort Calhoun Nuclear Station is only licensed for the normal four-pump configurations. In the future, the unit may be licensed for part loop pump configurations.

One three pump configuration was analyzed. This analysis assumed flow in three loops and no flow (forward or reverse) in the fourth loop. Inlet flow distribution and its associated exit pressure for the three pump configuration served as input to the thermal-hydraulics code. The results were then used to evaluate the Seized Rotor Incident (Section 14.6) and its impact on thermal margin degradation.

3.6.3 Peak Linear Heat Rate

The peak linear heat rate (PLHR), in the limiting fuel pin in the core shall not exceed that corresponding to the onset of fuel centerline melt. This fuel melt limit was calculated by GAPEX (29) to be 21 Kw/ft.

The parameters affecting this fuel design limit are as follows:

- Core Power;
- Axial Power Distribution;
- Radial Power Distribution;
- Azimuthal Tilt Magnitudes

3.6.4 Peak Linear Heat Rate Protection

The axial power distribution (APD) trip is provided to ensure that excessive axial peaking will not cause fuel damage. The APD trip performs the following two functions:

- It provides a reactor trip before the peak kw/ft exceeds that value corresponding to the centerline melting temperature of the fuel (21 kw/ft), by working in combination with the variable high power trip, rod block system and the LCO's shown in Figure 3.5-1.

- It provides a reactor trip before the axial power distribution becomes more severe than that assumed to exist by the thermal margin/low pressure trip.

The maximum radial power peak that can occur for power levels up to the variable high power trip limit (in the event of a design basis AOO) is factored into the axial power distribution LSSS. The radial power peak that is allowed at any steady-state or transient core power is specified through the Power Dependent Insertion Limit (PDIL). The rod block system assures that no single electrical component failure in the control element drive system (other than a dropped CEA) can result in CEA group insertion in violation of the PDIL. The rod block system also controls CEA group sequencing, deviation and overlap. A penalty is factored into the LSSS to allow the existence of a 3% azimuthal tilt in core power.

3.6.5 Thermal Margin Analysis

The basic objective of thermal margin analysis is to identify the combinations of steady state operating conditions which satisfy the Specified Acceptable Fuel Design Limit on minimum DNBR. To meet this objective, calculations are performed over a range of operating parameters to determine the power levels that would be required to reach the DNBR design limit. The ranges of these operating parameters are as follows:

• Inlet Temperature, deg. F	465-580
• System Pressure, psia	1750-2400
• Core Flow Rate, % LCO	80-120
• Core Power, % Rated	70-150
• Axial Power Distribution	-.500 to .500 ASI

These calculated powers to DNB or overpower margins are represented in curves which are used to assess and quantify available thermal margin. These curves, which constitute the Thermal Margin information, provide the upper limits on core power over the specified range of operating conditions. This information is used to establish the DNB related Limiting Safety System Settings (LSSS) (Figure 3.6-1) and Limiting Conditions for Operation (LCO) (Figure 3.6-2).

3.6.5.1 Engineering Factors

Engineering Heat Flux Factor

The effect on local heat flux of deviations from nominal design dimensions and specifications is accounted for by the engineering heat flux factor. Design variables that contribute to this factor are fuel density, fuel enrichment, pellet diameter, and clad outside diameter. These variables may be combined statistically to obtain the engineering heat flux factor. A design value of 1.03 is used for the engineering heat flux factor.

Engineering Enthalpy Rise Factor

The engineering enthalpy rise factor accounst for the effects of deviations in fuel fabrication from nominal dimensions or specifications on the enthalpy rise in the hot channel. Tolerance deviations (averaged over the length of the four fuel rods that enclose the hot channel) for fuel density, fuel enrichment, pellet diameter, and clad outside diameter, contribute to this factor.

The engineering enthalpy rise factor accounts for increased heat input resulting from higher-than-nominal U-235 content. Because of the difficulty in evaluatig average pellet tolerance variations for groups of four fuel rods, the enthalpy rise factor is conservatively assumed to be equal to the engineering heat flux factor.

Fuel Rod Bowing Effects

Fuel rod bowing effects on DNB margin for Fort Calhoun Unit 1 have been evaluated with the guidelines set forth in Reference 76.

A total of 70 fuel assemblies will exceed the NRC-specified DNB penalty threshold burnup of 24,000 MWD/T, as established in Reference 76, during Cycle 8. At the end of Cycle 8, the maximum burnup attained by any of these assemblies will be 40,880 MWD/T. From Reference 76 the corresponding DNB penalty for 40,880 MWD/T is 6.0 percent.

An examination of power distributions for Cycle 8 shows that the maximum radial peak at HFP in any of the assemblies that eventually exceed 24,000 MWD/T is at least ten percent less than the maximum radial peak in the entire core. Since the percent increase in DNBR has been confirmed to be never less than the percent decrease in radial peak, there exists at least ten percent DNB margin for assemblies exceeding 24,000 MWD/T relative to the DNB limits established by other assemblies in the core. This margin is considerably greater than the Reference reduction penalty of 6.0 percent imposed upon fuel assemblies exceeding 24,000 MWD/T in Cycle 8. Therefore, no penalty is needed on core power.

3.6.6 Departure From Nucleate Boiling

The margin to departure from nucleate boiling (DNB) at any point in the core is expressed in terms of the departure from nucleate boiling ratio (DNBR). The DNBR is defined as the ratio of the heat flux required to produce departure from nucleate boiling at specific local coolant conditions to the actual local heat flux. At some point in the core the DNBR is a minimum and it is at this point that the margin to DNB for the core is evaluated.

Because of the uncertainties associated with predicting DNB there is a finite probability that if a channel is operated at a specified DNB ratio greater than one based on a particular correlation, it will be at or above its DNB heat flux. Therefore, the proper interpretation of DNB ratio is that it is a measure of the probability that DNB would occur in the particular design situation to which the DNB correlation is applied. It is customary to establish the relationship between DNB ratio and probability of DNB by statistically evaluating the scatter between actual values of DNB heat flux, as measured experimentally for

many test geometries and operating conditions, and the corresponding values that are predicted by the correlation. Uncertainties associated with prediction of the operating conditions in the channel are subject to separate statistical interpretation. The approach used in design is to select core operating conditions and analytical methods in such a way that there is a very small probability that the actual hot channel coolant conditions are more severe than the calculated conditions used as input to the DNB correlation.

The CE-1 DNB correlation presented in References 63 and 64 is used for the Fort Calhoun design. The probability that the DNB heat flux has been exceeded for several values of the DNB ratio, according to Reference 65 is shown in Table 3.6-2. The CE-1 DNBR design limit was chosen such that a minimum DNBR of 1.19 will provide a 95% probability with 95% confidence of not experiencing critical heat flux on a hot rod.

TABLE 3.6-2

PROBABILITY DISTRIBUTION, DNB LIMITS

DNB Ratio	Probability That DNB Heat Flux Has Been Exceeded
1.44	.0001
1.22	.025
1.19	.050

3.6.7 Vapor Fraction

The high operating pressure of the reactor minimizes vapor formation. A calculation, assuming 2 percent overpower, maximum inlet temperature and design coolant flow rate, shows the core vapor fraction is less than 0.1 percent. A conservative value of 0.25 percent is assumed in assessing the effect of voids on reactivity (Section 3.4.1.3).

To avoid the possibility of departure from nucleate boiling as the result of local flow oscillations, a conservative limit has been established to prevent flow instabilities. The limits to assure stable flow are based on avoiding flow regime changes in the hot channel that could affect the flow-pressure drop characteristics so as to cause an instability. Figure 3.5-3 shows flow regimes and regions of stable flow as a function of local mass flow rate and void fraction based on the data in Reference 34.

An automatic reactor shutdown (thermal margin trip) will occur before the flow instability limit is reached; thus departure from nucleate boiling resulting from flow oscillations is prevented.

3.6.8 Thermal and Hydraulic Evaluation

Steady state DNBR analyses were performed using the TORC computer code (Reference 66), the CE-1 critical heat flux correlation (Reference 63-64), and the CETOP modeling and tuning methodology (References 67, 68). CETOP was used to develop the thermal margin model used for the DNBR analysis (Reference 69). Additional discussions of CETOP methodology are contained in the Arkansas

Nuclear One Unit 2 (ANO-2) docket in Reference 70 and on the Calvert Cliffs docket in Reference 71. CETOP was approved for use on ANO-2 and on Calvert Cliffs (References 72 and 73). CETOP differs from TORC in that enthalphy transport coefficients are used to improve modeling of coolant conditions in the vicinity of the hot subchannel and in that more rapid equation-solving routines are used. CETOP models are tuned to always give conservative MDNBR results relative to detailed TORC. CETOP is used only because it reduces computer costs signficantly; no margin gain is realized.

DTORC

The DTORC (66) thermal hydraulics computer code solves conservation equations for a 3-dimensional representation of the open lattice core to determine local coolant conditions at all points within the core. The code performs these calculations in three separate stages with the output of the previous stage coupled to the next stage. This type of model permits greater accuracy in predicting localized conditions.

D-TORC better represents assembly flow interactions. This is partly due to the explicit inlet flow (3.6.2.2) and exit pressure (3.6.2.3) distributions. Another important factor is the explicit representation of the loss coefficients associated with CE and ENC fuel assemblies (3.7.3.1)

CETOP

The CETOP hydraulics code (67) utilized in setpoint analysis. It is benchmarked against D-TORC to always give conservative results relative to D-TORC. In other words, CETOP always calculates smaller MDNBR's than does D-TORC for the same operating conditions.

3.6.9 Fuel Temperature Conditions

Fuel pellet temperature calculations were performed for the reload fuel design (Reference 30) to determine: 1) the maximum allowable rod linear heat generation rate withou calculated fuel centerline melt, and 2) the adequacy of 21.0 kw/ft as a limit over the life of the fuel. The values used in the calculations are shown in Table 3.5-6.

The results of the calculations are shown in Table 3.5-7 for several pellet exposures which are considered sufficient to represent the fuel pellet temperatures throughout life. For reference, selected values of the fel melting point are also given in Table 3.5-7.

These results indicate that for all pellet exposures likely to be encountered, a fuel rod LHGR $\leq$ 21.0 kw/ft will preclude fuel melting.

TABLE 3.6-3

FORT CALHOUN

FUEL PELLET CENTERLINE MELT CALCULATIONS

VARIABLE	VALUE
Fuel Pellet Diameter	0.3700 in.
Clad Inside Diameter	0.3795 in.
Active Fuel Length	128.0 in.
Clad Outside Diameter	0.442 in.
Initial Fill Gas Volume	0.809 $in.^3$
External Pressure	2088 psia
Initial Fuel Pellet Density Fraction	0.940
Maximum Fuel Pellet Radius Decrease Due to Densification	0.00216 in.
Enrichment	3.5 w/o U-235
Coolant Temperature	600°F
Film Coefficient	5000 Btu/hr-ft^2-°F
Film Gas Pressure	25.5 atmosphere
Helium Gas Fraction	1.000
Argon Gas Fraction	0.000
Sorbed Gas Hydrogen Fraction	0.00
Fuel Sorbed Gas Content	0.025 cm/gm
Pellet Surface Roughness	0.000063 in.
Clad Inside Surface Roughness	0.000032 in.
Clad Material	Zr-4
Rod Surface LHGR	See Table 3.5-7
Axial Peaking Factor	1.52
Fraction of Total Energy Generation in Fuel Pellet	0.975
Fuel Pellet Exposure	See Table 3.5-7

TABLE 3.6-4

FORT CALHOUN CALCULATED FUEL TEMPERATURES

Pellet Exposure Melting (MWD/MTU)	Fuel Rod LHGR (KW/FT)	Maximum Fuel Temperature (°F)	Fuel Melting Point (°F)
0	21.0	4753	5054
108	21.0	4697	5053
485	21.0	4422	5050
1024	21.0	4259	5045
2479	21.0	4178	5032
5389	21.0	4148	5005
10,779	21.0	4176	4957
16,168	21.0	4202	4908
21,557	21.0	4226	4860

TABLE 3.6-4 (Continued)

FORT CALHOUN CALCULATED FUEL TEMPERATURES

Pellet Exposure Melting (MWD/MTU)	Fuel Rod LHGR (KW/FT)	Maximum Fuel Temperature (°F)	Fuel Melting Point (°F)
26,947	21.0	4249	4811
32,336	21.0	4271	4763
37,725	21.0	4291	4714
43,115	21.0	4311	4665
48,504	21.0	4329	4617
53,893	21.0	4347	4568

3.6.10 Flow Stability

Flow oscillations of significant amplitude may be sustained in some channels when heat is added to two-phase flow in parallel channels. This possibility results from two conditions that exist within the core:

a. The pressure drop flow characteristics with two-phase flow are such that large changes in flow can occur for small changes in pressure drop;

b. With parallel channels, the flow has an alternate path.

The flow regimes may be classed as separated or homogeneous. Homogeneous flow is bubbly or froth flow. Separate flow is annular or slug. Reference 39 describes these flow regimes in detail. For homogeneous flow, the channel pressure drop continuously increases with increasing flow rate or increasing vapor fraction. A change in the flow regime to separated flow results in a change in the flow characteristics and flow oscillations in the parallel channels are then possible. Figure 3.5-3 shows flow regimes as a function of mass flow rate and void fraction based on the data of Reference 34. In general, increasing void fraction results in a transition to an annular type flow and decreasing void fraction results in a transition to slug flow. A comparison of this flow regime map with data of observed flow regimes reported in Reference 35, 36, 37 and 38 has been made to verify the effect of variation of such parameters as channel length, diameter and pressure and to check the consistency of the data. Good agreement was obtained, and the limits for stable flow as shown in Figure 3.5-3 are considered a reasonable and conservative representation of flow regime changes for core hot channel conditions.

The limit to ensure flow stability as applied to core conditions is conservative since the "openness" of the channels to crossflow tends to damp any flow oscillations. This is explained by the basic requirement that in order for flow oscillations to occur, a feedback effect (from the channel outlet to the channel inlet region) on channel flow and pressure loss is necessary. Crossflow tends to damp the feedback effect and tends to make the open channel array stable even when parallel closed channels would not be stable. This conclusion is supported by the observation of the absence of DNB conditions in the open array experiments reported in Reference 39. The experimental results of Reference 34 to 38 are all for closed channels.

3.7 MECHANICAL DESIGN AND EVALUATION

The reactor core and internals are shown in Figure 3.1-1. A cross section of the reactor core and internals is shown in Figure 3.1-2. Mechanical design features of the reactor internals, the control element drive mechanisms and the reactor core are described below. Mechanical design parameters are listed in Table 3.7-1.

TABLE 3.7-1

MECHANICAL DESIGN PARAMETERS

Fuel Assemblies

Type	No. of Assemblies	Fuel Rods No.	Poison Rods No./Dia.
G	29	176	---
H	40	176	---
I	36	176	---
J	28	176	---

Fuel Rod Array, square		14 x 14	
Fuel Rod Pitch, inches		0.580	
Spacers		G	H,I,J
Type		Leaf Spring	
Material		Zircaloy-4	
Number per Assembly		9	9
Weight of Fuel Assembly, pounds		1200	1200
Weight of Contained Uranium, kg U		364.74	356.86
Outside Dimensions			
Fuel Rod to Fuel Rod, inches		7.980 x 7.980	
Fuel Rod		G	H,I	J
Fuel Material (Sintered Pellets)		UO_2	UO_2	UO_2
Pellet Diameter, inches		0.3765 ± 0.0005	.3700 ± .0005	.3700 ± .0005
Pellet Dish Depth, inches		.021 ± .003	.0052	.0068
Pellet Dish Diameter, inches		0.1425	.270	.270
Pellet Length, inches		0.450 ± 0.050	0.275 ± .050	0.425 ± .050
Pellet Density, g/cc		10.248 ± 0.164	10.3	10.3
Pellet Density, % theoretical		93.5 ± 1.5	94.0 ± 1.5	94.0 ± 1.5
Stack Height Density, g/cc		10.097	10.19	10.19
Clad Material		Zircaloy-4	Zircaloy -4	Zircaloy -4
Clad ID, inches		0.3880 ± 0.0015	0.378 ± .0015	.0378 ± .0015

TABLE 3.7-1 (cont'd)

	D,F,G	H,I	J
Clad OD, inches (nominal)	0.440	0.442 ± .002	0.442 ± .002
Clad Thickness, inches (nominal)	0.026	0.032	.032
Clad Thickness, inches (minimum)	0.024	0.294	.0294
Diametral Gap, Cold Nominal, inches	0.0065	0.008	.008
Active Length, inches	128 ± 0.250	128 ± .128	128 ± .128
Total Length Between End Plates, inches	137.250	137.71	137.66

Control Element Assemblies (CEA's)	Full Length	Part Length
Number	45	4
Number of Absorber Elements	5	5
Type	Cylindrical Rods	Cylindrical Rods
Sheath Material	Inconel 625	Inconel 625
Sheath Thickness, inches	0.040	0.040
Poison Material	B_4C	B_4C
Corner Element Pitch, inches	4.64	4.64
Total Element Length, inches	148	148
Poison Length, inches	127	32
Element Diameter, inches	0.948	0.948
CEA Weight, pounds	73	73
Total Operating Assembly Weight, pounds	268	281

Core Arrangement	
Number of Fuel Assemblies in Core, Total	133
Number of CEA's	49
Number of Active Fuel Rods	23,408
CEA Pitch, min, inches	11.57
Spacing Between Fuel Assemblies, Fuel Rod Surface to Surface, inches	.198
Spacing, Outer Fuel Rod Surface to Core Shroud, inches	.179
Hydraulic Diameter, Nominal Channel, Feet	.04393
Total Flow Area (Excluding Guide Tubes), sq ft	32.61
Total Core Area, sq ft	62
Core Equivalent Diameter, inches	106.448
Core Circumscribed Diameter, inches	116.484
Core Volume, liters	18,726
Total Fuel Loading, kg U	47,691
Total Fuel Weight, kg UO_2	54,194
Total Heat Transfer Area, sq ft	28,864
Fuel Volume, cu ft	187.87

3.7.1 Reactor Internals

The reactor internals are designed to support and orient the reactor core fuel assemblies and control element assemblies, absorb the CEA dynamic loads and transmit these and other loads to the reactor vessel flange, provide a passageway for the reactor coolant, and support in-core instrumentation.

The internals are designed to safely perform their functions during all steady state conditions and during normal operating transients. The internals are designed to safely withstand the forces due to deadweight, handling, system pressure, flow impingement, temperature differential, shock and vibration. All reactor components are considered Class 1 for seismic design. The reactor internals design limits deflection where required by function. The structural components satisfy stress values given in Section III of the ASME Boiler and Pressure Vessel Code. Certain components have been subjected to a fatigue analysis. Where appropriate, the effect of neutron irradiation on the materials concerned is included in the design evaluation.

The components of the reactor internals are divided into three major parts consisting of the core support barrel (including the lower core support structure, the core shroud and the thermal shield), the upper guide structure (including the CEA shrouds and the in-core instrumentation guide tubes) and the flow skirt. These components are shown in Figure 3.1-1. The in-core instrumentation is described in Sections 7.5.1 and 7.5.2.

3.7.1.1 Core Support Assembly

The major support member of the reactor internals is the core support assembly. This assembled structure consists of the core support barrel, the core support plate and the support columns, the core shroud, the thermal shield, the core support barrel to pressure vessel snubbers and the core support barrel to upper guide structure guide pins. The major material for the assembly is Type 304 stainless steel.

The core support assembly is supported at its upper flange from a ledge in the reactor vessel flange. The lower end is restrained in its lateral movement by six core support barrel-to-pressure vessel snubbers. Within the core support barrel are axial shroud plates which are attached to the core support barrel wall by horizontal former plates and to the core support plate by anchor blocks. The core support plate is positioned within the barrel at the lower end and is supported both by a ledge in the core support barrel and by 44 columns. The core support plate provides support and orientation for the fuel assemblies. Also within the core support barrel just below the nozzles are four guide pins which align and prevent excessive motion of the lower end of the guide structure relative to the core support barrel during operation. The thermal shield is affixed to the outside of the core support barrel.

The effect of neutron irradiation on the core support structure will be a reduction in the ductility of the structures in the areas of highest fluence. In the design of the structures in these areas, the deflections and resultant strains were determined and compared with the estimated ductility values at end-of-service life in order to ensure adequacy of the design. Table 3.7-2 shows this comparison for certain areas in the core support structure which experience high fluence.

3.7.1.2 Core Support Barrel

The core support barrel net weight (325,000 pounds) consists of the entire core and other internals. It is a right circular cylinder with a nominal inside diameter of 120-5/8 inches and a minimum wall thickness in the weld preparation area of 1 inch. It is suspended by a 4-inch thick flange from a ledge on the pressure vessel. The core support barrel in turn supports the core support plate upon which the fuel assemblies rest. Press fitted into the flange of the core support barrel are four alignment keys located 90 degrees apart. The reactor vessel, closure head and upper guide structure assembly flanges are slotted in locations corresponding to the alignment key locations to provide proper alignment between these components in the vessel flange region.

Since the core support barrel is 26 feet long and is supported only at its upper end, it is possible that coolant flow could induce vibrations in the structure. Therefore, amplitude limiting devices, or snubbers, are installed near the bottom outside end of the core support barrel. The snubbers consist of six equally spaced double lugs around the circumference and are the grooves of the "tongue-and-groove" assembly; the pressure vessel lugs are the tongues. Minimizing the clearance between the two mating pieces limits the amplitude of any vibration. At assembly, as the internals are lowered into the vessel, the pressure vessel tongues engage the core support grooves in an axial direction. With this design, the internals may be viewed as a beam with supports at the furthest extremities. Radial and axial expansions of the core support barrel are accommodated, but lateral movement of the core support barrel is restricted by this design. The pressure vessel tongues have bolted, lock welded Inconel X shims and the core support barrel grooves are hardfaced with Stellite to minimize wear.

3.7.1.3 Core Support Plate and Support Columns

The core support plate is a 120-inch diameter, 2-inch thick, Type 304 stainless steel plate into which the necessary flow distributor holes for the fuel assemblies have been machined. Fuel assembly locating holes (five for each assembly) are also machined into this plate. Columns and support beams are placed between this plate and the bottom of the core support barrel in order to provide stiffness to this plate and transmit the core load to the bottom of the core support barrel.

3.7.1.4 Thermal Shield

The 3-inch thick, Type 304 stainless steel thermal shield is a cylindrical structure which reduces the neutron flux and radiation heating in the reactor vessel wall to an acceptable level. At the upper end, the shield is supported by

TABLE 3.7-2

COMPARISON OF AREAS IN THE CORE SUPPORT STRUCTURE WHICH EXPERIENCE THE HIGHEST FLUENCE WITH DUCTILITY AT END OF LIFE

COMPONENT	LOCATION	FLUENCE n/Cm^2	Calculated Strain %	Uniform Elongation % at Operat. Temp.
Core Barrel	Opposite Center of Core	1.30×10^{21}	.01	2.5
Core Support Columns	Top of Column	7.50×10^{21}	.04	0.5
Core Barrel	Upper Flange	$< 10^{20}$	.08	> 23%
Upper Guide Structure	Grid Beams	$< 10^{20}$	.08	> 23%
Lower Support Beams	Top of Beam	$< 10^{20}$	.08	> 23%

eight equally spaced lugs on the outer periphery of the core support barrel. A 0.005-inch gap between the thermal shield and the lower portion of the lug is provided to permit assembly of the core support barrel and the thermal shield. The lower end of the thermal shield is positioned radially utilizing 16 equally placed positioning pins which pass through the shield and butt against the core support barrel.

3.7.1.5 Core Shroud Plates and Centering Plates

The core shroud provides an envelope for the perimeter of the core and limits the amounts of coolant bypass flow. The shroud consists of rectangular plates 5/8-inch thick, 142-3/8 inches long and of varying widths. The bottom edges of these plates are fastened to the core support plate by use of anchor blocks.

The critical gap between the outside of the peripheral fuel assemblies and the shroud plates is maintained by eight tiers of centering plates attached to the shroud plates and centered during initial assembly by adjusting bushings located in the core support barrel. The overall core shroud assembly, including the rectangular plates, the centering plates, and the anchor blocks, is a bolted and lock welded assembly. In locations where mechanical connections are used, bolts and pins are designed with respect to shear, binding and bearing stresses. All bolts and pins are lock welded. In addition, all bolts (bodies and heads) are designed to be captured in the event of fracture; the bolt heads are trapped by lock bars or lock welds, and the bodies are trapped by the use of non-thru holes or by incomplete tapping of thru holes. Holes are provided in the core support plate to allow coolant to flow upward between the core shroud and the core support barrel, thereby minimizing thermal stresses in the shroud plates and eliminating stagnant pockets.

3.7 1.6 Flow Skirt

The Inconel flow skirt is a perforated (2-1/4-in. diameter holes) right circular cylinder, reinforced at the top and bottom with stiffening rings. The flow skirt is used to reduce inequalities in core inlet flow distributions and to prevent formation of large vortices in the lower plenum. The skirt provides a nearly equalized pressure distribution across the bottom of the core support barrel. The skirt is fastened to the pressure vessel lower head by nine equally spaced welds.

3.7.1.7 Upper Guide Structure Assembly

This assembly (Figure 3.7-1) consists of a plate, 41 control element assembly shrouds, a fuel assembly alignment plate and a ring shim. The upper guide structure aligns and laterally supports the upper end of the fuel assemblies, maintains the CEA spacing, prevents fuel assemblies from being lifted out of position during a severe accident condition and protects the CEA's from the effect of coolant crossflow in the upper plenum. It also supports the in-core instrumentation guide tubing. The upper guide structure is handled as one unit during installation and refueling.

The upper end of the assembly is a flanged grid structure consisting of a grid array of 24-inch deep beams. The grid is encircled by a 24-inch deep cylinder with a 3-inch thick plate welded to the cylinder. The periphery of the plate contains four accurately machined and located alignment keyways, equally spaced at 90-degree intervals, which engage the core barrel alignment keys. The reactor vessel closure head flange is slotted to engage the upper ends of the alignment keys in the core barrel. This system of keys and slots provides an accurate means of aligning the core with the closure head. The grid aligns and supports the upper end of the CEA shrouds.

The control element assembly shrouds extend from the fuel assembly alignment plate to an elevation about 8 inches above the support plate. There are 29 single-type shrouds. These consist of centrifugally cast cylindrical upper sections welded to cast bottom sections, which are shaped to provide flow passages for the coolant passing through the alignment plate while shrouding the CEA's from crossflow. There are also 12 dual-type shrouds which in configuration consist of two single-type shrouds connected by a rectangular section shaped to accommodate the dual control element assemblies. The shrouds are bolted to the fuel assembly alignment plate. At the upper guide structure support plate, the single shrouds are connected to the plate by spanner nuts which permit axial adjustment. The spanner nuts are torqued in place and lockwelded. The dual shrouds are attached to the upper plate by welding.

The fuel assembly alignment plate is designed to align the upper ends of the fuel assemblies and to support and align the lower ends of the CEA shrouds. Precision machined and located holes in the fuel assembly alignment plate align the fuel assemblies. The fuel assembly alignment plate also has four equally spaced slots on its outer edge which engage with Stellite hardfaced pins protruding out from the core support barrel to prevent lateral motion of the upper guide structure assembly during operation. Since the weight of a fuel assembly under all normal operating conditions is greater than the flow lifting force, it is not necessary for the upper guide structure assembly to hold down the core. However, the assembly would capture the core and limit upward movement in the event of an accident.

A ring shim bears on the flange at the top of the assembly to resist axial upward movement of the upper guide structure assembly and to accommodate axial differential thermal expansions between the core barrel flange, upper guide structure flange and pressure vessel flange support edge and head flange recess.

The upper guide structure assembly also supports the in-core instrument guide tubes. The tubes are conduits which protect the in-core instruments and guide them during removal and insertion operations.

3.7.2 Control Element Drive Mechanism

The control element drive mechanism (CEDM) drives the CEA within the reactor core and indicates the position of the CEA with respect to the core. The speed at which the CEA is inserted or withdrawn from the core is consistent with the reactivity change requirements during reactor operation. For conditions that require a rapid shutdown of the reactor, the CEDM drive releases to allow

the CEA and the supporting CEDM components to drop into the core by gravity. The reactivity is reduced during such a drop at a rate sufficient to control the core under any operating transient or accident condition. Since CEA speed is a direct function of drive motor power supply frequency, which is limited by the transmission frequency control system to 60 cycles/sec, CEA speed limiting features are not needed on Fort Calhoun and none are included as such.

The CEA is decelerated at the end of the drop by the CEDM which supports the CEA in the fully inserted position.

There are 37 CEDM's mounted on flanged nozzles on top of the reactor vessel closure head, located directly over the CEA's in the reactor core. Each CEDM is connected to a CEA by a locked coupling. The weight of the CEA's and CEDM's is carried by the vessel head. In order to provide lateral stability, particularly in resisting horizontal earthquake forces, the CEDM's are supported in the horizontal direction by a seismic support structure which is a cylindrical structure surrounding the CEDM's and attached to the reactor vessel head. This structure restricts bending deflection so as to limit stresses to allowable values in the lower housing and nozzle areas. Air is drawn through the structure for cooling (see Section 9.10).

The CEDM is designed to handle dual or single CEA's. The total stroke of the drive is 128 inches. The speed of the drive is 46 inches per minute. The time from receiving a trip signal to 90 percent of the fully inserted position of the CEA is less than 2-1/2 seconds under operating conditions. The CEA is allowed to accelerate to about 11 ft/sec and is decelerated to a stop at the end of the stroke.

The CEDM is of the vertical rack and pinion type with the drive shaft running parallel to the rack and driving the pinion gear through a set of bevel gears. The design of the drive is shown in Figure 3.7-2. The rack is driven by an electric motor operating through a gear reducer and a magnetic clutch. By de-energizing the magnetic clutch, the CEA drops into the reactor under the influence of gravity. The magnetic clutch incorporates an anti-reversing device which prevents upward CEA movement when the clutch is deenergized. For actuating part length CEA's, which maintain their position during a reactor trip, the CEDM is modified by replacing the magnetic clutch with a solid shaft assembly, which eliminates the trip function. Otherwise, this CEDM is the same as those attached to the full length CEA's. The drive shaft penetration through the pressure housing is closed by means of a face-type rotating seal. The rack is connected to the CEA by means of a rack extension containing an external collet-type coupling which expands and locks into a mating shouldered bore on top of the CEA. The rack extension is connected to the rack through a tie bolt by means of a nut and locking device at the upper end of the rack. A small diameter closure located at the top of the pressure housing provides tool access to this nut for releasing the CEA from the CEDM. The rack is guided at its upper end by a section having an enlarged diameter which operates in a tube extending the full length of the CEA travel. The final cushioning at the end of a CEA drop is provided by the dashpot action of the enlarged diameter of the rack entering a reduced diameter in the guide tube.

3.7.2.1 CEDM Pressure Housing

The pressure housing consists of a lower and an upper section joined near the top of the drive by means of a threaded autoclave type closure. The pressure housing design and fabrication conforms to the requirements of the ASME Boiler and Pressure Vessel Code, Section III, for Class A vessels. The housing is designed for steady state conditions as well as all anticipated pressure and thermal transients.

The lower housing section is a stainless steel tubular section welded to an eccentric reducer and flange piece at the lower end. This flange fits the nozzle flange provided on the reactor vessel closure head and is seal welded to it by an omega-type seal. Once seal welded and bolted into place, the lower pressure housing need not be removed since all servicing of the drive is performed from the top of this housing. The upper part of the lower housing is machined to form the autoclave-type closure and is provided with a recessed gasket surface for a spirally wound gasket.

The upper part of the pressure housing has a flange which mates with the lower housing autoclave-type closure, a cavity which contains the drive rotating seal, and a tubular housing extension with a small flange closure which provides access for attaching and detaching the CEA. The shaft seal is a face-type rotating seal with mating surfaces of Graphitar and tungsten carbide. The two parts of the seal are fitted with O-rings to prevent leakage around the seal. The O-rings are static seals. A cooling jacket surrounds the seal area to maintain the temperature of the seal and O-rings below 250°F. This cooling water is from the component cooling system (see Section 9.7) and is under low pressure and not connected to the reactor coolant system. A seal leak-off line is connected to the upper housing. A thermocouple in the seal leak-off connection at the upper housing monitors leak-off water temperature which provides an indication of seal leakage.

3.7.2.2 Rack and Pinion Assembly

The rack and pinion assembly is an integrated unit which fits into the lower pressure housing and couples to the motor drive package through the upper pressure housing. This unit carries the bevel gears which transmit torque from the vertical drive shaft to the pinion gear. The vertical drive shaft has splined couplings at both ends and may be lifted out when the upper pressure housing is removed. Ball bearings are provided for supporting the bevel gears and the pinion gear. The rack engages the pinion, and is held in proper engagement with the pinion by the backup rollers which carry the load due to gear tooth reactions. The gear assembly is attached to a stainless steel tube supported by the upper part of the pressure housing. This tube also carries and positions the guide tube which surrounds the rack. The rack is a tube with gear teeth on one side of its outer surface and a flat on the opposite side which forms a contact surface for guide rollers. The upper end of the rack is fitted with an enlarged section which runs in the guide tube and provides lateral support for the upper end of the rack. It also acts as a piston in controlling water flow in the lower guide tube dashpot. The top section also carries a permanent magnet which is used to operate a reed switch position indicator outside the

pressure housing. The guide tube is connected at its upper end to the support tube. The support for the guide tube contains an energy absorber at the top end of the tube which deforms to limit the stresses on the CEA, in case the mechanism is tripped without water in the dashpot. If such a "dry trip" should occur, the mechanism and CEA would not be damaged; however, it would be necessary to disassemble the CEDM and replace the energy absorber.

3.7.2.3 Motor Drive Package

Power to operate the drive is supplied by a fractional horsepower, 120-V, single-phase, 60-Hz motor. The output is coupled to the vertical drive shaft through a magnetic clutch and an anti-reverse clutch operating in parallel. When the magnetic clutch is energized, the drive motor is connected to the main shaft and can drive the CEA either up or down. When de-energized, the magnetic clutch separates and the CEA drops due to its own weight. The anti-reverse clutch prevents rotation of the drive in the up direction and holds the CEA in position against upward forces. The action is completely mechanical and does not rely on any outside source of power. The motor, brake, clutches, position indicator and limit switches are all mounted on a common frame for maintaining position and alignment. This entire drive package is assembled and checked as a unit and can be removed and replaced without disturbing the other parts of the mechanism. The frame for the drive package is provided with a flange which is bolted to a flange on the upper pressure housing for positioning the drive assembly. The electrical connections are located on the top of the drive package and are readily accessible.

3.7.2.4 Position Readout Equipment

Two independent position readout systems are provided for indicating the position of the CEA. One (primary system) is a synchro transmitter geared to the main drive shaft with readout provided by synchro receivers connected to the transmitter. The other (secondary system) position indicator consists of a series of reed switches built into a subassembly which is fastened to the outside of the CEDM along the pressure housing. The permanent magnet built into the top of the rack actuates the reed switches one at a time as it passes by them. A resistor network in conjunction with these switches controls the readout to indicate position. Limit switches located in the motor drive package are geared to the drive shaft and are used to provide indication of CEA position at certain predetermined points. These switches are used in the CEDM control system. The systems are described in Section 7.5.

3.7.2.5 Control Element Assembly Disconnect

The CEA is connected to the CEDM by means of an extension shaft with an internal collet-type coupling at its lower end. A tie rod connects the extension shaft to the rack. In order to disengage the CEA from the drive, the flange access closure at the top of the CEDM is removed. A tool is then inserted through this opening and, with the CEA in the full down position, the tool is used to release the nut locking device and to unscrew the nut on top of the tie rod. By turning another handle on the tool, the tie rod is rotated about a quarter turn and lifted about 2 inches to unlock the collet coupling and disengage the CEDM from the CEA.

3.7.2.6 CEDM Evaluation

Development models of internal and external drive components, subassemblies of the CEDM, as well as a complete model CEDM have undergone accelerated life tests under reactor conditions and have demonstrated that the CEDM fulfills all drive, trip and endurance requirements (see Section 1.4.4).

In addition to these development tests, a prototype CEDM with a simulated reactor core module was accelerated-life tested in an autoclave under reactor conditions to provide the overall adequacy of the CEDM during its design life. Each CEDM was tested at design pressure to prove its functional adequacy.

3.7.3 Core Mechanical Design

The core approximates a right circular cylinder with an equivalent diameter of 106.4 inches and an active fuel height of 128 inches. It is made up of 23,408 Zircaloy-4 clad fuel rods containing 47.69 metric tons of slightly enriched uranium in the form of sintered UO_2 pellets. The fuel rods are grouped into 133 assemblies.

Short term reactivity control is provided by 49 control element assemblies. Four of the CEA's contain poison in the lower end only. The CEA's are guided within the core by the guide tubes which are integral parts of the fuel assemblies.

3.7.3.1 Fuel Assembly

Figure 3.7-3 shows the details of the fuel assembly. The 133 assemblies consist of 176 fuel rods, five guide tubes, eight fuel spacer grids, and upper and lower end fittings. The structural frame of the assembly consists of the guide tubes, spacer grids and end fittings. All five guide tubes are mechanically attached to the stainless steel end fittings. Spacer grids for G fuel assemblies are welded to the guide tubes. The spacer grids contained in the H, I, and J assemblies are mechanically attached to the guide tubes. The Zircaloy-4 guide tubes are 1.115 inches in diameter and have an 0.040 in wall thickness.

The lower end fitting is a cast structure of 304 stainless steel. It is machined to accept alignment pins which fit in corresponding holes in the core support plate. The alignment pins provide lateral alignment of the lower end of the fuel assembly. The length of the alignment pin engagement has been determined to ensure that the spacing between fuel assemblies will not be altered even during postulated accident conditions when a fuel assembly is lifted into contact with the upper guide structure. The lower end fitting contains flow holes and holes for positioning the fuel rods and guide tubes.

The fuel assembly upper end fitting is a cast structure of 304 stainless steel. It serves as an attachment for the guide tubes and as the lifting fixture. The pin-shaped protrusions serve as guide pins and mate with precision-drilled holes in the alignment plate to provide the alignment of the upper ends of the fuel assembly.

The fuel rod spacer grids (Figure 3.7-4) maintain the fuel rod pitch over the full length of the fuel rods. The grids are fabricated from preformed zircaloy strips interlocked in an egg crate fashion and welded together. Each assembly G, fuel rod is supported by two leaf springs and two arches which are opposite these leaf springs. Each assmebly H, I and J fuel rod is supported by one (1) spring and four (4) support dimples. The springs press the rod against the arches to restrict relative motion between the grids and the fuel rods. The spring and arch positions are reversed from grid to grid to provide additional restriction to relative motion. The perimeter strips also contain springs and arches in addition to special features to prevent hang up of grids during a refueling operation. Spacer grids of this type have been hot-flow tested under a variety of conditions of velocity ranging from 15 to 25 feet per second, crossflow, and with simulated fully relaxed springs; no signifcant fretting has been detected.

Analysis of loss coefficients for both CE and ENC type grids has been performed, (Reference 74).

The results shown in Table 3.7.2.

TABLE 3.7-2
Grid Loss Coefficients

ENC	CE
$1.614\ Re^{-.067}$	$1.034Re^{-.040}$

The fuel rod spacer grids (Figures 3.7-4, 3.7-5) maintain the fuel rod pitch over the full length of the fuel rods. The grids are fabricated from preformed zircaloy strips interlocked in an egg crate fashion and welded together. Each assembly G, fuel rod is supported by two leaf springs and two arches which are opposite there leaf springs. Each assembly H, I and J fuel rod is supported by one (1) spring and four (4) support dimples. The springs press the rod against the arches to restrict relative motion between the girds and the fuel rods. The spring and arch positions are reversed from grid to grid to provide additional restriction to relative motion. The perimeter strips also contain springs and arches in addition to special features to prevent hang up of grids during a refueling operation. Spacer grids of this type have been hot-flow tested under a variety of conditions of velocity ranging from 15 to 25 feet per second, crossflow, and with simulated fully relaxed springs; no significant fretting has been detected.

3.7.3.2 Fuel Rods*

The fuel rods (see Figures 3.7-6, 3.7-7) consist of UO_2 pellets, a compression spring and spacer discs, all encapsulated within a Zircaloy-4 tube. The UO_2 pellets have a density of 10.25 g/cc (10.3 g/cc) and are dished at both ends. Dishing is used to accommodate the effects of thermal expansion and swelling and results in a pellet column density of approximately 10.1 g/cc (10.19 g/cc).

The fuel cladding is slightly cold worked Zircaloy-4 tubing. The cold nominal diametral gap between the pellet and clad ID is 0.0065 inch (.008 inch), and has been set taking into account clad stresses and strains and transfer of heat from the pellets. The compression spring located at the top of the fuel pellet column is of 302 stainless steel (X-750 Inconel) and maintains the column in its proper position during handling and shipping. It also provides support for the clad in the plenum region to prevent local buckling. The adequacy of the spring to perform its functions has been demonstrated in a series of long term creep buckling tests with plenum clad temperatures above those expected in the reactor.

There are two alumina spacers in each fuel rod. The spacers are located at either end of the fuel pellet stack. The lower spacer reduces the lower end cap temperature and prevents local boiling in the spiral pin area. The upper spacer prevents UO_2 chips from entering the plenum region.

The plenum above the pellet column provides space for axial thermal expansion of the fuel column and for expansion of fission gas. The maximum internal pressure at the end of life for hot operation conditions is 2760 psia. Gas release calculations are based on the most adverse fuel temperature and burnup conditions.

Each fuel rod is internally pressurized with helium. The internal pressurization with helium improves the thermal conductance between the fuel pellets and the cladding, resulting in a decrease in fuel temperature with an attendant reduction in the release of fission products and an increase in the margins between operating temperatures and allowable thermal limits. In addition, by reducing the differential pressure across the clad, internal pressurization affords a substantial reduction in the adverse effects of fuel-clad interaction and ensures that the fuel clad will be free standing against the possibility of collapsing under the effects of long-term creep due to differential pressure. The initial helium pressure is sufficient to prevent cladding collapse at the peak power location for the full design life of the fuel rod as discussed in Appendix L.

3.7.3.3 Clad Evaluation

The fuel rod cladding is designed to satisfy the design limits given in Section 3.2.3. The effects of irradiation of UO_2 and Zircaloy-4 have been considered in the design calculations. The predicted effects of anticipated transients have also been considered in the design process.

The design bases are conservative and the calculations used to demonstrate their compliance are conducted for limiting cases using limiting assumptions. This is considered advisable in the prediction of long term fuel behavior under irradiation.

A series of transverse and torsional deflection and thermal bow tests has been performed on a 12 x 12 fuel assembly to provide experimental support to the analytical effort in defining the structural action of a fuel assembly. The information gained from these tests has been used in the design of fuel assemblies and of lifting fixtures and shipping containers.

These tests show that the fuel assembly is sufficiently flexible to accommodate alignment tolerances, has adequate structural stablility for reactor operation and maintains its as-fabricated dimensions during handling. All handling from a horizontal to vertical position was performed using an auxiliary support structure.

Based upon the thermal tests, the maximum thermal bow expected under adverse temperature conditions is 7 mils. This amount of thermal bowing has no significant effect on CEA operation.

Clad stress-strain behavior is based upon a triaxial stress analysis which includes the effect of creep. The loads considered are those due to fuel thermal and fission growth, fission gas pressure and external coolant pressure.

The fuel thermal and fission growth was calculated considering the fuel as a solid rod with unrestrained thermal expansion and a volumetric growth rate of 0.16 percent for 10^{20} fissions/cm^3, (Reference 40), an average clad temperature of 688°F and a linear heat rate of 17.6 kW/ft. The fission gas pressure was calculated for a 31.5 percent fission gas release which was derived from the data of Hoffmann and Coplin (Reference 41) considering the change in plenum volume due to thermal expansion and growth of the rod.

The analysis is based upon an incremental approach which divides the 3-year fuel life span into discrete time intervals and evaluates the clad stress and strain, including the effect of creep, during these intervals. The relation between the incremental creep and the actual stress state is expressed by the Prandtl-Reuss formula (Reference 42). The basis for creep is given by the von Mises criterion, (Reference 48) and the relation between creep rate and generalized stress is that given by Scott (Reference 43). A rapidly convergent iterative technique is employed to solve the resulting nonlinear equations.

For the nominal pellet-to-clad gap, at about 1000 hours after the beginning of life, the fuel has expanded to completely fill the fuel/clad gap and to restore the clad to a circular shape after its initial creep onto the fuel. The fuel is subsequently assumed to swell unrestrained with the clad following. Based upon this conservative assumption, the final strain after 3-years' service is 0.42 percent; that is, for average fuel-to-clad gap at peak power density the strain criterion is satisfied without credit for fuel strain under load.

For the most adverse initial condition, i.e., minimum clad ID, maximum pellet OD coincident with the point of maximum power density which is assumed to be sustained over lifetime, application of the unrestrained fuel growth model results in a computed strain at end of life of about 0.91 percent. However, it has been shown (Reference 44, 45 and 46) that the effect of restraint from the exterior cooler regions of the fuel pellet, the clad and the external pressure results in a significant limitation on radial swelling with corresponding flow of pellet material into the dish provided. The assessment of this effect, using the methods of Reference 45, gives an upper limit strain for these adverse conditions of 0.73 percent.

These analyses have been conducted throughout with design beginning-of-life power density, although it is known that in fuel in its third burnup cycle, the local power density will be substantially below these values. Thus, the local power density increase which might be associated with overpower transients near end of fuel life has been conservatively considered. The maximum linear heat rating for the first core is 17.6 kW/ft at BOL (actual heat generated in fuel is 97.5 percent of the total heat generated in the core); therefore, actual peak linear heat rate is less than 17.6 kW/ft, and the maximum heat rating near EOC is estimated to be 14.9 kW/ft, resulting in a BOL/EOC ratio of 1.18. This is greater than the value of 1.12 for the ratio of maximum transient to steady state heat ratings. Thus, utilization of beginning-of-life power densities in these calculations for end-of-life transients ha provided considerable margin.

Studies by Notley et al (References 45 and 46), in which 27 fuel elements were irradiated without failure, reported measured clad strains up to 3.33 percent. In a series of experimental element irradiations, Westinghouse (Reference 44) reported strain values at failure for Zr-4 clad fuel elements of 0.78 percent to 2.6 percent, depending on the fuel properties assumed. Also, Lustman (Reference 47) has noted that failures in-pile have occurred at strain values between 0.5 percent and 1.0 percent. However, these results are based on relatively low Zr-4 cladding temperatures as compared to current large commerical PWR's. It is known (Reference 48) that permissible strain values for zircaloy increase above 650°F. The average Zr-4 cladding temperatures of about 688°F in the Fort Calhoun reactor should result in increased ductility and thus higher strain limit to failure.

Exxon Nuclear Company has conducted similar studies for the 14 x 14 fuel supplied for the Fort Calhoun Unit One reactor. A detailed discussion of this work can be found in XN-NF-79-69 (Reference 30).

3.7.3.4 Control Element Assembly

The CEA (shown in Figure 3.7-8) is comprised of five Inconel tubes 0.948 inch in diameter and containing boron carbide pellets with a density of approximately 72 percent of theoretical. Each tube is sealed by welded end caps. A gas expansion space is provided to limit maximum tube stress due to internal pressure developed by the release of helium gas and moisture from the boron carbide. The active length of the neutron absorber is 127 inches and the overall length of the control element assembly is 153 inches. Four tubes are assembled in a square array around the centrally located fifth tube. The tubes are joined by an upper end fitting. The hub of the upper end fitting also couples the CEA to the drive mechanism through the extension shaft and rack. A dashpot is provided in the CEDM to slow down the assembly in the last part of the stroke following a reactor trip, as described in Section 3.7.2.

Mechanical reactivity control is achieved by operational maneuvering of single or double CEA's. The double CEA is made up of two single CEA's connected to separate grippers and carried by one extension shaft. The arrangement of the CEA's in the core is shown in Figure 3.4-1.

There are 25 single CEA's, four of which are part length CEA's and 12 double CEA's all operated by a total of 37 control element drive mechanisms. Considering the 12 double CEA's as 24 single CEA's gives an overall equivalent number of 49 single CEA's in the core.

3.7.3.5 Control Element Assembly Evaluation

Several parallel experimental efforts (see Section 1.4) were pursued to assure that the CEA's will function under a wide variety of adverse conditions that could be encountered under normal and abnormal operation.

The results of the cold water tests indicate that the CEA's will operate satisfactorily and achieve acceptable scram times. Various hydraulic and friction forces developed in scramming a CEA have been ascertained. Measured drop times are less than those assumed in the accident analyses.

Additional cold water flow tests were conducted on CEA's to determine the effects on drop time of guide tube mechanical and thermal bow, core pressure drop, misalignments of all applicable components, guide structure clearance variations above the core, and CEA-to-guide tube clearance variation within the fuel assembly. These test conditions were more severe than the worst accumulations of tolerances and expected operating conditions.

Burst and collapse were also performed on the poison rod cladding. Reactor operating conditions for periods up to 10,000 hours were simulated using tubing which contained defects in the wall and tubes filled with B_4C pellets that have been water logged.

Full size and weight prototype CEA's were installed in a high temperature, high pressure test facility designed to simulate pressurized water reactor coolant conditions. It is an isothermal system with capabilities of operating at temperatures up to 625°F and pressures up to 2550 psig.

Hot flow tests exposing the fuel assemblies, CEA's and a CEDM to long term reactor conditions were also conducted. The main purpose of these tests was to proof test the CEA design. CEA scram time and operational characteristics, and wear and corrosion of CEA poison tube and guide tubes were evaluated.

3.7.3.6 Source Design

Two neutron source assemblies are installed in the reactor. The assemblies serve as both startup and sustainer sources. They are held in vacant CEA guide tubes by means of an axially loaded spring reacting against the upper fuel alignment plate.

The cladding is of a free standing design. The internal pressure is always less than reactor operating pressure. Internal gaps and clearances are provided to allow for differential expansion between the source material and cladding.

3.7.4 Vibration Analysis and Monitoring

Design analyses were performed to verify the structural integrity of the Fort Calhoun reactor internals and fuel assemblies. Emphasis was placed on the dynamic analysis of those components which are particularly critical and vulnerable to vibratory excitation. Thermal shields on reactors built prior to Fort Calhoun Station experienced some vibrational problems; however, for the Fort Calhoun reactor, a more reliable design was achieved by: using a top vs. a

bottom support design, which eliminates a free edge in the flow path; increasing the number of supports to provide a stiffer structure; and using an all welded shield to eliminate local flexibilities and relative motion at bolted joints. Operating data have shown that the thermal shield is stable on its support system when exposed to the axial annular flow.

The response of the fuel assemblies to mechanical and flow excitation was evaluated. The calculated response (amplitude and frequency) of the fundamental mode of vibration of the core support barrel was used as the mechanical excitation of the fuel assemblies. The calculated fuel assembly response was then used to assure that test conditions of fuel assemblies were more severe than expected operating conditions. Vibration analysis of the fuel assemblies demonstrates that the most likely modes of vibration do not coincide in frequency with known excitations.

A vibration-loose parts monitoring system as described in Reference 54 was installed following Cycle 1. This system was designed to provide monitoring, recording, and analysis for vibration and/or loose parts on the primary coolant loop major components and neutron flux related motion of the core and its components. The system contains accelerometers placed on the lower reactor vessel, seismic skirt flange, each steam generator and each reactor coolant pump plus four channels for neutron flux (from excore detectors) measurement of core internals vibration.

The core support barrel, the support structure for the core, was initially analyzed to provide assurance that this major structure does not exhibit excessive vibrations. Vibration analysis of the barrel based on inlet flow impingement forces and turbulent flow were performed to demonstrate that the anticipated RMS response of the barrel would be low. Spectral analyses of plant operations using the vibration-loose parts monitoring system have shown that although core barrel motion is present, it is within acceptable limits.

3.8 FUEL PERFORMANCE DURING ANTICIPATED TRANSIENTS AFTER LONG BURNUP

3.8.1 Fuel Design and Analysis

The fuel rod design accounts for cladding irradiation growth, external pressure, differential expansion of fuel and clad, fuel swelling, fuel densification, clad creep, fission and other gas releases, initial internal helium pressure, thermal stress, pressure and temperature cycling, and flow-induced vibrations. The clad will be initially pressurized with helium to an amount sufficient to prevent gross clad deformation under the combined effects of external pressure and long-term creep. The clad design will not rely on the support of fuel pellets or the holddown spring to prevent gross deformation. The structural bases for normal operation and anticipated transients are as stated in FSAR Sections 3.2.2, 3.2.3, and 3.7.

During normal operating and upset conditions, the maximum primary tensile stress in the Zircaloy clad shall not exceed two-thirds of the minimum unirradiated yield strength of the material at the applicable temperature. The corresonding limit under emergency conditions is the material yield strength. The use of the unirradiated material yield strength as the basis for allowable stress is conservative because the yield strength of Zircaloy increases with irradiation. The use of the two-thirds factor ensures a 50% factor with irradiation, and ensures 50% margin to component yielding in response to primary stresses. This 50% margin, together with its application to the minimum unirradiated properties and the general conservatism applied in the establishment of design conditions, is sufficient to ensure an adequate design.

Net unrecoverable circumferential strain shall not exceed 1% as predicted by computations considering clad creep and fuel-clad interaction effects. Data from O'Donnell[50] and Weber[51] were used to determine the present 1% strain limit. O'Donnell developed an analytical failure curve for Zircaloy cladding based upon the maximum strain of the material at its point of plastic instability. O'Donnell compared his analytical curve to circumferential strain data obtained on irradiated coextruded Zr-U metal fuel rods tested by Weber. The correlation was good, thus substantiating O'Donnell's instability theory. Since O'Donnell performed his analysis, additional data have been derived at Bettis[44,52,53] and AECL.[45,54] These new data are shown in Figure 3.8-1 along with O'Donnell's curve and Weber's data. This curve was then adjusted because of differences in anisotropy, stress states and strain rates.

The conservatism of the clad strain calculations is provided by the selection of adverse initial conditions and material behavior assumptions, and by the assumed operating history. The acceptability of the 1.0% unrecoverable circumferential strain limit is demonstrated by data from irradiated Zircaloy-clad fuel rods which show no cladding failures (due to strain) at or below this level, as illustrated in Figure 3.8-1.

Zircaloy-4 fuel cladding has been utilized in PWR reactors at temperatures and burnups anticipated in current designs with no failures attributable to radiation damage. Mechanical property tests on Zircaloy-4 cladding exposed to neutron irradiation of 4.7×10^{21} nvt (estimated) have revealed that the cladding retains a significant amount of ductility (in excess of 4 percent elongation). Typical results are shown in Table 3.8-1. It is believed that the

fluence of 4.7×10^{21} nvt is at saturation so that continued exposure to irradiation should not change these properties.

TABLE 3.8-1

TENSILE TEST RESULTS
ON
IRRADIATED SAXTON CORE III CLADDING

Fluence (<1 Mev) 4.7×10^{21} n/cm^2 (Estimated)

Rod ID	Location, Inches From Bottom	Testing Temp. °F	0.2% Yield Stress psi x 10^3	Ultimate Tensile Strength psi x 10^3	Uniform Strain % In 2" Gage Length	Total Strain % In 2" Gage Length
BO	11 - 17	650	61.4	65.6	2.2	6.8
BO	26 - 32	650	58.1	68.9	2.4	11.3
RD	3 - 9	650	62.2	70.0	2.0	4.2
RD	12 - 18	650	60.5	65.4	1.7	5.8
MQ	12 - 18	675	70.4	77.4	1.9	6.1
MQ	28 - 34	675	66.0	75.1	1.6	6.2
FS	28 - 34	675	57.2	71.4	3.9	12.9
GL	12 - 18	675	60.5	71.5	2.4	9.3

T. E. Caye, "Saxton Plutonium Project, Quarterly Progress Report for the Period Ending March 31, 1972," WCAP-3385-31, Nov. 1972.

Cumulative strain cycling usage, defined as the sum of the ratios of the number of cycles in a given effective strain range ($\Delta\varepsilon$) to the permitted number (N) at that range, as taken from Figure 3.8-2, will not exceed 1.0.

The cyclic strain limit design curve shown on Figure 3.8-2 is based upon the Method of Universal Slopes developed by S. S. Manson[55] and has been adjusted to provide a strain cycle margin for the effects of uncertainty and irradiation. The resulting curve has been compared with known data on the cyclic loading of Zircaloy and has been shown to be conservative. Specifically, it encompasses all the data of O'Donnell and Langer.[56]

Fuel swelling due to irradiation (accumulation of solid and gaseous fission products) and thermal expansion results in an increase in the fuel pellet diameter. The design makes provision for accommodating both forms of pellet growth. The fuel-clad diametral gap is more than sufficient to accommodate the thermal expansion of the fuel. To accommodate irradiation-induced swelling, it is conservatively assumed that the fuel-clad gap is used up by the thermal expansion and that only the fuel porosity and the dishes on each end of the

performance and from many basic experiments conducted in various research reactors which are available in the open literature. Each of these information sources will be discussed below. Evidence currently available indicates that Zircaloy and UO_2 fuel performance is satisfactory to exposures in excess of 55,000 MWD/MTU.

3.8.2.1 Public Information

General fuel performance information available in the open literature has provided part of the fuel rod design data base. Particular experiments that have been cited in the past as key references include:

Determination of the effect of fuel-cladding gap on the linear heat rating to melting for UO_2 fuel rods, conducted in the Westinghouse test reactor

Shippingport Irradiation Experience

Saxton Irradiation Experience

Combined Vallecitos Boiling Water Reactor 'VBWR)-Dresden irradiation

Large Seed Blanket Reactor (LSBR) Rod Experience

Joint U. S. - Euratom Research and Development Program to evaluate central fuel melting in the Big Rock Point Reactor operated by Consumers Power Co

Since the information from these programs is available in the open literature, it will not be described here. However, details as to the significance of the results to fuel burnup experience are presented in Reference 67.

3.8.2.2 Operating Fuel Experience

One of the two fuel vendors who have supplied fuel for Fort Calhoun Station, C-E, has fabricated over 597,000 Zircaloy-clad fuel rods both internally pressurized and unpressurized over a 10-year period. At the end of this period, 200,000 rods remained in operation with average burnups of up to 46,000/MWD/MTU. The remaining 397,000 rods were discharged with average burnups of 43,000 MWD/MTU. Overall performance of this fuel has been excellent. The fuel rod reliability level, estimated from coolant activities is 99.99%. This high reliability level is continually validated by extensive poolside fuel inspection programs conducted at reactor sites during refueling shutdowns.

Fuel for the Fort Calhoun Station is presently supplied by Exxon Nuclear Company. This fuel is of a design very similar to the fuel provided by C-E and comparable performance can be expected over the life of the fuel.

3.8.2.3 Fuel Irradiation Programs

Fuel vendors are involved in diversified fuel irradiation test programs to confirm the adequacy of the fuel rod design bases and models by experimental means. Some of these programs involve safety-related research while other programs provide confirmatory data on performance capability or evaluate design

pellets are available. Thermal and irradiation induced creep of the restrained fuel results in redistribution of fuel so that the swelling due to irradiation is accommodated by the free volume.

Demonstration of the margin which exists in accommodating fuel swelling is seen in the large seed blanket reactor (LSBR) irradiation. Two rods which operated in the B-4 loop of the MTR offer an interesting simulation for current PWR design.[54,57,58] Both rods were comprised of 95% theoretical density pellets with dished ends and clad in Zircaloy. The first of these, No. 79-21, was operated successfully to a burnup of 12.41 x 10^{20} fiss/cm^3 (>48000 MWD/MTU). The second fuel pin, No. 79-25, operated successfully to 15.26 x 10^{20} fiss/cm^3 (>60,000 MWD/MTU). The linear heat rating ranged from 7.1 to 16.0 kw/ft. The wall thickness for the latter pin was 0.028 inch as compared with 0.016 inch for the former. All other parameters were essentially identical. The two rods were assembled by shrinking the cladding onto the fuel. The maximum diametral increase measured at the ridge heights for Rod 79-21 was 0.005 inch, while it was less than 0.002 inch for Rod 79-25. From post-irradiation examination, it was concluded that approximately 84% of the total fuel swelling was accommodated by the porosity and dishes, while 16% caused diametral expansion of the clad and ridging at pellet interfaces. These results indicate that a comparable irradiation of the fuel elements for the Fort Calhoun Unit (cold diametral gap 0.007-.008 inch, wall thickness 0.024-.0294 inch, density 95% TD) would allow adequate margin for swelling accommodation.

The successful combined VBWR-Dresden irradiation of Zircaloy-clad uranium dioxide pellets provides additional confidence with respect to the design conditions for the fuel rods for this core.[59,60] Ninety-eight rods which had been irradiated in VBWR to an average burnup of about 10,700 MWD/MTU were assembled in fuel bundles and irradiated in Dresden to a peak burnup greater than 48,000 MWD/MTU. The reported maximum heat rating for these rods is 17.3 kw/ft which occured in VBWR. Post-irradiation examination[61] revealed that diametral increases in fuel rods ranges from 0.001 to 0.003 inch maximum. The maximum diametral change corresponds to 1.42% $\Delta V/V$ (or 0.12% $\Delta V/V$ per 10^{20} fiss/m^3) for these 0.424 inch diameter rods. The relevant fuel parameters are listed below for the above test and Fort Calhoun design.

	Fuel Density (% TD)	Cold Diametral Gap (in.)	Peak Burnup (MWD/MTU)
VBWR-Dresden	95	0.004 to 0.008	48,000
LSBR-MTR	95	0.001	50,000; 61,000
Fort Calhoun Design	95	0.007	55,000

A comparison of the design parameters above, relative to the test results, provides a demonstration of the clad strains resulting from swelling of fuel.

3.8.2 Summary of Fuels Irradiation Information

The fuel rod design is based on an extensive experimental data base and by an extension of experimental knowledge through design application of fuel rod evaluation codes. The experimental data base includes data from C-E/Kraftwerk Union (KWU) joint irradiation experiments, from operating commercial plant

and fabrication variables or methods which may improve and extend current knowledge of fuel rod performance.

Some of the key fuel performance evaluation programs that will be summarized below include:

Fuel densification experiments at the Battelle Research Reactor (BRR)

Joint C-E/KWU fuel densification experiments including tests in the MZFR reactor at Karlsruhe, West Germany, and the EEI experiments in the General Electric Test Reactor (GETR)

Participation in the Halden Project in Norway with access to all Halden base program fuel test data

Irradiation of special instrumented fuel rods to obtain dynamic in-reactor measurements in Halden experimental rigs

Ramp test programs on fuel rods to evaluate fuel load-follow capabilities and the pellet clad interaction/stress corrosion phenomenon in both the Studvik and Petten Test Reactors. Other in-reactor experiments have been conducted in the Obrigheim pressurized water reactor

Irradiation of special test and surveillance assemblies in operating reactors

Fuel Densification Experiments

Several experiments have provided data on the in-reactor densification behavior of various UO_2 fuel types. These include the BRR, EEI, and MZFR densification experiments.

BRR Fuel Densification Experiment

The object of this program was to examine the in-pile densification behavior of various fuel types and microstructures fabricated with and without poreformers. The non-poreformer fuel types had initial densities of 93% to 94% theoretical with a grain size of less than 6 microns and a large fraction of pores less than 4 microns in diameter. The poreformer fuel types had initial densities of 93% to 95% and were characterized by a combination of large grain size and/or large pore size. Fuel pellets of each experimental type were irradiated in six BRR capsules at linear heat ratings between 2.8 and 4.6 kw/ft for periods of up to 1500 hours. Post-irradiation examination of the BRR results showed significant differences in the densification behavior between poreformer and non-poreformer fuel. The poreformer fuel showed little change in density (high stability) while the non-poreformer fuel densified rapidly. A trend towards increased densification with lower initial density was apparent in the non-poreformer fuel. It was concluded that the UO_2 microstructure played a dominant role in the kinetics and extent of in-reactor densification.

Fuel Densification Experiment (MZFR)

As a follow-on to the experiment in the BRR, a joint C-E/KWU program has been conducted in the German MZFR to evaluate the performance of several non-densifying fuel types at higher power levels for longer times and to higher burnups.

Sixteen full-length fuel rods, each containing a different fuel type, were irradiated at powers up to 11 kw/ft for burnups up to 4000 MWD/MTU. Included in these rods were UO_2 and UO_2-PuO_2 fuels most of which were fabricated using techniques intended to minimize densification. Six rods employed C-E fabricated UO_2 fuels, five of which included poreformer additives and one fabricated without a poreformer to serve as a referencable control sample. Eight rods were fabricated using KWU experimental fuel representing a wide range of sintering times and temperatures, initial densities and enrichments. The remaining two rods were fabricated using UO_2-PuO_2 fuels of two different densities, with and without a poreformer additive. Each of the fuel pellet types and fuel rods was extensively characterized prior to testing to permit comparison with similar post-irradiation measurements.

The results of the post-irradiation examination showed that fuel types fabricated with poreformers (similar to current production fuel) experienced significantly less in-pile densification compared to those fabricated without poreformers. The data also supports use of a standardized out-of-pile resintering test to characterize expected in-pile densification at the time of fabrication. This simulation test has been submitted to the NRC and approved for use in LOCA calculations.

EEI Fuel Densification Experiment

The prime objective of the EEI Fuel Irradiation Test Program conducted in the General Electric Test Reactor (GETR) was to isolate and characterize the in-reactor densification behavior of poreformer (or stable) fuel types.

This program provided densification data on basic program fuel pellet types with varying microstructures. The pellets in the program were well characterized prior to irradiation. Four of the fuel types were irradiated in one pressurized (53 atmospheres) capsule. Two of the fuel types were also irradiated in a separate nonpressurized capsule (one atmosphere). Each of the capsules contained thermocouples to continuously monitor capsule power generation during irradiation to assure that the desired operating conditions were maintained. Post-irradiation examination of these test capsules confirmed that UO_2 fuel with specific ranges of microstructural characteristics, such as produced by poreformer additives, are stable with respect to densification. The largest in-reactor density changes occurred for those types having a combination of the smallest pore size, the largest volume percent of porosity in pores less than 4 microns in diameter, the smallest initial grain size and the lowest initial density.[57]

Halden Program

The experimental facilities and programs of the OECD Halden Reactor Project in Norway represent one of the most advanced efforts in quantifying the effects and interaction of the various design parameters of Zircaloy-clad.

The Halden test reactor has unique capabilities for measuring fuel rod operation during irradiation. These capabilities have been utilized to provide information in the following areas:

Fuel densification phenomenon including measurements of the rate of fuel column shortening as a function of the initial fuel density, power level and fuel fabrication process

Fuel clad mechanical interaction involving studies of the effects of pellet design (shape and density) and operating parameters on cladding deformation

Modelling of fuel rod behavior with emphasis on heat transfer characteristics

The first three test assemblies contained 24 well characterized fuel rods. The objectives of these tests were to determine the dynamic changes in fuel rod internal pressure, fuel centerline temperature and fuel stack length during operation, as a function of burnup. These assemblies included the following range of design and operating parameters:

Helium fill pressures from 22 to 35 atmospheres

Initial fuel densities from 91 to 96% TD

Linear heat ratings to 15 kw/ft

U_{235} enrichments from 6 to 12%; 9 rods fabricated with mixed-oxide fuel

Two of these assemblies (6 test rods each) were discharged from the reactor after receiving peak burnups of ~24,000 MWD/MTU. The third rig (12 rods) was discharged after reaching ~45,000 MWD/MTU. The objectives of a fourth six-rod test assembly were to evaluate the effects of such design variables as pellet-clad gap, fill-gas composition, and linear heat rating (to 14 kw/ft) on heat transfer characteristics. This experiment also provided gap conductance data on UO_2 and mixed-oxide fuel. This test was discharged from the reactor after reaching a peak burnup of ~4,000 MWD/MTU.

Instrumentation used to measure fuel behavior during irradiation included centerline thermocouples, internal pressure transducers, linear variable differential transformers (LVDTs) for fuel column length changes and flux monitors for axial and radial power profiles.

Hot-cell examinations of three of the four discharged test assemblies have been completed. Fuel column length change data obtained supports data generated by the EEI, BRR, and MZFR experiments and confirms the in-reactor stability of poreformer fuel types. In addition, the internal pressure monitors and centerline thermocouple data have confirmed the adequacy of thermal performance design models.

In addition to these test assemblies, three rods have been designed and irradiated in the Halden high temperature, high pressure loop to simulate PWR coolant temperature and pressure conditions. The purpose of these experiments

was to distinguish the effects of pellet configuration on the formation of circumferential ridging and on the elongation of the rods. Each rod contained three pellet types with one type as a standard. This program, in combination with the results of other experiments, provides a firm basis upon which to optimize fuel rod design with respect to dimensional changes and to improve fuel performance models developed to predict rod dimensional stability.

Power Ramp Programs

The Pathfinder/Petten and Studsvik programs were initiated to evaluate fuel rod performance under power ramp conditions. Power ramps can occur either after refueling or after extended periods of low power operation or during control rod maneuvers. The effects of various fuel rod design variables on power ramp limits is also investigated as a means to further optimize design. The Petten/Pathfinder program, which began in 1973, is being conducted in the Obrigheim PWR reactor and Petten test reactor facilities. Special test assemblies have been irradiated each year since 1973 in the Obrigheim reactor. Included in these assemblies, which are designed to facilitate fuel rod removal and replacement, are well-characterized segmented rods or "rodlets" which are axially connected to form a complete fuel rod. These rodlets are "pre-irradiated" in the Obrigheim reactor for one of four operating cycles, and then separated and irradiated in a test reactor to evaluate performance under power ramp conditions. To date, approximately 840 rodlets have been irradiated in Obrigheim. Approximately 100 of these rodlets have been discharged and ramped in Petten after achieving burnups of 7,000 to 36,000 MWD/MTU. An additional 44 rodlets have been supplied to the Studsvik Overramp and Superramp projects for ramp testing in the R-2 reactor at Studsvik. In addition, a DOE sponsored ramp program in Petten will ramp test burnup rodlets having exposures of 30,000 to 46,000 MWD/MTU. Post-irradiation, hot-cell examination programs form an integral part of both the Petten and Studsvik experiments to characterize fuel rod behavior, particularly with respect to dimensional stability and fission product release. These test programs are designed to distinguish between fuel rod power ramps which occur on start-up and those which might occur during reactor power maneuvering operations.

Operating flexibility of a plant requires that the fuel rods maintain integrity during periodic changes in power. Power cycling tests of this type have been jointly conducted in Obrigheim and Petten. In the Petten test, a single unpressurized fuel rod was power cycled between 9 kw/ft and 17 kw/ft at a power change rate of about 3 kw/ft/min. The fuel rod successfully completed 400 cycles and achieved a burnup of 8,000 MWD/MTU. Power cycling tests were then conducted in Obrigheim on eight short pressurized and unpressurized fuel rods. The test fuel rods were attached to a control rod drive mechanism and driven from a low power to a high power position. Power changes from 50% to 100% at rates of 20% per minute for 880 cycles were included. After successfully completing the experiment, the test rods achieved a peak burnup of 30,000 MWD/MTU without substantial cladding deformation or fuel rod perforation.

3.8.2.4 Fuel Surveillance Programs

A number of fuel surveillance programs have been conducted on fuel in operating plants. Thus far, over twenty poolside fuel inspection programs of varying details have been performed on fuel similar to that used at Fort Calhoun. In this case, a total of 542 assemblies have been examined having burnups of up

to 45,900 MWD/MTU. Fuel bundle disassembly operations have been conducted either as part of test assembly surveillance programs or to reconstitute fuel assemblies having failed fuel rods. A total of over 2,300 fuel rods have been individually examined. The results of these poolside inspection programs have verified fuel assembly operation and have provided data in support of the design.

3.8.3 Summary

Design bases have been established for the Zircaloy-clad stresses, circumferential strain and cumulative strain cycling which are conservative with respect to the reported data. Evidence currently available indicates that UO_2 fuel performance is satisfactory to burnups in excess of 55,000 MWD/MTU. Heat rating and burnup analyses, including those under expected overpower conditions, have been conducted using the design beginning-of-life conditions, although it is known that local power density decreases with burnup. Thus, the local power density increase associated with over-power transients at any time in life has been conservatively assessed.

3.9 SECTION 3 REFERENCES

1. Prediction of Departure from Nucleate Boiling for an Axially Non-Uniform Heat Flux Distribution, Tong, L. S., Journal of Nuclear Energy, 21, 241 to 248 (1967).

2. Development and Verification of a Fuel Temperature Correlation for Power Feedback and Reactivity Coefficient Application, Gavin, P. H. and Rohr, P. C., "Transactions American Society", 30, 714 (1978).

3. Post-Irradiation Evaluation of Reactor-Vessel Surveillance Capsule W-225, TR-O-MCM-001, Revision 1, August 1980.

4. PDQ-7 Reference Manual, Cadwell, W. R., WAPD-TM-678, (January 1968).

5. XTG - A Two-Group Three Dimensional Reactor Simulator Utilizing Coarse Mesh Spacing, Stout, R. B., XN-CC-28, Revision 3 (January 1965).

6. CEPAK - Combustion Engineering Lattice Program Consisting of Codes and as FORM, THERMOS, CINDER, etc.

7. HARMONY - System for Nuclear Reactor Depletion Computation, Breen, R. J., et al, WAPD-TM-478 (January 1965).

8. Theory Capabilities and Use of the Three-Dimensional Reactor Operation and Control Simulator (ROCS), Ober, T. G., et al, Nuclear Science and Engineering, 64, 605-623 (1977).

9. Spectral Shift Control Reactor, Basic Physics Program, Engelder, T. C., et al, B&W-1273 (November 1963).

10. Physics Vertification Program, Final Report, Clark, R. H., et al, B&W-3647-3 (March 1967).

11. Yankee Critical Experiments, Davidson, P. W., et al. YAEC-94 (April 1959).

12. Reactivity and Neutron Flux Studies in Multi-Region Loaded Cores, Eich, W. J. and Rocacik, W. P., WCAP-1433 (1961).

13. An Evaluation of Some Uncertainties in the Comparison Between Theory and Experiments for Regular Light Water Lattices, Fayer, F. J., et al, Brit. Nuc. En. Soc. J., 6 (April 1967).

14. Kinetic and Buckling Measurements on Lattices of Slightly enriched Uranium and UO_2 Rods in Light Water, Brown, J. R., et al, WAPD-176 (1958).

15. Uranium-Water Lattice Compliation, Part I, Price, G. A., BNL 50035 (T-449) (December 1966).

16. Spectral Shift Control Reactor, Basic Physics Program, Barrett, L. E., et al, B&W-1233 (March 1962).

17. Critical Masses and Buckling of PuO_2-UO_2-H_2O Systems, Schmid, L. C., et al. ANS Trans, 1, 216 (1964).

3.9 SECTION 3 REFERENCES (Cont'd)

18. Plutonium Utilization Program Annual Report, Dawson, F. G., BNWL-624 (December 1964).

19. PuO_2-H_2O Fueled Critical Experiments, Leamer, R. D., WCAP-3726-1 (July 1967).

20. Neutronenphysikalische Untersuchungen Bei Inbetriebnahme des KWO, Bronner, G., et al, Atomwirtschaft, December, 1968 p. 618.

21. The Start-up Test Program of the Conn. Yankee Reactor, Hemmelwright, J. R., (Sept. 1967).

22. Yankee Core Evaluation Program - Quarterly Report for the Period Ending September 30, 1963, Chison, L., et al, WCAP-6056 (October 1963).

23. AEC-NFS Measurement Date Comparison - Yankee Reactor Fuel, Peck, C. C., (January 1968).

24. INCA/CECOR Power Peaking Uncertainty, Jonsson, A., et al, CENPD-153-P, Revision 1-P-A, (May 1980).

25. Xenon Spatial Oscillations, Randall, D., Nucleonics 16, 3, P 82-86 (1958).

26. CEND-TP-26, Daitch, P. B.

27. Linear Analysis of Xenon Spatial Oscillations, Stacey, W. M., Jr. Nuc Sci Eng 30, 453-455 (1967).

28. The Effect of a Finite Time Step Length on Calculated Spatial Xenon Stability Characteristics in Large PWR's, Poncelet, C. G., Trans ANS, 10, 2, 571 (1967).

29. "GAPEX: A Computer Program for Predicting Pellet-to-Cladding Heat Transfer Coefficients", XN-73-25, August 13, 1973.

30. Fort Calhoun Reload Fuel Design Report - Mechanical, Thermal-Hydraulic and Neutron Analysis, Exxon Nuclear Company, XN-NF-79-69, (September 1979).

31. Definition and Justification of Exxon Nuclear Company, DNB Correlation for PWR's, Galbraith, K. P., et al, XN-75-48, (October 1975).

32. XCOBRA II-C: A Computer Code to Determine the Distribution of Coolant During Steady State and Transient Core Operation, Exxon Nuclear Company, XN-75-21, (April 1975).

33. Critical Heat Flux on a Heater Rod in the Center of Smooth and Rough Square Sleeves, and in Line Contact with an Unheated Wall, Tong, L. S., Steer, R. W., Wenzel, A. H., Bogaardt, M. and Spigt, C. L., ASME Paper, 67-WA/HT-29 (November 1967).

34. Investigation of Boiling Water Flow Regimes at High Pressure, Bergles, A. E., and Suo, M., NYO-3304-8 (February 1966).

3.9 SECTION 3 REFERENCES (Cont'd)

35. Simultaneous Flow of Oil and Gas, Baker, O., Oil and Gas Journal, Vol 53, 185 (1954).

36. Flow Patterns in High Pressure Two Phase (Steam-Water) Flow with Heat Addition, Hosler, E. R., ALCHEP Preprint 22, 9th National Heat Transfer Conference (August 1967).

37. Flow Properties of Bubbly Mixtures, Rose, S. C., and Griffith, P., ASME Paper No. 65-HT-58 (August 1965).

38. Critical Heat Fluxes and Flow Patterns in High Pressure Boiling Water Flow, Tippets, F. E., ASME Paper No. 62-WA-162 (1962).

39. Experimental Determination of the Departure From Nucleate Boiling in Large Rod Bundles at High Pressures, Tong, L. S., et al, ALChe preprint No. 29, 9th National Heat Transfer Conference (August 1967).

40. Effects of High Burnup on Oxide Ceramic Fuel, Bleiberg, M. L., Berman, R. M., and Justman, B., WAPD-T-1455 (March 1962).

41. The Release of Fission Gases for Uranium Dioxide Pellet Fuel Operated at High Temperatures, GEAP-4596 (September 1964).

42. The Mathematical Theory of Plasticity, Hill, R., Oxford Press (1965).

43. Physical and Mechanical Properties of Zircaloy-2 and 4, Scott, D. B., WCAP-3269 (May 1965).

44. Comparisons with Experiment of Calculated Dimensional Changes and Failure Analysis of Irradiated Bulk Oxide Fuel Test Rods Using the CYGRO-I Computer Program, Duncombe, E., Meyer, H. E., and Coffman, W. A., WAPD-TM-583 (September 1966).

45. The Longitudinal and Diametral Expansion of UO_2 Fuel Elements, Notley, Bain and Robertson, AECL-2143 (November 1964).

46. The Effect of UO_2 Density on Fission Product Gas Release and Sheath Expansion, Notley, M. J. F., and MacEwan, J. R., AECL-2230 (March 1965).

47. Fuel Clad Design Basis for Thermal Reactors, Lustman, B., Bettis Atomic Laboratory (May 1966).

48. Creep Properties of Zircaloy-2 for Design Application, Pankaskie, P. J., HW-75267 (October 1962).

49. Vibration and Loose Parts Monitoring System - Operation and Maintenance Manual, Rockwell International, AI-73-1.

50. Fracture of Cylindrical Fuel Rod Cladding due to Plastic Instability, O'Donnel, W. J., WAPD-TM-651, April 1967.

3.9 SECTION 3 REFERENCES (Cont'd)

51. Plastic Stability of Zr-2 Fuel Cladding, Effects of Radiation of Structural Metals, Weber, J. M., ASTM STP 426, Am. Soc. Testing Mats, pp 653-669, 1967.

52. Performance of Fuel Rods Hahing 97 Percent Theoretical Density UO_2 Pellets Sheathed in Zircaloy-4 and Irradiated at Low Thermal Ratings, Engle, J. T. and Meieran, H. B., WAPD-TM-631, July 1968.

53. Evaluation of the Irradiation Performance of Zircaloy-4 Clad Testing Rod Containing Annular UO_2 Fuel Pellets (Rod 79-19), McCauley, J. E. et al., WAPD-TM-595, December 1966.

54. The Thermal Conductivity of Columnar Grains in Irradiated UO_2 Fuel Elements, Notley, M. J. F., AECL-1822, July 1962.

55. Fatigue: A Complex Subject - Some Simple Approximations, Manson, S. S. Experimental Mechanics, Vol. 22, No. 2, pp. 193-226, July 1965.

56. Fatigue Design Basis for Zircaloy Components, O'Donnel, W. J. and Langer, B. F., Nuc. Sci. Eng., Vol. 20, pp 1-12, 1964.

57. EEI/EPRI Fuel Densification Program Final Report, Brite, D. W. et al, Battelle Pacific Northwest Laboratories, March 1975.

58. Irradiation Behavior of Zircaloy-Clad Fuel Rods Containing Dished End UO_2 Pellets, Berman, R. M., Meieran, H. B, and Patterson, P., (LWBR-LSBR Development Program), WAPD-TM-629, July 1967.

59. Comparative Performance of Zircaloy and Stainless Steel Clad Fuel Rods Operated to 10,000 MWD/MTU in the VBWR, Baroch, S. J., et al., GEAP-4849, April 1966.

60. Zircaloy-Clad UO_2 Fuel Rod Evaluation Program, Quarterly Progress Report No. 8, Megerth, F. H., August 1969-October 1969, GEAP-10121, November 1969.

61. Zircaloy-Clad UO_2 Fuel Rod Evaluation Program, Quarterly Progress Report No. 1, Megerth, F. H., November 1967-January 1968, GEAP-5598, March 1968.

62. Final Safety Analysis Report, San Onofre Nuclear Generating Station, Units 2 & 3, Volume-9, pages 4.2-59 - 4.2-61.

63. CE Critical Heat Flux, CENPD-162-P-A, Combustion Engineering, September, 1976.

64. CE Critical Heat Flux, Part 2, CENPD-207-P-A, Combustion Engineering. June, 1976.

65. Letter: From H. Bernard (NRC) to AE Scherer (CE), May 12, 1982.

66. CENPD-161-P, TORC Code, A Computer Code for Determining the Thermal Margin of a Reactor Core, Combustion Engineering. July, 1975.

67. CENPSD-150-P, CETOP: Thermal Margin Model Development, Combustion Engineering. May 1981.

3.9 SECTION 3 REFERENCES (Cont'd)

68. CENPSD-148-P, CE-Thermal Margin Model Development, Combustion Engineering. May 1981.

69. CENPDS-156-P, CE Thermal Margin Analysis Using CETOP-D/CE-1 Methodology, Combustion Engineering, May 1981.

70. Letter, D.C. Trible (AP&L) to Director, NRR, "CETOP-D Code Structure and Modeling Methods, Response to First Round Questions on the Statistical Combination of Uncertainties Program (CEN-139 (A)-P)", July 15, 1981.

71. CEN-124(B)-P, "Response to First Round Questions on the Statistical Combination of Uncertainties Program: CETOP Code Structure and Modeling Methods," May 1981.

72. Final Safety Evaluation Report Supporting Facility Operating License Amendment No. 26 on Docket No. 50-368 and Operation of ANO-2 During Cycle 2, July 21, 1981.

73. Safety Evaluation by the Office of Nuclear Reactor Regulation Supporting Amendment No. 71 to Facility Operating License No. DPR-53 Calvert Cliffs Nuclear Power Plant Unit No. 1 Docket No. 50-317.

74. Single Phase Hydraulic Performance of Exxon Nuclear and Combustion Engineering Fort Calhoun Fuel Assemblies. Exxon Nuclear Company XN-NF-76-16. March 1979.

75. CEN-191(B)-P CETOP-D, Code Structure and Modeling methods for Calvert Cliffs Units 1 & 2. Combustion Engineering. December 1981.

76. "Interim Safety Evaluation Report on Effects of Fuel Rod Bowing on Thermal Margin Calculations for Light Water Reactors," NRC Report.

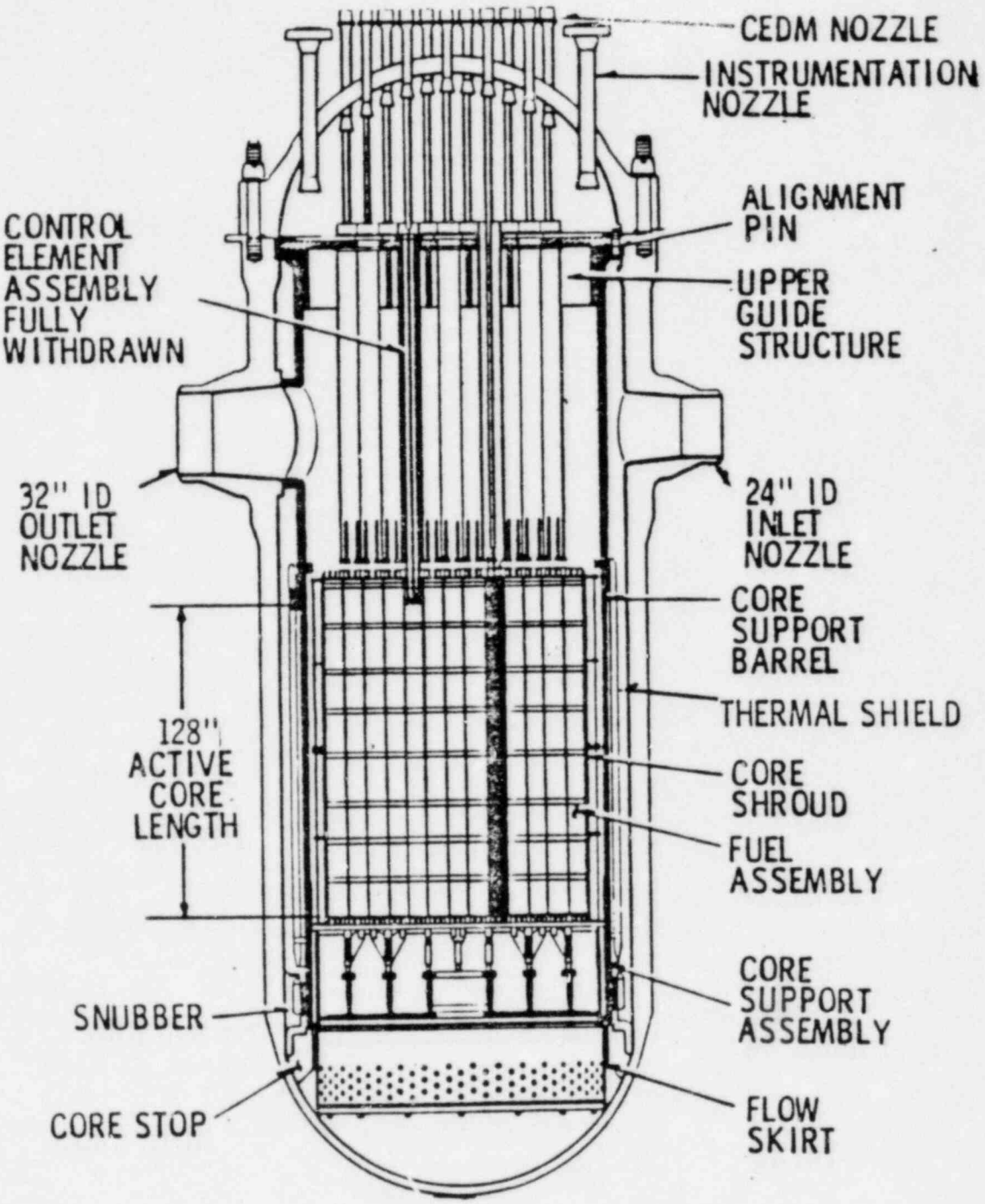

Reactor Arrangement	Omaha Public Power District Fort Calhoun Station-Unit No. 1	Figure 3.1-1

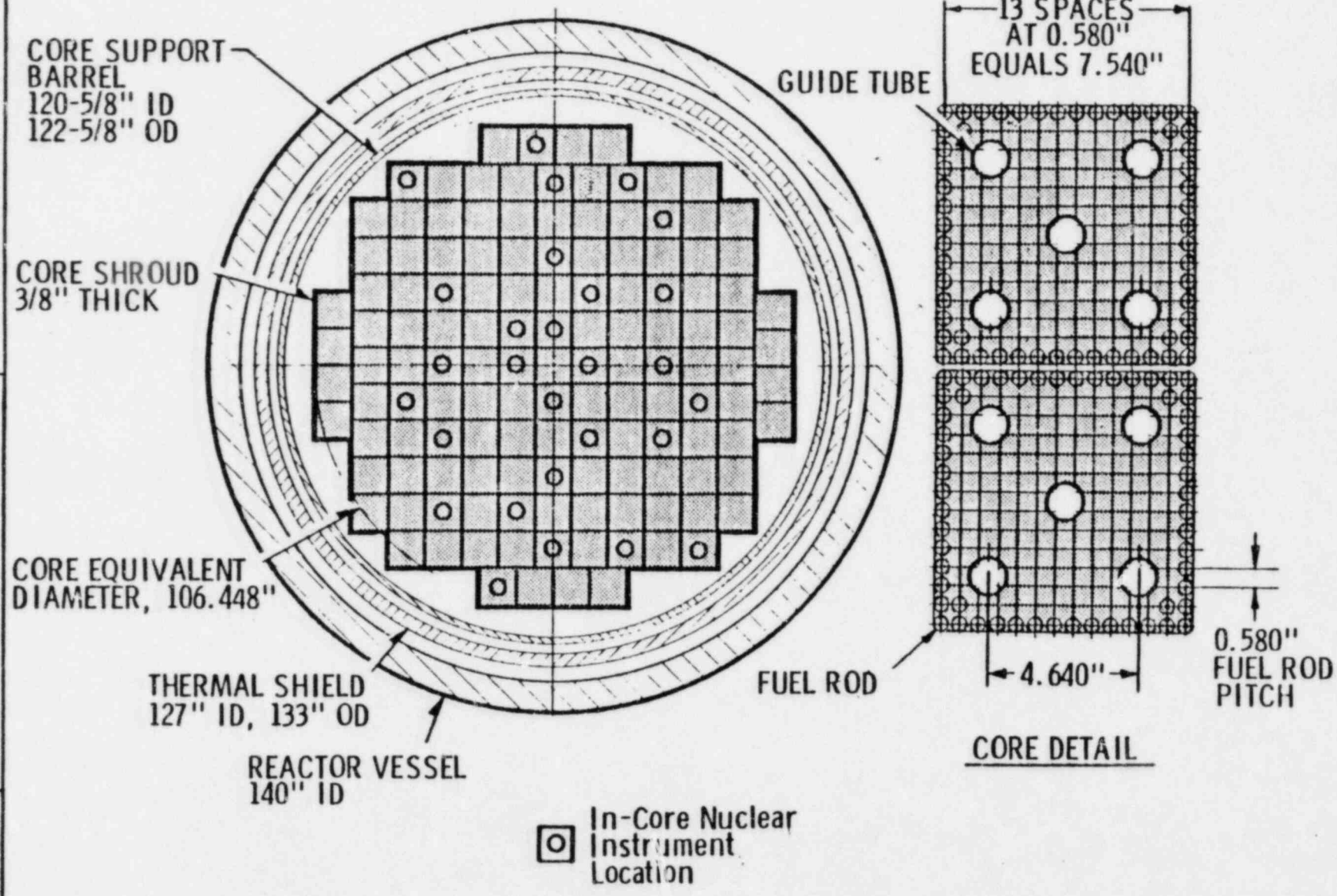

Reactor Core Cross Section

Omaha Public Power District
Fort Calhoun Station-Unit No. 1

Figure 3.1-2

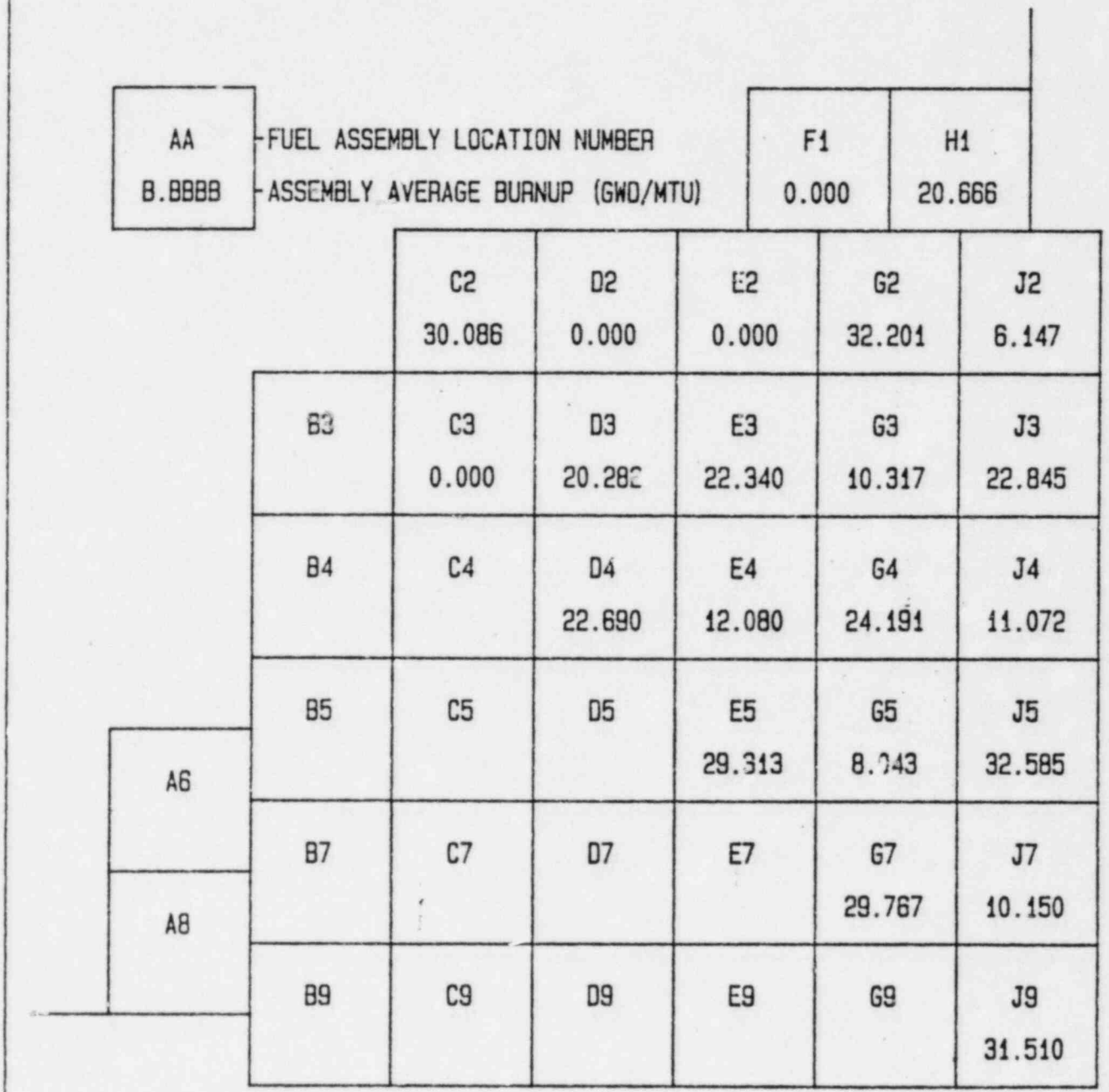

Assembly Average Burnup Distribution Beginning of Cycle	Omaha Public Power District Fort Calhoun Station-Unit No. 1	Figure 3.4-1

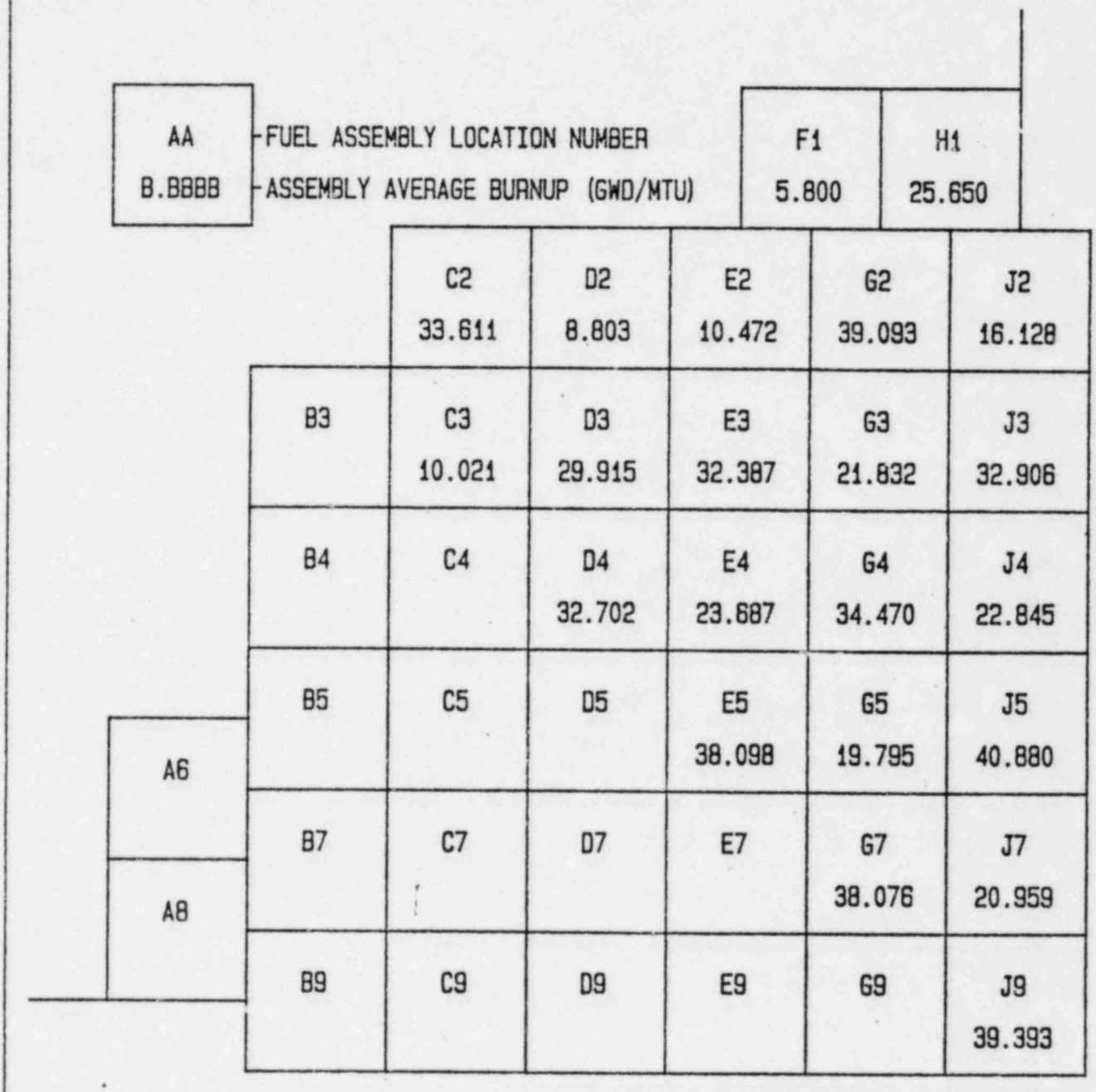

Assembly Average Burnup Distribution End of Cycle (9000 MWD/MTU)	Omaha Public Power District Fort Calhoun Station-Unit No. 1	Figure 3.4-2

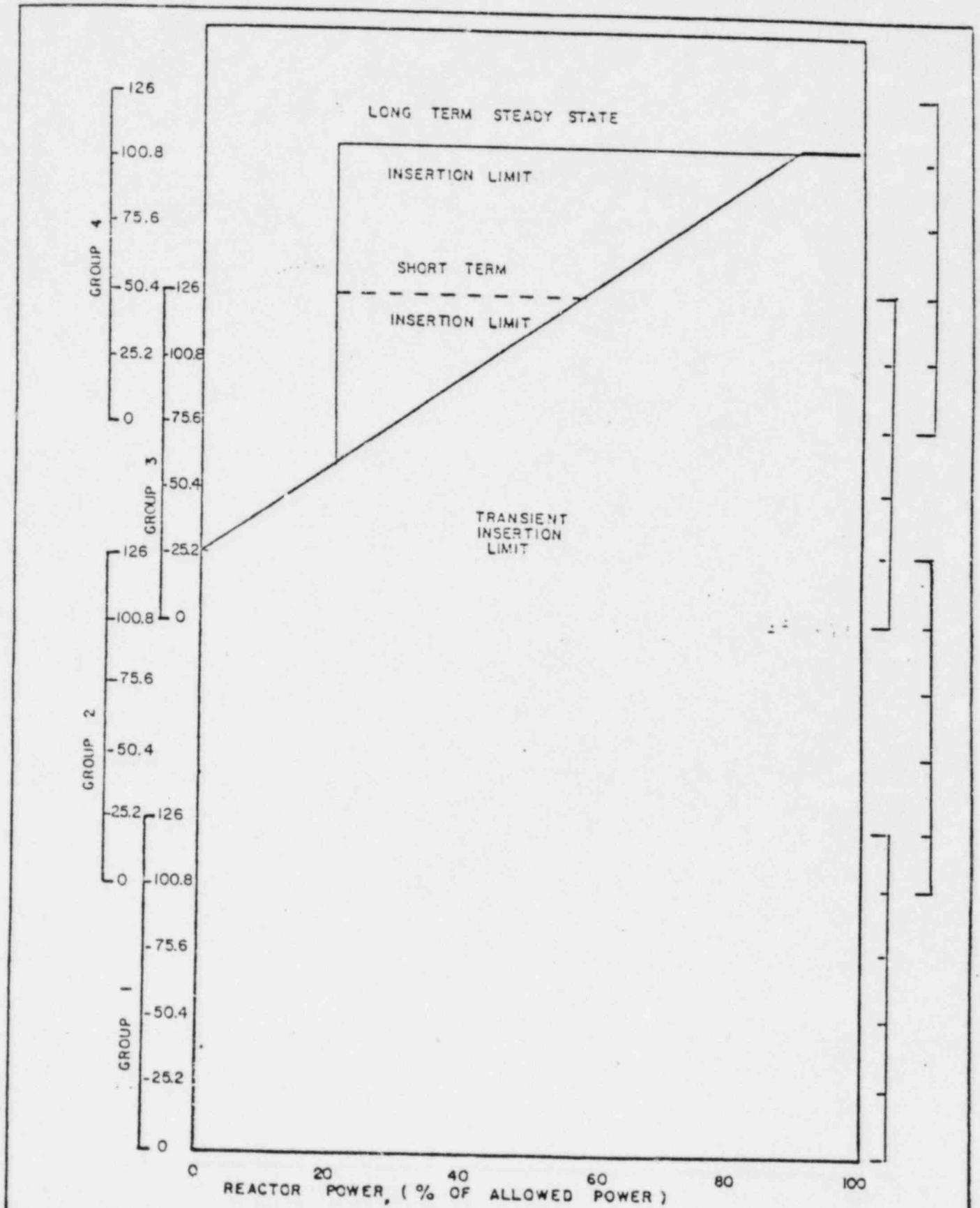

POWER DEPENDENT INSERTION LIMIT	OMAHA PUBLIC POWER DISTRICT FORT CALHOUN STATION UNIT NO. 1	Figure 3.4-3

CEA GROUPS
1, 2, 3, 4 REGULATING
A, B SHUTDOWN
P PART LENGTH

AA	FUEL ASSEMBLY LOCATION NUMBER
B	CEA GROUP IDENTIFICATION
C	FUEL ASSEMBLY TYPE

			C2 G	D2 A J	E2 J	G2 2 H	J2 I
		B3 G	C3 4 J	D3 H	E3 A H	G3 I	J3 P H
		B4 A J	C4 H	D4 B I	E4 H	G4 I	J4 H
		B5 J	C5 A H	D5 H	E5 B I	G5 G	J5 3 I
	A6 J	B7 2 H	C7 I	D7 1* I	E7 G	G7 J	J7 G
	A8 G	B9 I	C9 P H	D9 H	E9 3 I	G9 G	J9 4 G
			F1 J	H1 G			

* CORRESPONDING CEA LOCATED ASSYMETRICALLY IN OTHER QUADRANTS

Position of Fuel Assemblies and CEA Groups	Omaha Public Power District Fort Calhoun Station-Unit No. 1	Figure 3.4-4

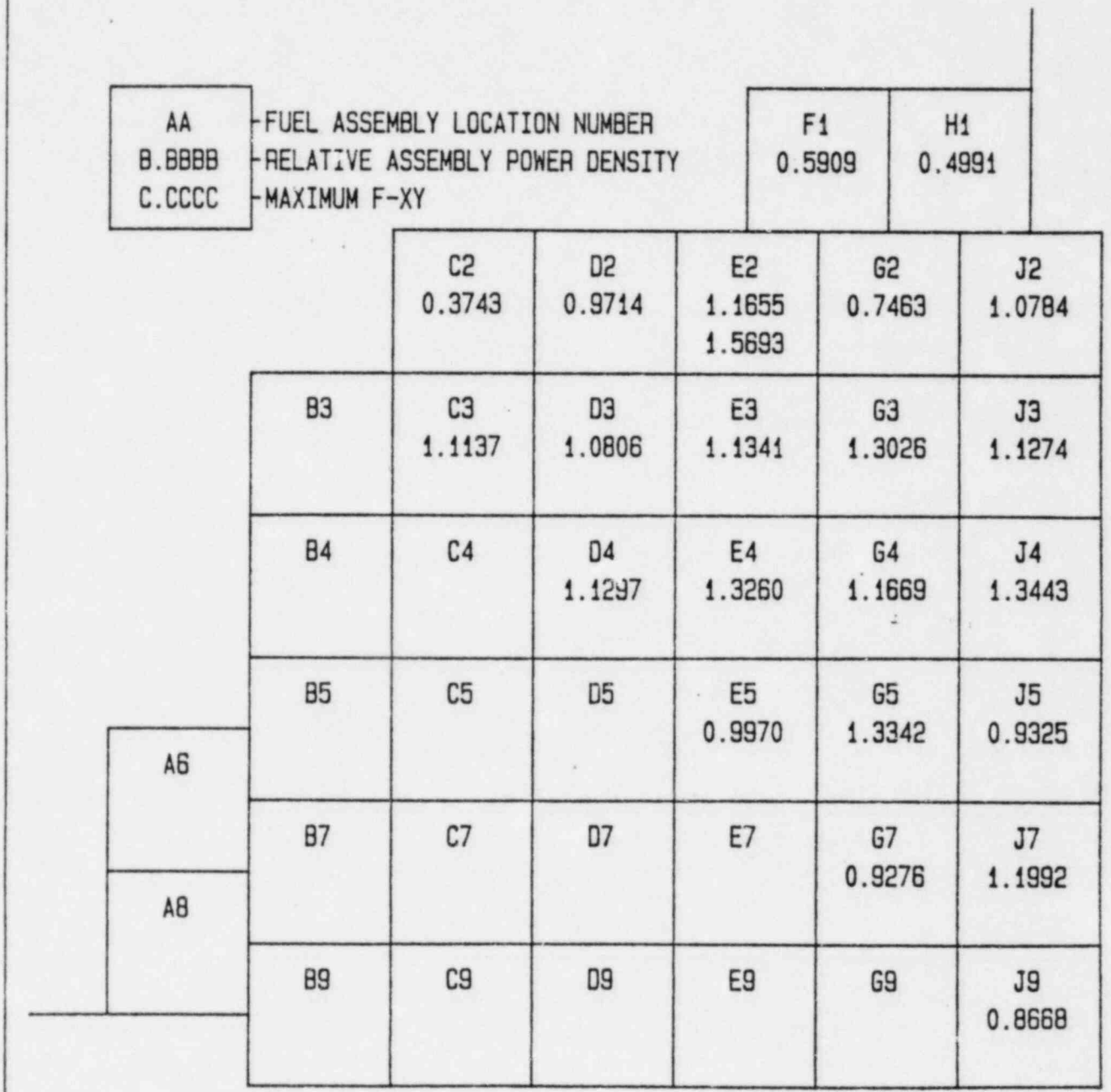

Core Radial Power Distribution Beginning of Cycle ARO	Omaha Public Power District Fort Calhoun Station-Unit No. 1	Figure 3.4-5

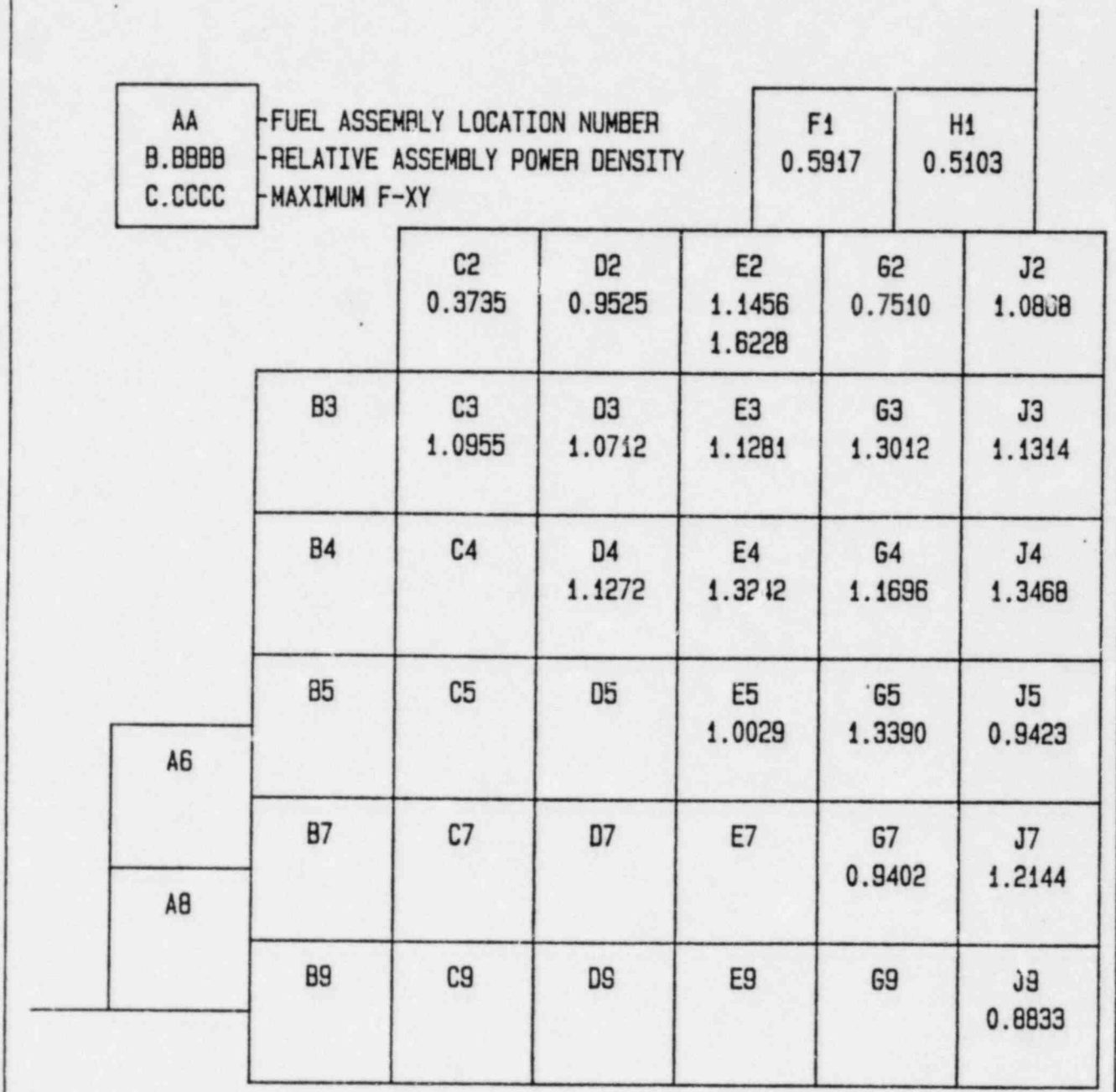

Core Radial Power Distribution at 1000 MWD/MTU Burnup ARO	Omaha Public Power District Fort Calhoun Station-Unit No. 1	Figure 3.4-6

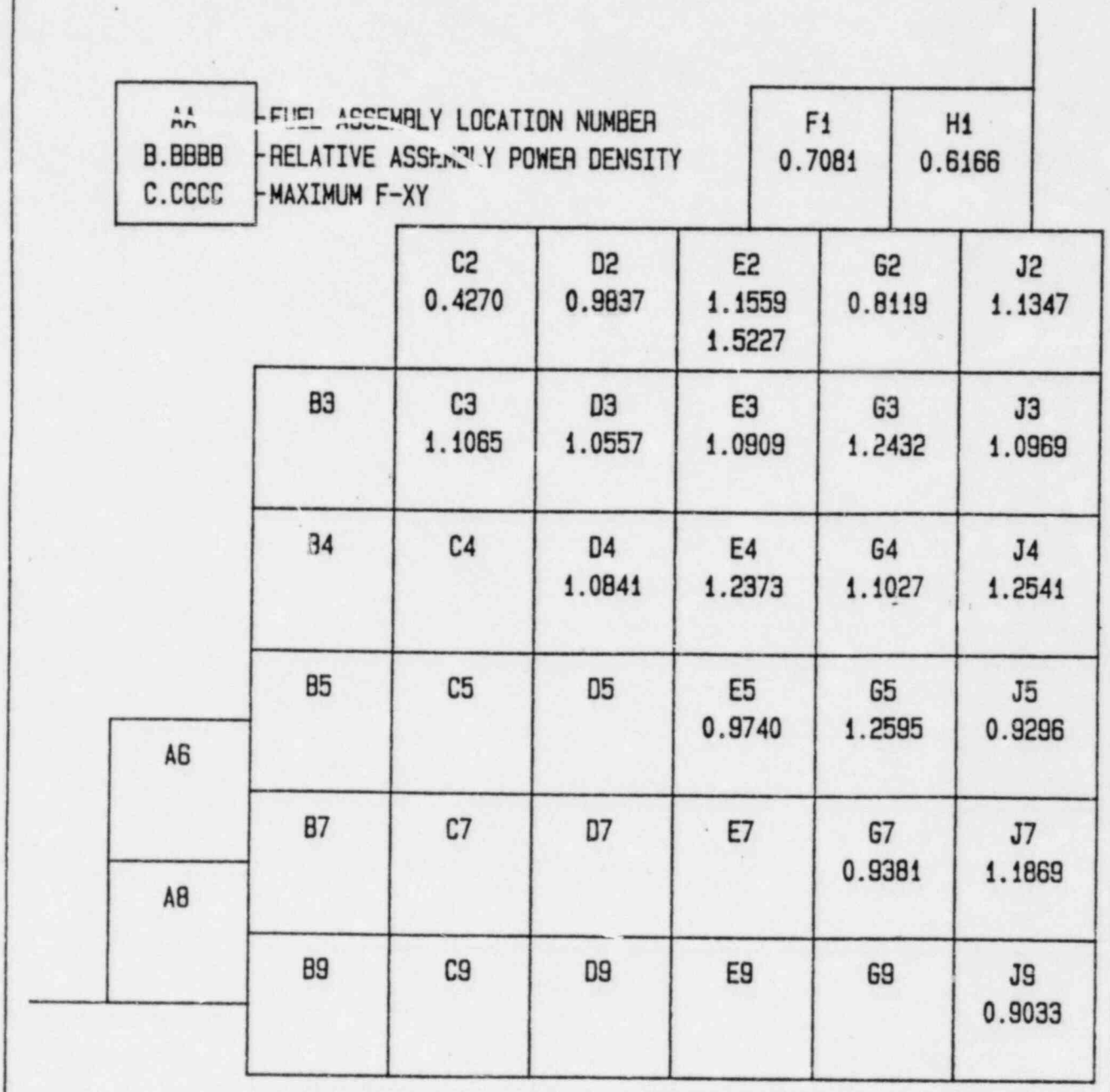

Core Radial Power Distribution End of Cycle (9000 MWD/MTU) ARO	Omaha Public Power District Fort Calhoun Station-Unit No. 1	Figure 3.4-7

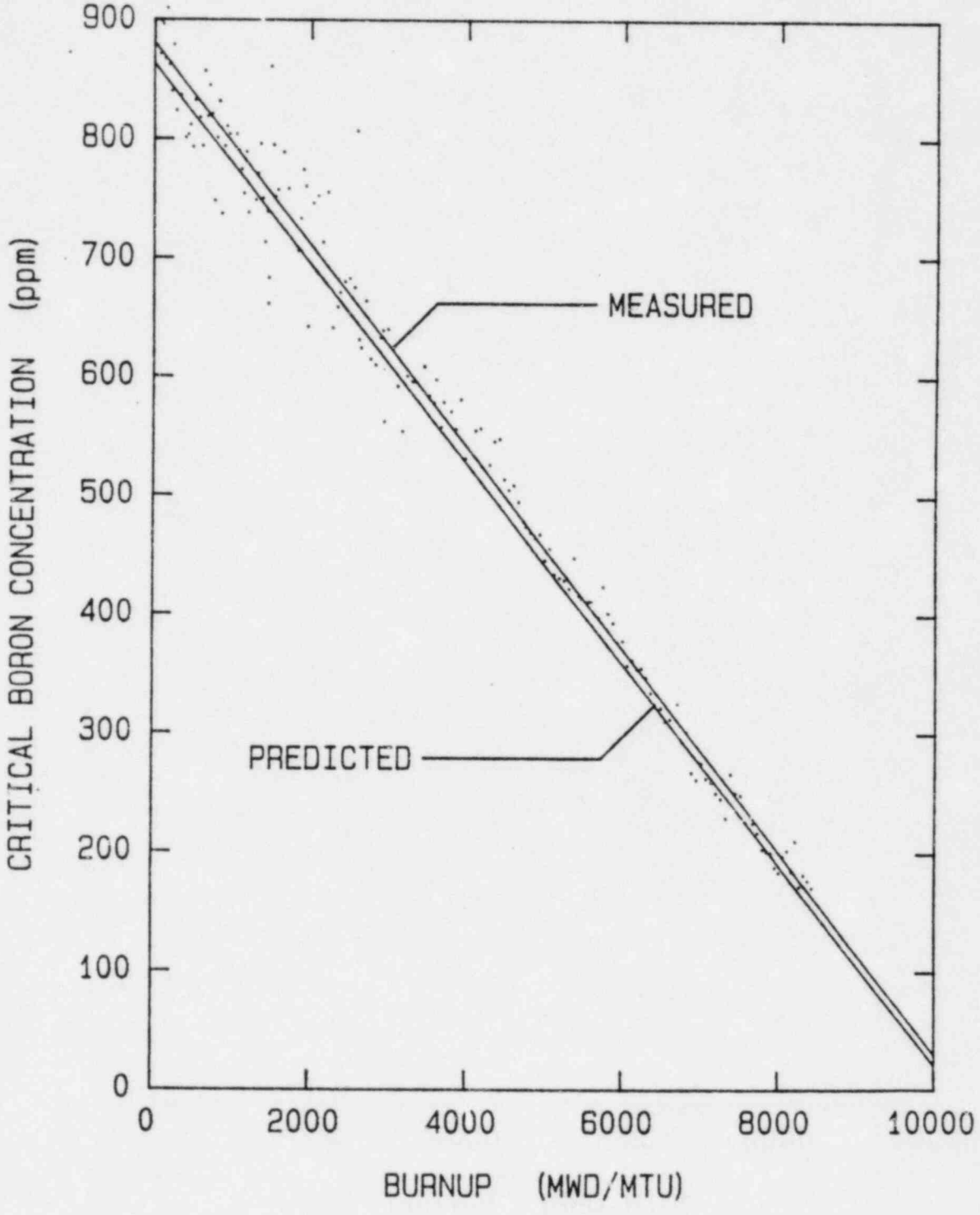

Critical Boron Concentration vs Burnup for Cycle 7	Omaha Public Power District Fort Calhoun Station-Unit No. 1	Figure 3.4-8

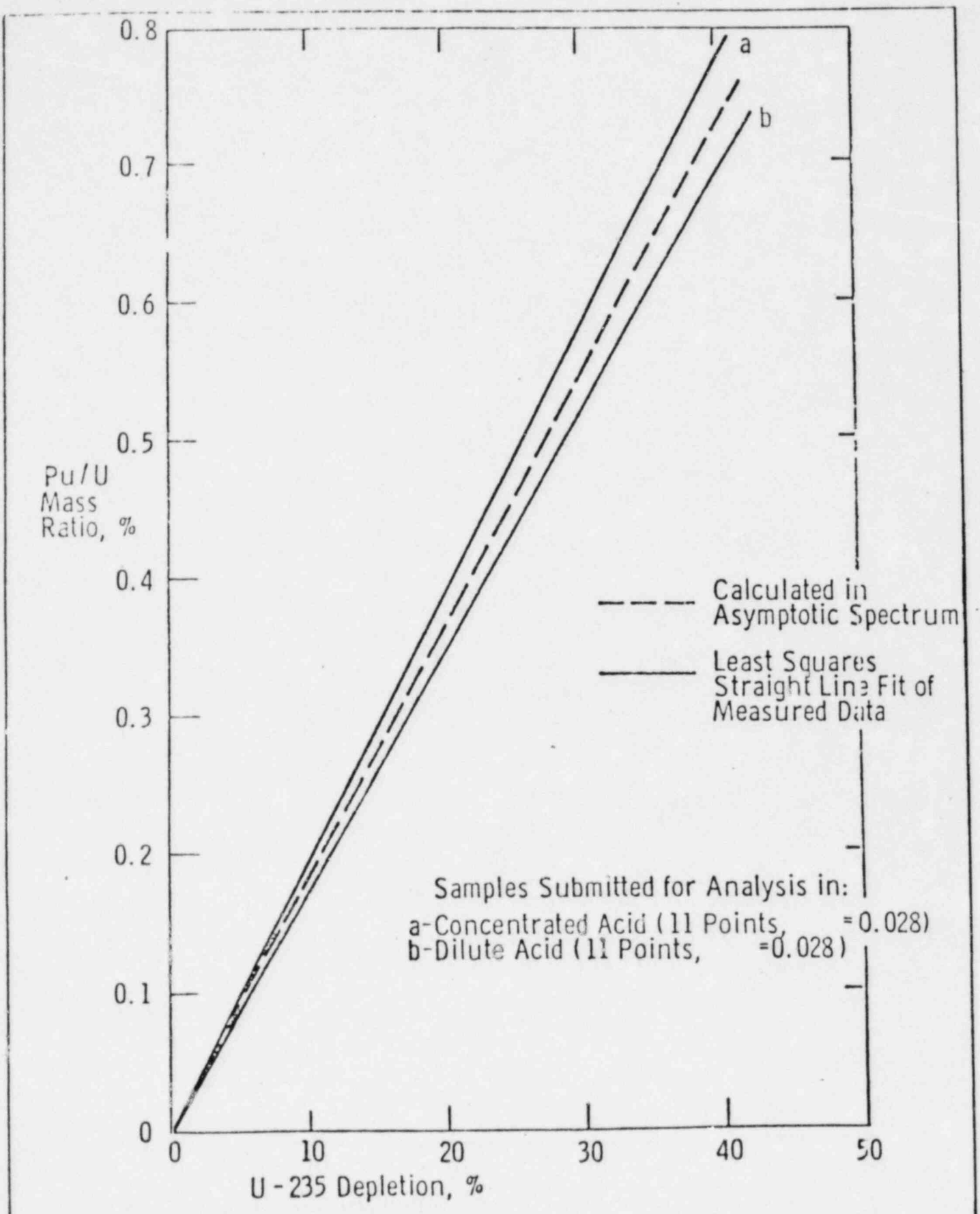

Comparison of Calculated and Measured Plutonium-to-Uranium Mass Ratio in the Asymptotic Neutron Spectrum for Yankee

Omaha Public Power District
Fort Calhoun Station-Unit No. 1

Figure 3.4-9

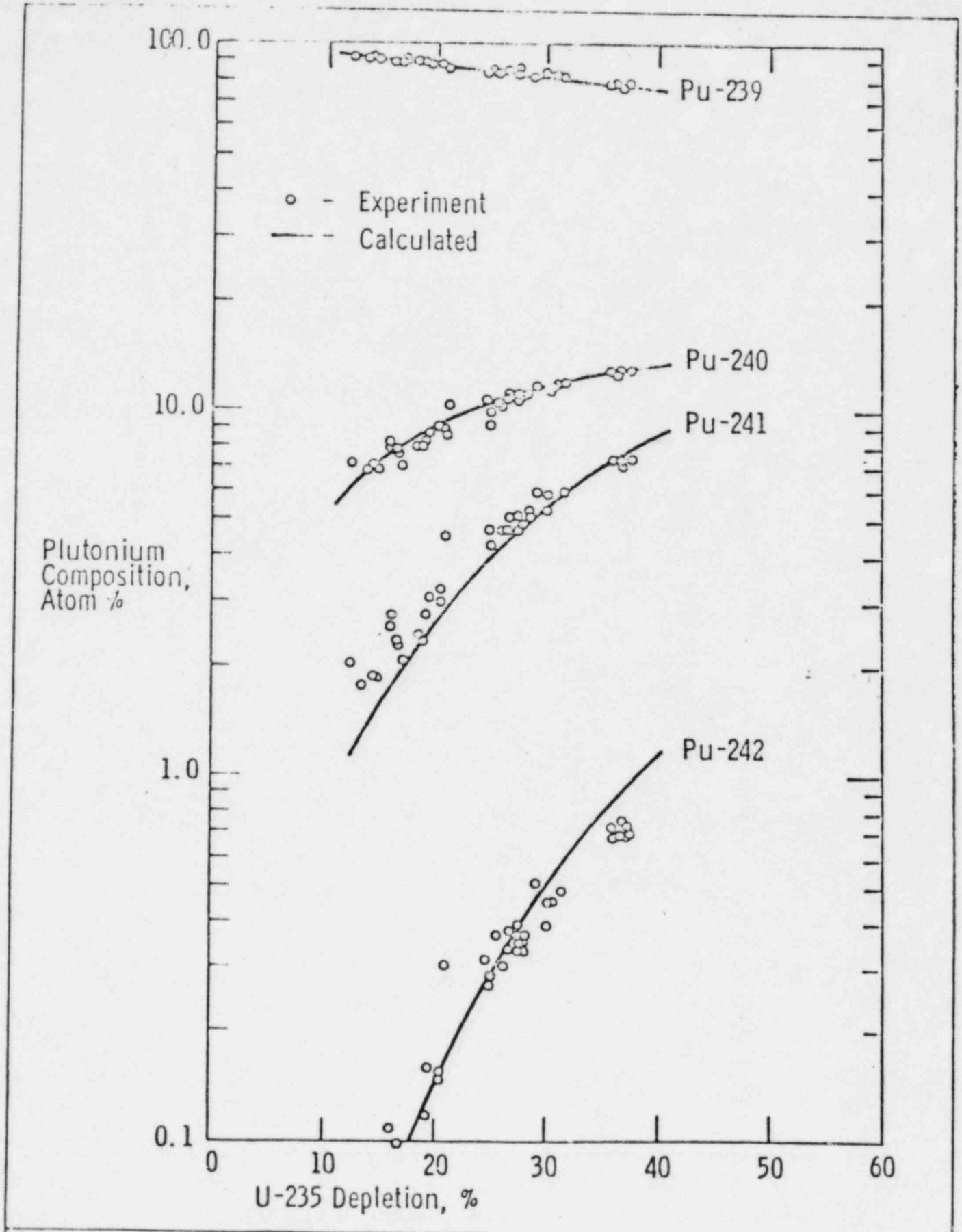

Plutonium Isotopic Composition vs Fuel Depletion in the Asymptotic Spectrum for Yankee

Omaha Public Power District
Fort Calhoun Station-Unit No. 1

Figure 3.4-10

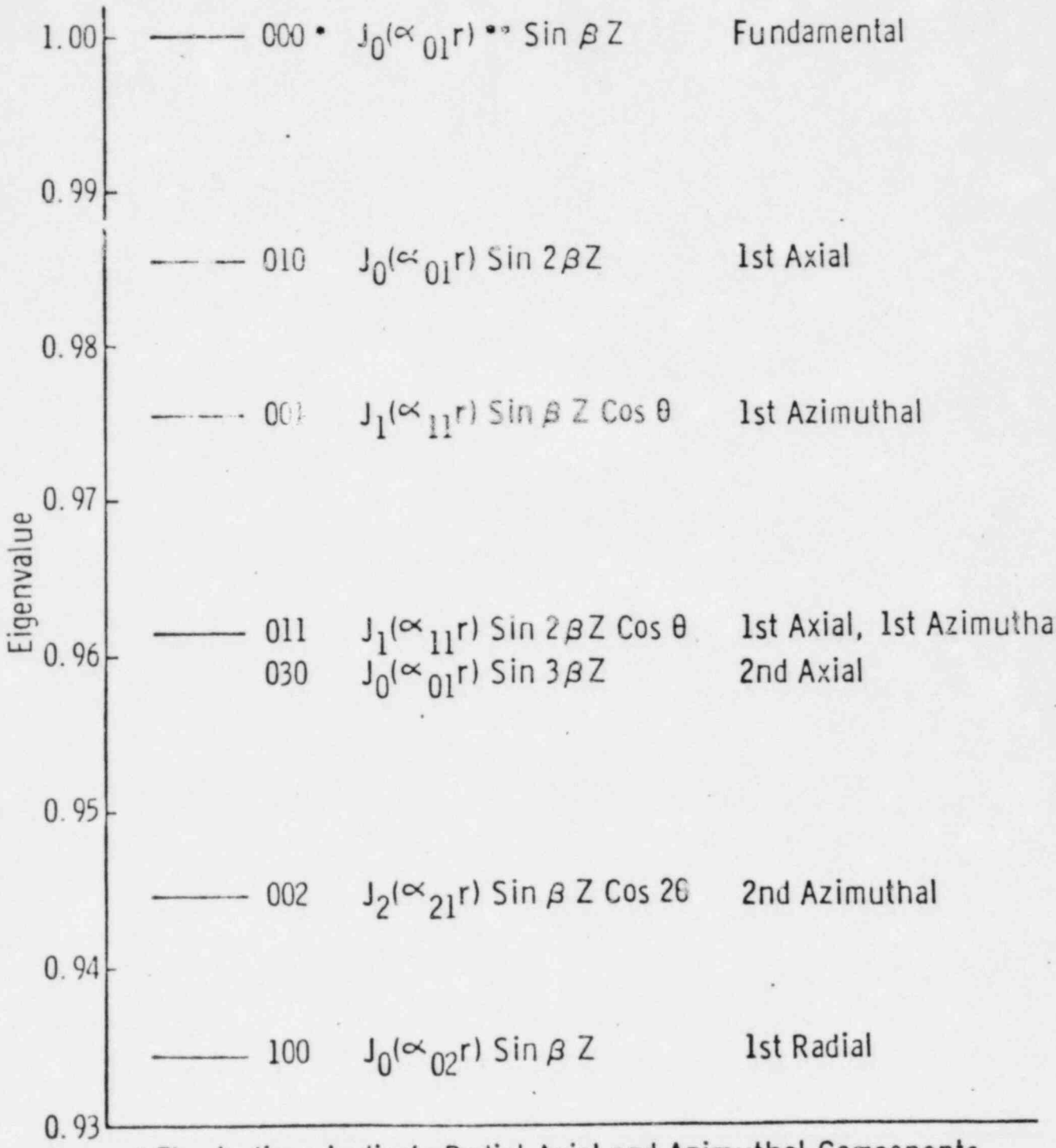

• The Indices Indicate Radial Axial and Azimuthal Components of the Separable Modes in That Order

•• ij Indicates the j^{th} Zero of the i^{th} Bessel Function

Reactivity Difference Between Fundamental and Excited States of a Bare Cylindrical Reactor

Omaha Public Power District
Fort Calhoun Station-Unit No. 1

Figure 3.4-11

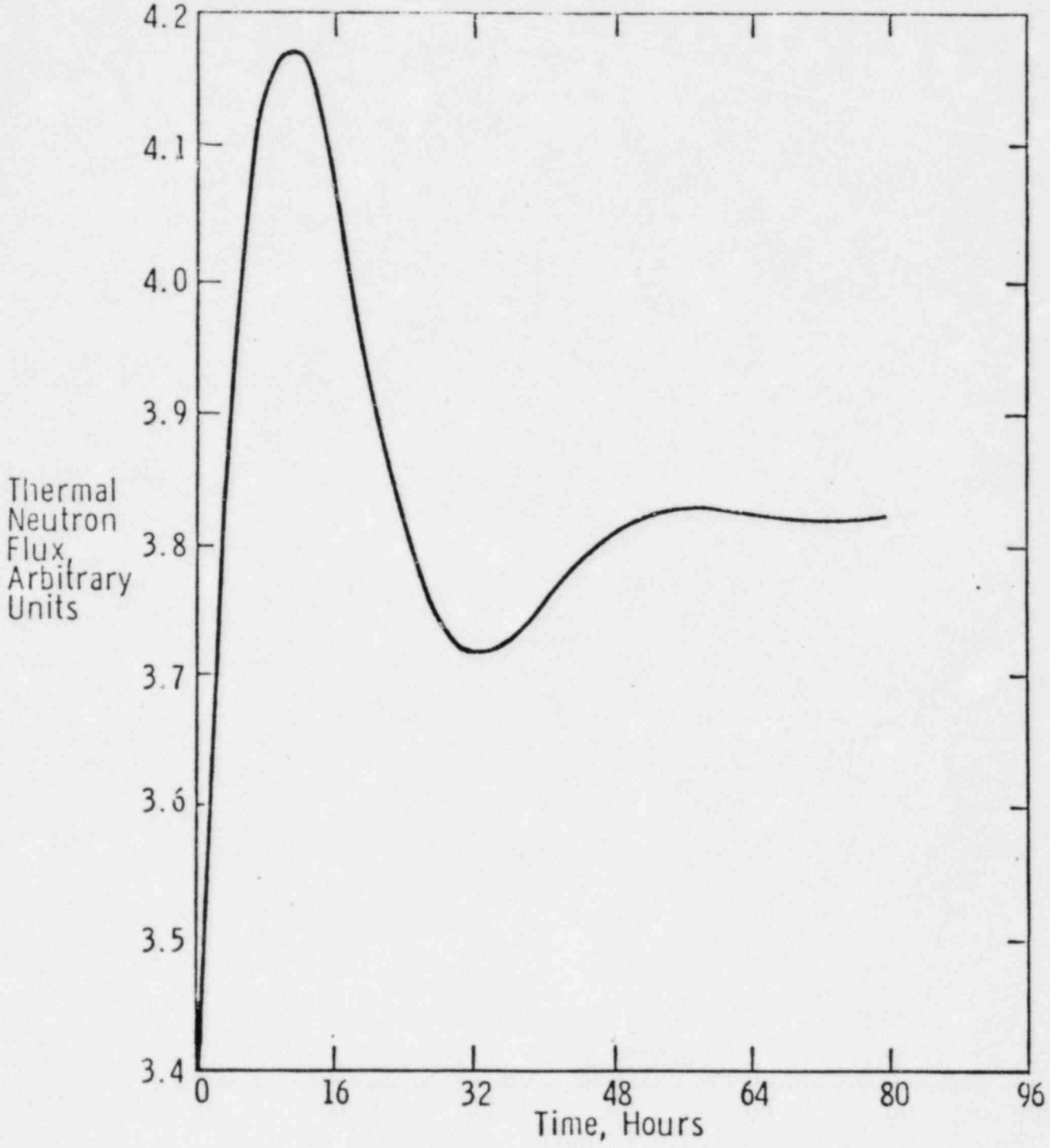

Thermal Neutron Flux at the Center of the Core vs Time	Omaha Public Power District Fort Calhoun Station-Unit No. 1	Figure 3.4-12

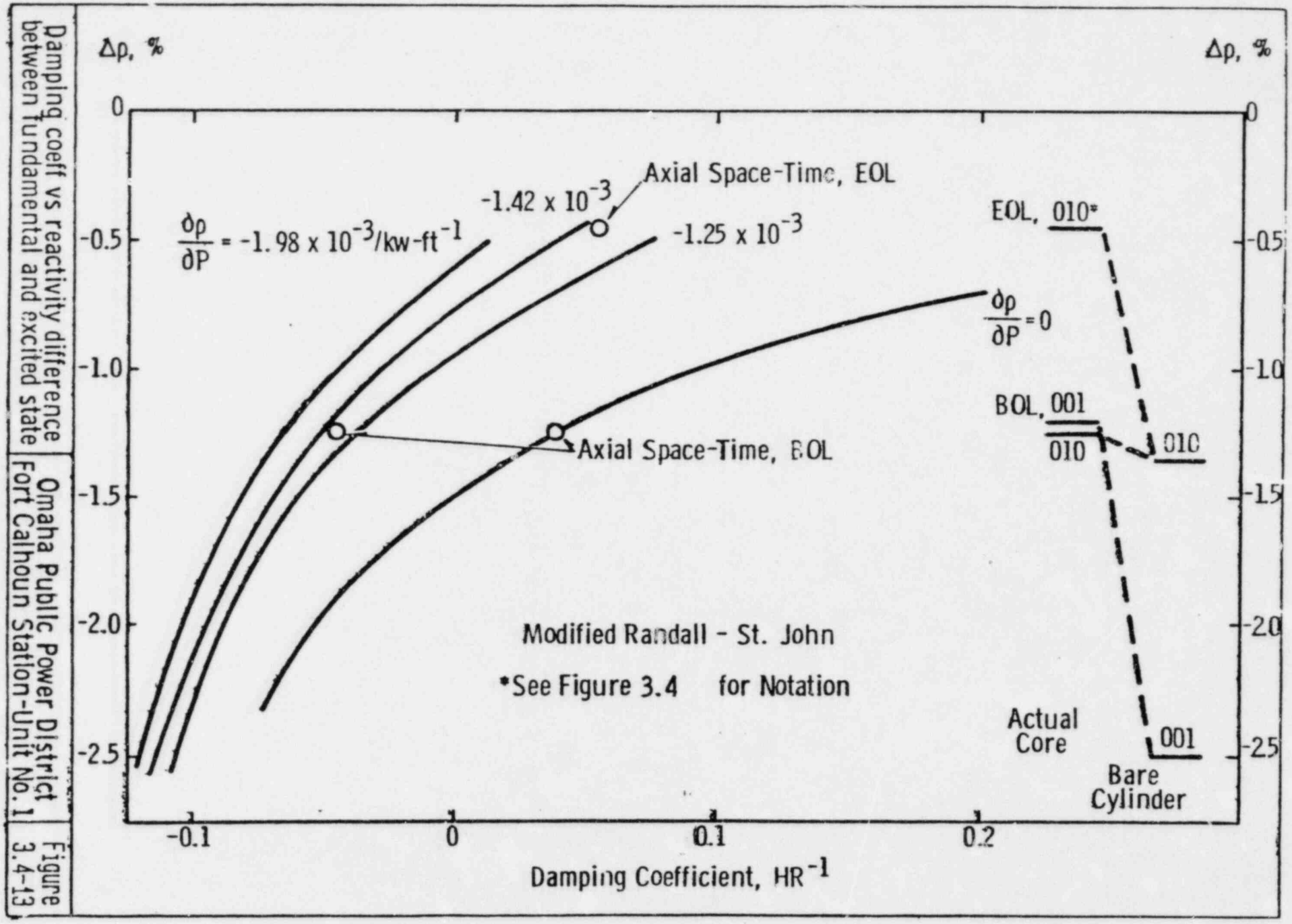

Damping coeff vs reactivity difference between fundamental and excited state

Omaha Public Power District
Fort Calhoun Station-Unit No. 1

Figure 3.4-13

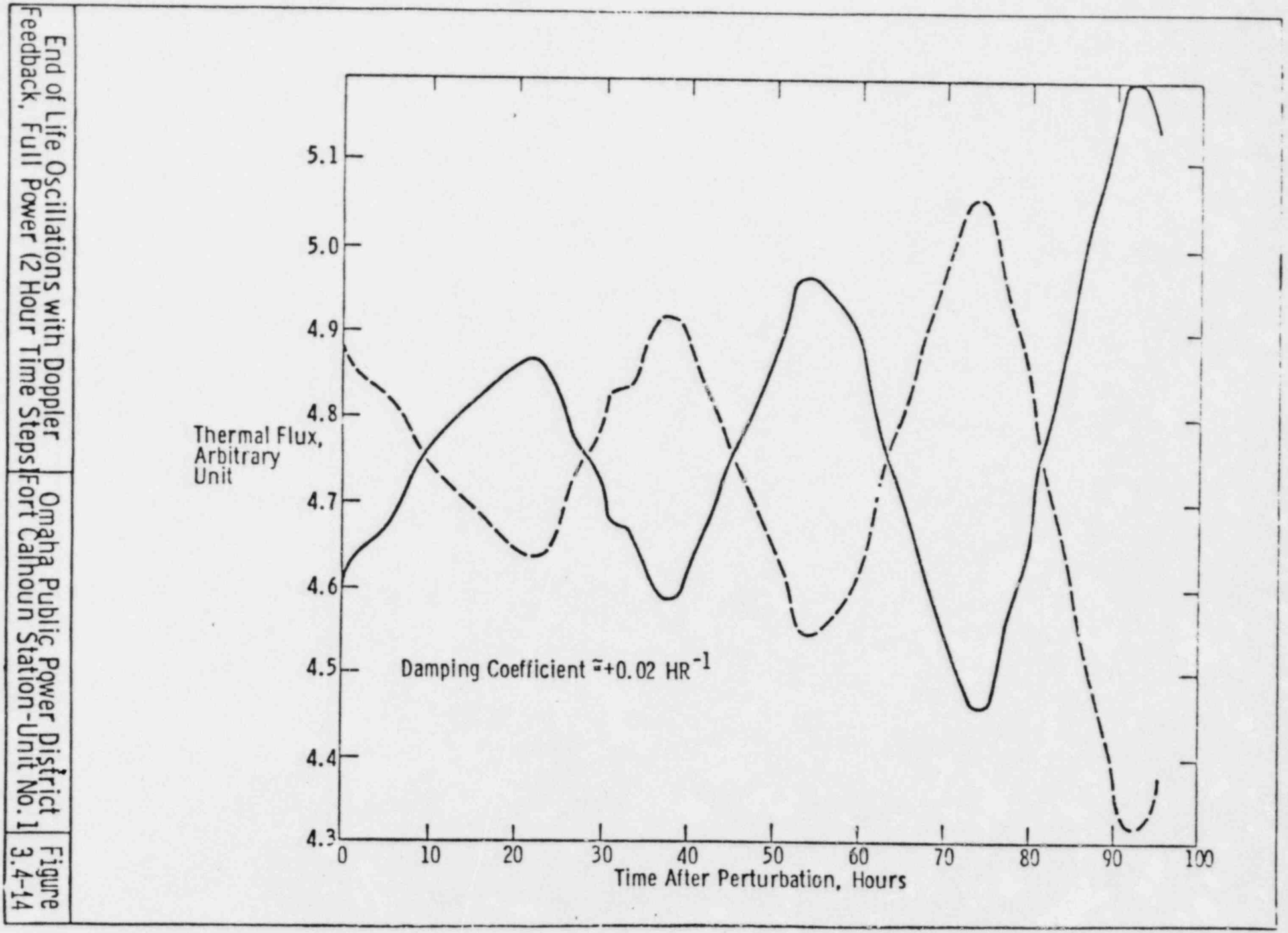

End of Life Oscillations with Doppler Feedback, Full Power (2 Hour Time Steps)

Omaha Public Power District
Fort Calhoun Station-Unit No. 1

Figure 3.4-14

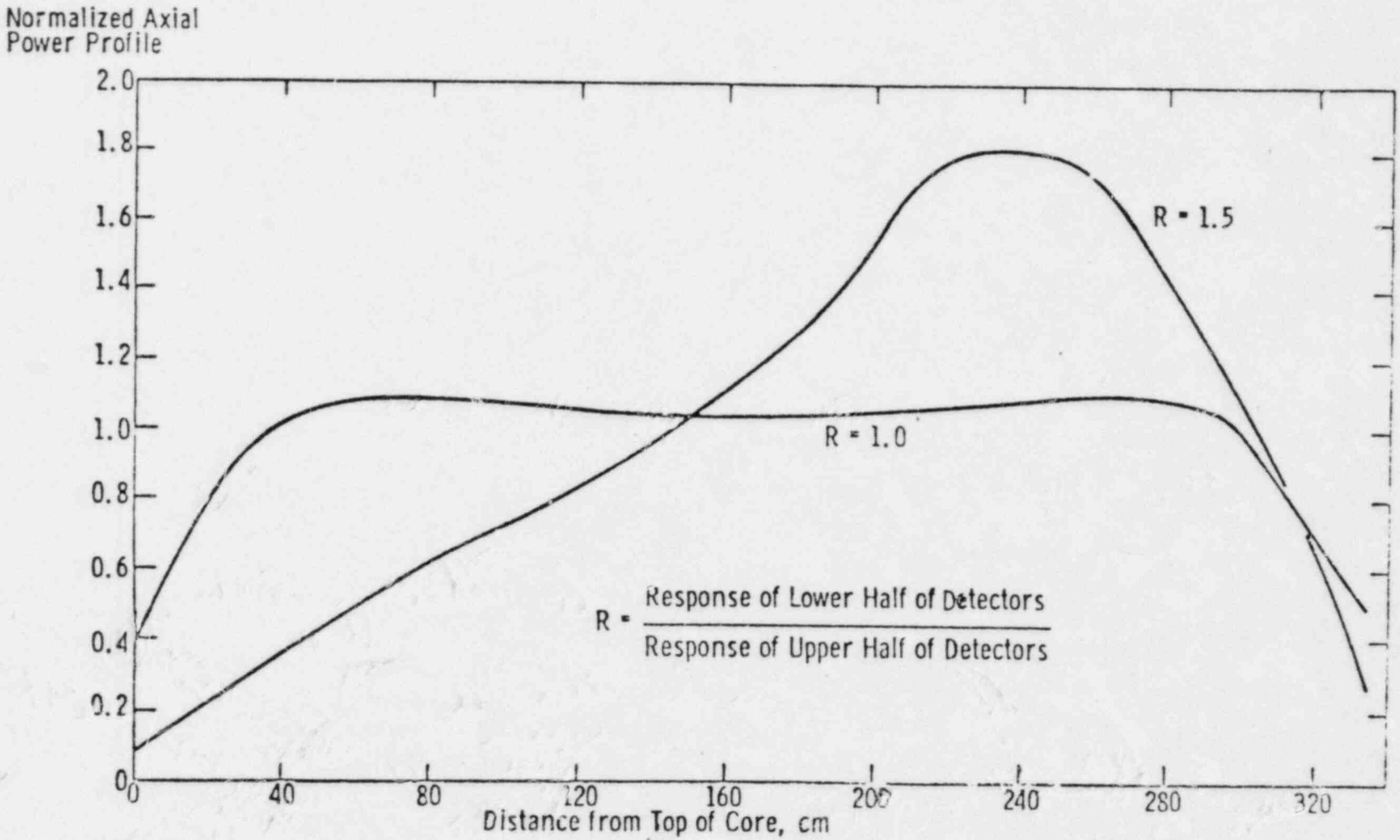

Split Detector Response to Axial Power Profiles in the Core

Omaha Public Power District
Fort Calhoun Station-Unit No. 1

Figure 3.4-15

Omaha Public Power District
Fort Calhoun Station
Unit No. 1

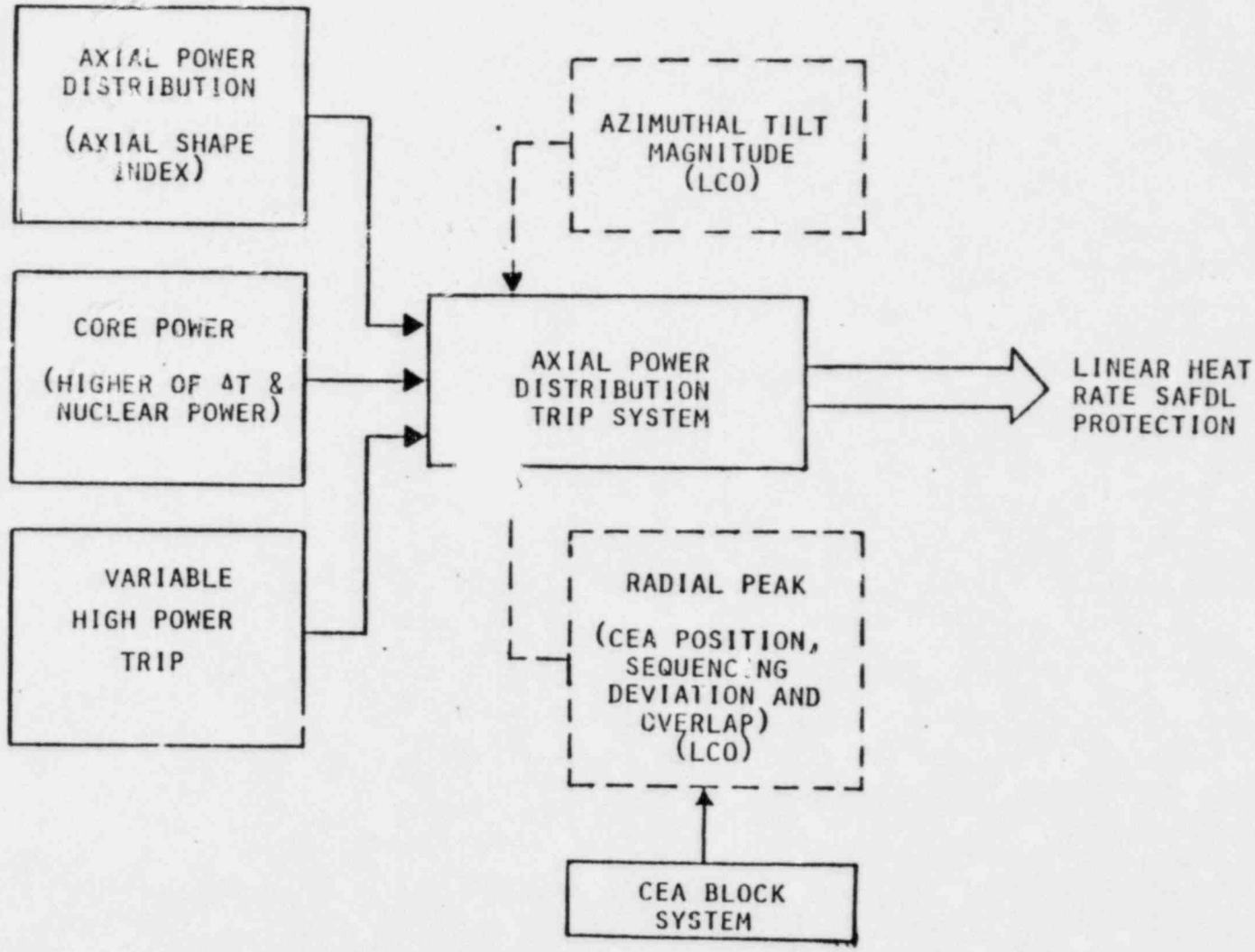

LINEAR HEAT RATE SAFDL PROTECTION BY APD TRIP

FIGURE 3.5-1

Omaha Public Power District Fort Calhoun Station Unit No. 1	INLET TEMPERATURE VS CORE POWER FOR THERMAL MARGIN LIMITS	FIGURE 3.5-2

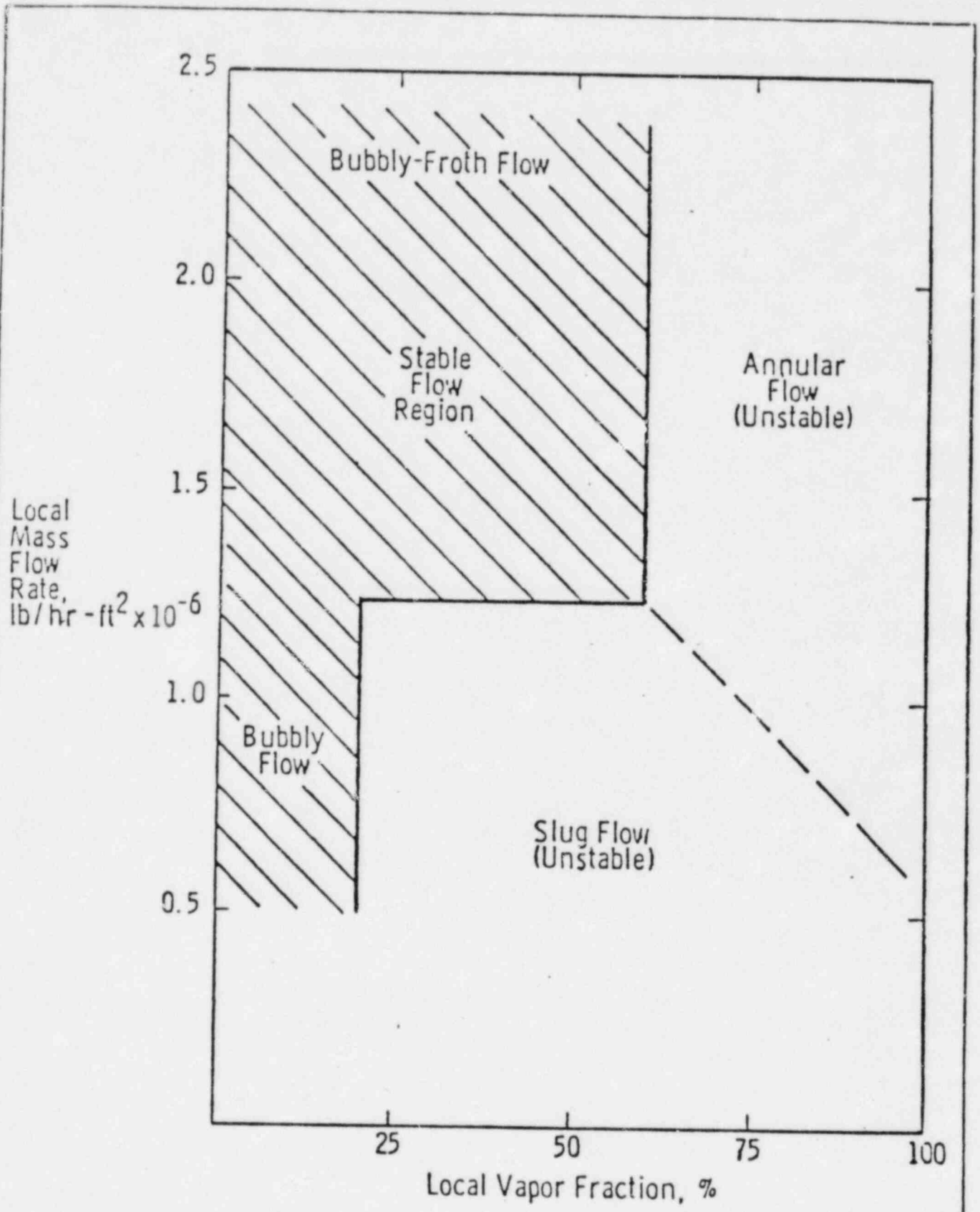

Two Phase Flow Regime Transitions Stable Flow Limits	Omaha Public Power District Fort Calhoun Station-Unit No. 1	Figure 3.5-3

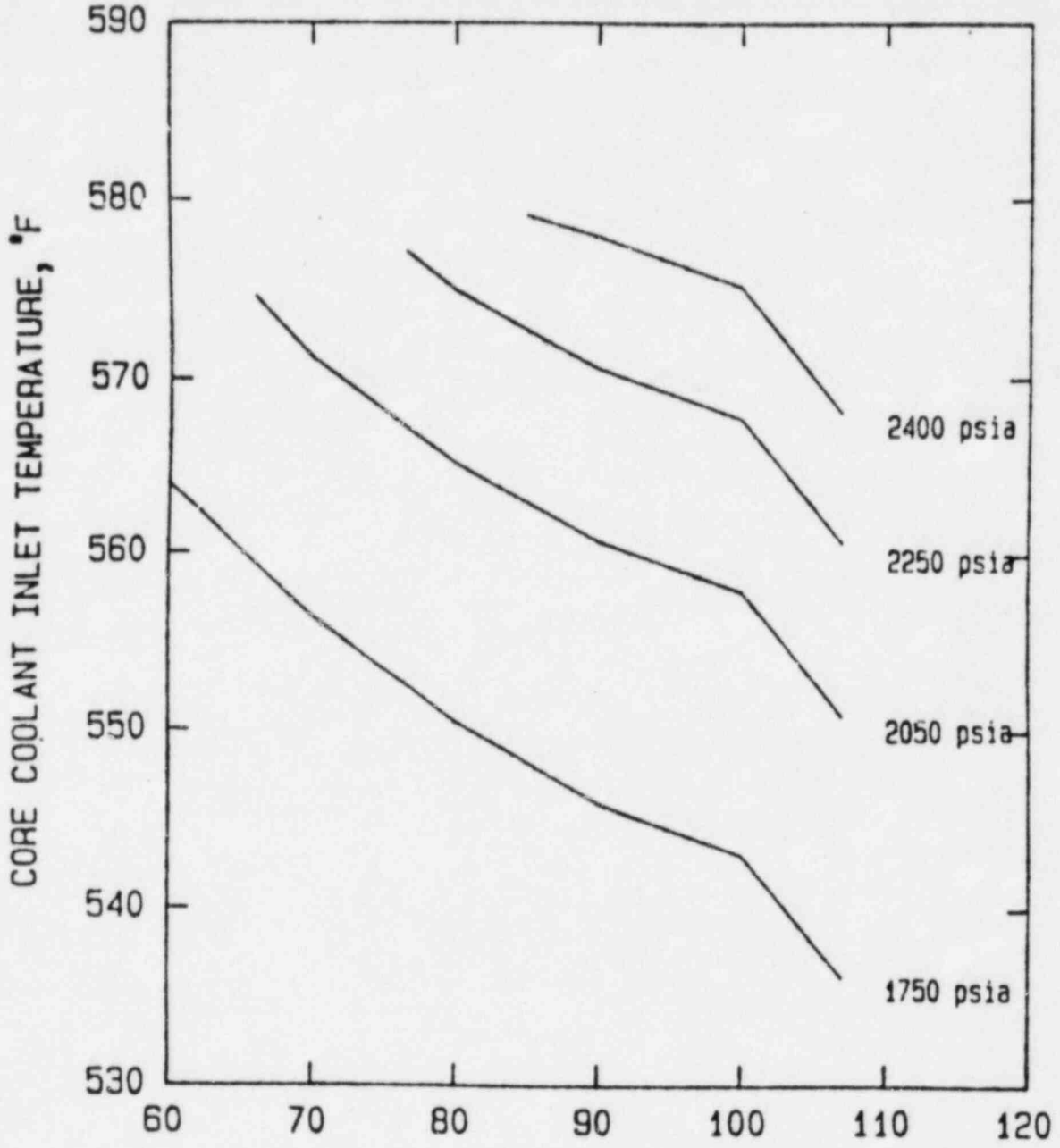

$$P_{VAR} = 20.3\ PF(2)\ B + 20.3\ T_{IN} - 11,283$$

$$PF(B) = 1.0 \quad B \geq 100\%$$
$$= -.008\ B + 1.8 \quad 50\% \leq B \leq 100\%$$
$$= 1.4 \quad B \leq 50\%$$

Thermal Margin/Low Pressure LSSS 4 Pump Operation	Omaha Public Power District Fort Calhoun Station-Unit No. 1	Figure 3.6-1

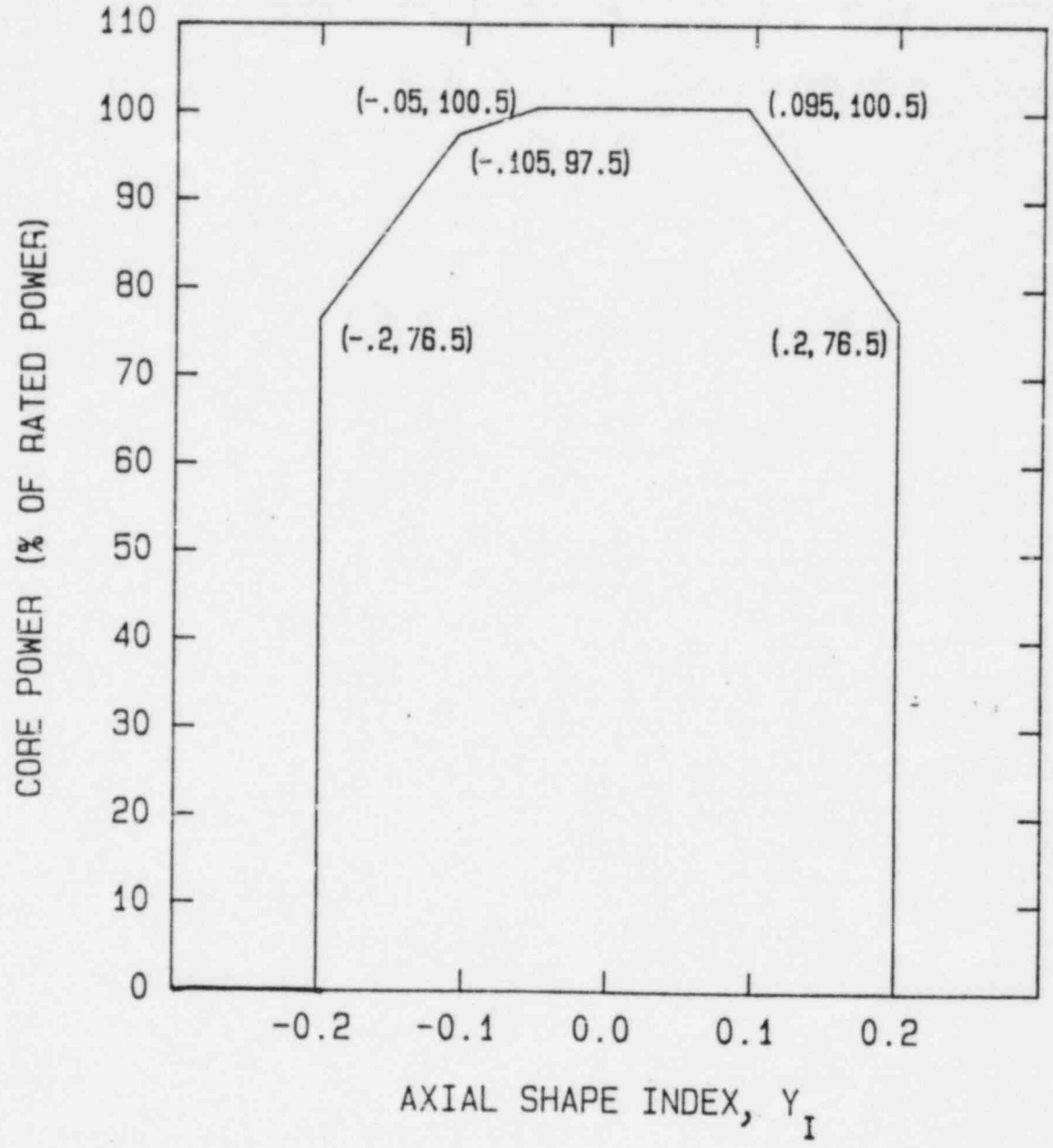

Limiting Condition for Operation for DNB Monitoring	Omaha Public Power District Fort Calhoun Station-Unit No. 1	Figure 3.6-2

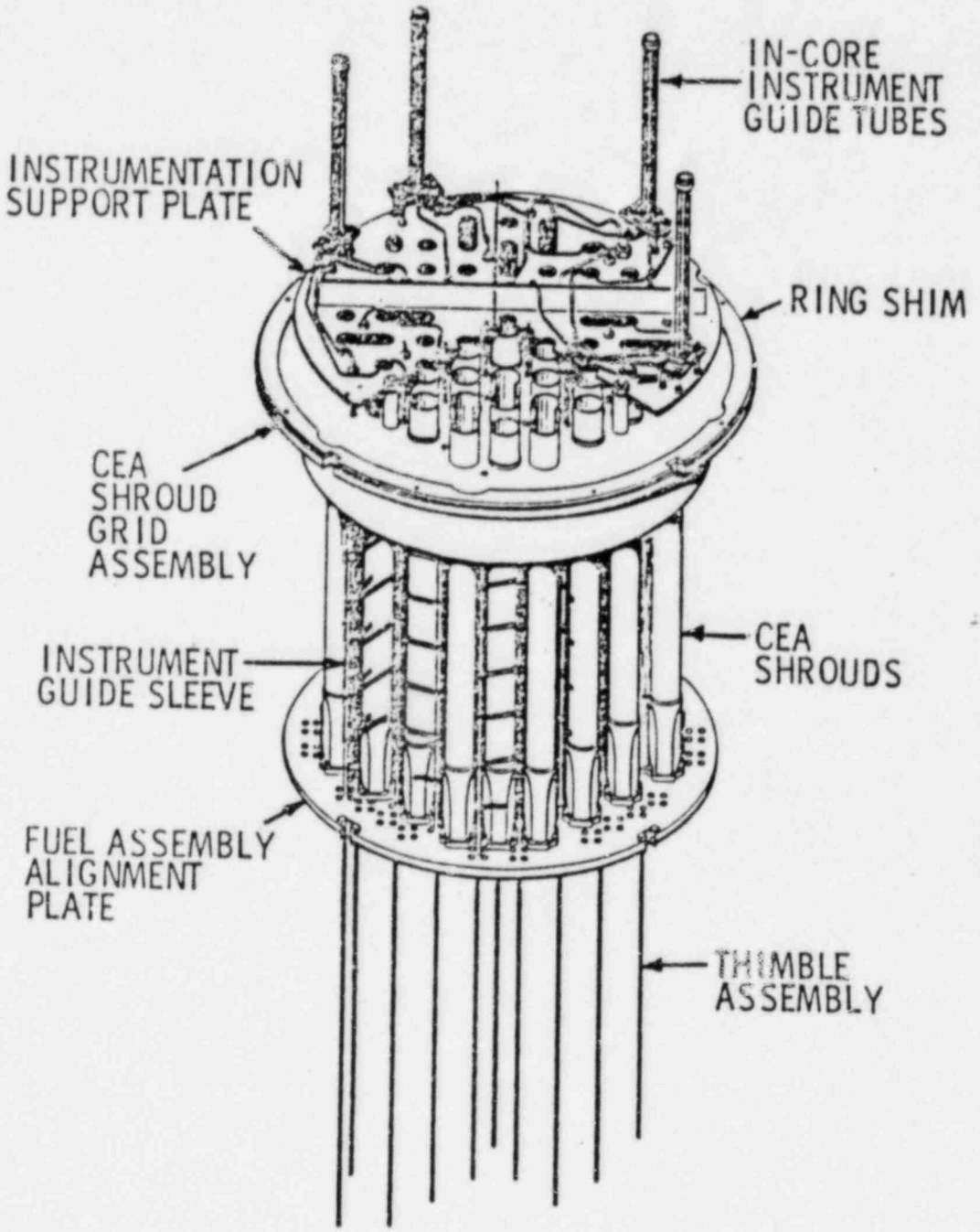

Upper Guide Structure Assembly	Omaha Public Power District Fort Calhoun Station-Unit No. 1	Figure 3.7-1

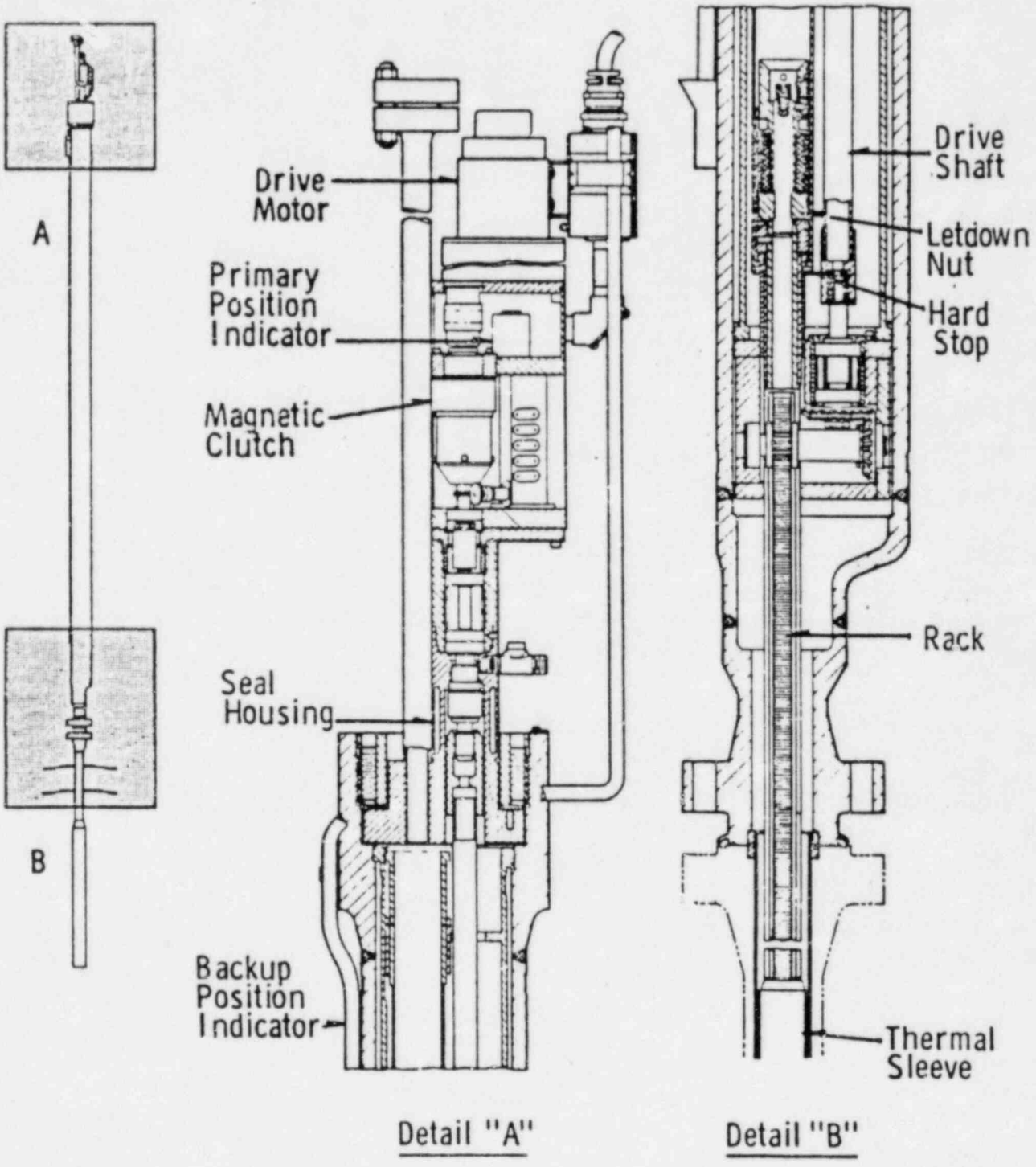

Control Element Drive Mechanism	Omaha Public Power District Fort Calhoun Station-Unit No. 1	Figure 3.7-2

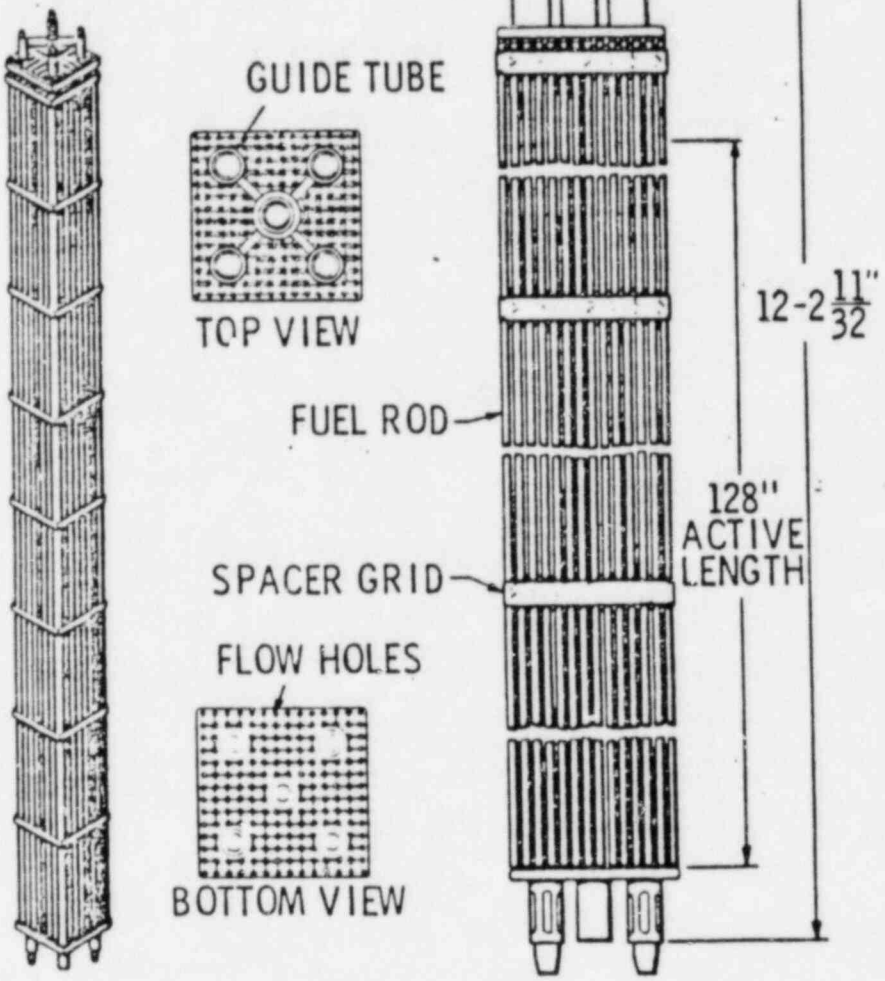

Fuel Assembly	Omaha Public Power District Fort Calhoun Station-Unit No. 1	Figure 3.7-3

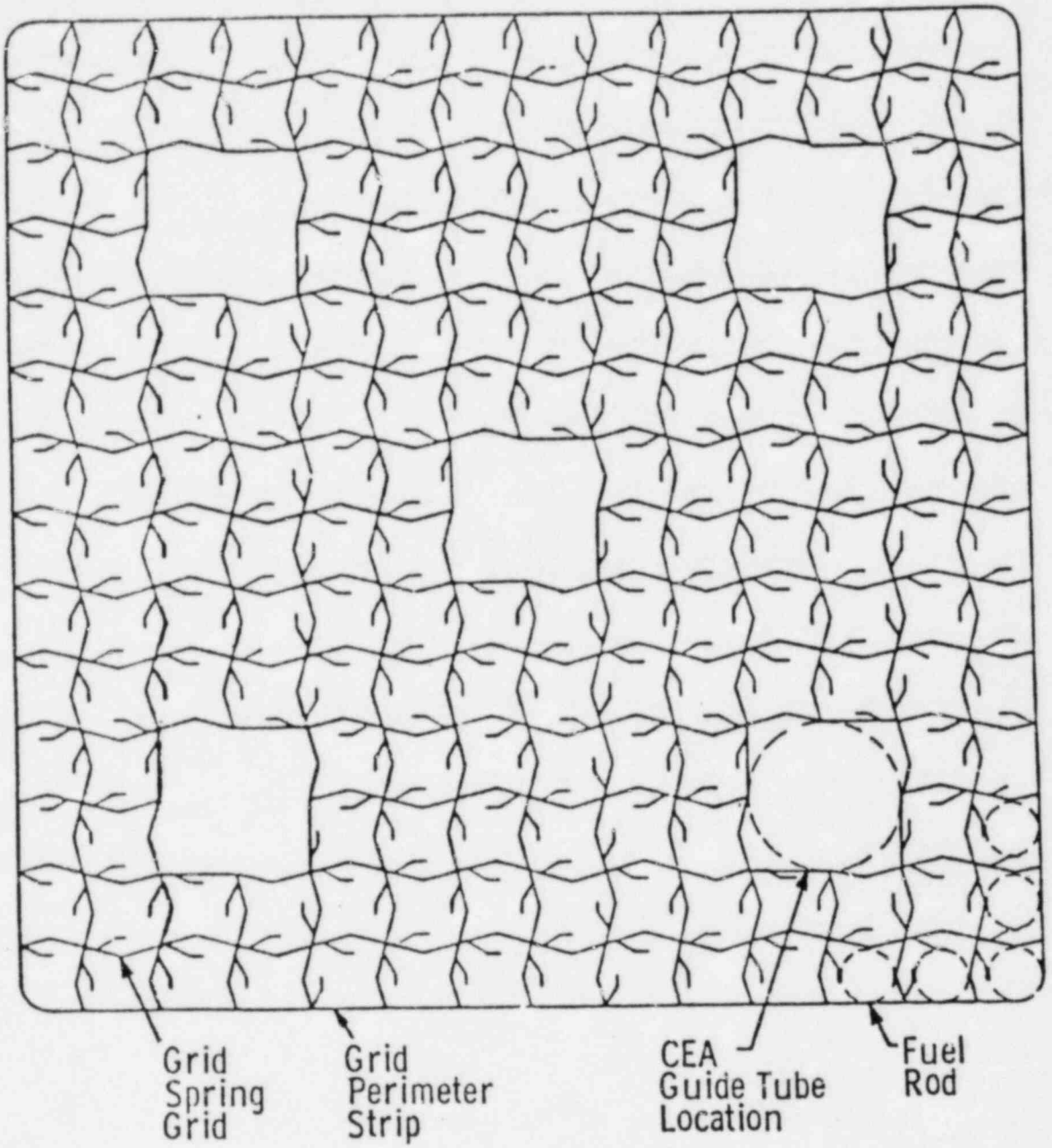

BATCH G FUEL SPACER GRID	Omaha Public Power District Fort Calhoun Station-Unit No. 1	Figure 3.7-4

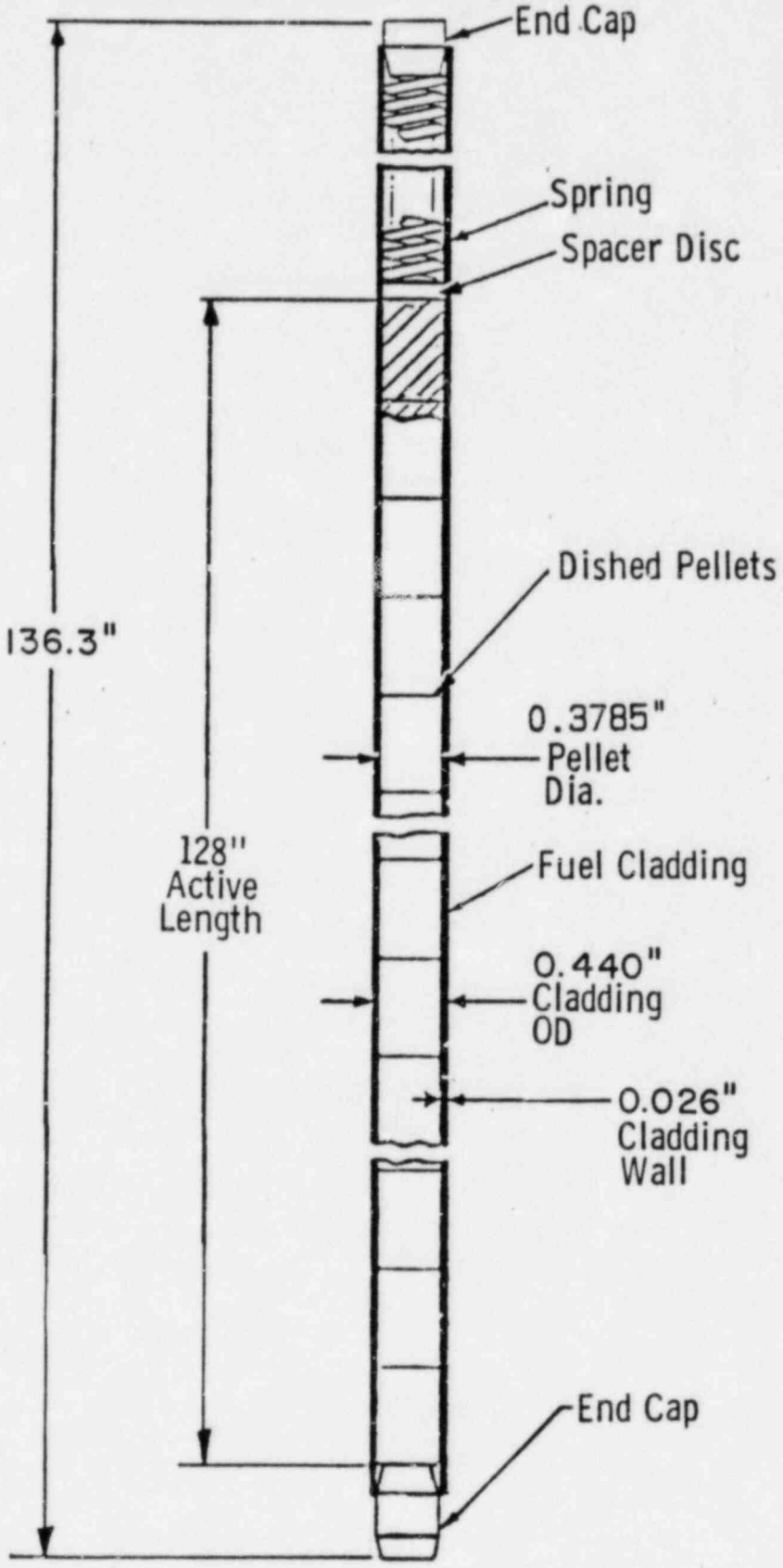

BATCH G FUEL ROD	Omaha Public Power District Fort Calhoun Station-Unit No. 1	Figure 3.7-5

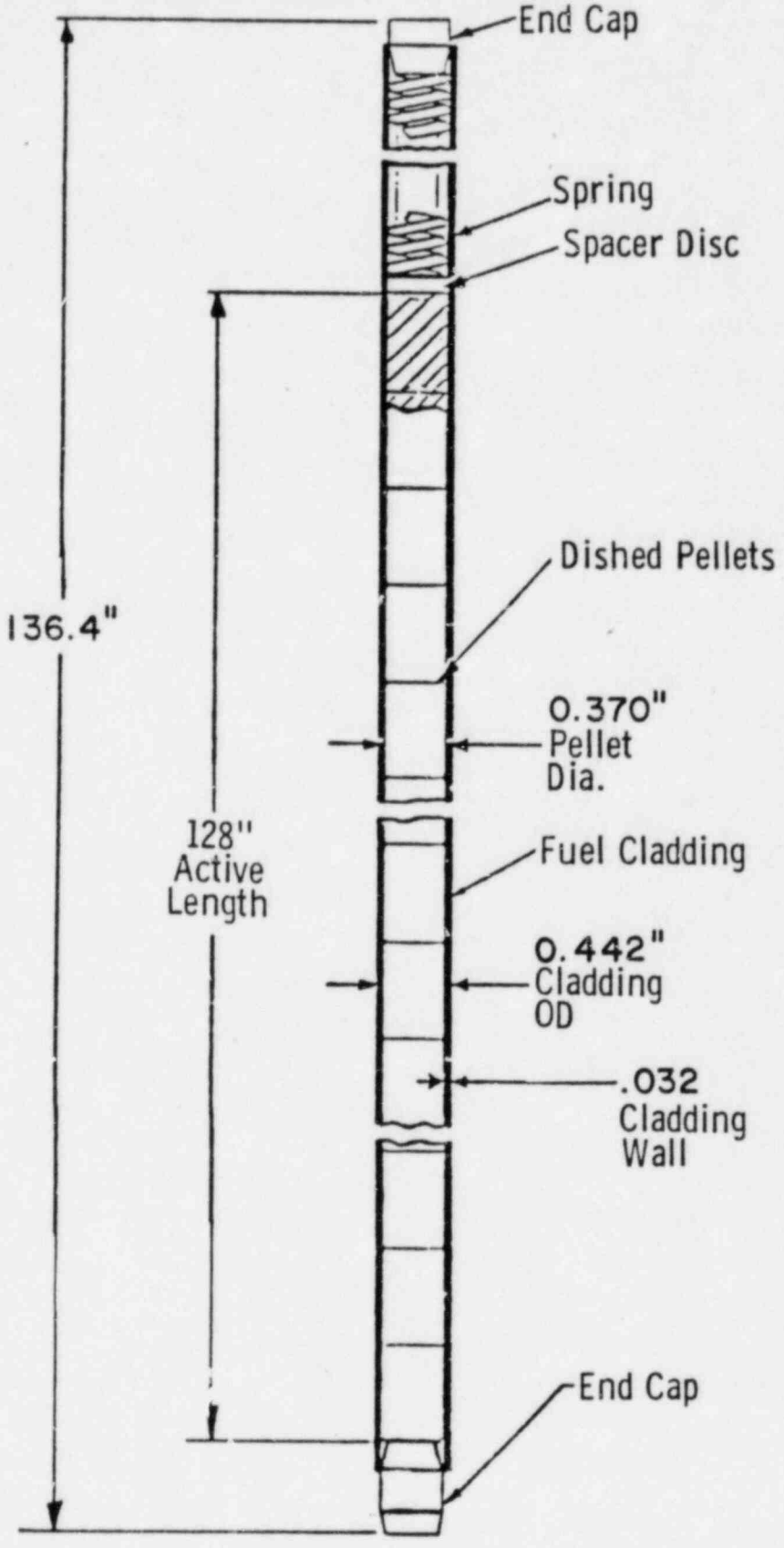

BATCH H & I FUEL ROD	Omaha Public Power District Fort Calhoun Station-Unit No. 1	Figure 3.7-8

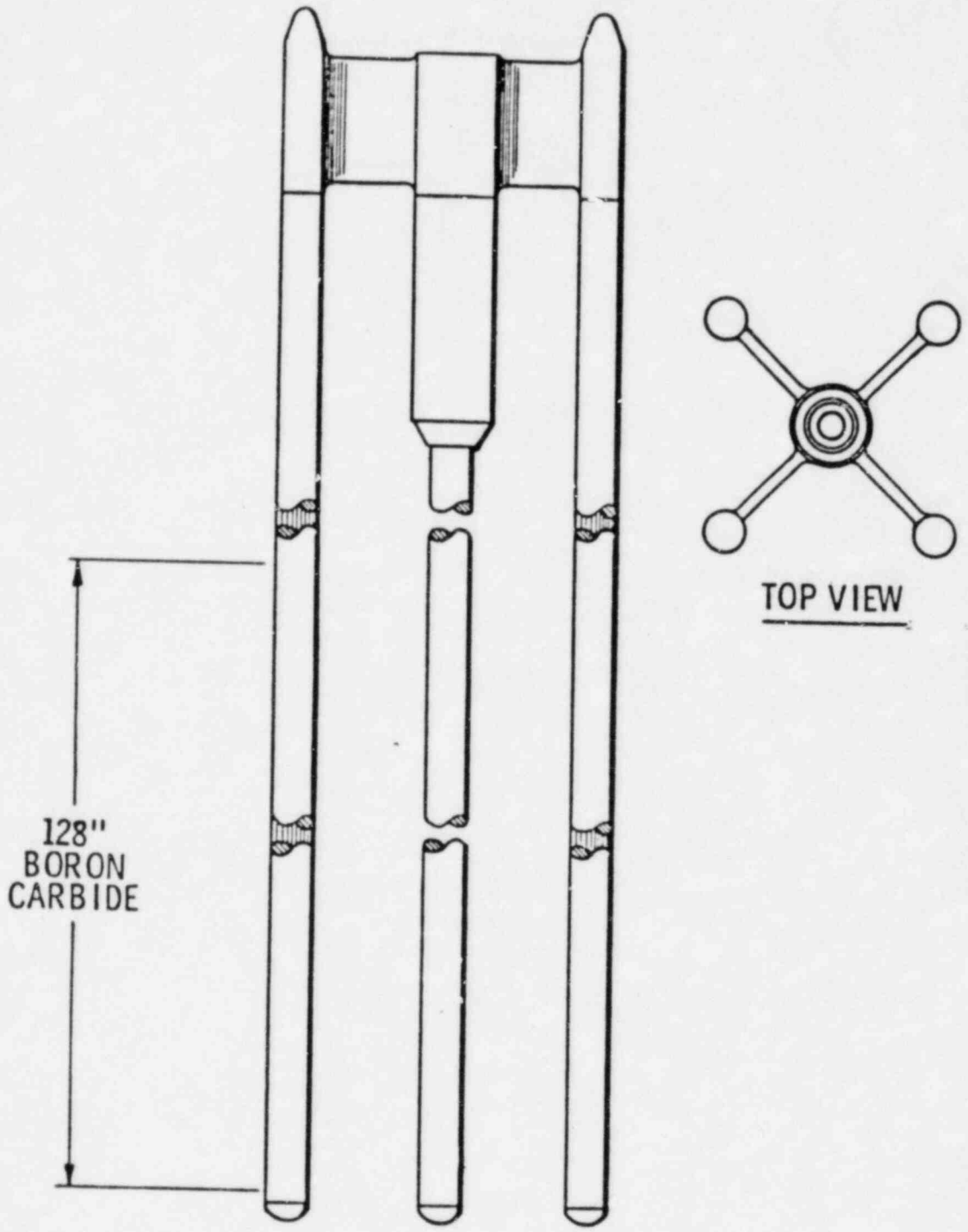

Control Element Assembly, (CEA)	Omaha Public Power District Fort Calhoun Station-Unit No. 1	Figure 3.7-1

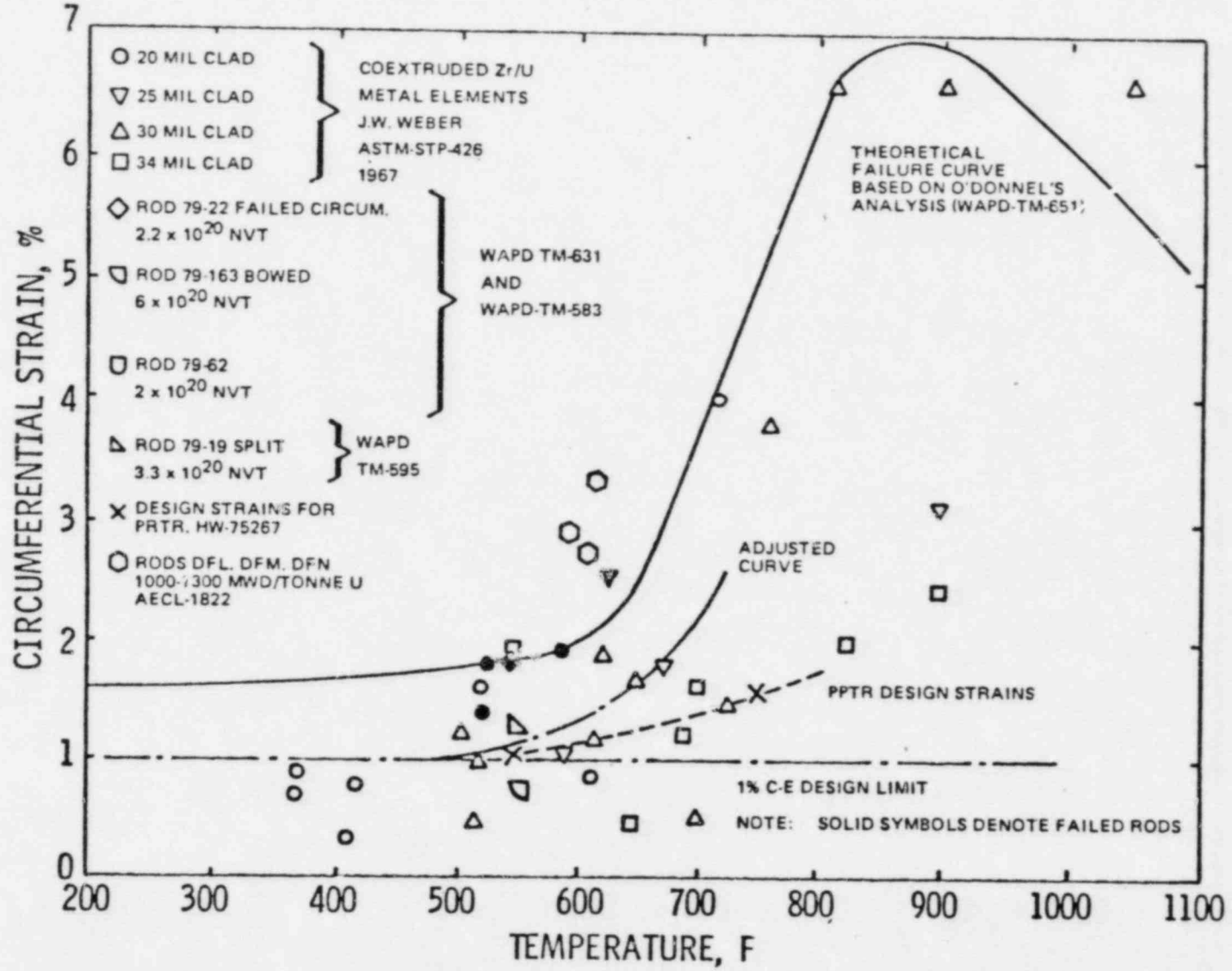

Circumferential Strain vs Temperature

Omaha Public Power District
Fort Calhoun Station-Unit No. 1

Figure 3.8-1

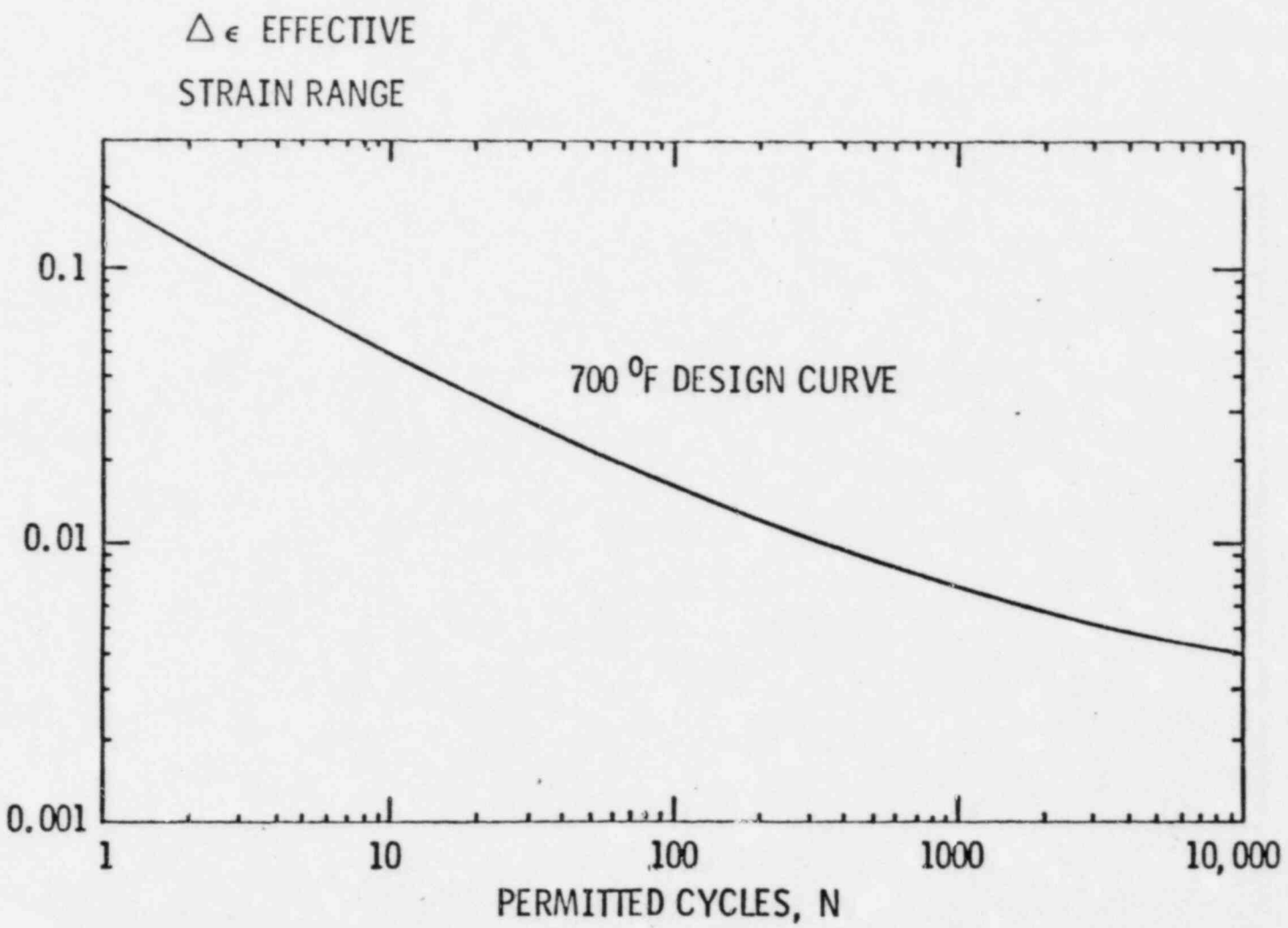

Design Curve For Cyclic Strain Usage Of Zircaloy-4 at 700 Degrees F

Omaha Public Power District
Fort Calhoun Station-Unit No. 1

Figure 3.8-2

14.2 CONTROL ELEMENT ASSEMBLY WITHDRAWAL INCIDENT

14.2.1 General

The sequential CEA group withdrawal event is assumed to occur as a result of a failure in the control element drive mechanism control system or by operator error. The CEA Block System, which was installed after Cycle 1, has eliminated the possibility of an out-of-sequence bank withdrawal or a single CEA withdrawal due to a single failure.

An uncontrolled or unplanned withdrawal of the CEA's results in a positive reactivity addition, which causes the core power, core average heat flux, and reactor coolant system temperature and pressure to rise inturn decreasing the DNB and the linear heat rate (LHR) margins. The pressure increase, if large enough, activates the pressurizer sprays which mitigate the pressure rise. In the presence of a positive moderator temperature coefficient (MTC) of reactivity, the temperature increase results in an additional positive reactivity addition further increasing the severity of the power transient and reducing the DNB and LHR margins.

The withdrawal of the CEA's also causes the axial power distribution to shift to the top of the core. The associated increase in the axial peak is partially compensated by a corresponding decrease in the integrated radial peaking factor. The magnitude of the 3-D peak change depends primarily on the initial CEA configuration and the axial power distribution. Furthermore, the the neutron flux measured by the excore detectors becomes decalibrated due to CEA motion (i.e., rod shadowing effects). This decalibration of excore detectors, however, is partially compensated by reduced neutron attenuation arising from moderator density changes (i.e., temperature shadowing effects).

As the core power and heat flux increase, a reactor trip on high power, variable power, or thermal margin/low pressure may occur to terminate the event depending on the initial operating conditions and the rate of reactivity addition. Other potential reactor trips include axial power distribution and high pressurizer pressure. If a trip occurs, the CEA's drop into the core and insert negative reactivity which quickly terminates further thermal margin degradation. If no trip occurs and corrective action is not taken by the operator, the CEA's fully withdraw and the NSSS achieves a new steady state equilibrium with higher power, temperature, peak LHR and lower hot channel DNBR value.

14.2.1.1 Hot Full Power CEA Withdrawal

Withdrawal of CEA's from full power operating conditions results in a small rate of reactivity addition since the lead bank (normally a low worth bank) can only be inserted 25%. The small positive reactivity addition causes the core power, core average heat flux, and reactor coolant system pressure and temperature to rise. This rise in power is mitigated by the high power trip. It should be noted that for Cycle 8 a TM/LP is not required because the high power trip in conjunction with the initial steady state LCO's prevent the DNBR limits from being exceeded. The calculated TM/LP trip pressure is always less than the actual reactor coolant system pressure (which is increasing).

14.2.1.2 Hot Zero Power CEA Withdrawal

A CEA withdrawal event initiated from lower power levels will exhibit trends similar to the full power CEA withdrawal except that the rate of reactivity addition (and margin degradation) will be greater due to the greater insertion of CEA's allowed by the Technical Specification Power Dependent Insertion Limit LCO (see Technical Specification Figure 2-4). The rate and magnitude of the power, temperature, heat flux and pressure increase is therefore, greater due to the greater reactivity addition. At hot zero power (including subcritical conditions) the withdrawal can result in a significant power spike. The heat flux follows the fission power but is limited by the fuel temperature feedback. The event is terminated by the variable high power trip. The TM/LP trip will not occur because the Pvar calculated pressure will be less than the actual reactor coolant system pressure.

14.2.2 Method of Analysis

The CEA withdrawal incident was analyzed using the CESEC computer code which models neutron kinetics with fuel and moderator temperature feedback, the reactor control system, the reactor coolant system, the steam generators, and the main steam and feedwater systems. The results of the transient simulation, the transient average core heat flux, average channel mass flow rate, reactor core inlet temperature, and reactor coolant system pressure serve as input to CETOP which uses open channel pressure balancing calculations. This code uses the CE-1 correlation to calculate the DNB ratio for the hot channel as a function of time and axial position (see Section 3.6).

Reactivity addition by withdrawal of CEA regulating groups is dependent on the initial position of the groups prior to the withdrawal and on the integral worth of these groups. The regulating groups are withdrawn in a specified sequence having 20 percent group overlap, with the exception of groups 3 and 4 which have a 40 percent overlap, and the position of the groups under steady state conditions is a function of power level (see Technical Specification Figure 2-4).

For both the full power and zero power cases the most positive MTC was used to maximize the positive reactivity feedback from increasing coolant temperatures. To minimize negative reactivity feedback from increasing fuel temperature a 0.85 multiplier was applied to the Doppler coefficient of reactivity. The initial RCS pressure was chosen to be 2053 psia which corresponds to the minimum allowed pressure minus uncertainties. These assumptions yield lower transient minimum DNBR's. The maximum positive reactivity insertion rate, due to the CEA withdrawal, was determined to be bounded by 1.0×10^{-4} $\Delta\rho$/sec for both full power and zero power conditions.

14.2.2.1 Hot Full Power Case

Table 14.2-1 contains a list of the initial conditions and assumptions including uncertainties for Cycle 8 used in the analysis of the full power CEA withdrawal. For the full power case it is conservative not to take credit for the decalibration of the excores due to CEA motion or temperature shadowing effects. A trip on High Power at 112% of rated thermal power was assumed in the analysis.

TABLE 14.2-1
CYCLE 8 KEY PARAMETERS FOR THE HFP CEA WITHDRAWAL EVENT

Parameter	Units	Value
Initial Core Power Level	MWth	1530
Core Inlet Coolant Temperature	°F	547
Reactor Coolant System Pressure	psia	2053
Moderator Temperature Coefficient	10^{-4} Δρ/°F	+.5
Doppler Coefficient Multiplier		0.85
CEA Worth at Trip	% Δρ	5.98
Maximum Reactivity Insertion Rate	10^{-4} Δρ/sec	1.0
CEA Group Withdrawal Rate	in/min	46.0
Total Trip Delay Time	sec	1.4
RTD Time Constant	sec	12.0

14.2.2.2 Hot Zero Power Case

The list of the initial conditions and assumptions including uncertainites for Cycle 8 used in the zero power CEA withdrawal case can be found in Table 14.2-2. In this case, it was conservative to credit the decalibration of the excores due to the CEA motion (i.e., rod shadowing effects) and again, conservatively, no credit was taken for temperature shadowing effects. A reactor trip, initiated by the Variable High Power Trip at 29.1% (19.1% plus 10% uncertainty) of rated thermal power, was assumed in the analysis.

TABLE 14.2-2
CYCLE 8 KEY PARAMETERS FOR THE HZP CEA WITHDRAWAL EVENT

Parameter	Units	Value
Initial Core Power Level	MWth	1.0
Core Inlet Coolant Temperature	°F	532
Reactor Coolant System Pressure	psia	2053
Moderator Temperature Coefficient	10^{-4} Δρ/°F	+.5
Doppler Coefficient Multiplier		0.85
CEA Worth at Trip	% Δρ	5.26
Maximum Reactivity Insertion Rate	10^{-4} Δρ/sec	1.0

TABLE 14.2-2 (Continued)
CYCLE 8 KEY PARAMETERS FOR THE HZP CEA WITHDRAWAL EVENT

Parameter	Units	Value
CEA Group Withdrawal Rate	in/min	46.0
Total Trip Delay Time	sec	.9
RTD Time Constant	sec	12.0

14.2.3 Results

The CEA Withdrawal event was reanalyzed for Cycle 8 to determine the initial margins that must be maintained by the Limiting Conditions for Operation (LCO's) such that the DNBR and the peak LHR design limits will not be exceeded in conjunction with the High Power and Variable High Power Trips.

Protection against exceeding the DNBR limit for the CEA withdrawal at full power is provided by the initial steady state thermal margin which is maintained by adhering to the Technical Specifications LCO's on DNBR margin and by the response of the RPS which provides an automatic reactor trip on high power level. The minimum DNBR for this event, when initiated from the extremes of the LCO's is 1.30 using the CE-1 correlation. The analysis shows that the peak LHR is well below the acceptable value of 21 kw/ft. The sequence of events for the full power case is presented in Table 14.2-3. Figures 14.2-1 through 14.2-4 show the transient behavior of core power, core average heat flux, reactor coolant system temperatures, and the RCS pressure for the full power case.

The zero power case intiated at limiting conditions of operation results in a minimum CE-1 DNBR of 6.01. Also, the analysis shows that the peak linear heat rate acquired is well within the acceptable limit. Table 14.2-4 contains the sequence of events for the zero power case. The transient behavior of the core power, core average heat flux, reactor coolant system temperatures, and the RCS pressure are presented in Figures 14.2-5 through 14.2-8.

TABLE 14.2-3
CYCLE 8
SEQUENCE OF EVENTS FOR THE HFP CEA WITHDRAWAL EVENT

Time (sec)	Event	Setpoint or Value
0.0	CEA Withdrawal Causes Uncontrolled Reactivity Insertion	---
4.571	High Power Trip Signal Was Generated	112% of 1500 MWt
5.471	Reactor Trip Breakers Open	---
5.971	CEA's Begin to Drop Into Core	---
6.190	Maximum Core Power	115.61% of 1500 MWt

TABLE 14.2-3 (Continued)
CYCLE 8
SEQUENCE OF EVENTS FOR THE HFP CEA WITHDRAWAL EVENT

Time (sec)	Event	Setpoint or Value
6.475	Maximum Heat Flux	110.0% of 1500 MWt
6.475	Minimum CE-1 DNBR	1.30
6.570	Maximum RCS Pressure, psia	2075.67

TABLE 14.2-4
CYCLE 8
SEQUENCE OF EVENTS FOR THE HZP CEA WITHDRAWAL EVENT

Time (sec)	Event	Setpoint or Value
0.0	CEA Withdrawal Causes Uncontrolled Reactivity Insertion	---
34.173	Variable High Power Trip Signal Generated	29.1% of 1500 MWt
34.573	Reactor Trip Breakers Open	---
35.073	CEA's Begin to Drop Into Core	---
35.449	Maximum Core Power	40.66% of 1500 MWt
36.298	Maximum Heat Flux	27.94% of 1500 MWt
36.298	Minimum CE-1 DNBR	6.01
39.877	Maximum RCS Pressure, psia	2210.54

14.2.4 Conclusions

The CEA Withdrawal Incident when initiated at either hot full power or hot zero power conditions from the Technical Specification LCO's will not lead to a DNBR or a LHR which will exceed the design limits. Neither of the design limits are exceeded for this event and no pins are predicted to fail.

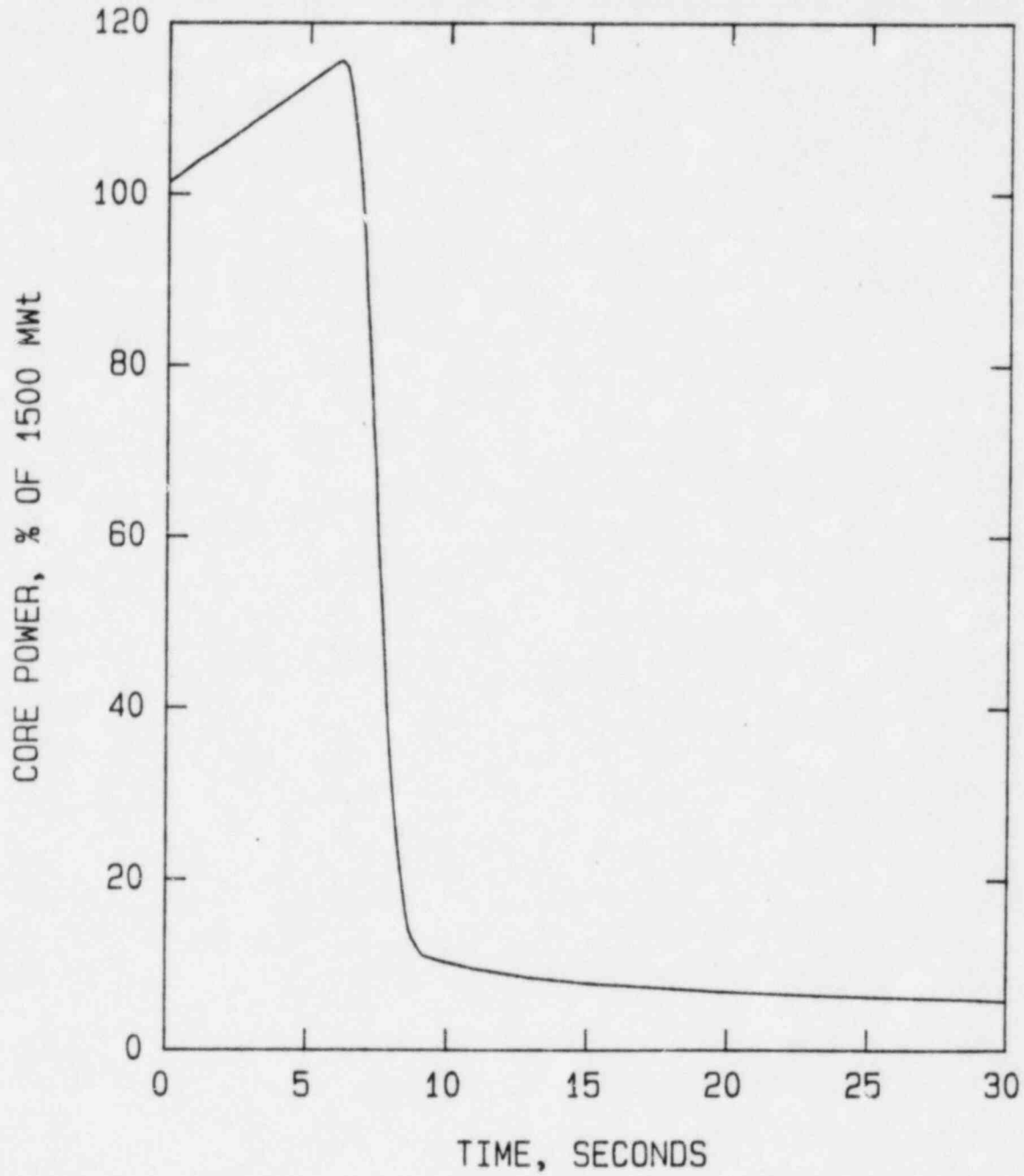

NOTE:

Initial Power Level At 1530 MWt

Reactivity Addition Rate Of $1.0 \times 10^{-4} \Delta\rho$/sec

CEA Withdrawal Incident Core Power vs Time	Omaha Public Power District Fort Calhoun Station-Unit No. 1	Figure 14.2-1

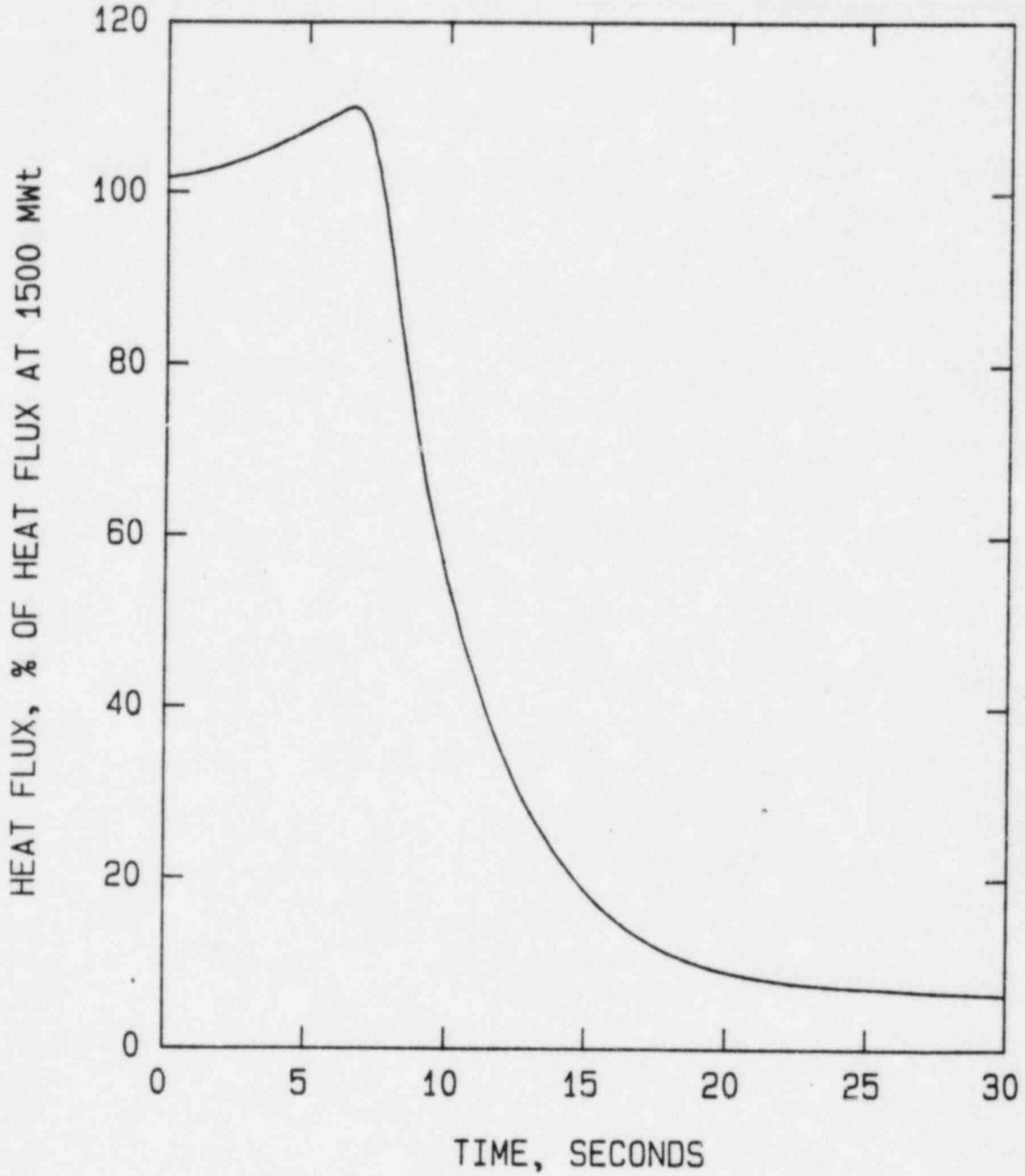

NOTE:

Initial Power Level At 1530 MWt
Reactivity Addition Rate Of $1.0 \times 10^{-4} \Delta\rho$ /sec

CEA Withdrawal Incident Core Average Heat Flux vs Time	Omaha Public Power District Fort Calhoun Station-Unit No. 1	Figure 14.2-2

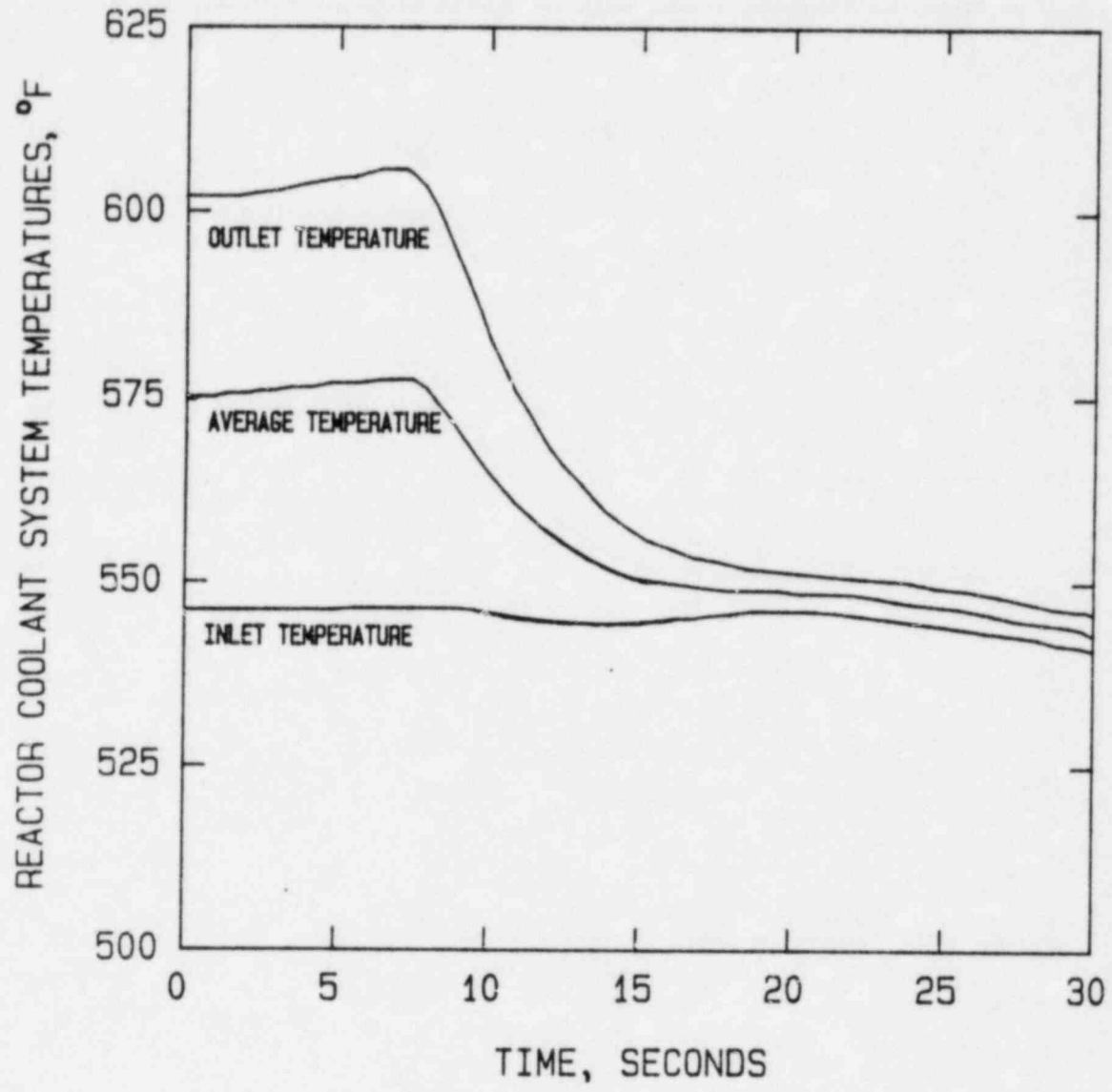

NOTE:

Initial Power Level At 1530 MWt
Reactivity Addition Rate Of $1.0 \times 10^{-4} \Delta\rho$/sec

CEA Withdrawal Incident Coolant Temperatures vs Time	Omaha Public Power District Fort Calhoun Station-Unit No. 1	Figure 14.2-3

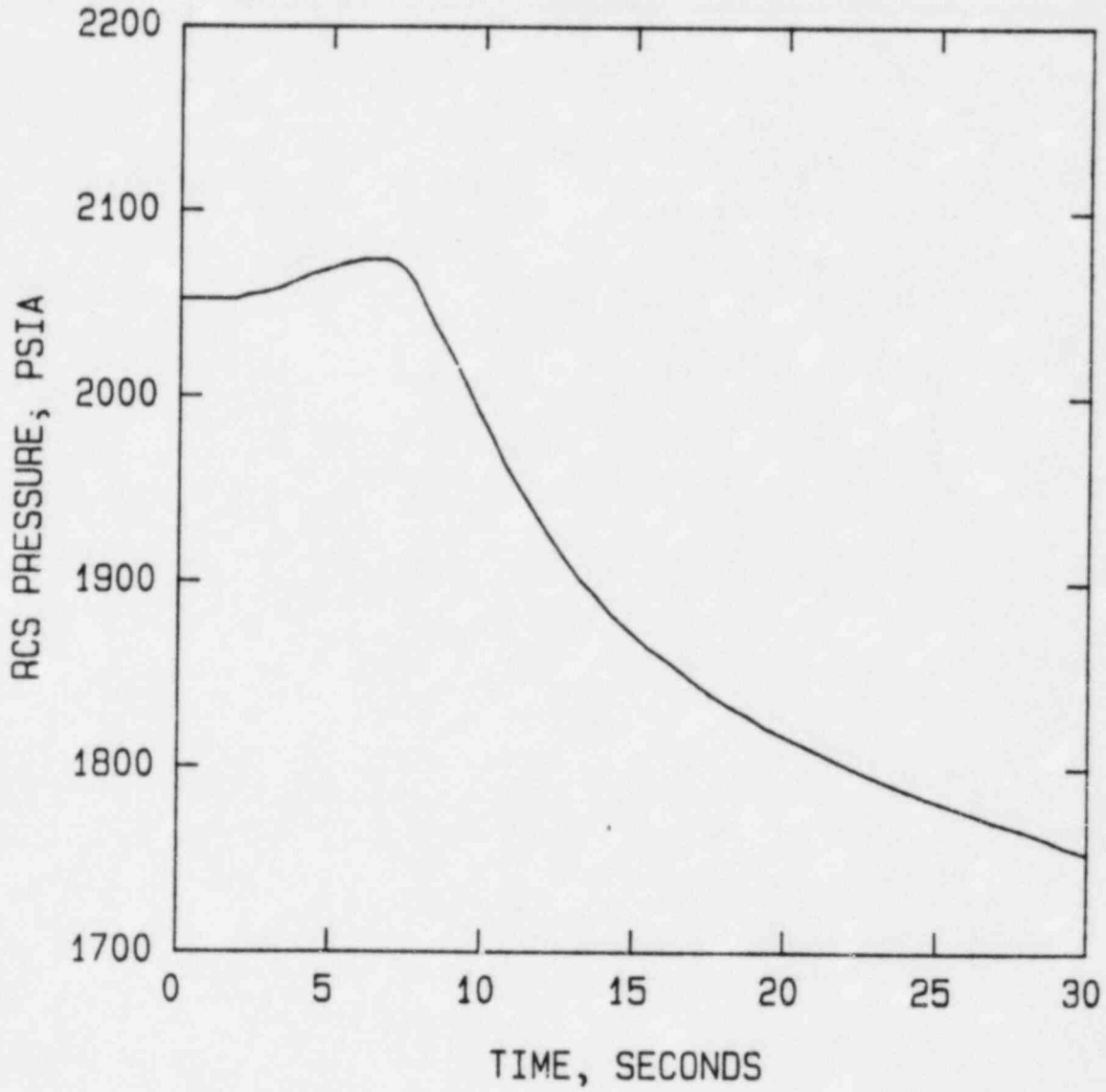

NOTE:

Initial Power Level At 1530 MWt
Reactivity Addition Rate Of $1.0 \times 10^{-4} \Delta\rho$/sec

CEA Withdrawal Incident RCS Pressure vs Time	Omaha Public Power District Fort Calhoun Station-Unit No. 1	Figure 14.2-4

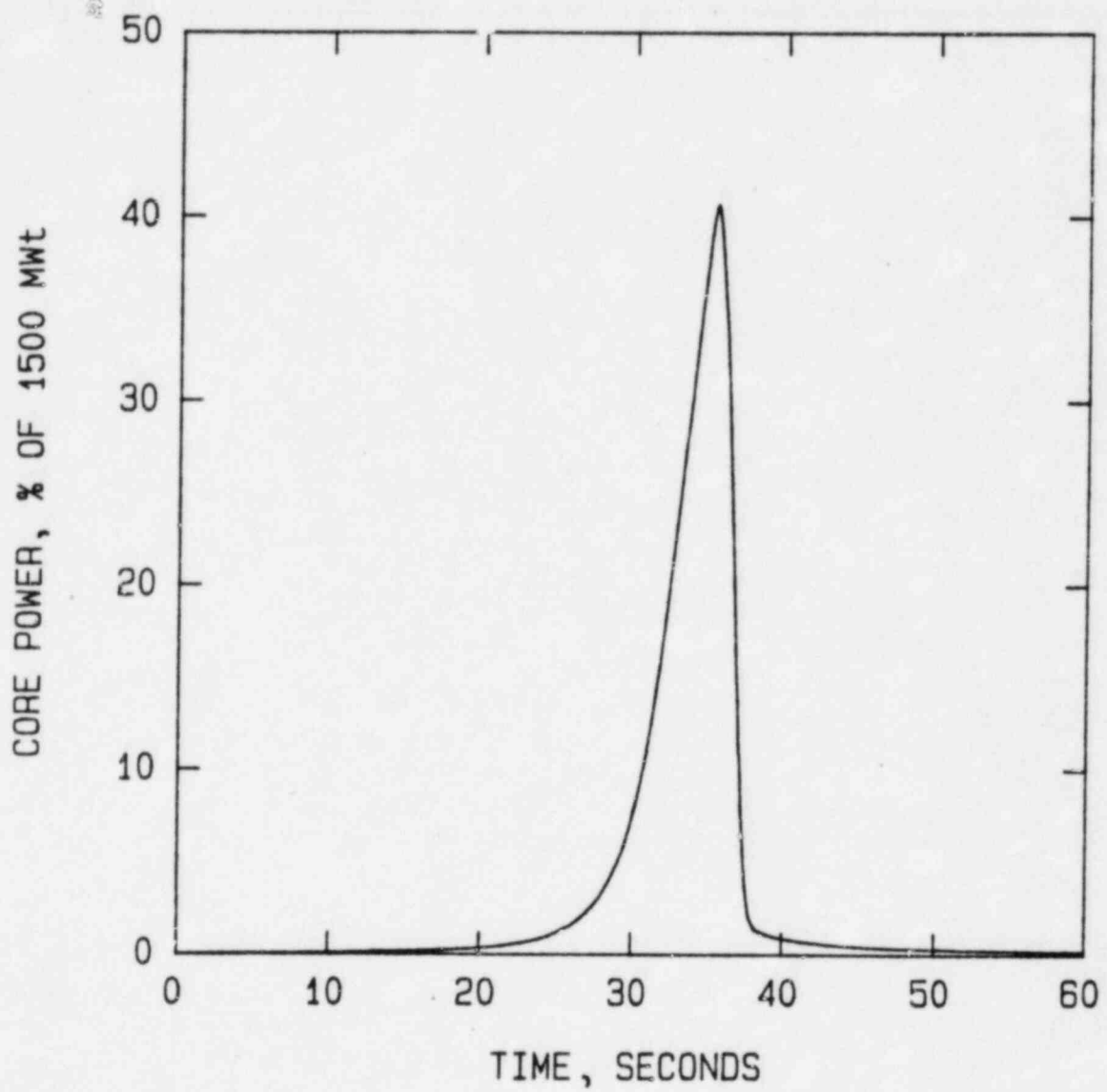

NOTE:

Initial Power Level At 1.0 MWt
Reactivity Addition Rate Of $1.0 \times 10^{-4} \Delta\rho$/sec

CEA Withdrawal Incident Core Power vs Time	Omaha Public Power District Fort Calhoun Station-Unit No. 1	Figure 14.2-5

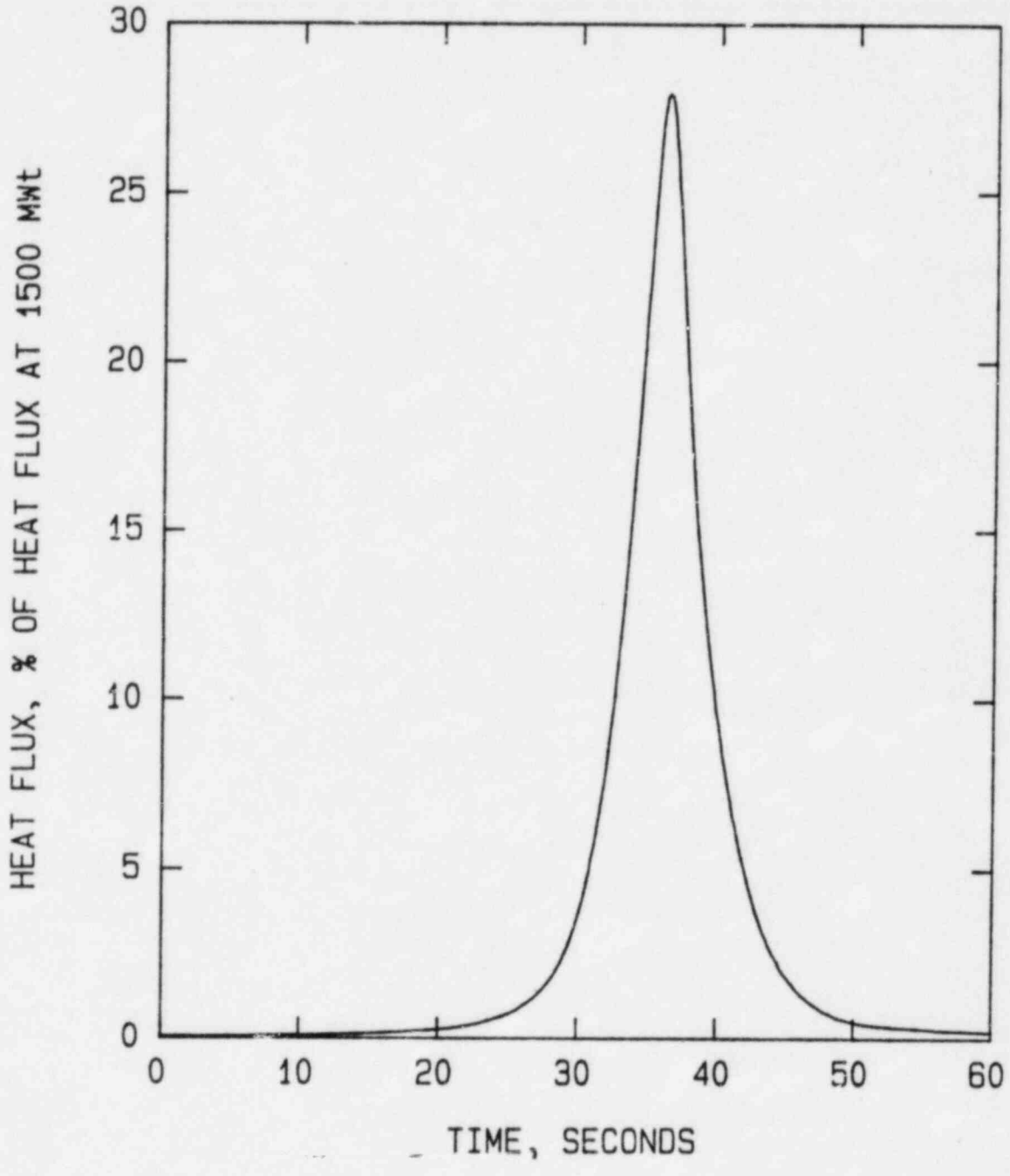

NOTE:

Initial Power Level At 1.0 MWt
Reactivity Addition Rate Of $1.0 \times 10^{-4} \Delta\rho$/sec

CEA Withdrawal Incident Core Average Heat Flux vs Time	Omaha Public Power District Fort Calhoun Station-Unit No. 1	Figure 14.2-6

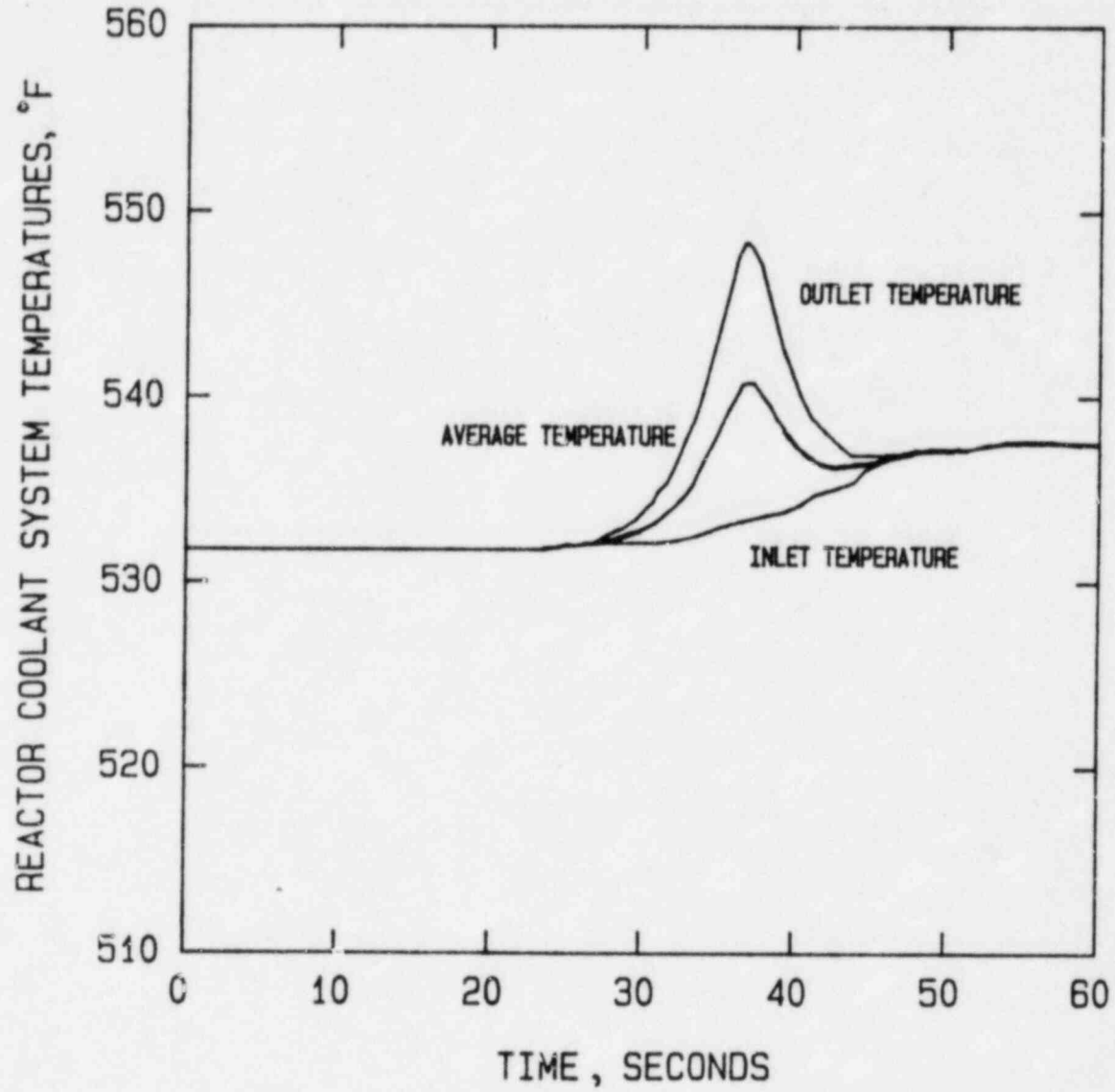

NOTE:

Initial Power Level At 1.0 MWt
Reactivity Addition Rate Of $1.0 \times 10^{-4} \Delta\rho$/sec

CEA Withdrawal Incident Coolant Temperatures vs Time	Omaha Public Power District Fort Calhoun Station-Unit No. 1	Figure 14.2-7

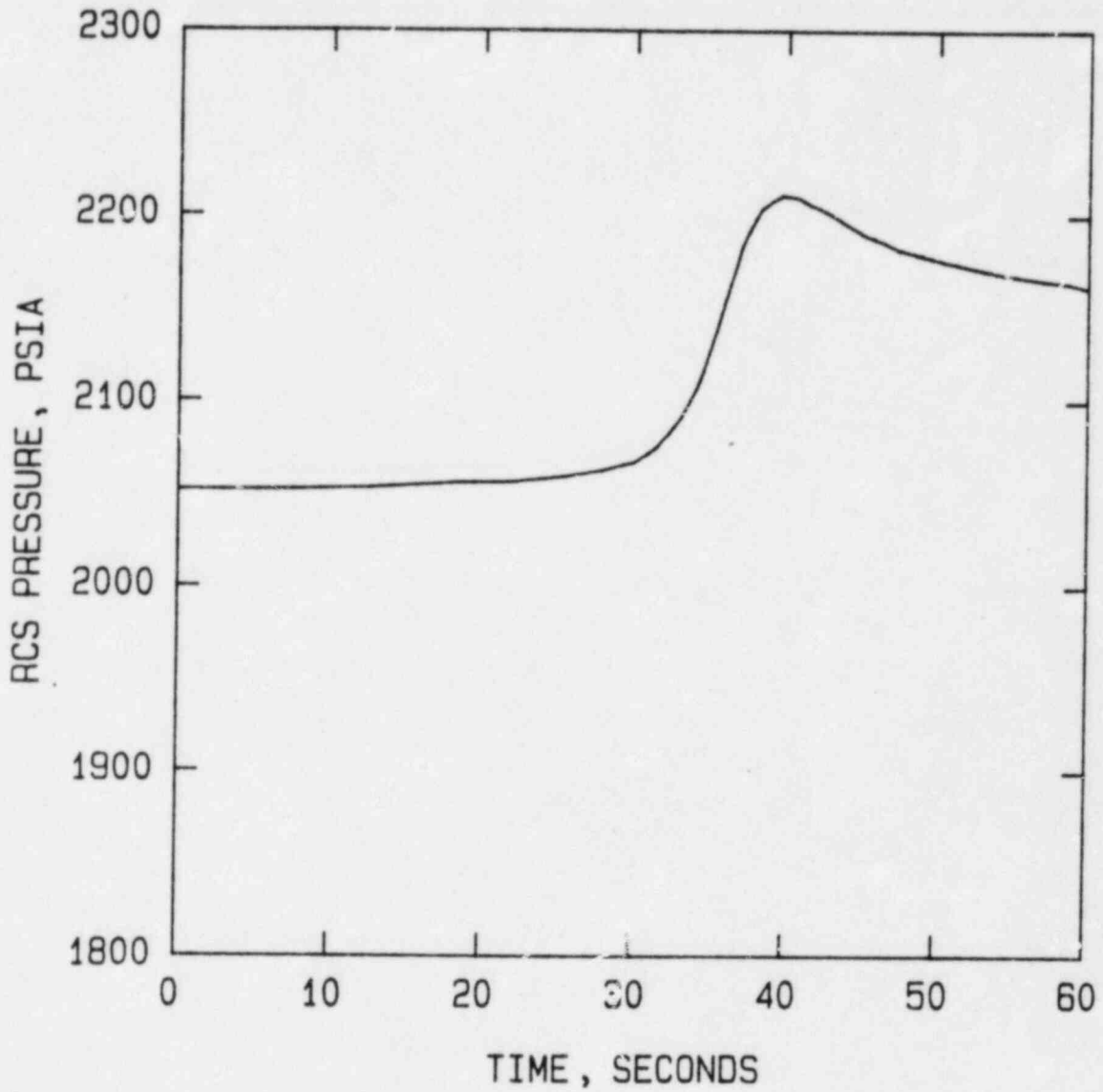

NOTE:

Initial Power Level At 1.0 MWt
Reactivity Addition Rate Of $1.0 \times 10^{-4} \Delta\rho$/sec

CEA Withdrawal Incident RCS Pressure vs Time	Omaha Public Power District Fort Calhoun Station-Unit No. 1	Figure 14.2-8

14.3 BORON DILUTION INCIDENT

14.3.1 General

The chemical and volume control system regulates both the chemistry and the quantity of coolant in the reactor coolant system. Changing the boron concentration in the reactor coolant system is a part of normal plant operation, compensating for long term reactivity effects such as fuel burnup, xenon buildup and decay, and plant cooldown. For refueling operations, borated water is supplied from the safety injection and refueling water tank.

Boron dilution is a manual operation, conducted under strict procedural controls which specify permissible limits on the rate and magnitude of any required change in boron concentration. Boron concentration in the reactor coolant system can be decreased either by controlled addition of unborated makeup water with a corresponding removal of reactor coolant (feed and bleed) or by using the deborating ion exchangers. The deborating ion exchangers are used for boron removal when the boron concentration is low, and the feed and bleed method becomes inefficient. A boronometer is located in parallel with the deborating and purification ion exchangers in the chemical and volume control system (Figure 9.2-2). This instrument measures and indicates the boron concentration in the letdown flow.

During normal operation, concentrated boric acid solution is mixed in the manual mode with primary makeup water (demineralized water) to achieve the concentration required for proper plant operation and added to the volume control tank as needed to maintain the proper level. To effect boron dilution, the makeup controller mode selector switch must be set to "Dilute" and the demineralized water batch quantity selector set to the desired quantity. When the specific amount has been injected, the demineralized water control valve is shut automatically.

Dilution of the reactor coolant can be terminated by isolation of the primary makeup water system or by stopping both the deaerated water booster pump and the charging pumps or by closing the charging isolation valves. A charging pump must be running in addition to a deaerated water booster pump for boron dilution to take place.

The chemical and volume control system is equipped with the following indications and alarm functions which will inform the reactor operator when a change in boron concentration in the reactor coolant system may be occurring:

a. Volume control tank level and high level alarm;

b. Letdown diverter valve position;

c. Makeup controller flow indication and alarms which alert the operator to flow deviation from the set value;

d. Boronometer indication; and

e. Letdown flow temperature indication at outlet of regenerative heat exchanger.

Because of the procedures involved and the numerous alarms and indications available to the operator, the probability of a sustained or erroneous dilution is very low.

14.3.2 Analysis And Results

Although the possibility is remote, a boron dilution incident could occur either with the reactor shutdown or operating. Therefore, Cycle 8 boron dilution incidents have been analyzed for power operation (Mode 1), hot standby (Mode 2) hot shutdown (Mode 3), cold shutdown (Mode 4), and refueling (Mode 5). A shutdown margiin of 3.0% $\Delta\rho$ was conservatively assumed for the Cycle 8 analysis even though the required shutdown margin determined from the hot zero power main steamline break is greater. The 3.0% $\Delta\rho$ shutdown margin is still adequate to provide acceptable results for the boron dilution event.

14.3.2.1 Dilution at Power (Mode 1)

Inadvertent charging of unborated primary makeup water into the reactor coolant system while the reactor is at power would result in a reactivity addition producing power and temperature increases which result in a reduction in the margin to both the DNBR and KW/ft SAFDL's. Since the Thermal Margin/Low Pressure (TM/LP) trip system monitors the transient behavior of core power level and core inlet temperature, the TM/LP trip assures that the DNBR SAFDL is not exceeded for power increases less than the Variable High Power Trip (VHPT) setpoints. For power excursions in excess of the VHPT, a reactor trip is actuated. The approach to the KW/Ft SAFDL is terminated by either the Axial Power Distribution trip, VHPT or the TM/LP trip. For a boron dilution initiated from hot zero power critical, the power transient resulting from the slow reacting insertion rate is terminated by the VHPT prior to approaching the SAFDL's.

The boron dilution event is similar to and bounded by the CEA withdrawal event with the exceptions that the dilution transient has a slower reactivity insertion rate and lacks the local power peaking associated with a withdrawn CEA.

Alarms and/or indications that the event is taking place are the same as in Section 14.3.1. Because of the available alarms and indications, there is ample time and information available to allow the operator to take corrective action. Protracted, unidentified erroneous dilution is improbable.

14.3.2.2 Dilution To Hot Standby (Mode 2)

This event was assumed to be initiated from 3% hot shutdown at 532°F. The critical boron concentration and inverse boron worth assumed in the analysis are listed in Table 14.3-1. These values were generated using methods described in Section 3.4. The reactor coolant system volume was 5506 ft^3, and the charging rate was 120 gpm. The time for dilution to critical was 82.5 minutes which is greater than the minimum acceptable time of 15.0 minutes (as summarized in Table 14.3-2). The acceptance criteria times are consistent with those assumed in the reload license submittals since Cycle 3. Alarms and indications that a dilution is taking place are the same as for the event at power except that an audible count rate indication is available. The 82.5 minute value allows more than adequate time for operator intervention to terminate the event and restore the proper shutdown margin.

The method used to calculate the dilution time to critical for modes 2 through 5 is through the use of the following equation:

$$\Delta t_{crit} = \tau_{BD} \ln \left[\frac{C_B + SDM*IBW}{C_B} \right]$$

Where τ_{BD} = boron dilution time constant, which is a function of RCS volume and temperature (sec)
C_B = critical boron concentration (ppm)
SDM = shutdown margin (%$\Delta\rho$)
IBW = inverse boron worth (ppm/%$\Delta\rho$)

As can be seen from this equation the greater the critical boron concentration, the smaller the inverse boron worth, or the smaller τ_{BD}, the smaller the dilution time to critical will be.

14.3.2.3 Dilution at Hot Shutdown (Mode 3)

This event was assumed to be initiated from 3% shutdown at 210°F. The assumptions were the same as for the hot standby case except the inverse boron worth was assumed to be 55 ppm/% $\Delta\rho$ which results in a dilution time to critical of 40.1 minutes. This is substantially greater than the minimum limit of 15 minutes.

14.3.2.4 Dilution at Cold Shutdown (Mode 4)

The cold shutdown boron dilution event was analyzed at 68°F with a 3% $\Delta\rho$ shutdown margin, and a dilution rate of 120 gpm. Two cases were considered - one with the RCS at a normal volume of 5506 Ft^3 and the other with a partially drained volume. The second configuration may occur when the RCS is drained to the centerline of the reactor vessel outlet nozzles. To be conservative the minimum RCS volume, corresponding to the refueling condition (2036 ft^3), was utilized in the partially drained system analysis.

The results of the 5506 ft^3 system analysis showed a dilution time to critical of 39.8 minutes which is greater than the 15.0 minute minimum limit. Rather than assume an all rods out configuration which is overly conservative, the partially drained system analysis used a critical boron concentration which assumed that Shutdown Groups A and B were withdrawn from the core, and all Regulating Groups were inserted into the core, except the most reactive Regulating Rod, which was assumed to be in the fully stuck-out position. These assumptions are consistent with the Technical Specifications for cold shutdown conditions. The dilution time to critical was 17.0 minutes which meets the acceptance criteria (see Tables 14.3-1 and 14.3-2).

14.3.2.5 Dilution During Refueling (Mode 5)

The boron dilution event analysis for refueling conditions contained the following assumptions:

a. Reactor refueling has just been completed and the head is in place, but the coolant volume is just sufficient to fill the reactor vessel to the bottom of the piping nozzles (2036 ft^3).

b. Demineralized water is added by the charging system at the maximum flow rate of 120 gpm.

c. The minimum permissable boron concentration allowed by Technical Specifications for refueling exists (1700 ppm). All CEA's are withdrawn from the core. (It is improbable that more than a few CEA's would be removed at any one time during refueling.)

These assumptions represent a shutdown condition wherein the core reactivity is the greatest, the water volume and total boron content is at a minimum, and the rate of dilution is the largest possible. Hence, this condition represents the minimum time to achieve inadvertent criticality in the event of uncontrolled boron dilution.

The dilution time from 1700 to 1260 ppm boron allows 38.0 minutes for the operator to acknowledge the audible count rate signal and makeup controller alarm prior to criticality. Corrective action can then be taken to isolate the primary makeup water source by closing valves and/or stopping the primary makeup water pumps or the charging pumps. With the control rods in the all-in position, more time is required to achieve a critical condition.

If the reactor coolant system was full and the chemical and volume control system was in operation (the normal startup mode), the boronometer would warn the operator of any change in boron concentrations. Should dilution occur, the operator would have additional indirect indication of the condition from the volume control tank level alarms and from operation of the letdown diverter valves. Should the makeup controller fail to shut the primary makeup water stop valve, the operator also has control room indication and manual control of the makeup water flow.

14.3.3 Conclusions

Because of the equipment and controls and the administrative procedures provided for the boron dilution operation, the probability of erroneous dilution is considered very small. Nevertheless, if an unintentional dilution of boron in the reactor coolant does occur, numerous alarms and indications are available to alert the operator to the condition. For the hot standby, hot shutdown, cold shutdown, and refueling modes, the maximum reactivity addition due to the dilution is slow enough to allow the operator to determine the cause of the dilution and take corrective action before the initially required shutdown margin is completely lost, i.e. criticality occurs. Additional margin exists in the Cycle 8 times for modes (2)and (3) with the conservative assumption of only a 3.0% shutdown margin. The actual shutdown margin (as determined) from the hot zero power main steamline break and incorporated into the Technical Specifications is significantly higher. The boron dilution event at power is less severe than and bounded by the CEA withdrawal event.

Table 14.3-1

CYCLE 8

ASSUMED INPUT PARAMETERS FOR BORON DILUTION INCIDENT ANALYSIS

Mode	Critical Boron Concentration, PPM (All-rods-out, No Xenon)	Inverse Boron Worth, PPM/% Δρ
Hot Standby	1330	90
Hot Shutdown	1330	55
Cold Shutdown- Normal RCS Volume	1340	55
Cold Shutdown- Minimum RCS Volume	1145*	55
Refueling	1260	55

* Shutdown Groups A and B out, all Regulating Groups inserted except most reactive rod stuck out.

Table 14.3-2

CYCLE 8

RESULTS OF BORON DILUTION INCIDENT

Mode	Time to Lose Prescribed Shutdown Margin (Min)	Acceptance Criteria for Time to Lose Prescribed Shutdown Margin (Min)	Minimum Shutdown Margin Assumed (Δρ)
(2) Hot Standby	82.5	15.0	3.0%
(3) Hot Shutdown	40.1	15.0	3.0%
(4) Cold Shutdown - Normal RCS Volume	39.8	15.0	3.0%
Cold Shutdown - Minimum RCS Volume	17.0	15.0	3.0%
(5) Refueling	38.0	30.0	*

* 1700 ppm boron initially

14.4 CONTROL ELEMENT ASSEMBLY DROP INCIDENT

14.4.1 General

The CEA drop incident is defined as the inadvertent release of a CEA causing it to drop into the reactor core. The CEA drive is of the rack and pinion type, with the drive shaft running parallel to and driving the rack through a pinion gear and a set of bevel gears. The drive mechanism is equipped with a mechanical brake which maintains the position of the CEA. A CEA drop may occur due to either an inadvertent interruption of power to the CEA holding coil (i.e. magnetic clutch) or an electrical or mechanical failure of the mechanical brake in the CEA drive mechanism when the CEA's are being moved.

The drop of a single CEA into the core reduces the fission power in the vicinity of the dropped CEA and adds negative reactivity on a core-wide basis. The negative reactivity insertion causes a prompt drop in core power and heat flux with the magnitude ranging from approximately 4 to 35%, depending on the worth of the dropped CEA. The turbine runback circuitry at the Fort Calhoun Station has been removed along with the automatic mode of operation. Therefore, the turbine continues to demand the same power as it did prior to the drop. This results in a power mismatch between the primary and secondary systems resulting in a cooldown of the reactor coolant system. In the presence of a negative moderator temperature coefficient (MTC) of reactivity, the decreasing average coolant and fuel temperatures add positive reactivity to the core. The radial and axial power distributions begin to shift as a result of the reactivity feedback effects and the neutron flux asymmetry caused by the dropped CEA. A new tilted asymptotic radial power distribution with higher radial peaking is reached within a few minutes. Xenon redistribution will cause further tilting and increase the radial peak by approximately 5% within one hour if the event is not terminated. The positive reactivity addition due to feedback from the moderator and Doppler is eventually sufficient to compensate for th d rod's negative reactivity. The final result is that the core powe rn to the pre-drop level and the coolant temperature will be slightly red. this configuration or in the process of achieving it, local power d l heat fluxes may exist which are in excess of the design limits.

The full length CEA drop event is classified as an anticipated operational occurrence (AOO) which does not require a reactor protective system trip to maintain a DNBR (using the CE-1 correlation) greater or equal to 1.19 and a peak linear heat rate (PLHR) less than the linear heat rate (LHR) limiting condition of operation (LCO) and limiting safety system setting (LSSS). For Fort Calhoun Station, this event is the limiting AOO in terms of DNBR and required overpower margin. The DNBR criterion is met by maintaining the following parameters within their LCO limits:

(1) Cold leg temperature $\leq$ 545°F
(2) Pressurizer pressure $\geq$ 2075 psia
(3) Reactor coolant flow $\geq$ 197,000 gpm
(4) Axial shape index within limits of Technical Specification Figure 2-7 (Limiting Condition of Operation for DNB Monitoring)
(5) CEA configurations within power dependent insertion limit (Technical Specification Figure 2-4)

(6) Integrated radial peaking factor F_R^T, within limits of Technical Specification Figure 2-9.

During the reload analysis, sufficient initial steady state margin must be built into these LCO's to allow the reactor to ride out the event.

Detection of a dropped CEA is accomplished from any one of three sources. Alarms indicating four and eight inch deviations from the group position are provided from the position indications for every CEA. This means of detection is independent of the location and reactivity worth of the dropped CEA and is also independent of spatial distribution of core power. The rod block circuitry, which contains a visual display of rod positions, provides another method of determining that a rod drop has occurred. The CRT screen will flash for this condition, and the circuitry will limit CEA movement to the manual individual mode (where only one rod can be moved at a time). A third method for sensing a dropped CEA utilizes the out-of-core power range nuclear instruments. A first order time lag network is used to distinguish between the relatively rapid power reduction caused by a dropped CEA as compared with normal changes in load demand. Dropping of even the most remote CEA (a CEA near the core center) is expected to cause a reduction of approximately 10 percent in the signal from the out-of-core detectors. Should a CEA drop from a partially inserted position, causing a smaller change in neutron flux, the corresponding change in power distortion would be smaller.

14.4.2 Method of Analysis

The dropped CEA incident analysis was performed using the computer code CESEC which models neutron kinetics with fuel and moderator temperature feedback, the reactor control system, the reactor coolant system (RCS), the steam generators, and the main steam and feedwater systems.

The methodology used in deriving the DNBR and LHR Required Overpower Margins* (ROPM's) is consistant with that use in Cycle 5. Table 14.4-1 contains a list of the assumptions including uncertainties for the analysis. A Doppler multiplier of 1.15 was used to enhance the positive reactivity feedback from the reactor coolant temperature decrease. Likewise, the most negative moderator temperature coefficient of reactivity was chosen. The initial pressurizer pressure was chosen to be 2053 psia which corresponds to the minimum allowed pressure minus uncertainties. This results in a lower final RCS pressure and thus in a lower minimum DNBR. The minimum dropped rod worth allowed by the PDIL was chosen so that the prompt drop in power and inlet temperature drops would be minimized. Consequently, the initial condition LCO's are more restrictive, because the inlet temperature remains higher resulting in a lower DNBR value.

*The ratio between the margin that is available at the initiation of the transient and that which exists for the most adverse conditions at any time during the transient expressed as a percentage change.

TABLE 14.4-1

FULL LENGTH CEA DROP ASSUMPTIONS INCLUDING UNCERTAINTIES

Parameter	Units	Cycle 8
Initial Core Power Level	MWt	102% of 1500
Core Inlet Temperature	°F	547
Pressurizer Pressure	psia	2053
Core Mass Flow Rate	10^6 lbm/hr	70.9
Moderator Temperature Coefficient	10^{-4} $\Delta\rho$/°F	-2.7
Doppler Coefficient Multiplier		1.15
CEA Insertion at Full Power	% Insertion of Bank 4	25.0
Dropped CEA Worth	% $\Delta\rho$	-0.28
Radial Peaking Distortion Factor		
Integrated Radial Peaking	Unrodded	1.16
	Bank 4 Inserted	1.17
Planar Radial Peaking	Unrodded Bank 4	1.25
	Inserted Region	1.24

14.4.3 Results

The CEA Drop event was reanalyzed for Cycle 8 to accommodate an increase in the total unrodded integrated radial peaking factor (F_R^T) to 1.62 and an increase in the total unrodded planar radial peaking factor (F_{XY}^T) to 1.67. Conservative bounding values of 1.65 and 1.72 for F_R^T and F_{XY}^T, respectively, were used in the analysis.

Table 14.4-2 presents the sequence of events for the Full Length CEA Drop event initiated from the full power initial conditions contained in the Table 14.4-1. Figures 14.4-1 through 14.4-5 show the results of the transient analysis as presented in plots of core power, core heat flux, reactor coolant system temperatures, pressurizer pressure, and steam generator steam flow versus time.

The incident is initiated by the insertion of -0.28% $\Delta\rho$ over a time period of 1.0 second. The maximum increase in the value of F_R^T for the dropped CEA is 16% for the initially unrodded case and 17% for the initially rodded case. These distortion factors which were used in the calculation of the DNBR Required Overpower Margin were derived on the basis of a three-dimensional power distribution analysis rather than on the synthesis of a two dimensional model using separate rodded and unrodded distortion factors in conjunction with the rodded and unrodded F_{XY} values and the most adverse axial power distribution.

For Cycle 8, a CEA drop initiated at an axial shape index of +0.002 produces a DNBR transient that results in the closest approach to 1.19 DNBR using the CE-1 correlation. The associated ROPM is 113.3% of initial power. The results show that for Cycle 8 this incident is the most limiting Anticipated Operational Occurance (AOO) for determining the DNBR ROPM.

For the full length CEA Drop, a maximum allowable initial linear heat generation rate of 16.8 kw/ft could exist as an initial condition without exceeding the Specified Acceptable Fuel Design Limit of 21 kw/ft during this transient. This amount of margin is maintained operationally by setting the Linear Heat Rate LCC based on the allowable linear heat rate for LOCA.

Since the limiting conditions for operation maintain the required DNB thermal margin, and the allowable linear heat generation rate LCOs are based on more stringent LOCA limits, the Specified Acceptable Fuel Design Limits (SAFDLs) will not be exceeded during a dropped CEA incident.

TABLE 14.4-2

SEQUENCE OF EVENTS FOR FULL LENGTH CEA DROP INCIDENT

TIME (Sec)	Event	Value
0.0	CEA begins to drop into core	
1.0	CEA reaches fully inserted position	100% insertion
1.06	Core power level reaches a minimum and begins to return to power due to reactivity feedbacks	68.7% of 1500 MWt
200.0	Pressurizer pressure reaches a minimum value	1956 psia
200.0	Minimum DNBR is reached	>1.19(CE-1 correlation)
200.0	Core power returns to its maximum value	99.8% of 1500 MWt

14.4.4 Conclusions

The dropped rod incident is the most limiting AOO for Fort Calhoun Station in terms of DNBR not requiring an RPS trip. The DNBR LCO limits of core and RCS parameters ensure that the reactor will ride out the event without tripping while maintaining a DNBR greater or equal to 1.19 using the CE-1 correlation.

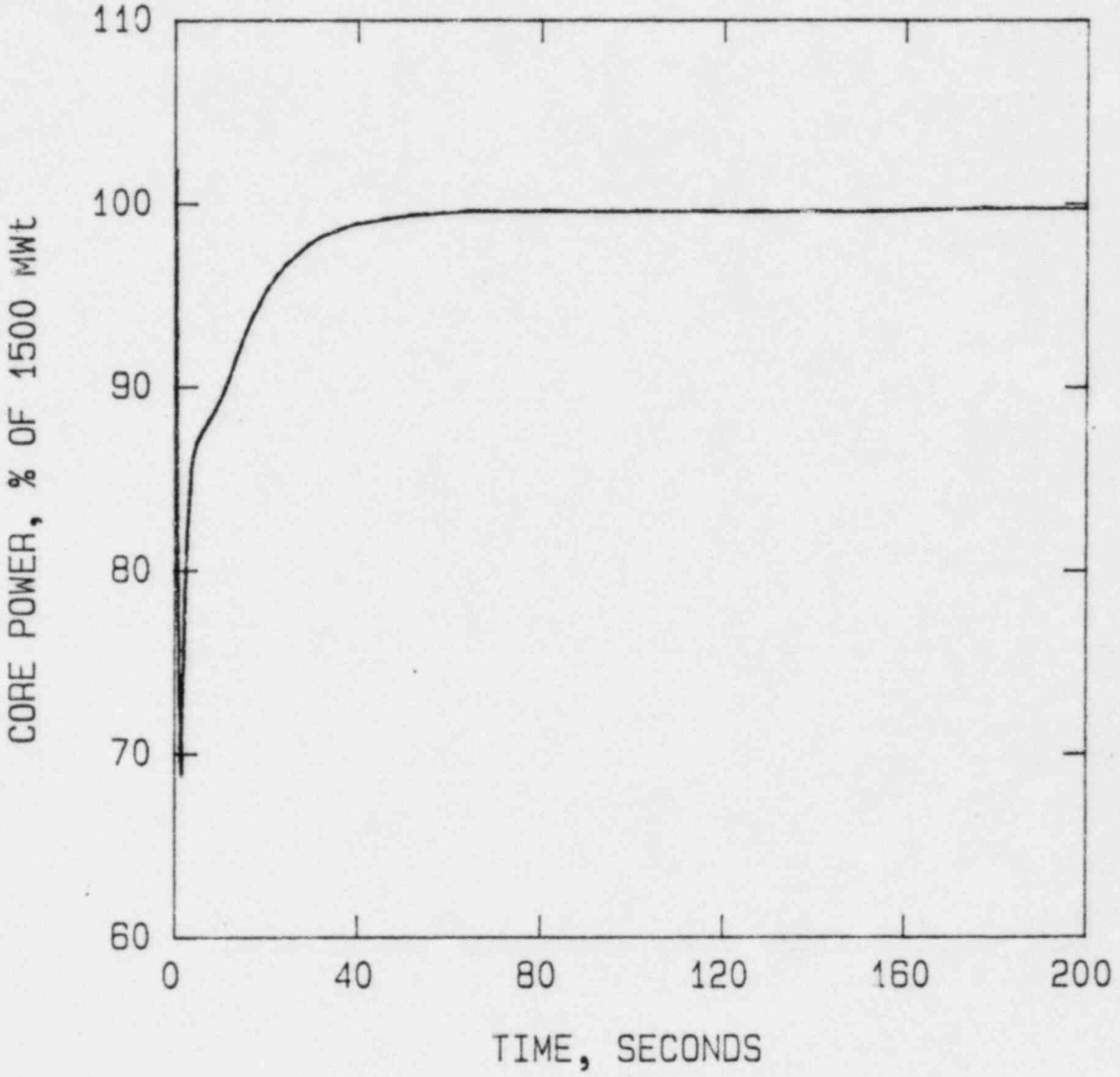

NOTE:
Cycle 8

CEA Drop Incident Core Power vs Time	Omaha Public Power District Fort Calhoun Station-Unit No. 1	Figure 14.4-1

NOTE:
Cycle 8

CEA Drop Incident Core Average Heat Flux vs Time	Omaha Public Power District Fort Calhoun Station-Unit No. 1	Figure 14.4-2

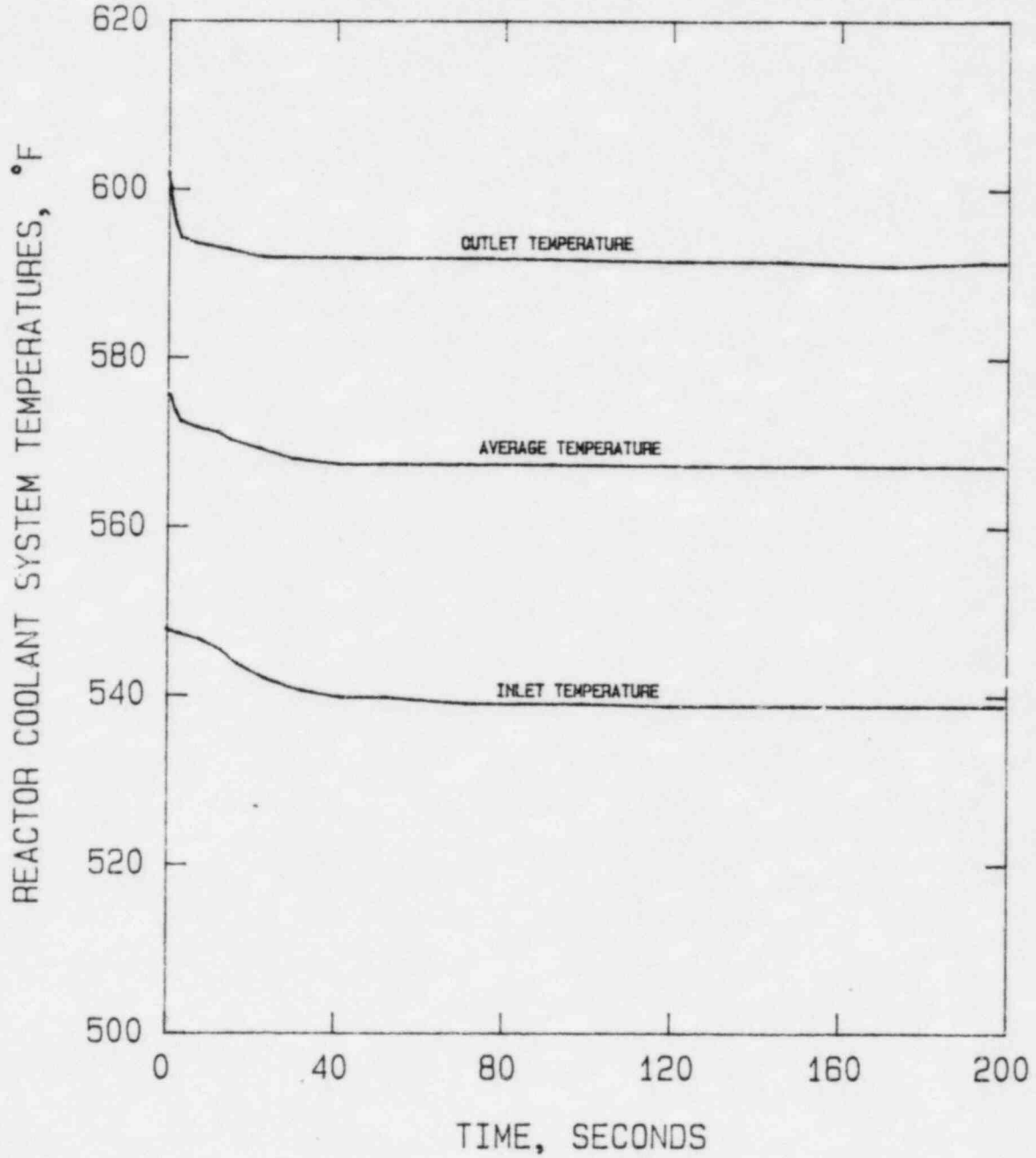

NOTE:
Cycle 8

CEA Drop Incident Coolant Temperatures vs Time	Omaha Public Power District Fort Calhoun Station-Unit No. 1	Figure 14.4-3

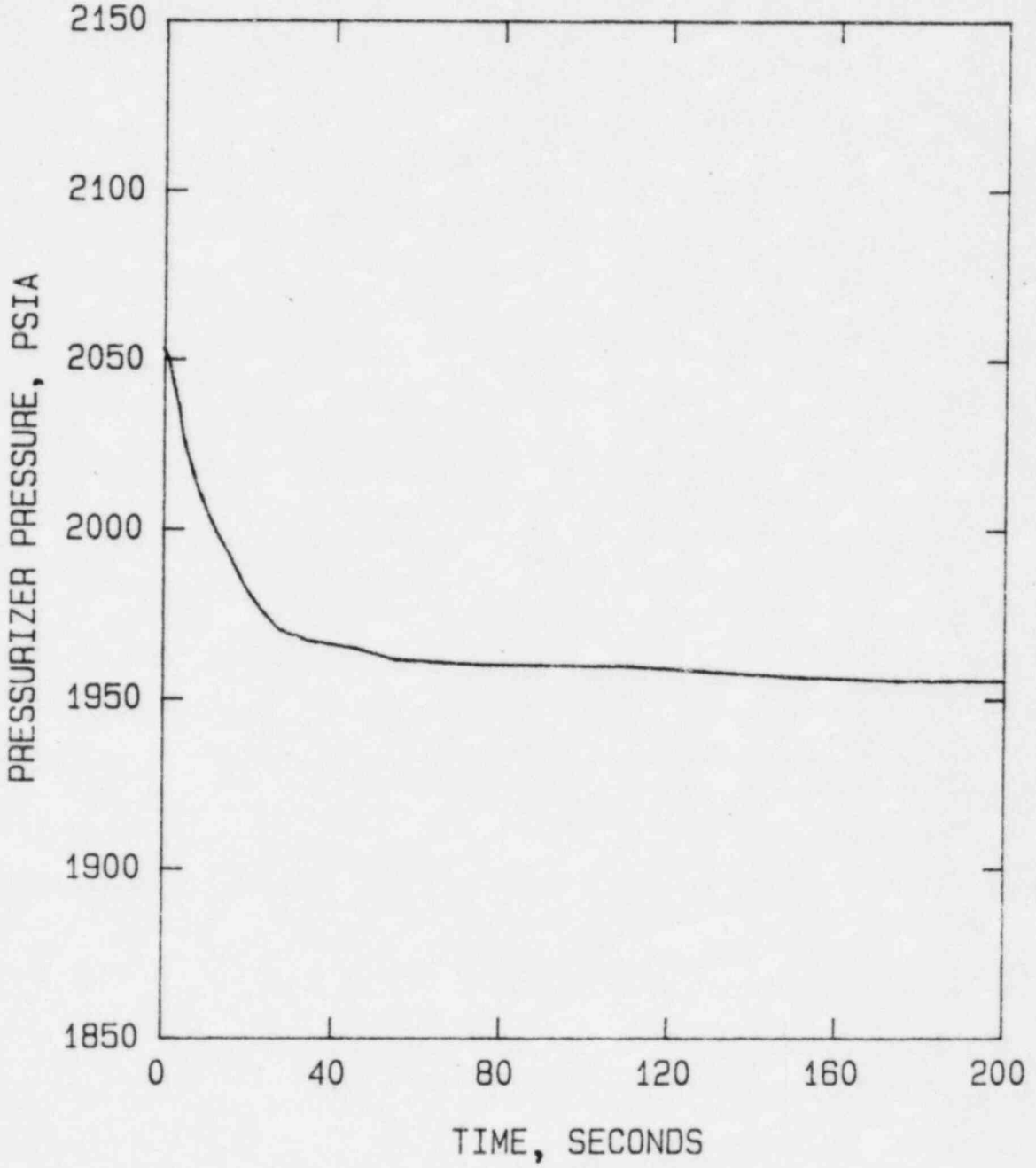

NOTE:
Cycle 8

CEA Drop Incident Pressurizer Pressure vs Time	Omaha Public Power District Fort Calhoun Station-Unit No. 1	Figure 14.4-4

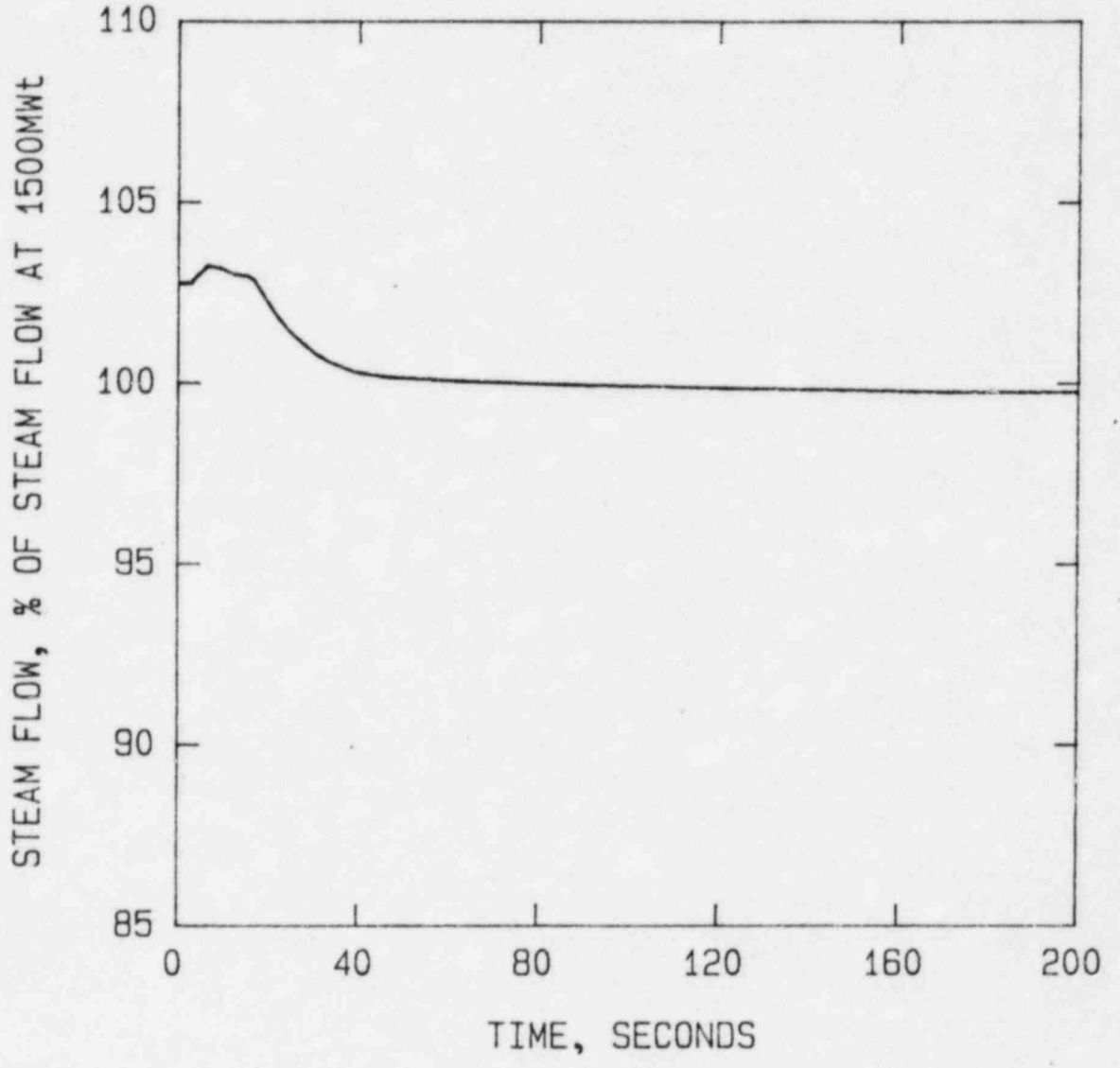

NOTE:
Cycle 8

CEA Drop Incident Steam Flow vs Time	Omaha Public Power District Fort Calhoun Station-Unit No. 1	Figure 14.4-5

14.12 MAIN STEAM LINE BREAK ACCIDENT

14.12.1 General

A large break of a pipe in the main steam system causes a rapid depletion of steam generator inventory and an increased rate of heat extraction from the primary system. The resultant cooldown of the reactor coolant, in the presence of a negative moderator temperature coefficient of reactivity, will cause an increase in nuclear power and trip the reactor. A severe decrease in main steam pressure will also initiate reactor trip and cause the steam line isolation valves to trip closed. If the steam line rupture occurs between the isolation valve and the steam generator outlet nozzle, blowdown of the affected steam generator would continue. (However, closure of the check valve in the ruptured steam line, as well as closure of the isolation valves in both steam lines, will terminate blowdown from the intact steam generator.) The fastest blowdown, and therefore, the most rapid reactivity addition, occurs when the break is at a steam generator nozzle. This break location is assumed for the cases analyzed. Inadvertent opening of valves in the main steam system is discussed in Section 14.11 (Excess Load Increase event).

Both full power and no-load (hot standby) initial condition cases were considered for two-loop operation (i.e., four reactor coolant pumps). Also included is a no-load case for one-loop operation (i.e., two reactor coolant pumps and one steam generator). Although Technical Specifications prohibit operation with less than four reactor coolant pumps in use (with the exception of physics testing done at less than 10^{-1}% power), the one-loop, no-load case will be included to document the analysis performed for Cycle 1. With one loop in operation the break is assumed to occur in the active steam generator. If the break was in the inactive steam generator, the cooldown rate of the reactor coolant would be significantly reduced; because the flow through the idle loop is only about 15 percent of full flow.

Since the steam generators are designed to withstand reactor coolant system operating pressure on the tube side with atmospheric pressure on the shell side, the continued integrity of the reactor coolant system barrier is assured.

14.12.2 Method of Analysis

The analysis of the main steam line break (MSLB) accident was performed using the digital computer code CESEC which models neutron kinetics with fuel and moderator temperature feedback, the reactor protection system, the reactor coolant system, the steam generators, and the main steam and feedwater systems.

The MSLB accident is assumed to start from steady state conditions with the initial power being 1530 MWt (102%) for the full power case and 1 MWt for the no load case. The reactor coolant system cooldown causes the greatest positive reactivity insertion into the core when the moderator temperature coefficient (MTC) of reactivity is the most negative. For this reason the Technical Specification negative MTC limit corresponding to the end-of-cycle was assumed for the analysis. Since the reactivity change associated with moderator feedback varies significantly over the temperature range covered in the analysis, a curve of reactivity insertion versus temperature rather than a single value of MTC is assumed. The moderator cooldown curve utilized is shown in Figure 14.12-1.

This curve was derived on the basis that upon reactor trip the most reactive CEA is stuck in the fully withdrawn position thus yielding the most adverse combination of scram worth and reactivity insertion. Although no single value of MTC is assumed in the analysis, the moderator cooldown reactivity function is calculated assuming an initial MTC equal to the most negative Technical Specification limit, i.e. -2.3×10^{-4} $\Delta\rho/°F$ for Cycle 1 and -2.5×10^{-4} $\Delta\rho/°F$ for Cycle 8.

Reactivity feedback effects from the variation of fuel temperature (i.e., Doppler) are included in the analysis. The most negative Doppler defect function, which occurs at beginning of cycle for Fort Calhoun (for Cycle 8), when used in conjunction with the decreasing fuel temperature causes the greatest positive reactivity insertion during the MSLB event. For Cycle 8, in addition to assuming the most negative Doppler defect function, an additional 15% uncertainty was assumed, i.e., a 1.15 multiplier. This multiplier conservatively increases the subcritical multiplication and results in a larger return-to-power.

The delayed neutron precursor fraction, β, assumed is the maximum absolute value including uncertainties for end of cycle conditions. This is conservative since it also maximises subcritical multiplication and thus, enhances the potential for a return-to-power.

The most probable trip signals resulting from an MSLB include low steam generator pressure, high power, low steam generator level, thermal margin/low pressure, and high rate-of-change of power (for the no-load case). The steam generator low pressure trip, which occurs at 478 psia (including a 22 psia uncertainty below the nominal trip setting of 500 psia), was the trip assumed in the analysis. No credit is taken for the high power trip which occurs at approximately the same time for the full power case. For the cases analyzed, it was assumed that the most reactive CEA was stuck in the withdrawn position. The CEA configuration at no load operation is such that the most reactive CEA of those in the withdrawn position is worth less than the most reactive CEA of those withdrawn at full power. If all CEA's insert (no stuck CEA), there is no return to criticality and no power transient following trip.

The power distribution following CEA insertion is distorted by the stuck CEA. The coincident high radial peaking and low reactor coolant pressure can lead to local boiling at moderate power levels. The power flattening effect of the voids and of the locally high fuel temperature is included in the analysis, but no credit is taken for the corresponding reactivity feedback. In addition, cold edge temperatures were used to calculate moderator reactivity insertion during the cooldown, thus maximizing the return-to-critical and return-to-power potentials. The computed power peaks after trip are thus conservative.

Current Emergency Operating Procedures require that the reactor coolant pumps (RCP's) be manually tripped following the receipt of a safety injection actuation signal (SIAS). The MSLB case with the RCP's tripped is similar to the MSLB case with a loss of offsite power (LOOP) since the RCP's coastdown in both events. As discussed in Reference 1, the loss of offsite power delays safety injection due to the time delay for the emergency diesel generators to restore power to the safety injection pumps and causes a coastdown of the RCP's. The coastdown affects the degree of overcooling and increases the time for safety injected borated water to reach the core midplane. Because manual tripping of the RCP's results in a later coastdown of the RCP's and because safety injection is not delayed since offsite power is available (i.e., the diesel generator

startup and pump loading delays are not present), the injected boron will arrive at the core midplane sooner for a MSLB with the RCP's tripped than for a MSLB with a loss of offsite power. Therefore the reactivity effects of a MSLB with the RCP's tripped are less severe than for the MSLB with a loss of offsite power.

Reference 1 states that the MSLB case with a loss of offsite power results in the injected boron being dominant over the RCS cooldown and concludes that the reactivity effects of a MSLB accident would be reduced in severity with a concurrent loss of offsite power when compared to the same event with offsite power available and the RCP's operating. Because the reactivity effects of a MSLB with the RCP's tripped after SIAS are less severe than a MSLB with a concurrent loss of offsite power, it is concluded that the reactivity effects for the MSLB case with the RCP's tripped after SIAS are less severe than for a MSLB with offsite power available and RCP's operating. Therefore, to maximize the severity of the reactivity effects, the Cycle 8 MSLB analysis was performed with the four reactor coolant pumps operating at the limiting condition of operation volumetric flow rate.

The reactor coolant volumetric flow rate is assumed to be constant during the incident. The limiting condition of operation flow rate (197,000 gpm) was used in order to obtain the most adverse results. A lower flow rate increases the initial fuel and average primary coolant temperatures and consequently results in a higher steam generator pressure and a greater steam generator mass inventory. These effects cause a longer blowdown, a greater blowdown rate and a greater decrease in average primary coolant temperature. After MSIV closure the lower flow rate decreases the rate of reverse heat transfer from the intact steam generator, thereby increasing the heat extracted from the primary system by the ruptured steam generator. The overall effect is that the potential for a return-to-power is maximized. The Cycle 1 analysis assumed a higher flow rate of 209,500 gpm for the two-loop cases and 102,200 gpm for the one-loop case.

Maximum values for the heat transfer coefficient across the steam generator are used for the no-load initial condition case, while nominal values are used for the full-load initial condition. These heat transfer coefficients result in the most severe conditions during the incident because of the shape of the reactivity versus moderator temperature function and the difference in average moderator temperature for the maximum and minimum values of the steam generator heat transfer coefficients.

The fast cooldown following an MSLB results in a rapid shrinking of the reactor coolant. After the pressurizer is emptied, the reactor coolant pressure is assumed to be equal to the saturation pressure corresponding to the highest temperature in the system.

Safety injection actuation occurs at 1578 psia (i.e., 1600 psia minus the 22 psia uncertainty) after the pressurizer empties. Additional time is required for pump acceleration, valve opening, and flushing of the unborated part of the safety injection piping along with the requirement that the RCS pressure decrease below the shutoff head of the safety injection pumps (1376 psia for high pressure safety injection [HPSI] pumps and 201 psia for low pressure safety injection [LPSI] pumps). The Cycle 1 analysis assumed that two of the three HPSI pumps and two of the three charging pumps were available; whereas the Cycle 8 analysis takes credit for one HPSI pump, one LPSI pump, and the safety injection tanks.

For one-loop operation, no credit is taken for boron injected into the idle loop because of the long transport time to the core. Further, 13 percent of the boric acid injected in the active loop will enter the core via the idle loop, and the effect of this boron has been neglected. The boric acid is assumed to mix homogeneously with the reactor coolant at the points of injection into the cold legs. The reactor coolant loop transit time is 11.4 seconds for the 209,500 gpm two-loop case (Cycle 1), 12.5 seconds for the 197,000 gpm two-loop case (Cycle 8), and 19.3 seconds for the one-loop case. Slug flow is assumed for movement of the mixture through the piping, plena, and core. After the boron reaches the core midplane, the concentration within the core is assumed to increase as a step function after each loop transit interval.

The boron concentration of the safety injection water is 1700 ppm. The charging pumps deliver concentrated boric acid solution containing 10,925 ppm boron. The values of the inverse boron worth were conservatively chosen to be large to minimize the negative reactivity insertion from safety injection.

Since the rate of temperature reduction in the reactor coolant system increases with rupture size and with steam pressure at the point of rupture, it is assumed that a circumferential rupture of a 26-inch (inside diameter) steam line occurs at the steam generator main steam line nozzle, with unrestricted blowdown. Critical flow is assumed at the point of rupture, and all of the mass leaving the break is assumed to be in the steam phase. This assumption results in the maximum heat removal from the reactor coolant per pound of secondary water, since the latent heat of vaporization is included in the net heat removal. A single failure of the reverse flow check valve in the ruptured steam generator is assumed; so that the intact steam generator will have steam flow through the unaffected steam line and back through and out the ruptured line. The analysis conservatively neglects a choke which is installed in each steam line immediately above the steam generator and assumes the steam flow from the intact steam generator is through an unrestricted 24 inch steam line. This flow will be terminated upon MSIV closure.

The feedwater flow at the start of the MSLB corresponds to the initial steady state operation. For the full load initial condition, it is automatically reduced from 100 percent to 10.66 percent within 40 seconds following reactor trip. For the no load initial condition, feedwater flow is assumed to match energy input by the reactor coolant pumps and the 1 MWt core power. Feedwater isolation upon the receipt of a low stream generator pressure (at 478 psia) was credited for both the full load and no load cases for Cycle 8. A valve closure time of 30 seconds was used.

14.12.3 Results

14.12.3.1 No-Load Initial Condition, Two-Loop Operation

Results indicating the plant response to the postulated rupture for the no-load, two-loop case are shown in Figures 14.12-2 through 14.12-7. Cycle 1 results, which are more limiting than those of Cycle 8 are also plotted. In addition, the Cycle 1 values of power and heat flux have been rescaled to a full power rating of 1500 MWt rather than 1420 MWt. For Cycle 1 (the limiting cycle), the low steam generator pressure trip signal occurs at 4.0 seconds and CEA motion begins at 4.9 seconds. At 14 seconds the pressurizer has emptied, at which time the pressure drops below 1578 psia, and therefore, the safety injection actuation signal (SIAS) occurs. At 38 seconds the first boron from the HPSI pumps reaches the core midplane, and at 140 seconds boron from the concentrated boric acid tank reaches the core midplane. At 112 seconds the affected steam

generator is emptied, the moderator temperature begins to increase and power decreases towards zero. During the incident, reactor power and reactor heat flux reach peak values of 28 percent and 26 percent of 1500 MWt, respectively.

Table 14.12-1 contains the conditions from which the Cycle 8 no-load, two-loop Main Steamline Break event was initiated and the assumptions used. Table 14.12-2 presents the sequence of events and pertinent parameter values occurring during the Cycle 8 event. From this table and Figures 14.12-2 through 14.12-7, it can be seen that this event is less severe than that analyzed for Cycle 1. The peak reactivity during the return-to-critical exceeds the Cycle 1 peak, however the duration of criticality is less resulting in the lower peak return-to-power and core heat flux values of 19.2% and 19.1%, respectively. Boron from the safety injection tanks quickly terminates the reactivity transient when the RCS pressure falls below the nitrogen overpressure of 255 psia. An additional cooldown from automatic auxiliary feedwater actuation is prevented by the existence of a low steam generator pressure condition in the ruptured steam generator and by an adequate level in the intact steam generator.

TABLE 14.12-1

KEY PARAMETERS ASSUMED IN THE MAIN STEAM LINE BREAK ANALYSIS FOR NO-LOAD AND 2-LOOP OPERATION CYCLE 8

Parameter	Units	Cycle 1	Cycle 8
Initial Core Power*	MWT	1.0	1.0
Initial Core Inlet Temperature	°F	532	532
Initial Pressurizer Pressure	psia	2100	2172
Initial Steam Generator Pressure	psia	750	895
Initial Steam Generator Mass Inventory (Level)	% Narrow Range Scale	63	70
RCS Flow Rate	gpm	209,500	197,000
Minimum CEA Worth Available at Trip	%Δρ	-2.4	-4.0
Doppler Multiplier		1.0	1.15
Moderator Cooldown Curve	%Δρ vs temp.	See Figure 14.12-1	See Figure 14.12-1
Inverse Boron Worth	PPM/%Δρ	-80	-94
Effective MTC	$x10^{-4}$Δρ/°F	-2.3	-2.5
β Fraction (including uncertainty)		**	0.0058

*Reactor coolant pump heat assumed to be zero.
** data not available.

TABLE 14.12-2

SEQUENCE OF EVENTS FOR THE MAIN STEAMLINE BREAK EVENT
FOR NO-LOAD AND TWO-LOOP OPERATION
CYCLE 8

TIME(Sec)	EVENT	SETPOINT or VALUE
0.0	Main Steam Line Break Occurs	-
4.6	Low Steam Generator Pressure Trip	478 psia
	Main Steam and Feedwater Isolation Signal	478 psia
5.1	CEA's Begin to Drop Into Core	-
5.6	Main Steam and Feedwater Isolation Valves Begin to Close	-
9.6	Main Steam Iolation Valves Completely Closed	-
12.1	Pressurizer Empties	-
12.9	Safety Injection Actuation Signal	1578 psia
24.9	Safety Injection Pumps Reach Full Speed	-
35.6	Main Feedwater Isolation Valves Completely Closed	-
69.9	Return-to-Critical	-
101.0	Peak Reactivity	+0.353%$\Delta\rho$
128.5	Peak Return-to-Power	19.20%
131.5	Boron Reaches Core Mid-Plane	-
131.8	Peak Return-to-Power Core Heat Flux	19.10%
134.3	Subcritical	-
146.5	Dryout of Ruptured Steam Generator	-

14.12.3.2 No-Load Initial Condition, One-Loop Operation (Cycle 1)

It is assumed that only the two reactor coolant pumps of one loop are in operation. Due to the lower pressure drop, flow in the active loop is 112 percent of nominal flow rate, but only 87 percent of this amount flows through the reactor core, while 13 percent flows backwards through the idle loop. The reactor core flow is thus 49 percent of the nominal value. A coolant particle travels through the idle loop from the lower to the upper plenum of the pressure vessel in 39 seconds.

Results for the no-load, one-loop case are shown in Figure 14.12-8 through 14.12-13. Since it was assumed that only one loop participates in the incident, conditions for only one steam generator are shown. The pressure on the secondary side of this steam generator also drops to 478 psia within 3.9 seconds, and a reactor trip is initiated. Emptying of the pressurizer at 17 seconds results in a rapid pressure decrease to the highest saturation pressure in the reactor coolant system. Safety injection is initiated simultaneously.

Boron from the HPSI system reaches the core midplane first at 47 seconds, followed by boron from the concentrated boric acid tank at 146 seconds. The affected steam generator is empty at 163 seconds, and the rising coolant temperatures as well as the increasing boron concentration terminate the transient.

Reactor power and reactor heat flux show peak values of 27 percent and 22 percent of 1500 MWt, respectively.

14.12.3.3 Full-Load Initial Condition, Two-Loop Operation

Figures 14.12-14 through 14.12-19 show the results of the most limiting, acceptable analysis (Cycle 1) and the Cycle 8 analysis for the full load MSLB accident. The Cycle 1 values of power and heat flux have been rescaled to a full-power rating of 1500 MWt rather than 1420 MWt.

Cycle 1

The full power MSLB was analyzed for two different steam generator heat transfer coefficients. The first case, with the maximum heat transfer coefficient (zero resistance due to fouling on the steam side tube surface) had to be combined with relatively low reactor coolant temperatures in order not to exceed permissible main steam pressure. The second case was run for the nominal steam pressure (770 psia), and the initial core inlet temperature was 547°F resulting in an average coolant temperature of 572°F. A higher maximum heat flux was obtained in the second case due to the more negative moderator temperature coefficient of reactivity at the higher temperature.

The pressure in the affected steam generator drops to 478 psia at 2.5 seconds following the rupture, and a reactor trip is initiated. CEA insertion starts at 3.4 seconds. At the same time, feedwater flow reduction is initiated. The reduction is linear from full power flow to 5 percent flow within 60 seconds. Emptying of the pressurizer causes a rapid pressure drop in the reactor coolant system, and therefore, a SIAS occurs at this time, i.e., 28 seconds. After reaching a minimum of 9.5 percent (half of which is fission product decay power) at 22 seconds, the continued cooldown of the moderator combined with the negative moderator coefficient results in a return to criticality and increase in power level. The power rise is interrupted at 54 seconds and 65.4 seconds by the first two cycles of borated high pressure safety injection water arriving at the core midplane. The steam generator associated with the ruptured line empties at 73 seconds. The subsequent rise of the moderator temperature decreases the core reactivity, and a subcritical condition is attained again which causes the power to decrease rapidly to the decay heat level. Boron from the concentrated boric acid tank pumped by the charging pumps reaches the core after 157 seconds. The peak power after trip is 30 percent of nominal, and the peak heat flux is 27 percent. The minimum reactor coolant pressure, 424 psia is reached at 81 seconds.

The intact steam generator, isolated on its secondary side after the start of the incident, delivers heat into the reactor coolant during the interval from 21 seconds to 88 seconds.

Cycle 8

Table 14.12-3 contains the conditions from which the Cycle 8 full-load, two-loop Main Steamline Break event was initiated and the assumptions used. Table 14.12-4 presents the sequence of events and pertinent parameter values occurring during the Cycle 8 event. This table and Figures 14.12-14 through 14.12-19 show that this event is bounded by Cycle 1. There is no return-to-critical, as in Cycle 1, and the peak return-to-power and core heat flux values are 12.9% and 13.9%, respectively. The reactivity transient has already terminated due to dryout of the ruptured steam generator (at 70.1 seconds) by the time boron from safety injection reaches the core midplane (at 143.4 seconds). An additional cooldown from automatic auxiliary feedwater actuation is prevented by the existence of a low steam generator pressure condition in the ruptured steam generator and by an adequate level in the intact unit.

TABLE 14.12-3
KEY PARAMETERS ASSUMED IN THE MAIN STEAM LINE BREAK ANALYSIS FOR FULL-LOAD AND 2-LOOP OPERATION CYCLE 8

Parameter	Units	Cycle 1	Cycle 8
Initial Core Power*	MWT	1420	1530
Initial Core Inlet Temperature	°F	547	547
Initial Pressurizer Pressure	psia	2100	2172
Initial Steam Generator Pressure	psia	770	895
Initial Steam Generator Mass Inventory (Level)	% Narrow Range Scale	63	70
RCS Flow Rate	gpm	209,500	197,000
Feedwater Pumpdown After Trip		5%/60 sec	10.66%/40 sec
Minimum CEA Worth Available at Trip	%Δρ	-5.0	-6.68
Doppler Multiplier		1.20	1.15
Moderator Cooldown Curve	%Δρ vs temp.	See Figure 14.12-1	See Figure 14.12-1
Inverse Boron Worth	PPM/%Δρ	-80	-94
Effective MTC	$x10^{-4}$Δρ/°F	-2.3	-2.5
β Fraction (including uncertainty)		**	0.0058

* Reactor coolant pump heat of 5.6 MWT not included in this value.
** Data not available.

TABLE 14.12-4

SEQUENCE OF EVENTS FOR THE MAIN STEAMLINE BREAK EVENT
FOR FULL-LOAD AND TWO-LOOP OPERATION
CYCLE 8

TIME(Sec)	EVENT	SETPOINT or VALUE
0.2	Main Steam Line Break Occurs	-
4.9	Low Steam Generator Pressure Trip	478 psia
	Main Steam and Feedwater Isolation Signal	478 psia
5.4	CEA's Begin to Drop Into Core	-
5.9	Main Steam ad Feedwater Isolation Valves Begin to Close	-
9.9	Main Steam Iolation Valves Completely Closed	-
13.5	Pressurizer Empties	-
13.6	Safety Injection Actuation Signal	1578 psia
35.9	Main Feedwater Isolation Valves Completely Closed	-
65.8	Peak Return-to-Power Core Heat Flux	13.94%
70.1	Dryout of Ruptured Steam Generator	-
72.8	Peak Reactivity	-0.204%$\Delta\rho$
	Peak Return-to-Power	12.92%
143.4	Boron from Safety Injection Reaches Core Mid-Plane	-

14.12.3.4 Margin to DNB during the Transients

The critical heat flux was calculated, (Reference 2) for the worst conditions occurring during the Cycle 1 no-load, one-loop case. These conditions are 22 percent core heat flux, 140 psia coolant pressure and 22°F subcooling. The radial power distribution was determined for one stuck CEA, with Doppler and moderator void feedback. The resulting critical heat flux is greater than the maximum local core heat flux for this case, and DNB is not expected to occur.

The peak flux during the Cycle 1 no-load, two-loop incident is slightly greater than in the one-loop case. However, full core flow is available, and the minimum coolant pressure of 190 psia is high enough to provide comparable margin to the critical heat flux.

The minimum coolant pressure is still higher in the Cycle 1 full-power, two-loop incident. Therefore, the void feedback is not as effective in flattening the radial power distribution as for the no load cases, but the peak heat flux is still below the calculated critical heat flux.

The margin to DNB, for the Cycle 8 MSLB no-load, two-loop and full-load, two-loop cases, is greater than for Cycle 1 due to significantly lower peak heat fluxes when combined with both similar RCS pressures and coolant temperatures.

The DNB consequences of a steam line break with the reactor coolant pumps tripped were addressed in Reference 3. This analysis concluded that the margin to fuel failure is decreased by reducing RCS flow prior to the post-trip return to power but the consequences of the steam line break would be acceptable. The NRC review of ths analysis is contained in Reference 4. Based on this analysis and review it is concluded that sufficient margin to DNB is maintained.

14.12.4 Radiological Consequences of MSLB

The radiological consequences of MSLB are determined based on the conservative assumption that there is a complete severance of a mian steam line outside the containment with the plant in a hot zero power condition where the transient is initialed shortly after full power operation. The hot zero power condition assures the maximum water inventory in the steam generators and the shutdown from full power assures the maximum decay heat which must be removed by manual control of the atmospheric dump valve associated with the intact steam generator. The MSIV's are installed in the min steam lines from each steam generator, downstream from the safety relief valves and atmospheric dump valves outside the containment. The MSLB is assumed to beupstream of the MSIV. Following a reactor trip, the affected steam generator blows down completely and the steam is vented directly to the atmosphere. Mass release from the intact steam generator is terminated when the shutdown cooling system is initiated at a reactor coolant system temperature of 300°F.

The following assumptions are postulated in the calculation of radiological consequences:

1. The reactor coolant equilibrium activity is based on long term operation at 100 percent of the ultimate core power level of 1500 MWt nd 1% failed fuel. The RCS equilibrium activity is 60 μCi/gm DEC I-131.

2. The activity in the secondary coolant is assumed to be equal to 0.1 μVi/gm DEC I-131.

3. The primary-to-secondary leakage of 1 gpm was assumed to continue through the affected steam generator at a constant rate until shutdown cooling is initiated.

4. Offsite power is lost; the main condenser is not available for steam relief via the turbine bypass system.

5. The activity released from the steam generators is immediately vented to the atmosphere. No credit is taken for radioactive decay for isotopes in transit to the dose points.

6. The mass of primary-to-secondary leakage for the 30-minute duration is 491 lbs.

7. The secondary mass release to atmosphere from the affected steam generator is 233,498 lbs.

8. A post-accident steam generator decontamination factor between steam and water phase is 1.0.

9. The total activity released from the steam generator for various nuclides is provided in Table 14.12-5.

10. The dispersion factors for the EAB and the LPZ outer boundary are 4.4 E-04 sec/m^3 and 1.57 E-05 sec/m^3, respectively.

11. The adult breathing rate for the EAB and LPZ is 3.47 E-04 m^3/sec.

Based on these assumptions, the resulting doses are as follows:

	Thyroid (Rems)	Whole Body (Rems)
EAB	5.41 E+00	5.66 E-04
LPZ	1.93 E-01	2.02 E-05

TABLE 14.12-5

ACTIVITY RELEASED FROM THE STEAM GENERATOR

Nuclide	Activity (Curies)
DEC I-131	2.39 E+01
Kr-83m	1.86 E-02
Kr-85m	1.08 E-01
Kr-85	1.93 E+00
Kr-87	4.80 E-02
Kr-88	2.12 E-01
Xe-131m	1.61 E-01
Xe-133m	2.44 E-01
Xe-133	2.20 E+01
Xe-135m	4.83 E-03
Xe-135	3.63 E-01
Xe-138	1.54 E-02

14.12.5 Conclusions

A steam line rupture may lead to a rapid cooldown of the reactor coolant and a corresponding increase in reactivity. The assumption of one CEA not falling into the core after trip causes a redistribution in the radial power that is used in determining peak local power during the post-trip power transient. The complete rupture of the steam line at the outlet of a steam generator (for radiological evaluation the break is assumed outside the containment) with the

most negative moderator temperature coefficient of reactivity was analyzed for different operating conditions. Conservatism is added by inclusion of uncertainties for the moderator and fuel temperature coefficients of reactivity, by taking no credit for void reactivity feedback, and by taking credit for only two of the three HPSI pumps for Cycle 1 and for only one HPSI pump for the current analysis. Based on the results of the Cycle 1 and Cycle 8 analyses, no fuel damage will occur, since the critical heat flux is not exceeded.

The results of radiological consequences due to a postulated MSLB are presented above. The values for thyroid dose and whole body dose show that the calculated doses using the conservative assumptions are well within the limits of 10CFR Part 100.

14.12.6 SECTION 14.12 REFERENCE

1. Fort Calhoun SER on Automatic Initiation of Auxiliary Feedwater, contained in the letter to W.C. Jones from Robert A. Clark, dated February 20, 1981.

2. Burnout Analysis Part 4: Application of a Local Conditions Hypothesis to World Data for Uniformily Heated Round Tubes and Rectangular Channels, MacBeth, R. V., AEEW-R-267, August, 1963

3. CEN-115, Response to NRC IE Bulletin, 79-06C for Combustion Engineering Nuclear Steam Supply System, August 1979.

4. NUREG-0623, Generic Assessment of Delayed Reactor Coolant Pump Trip during Small Break Loss-of-Coolant Accidents in Pressurized Water Reactors, November, 1979.

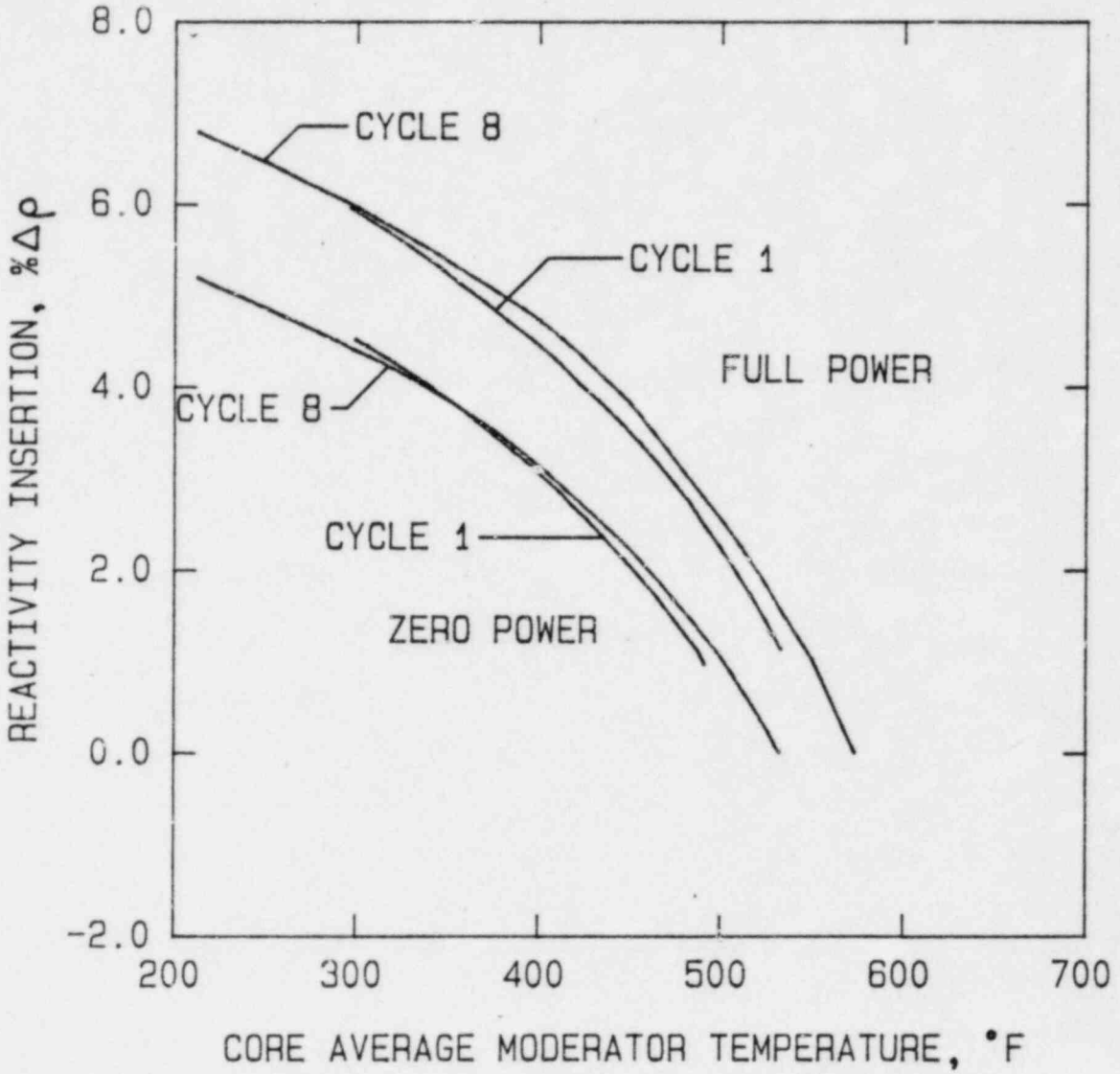

Steam Line Break Incident Reactivity vs Moderator Temperature	Omaha Public Power District Fort Calhoun Station-Unit No. 1	Figure 14.12-1

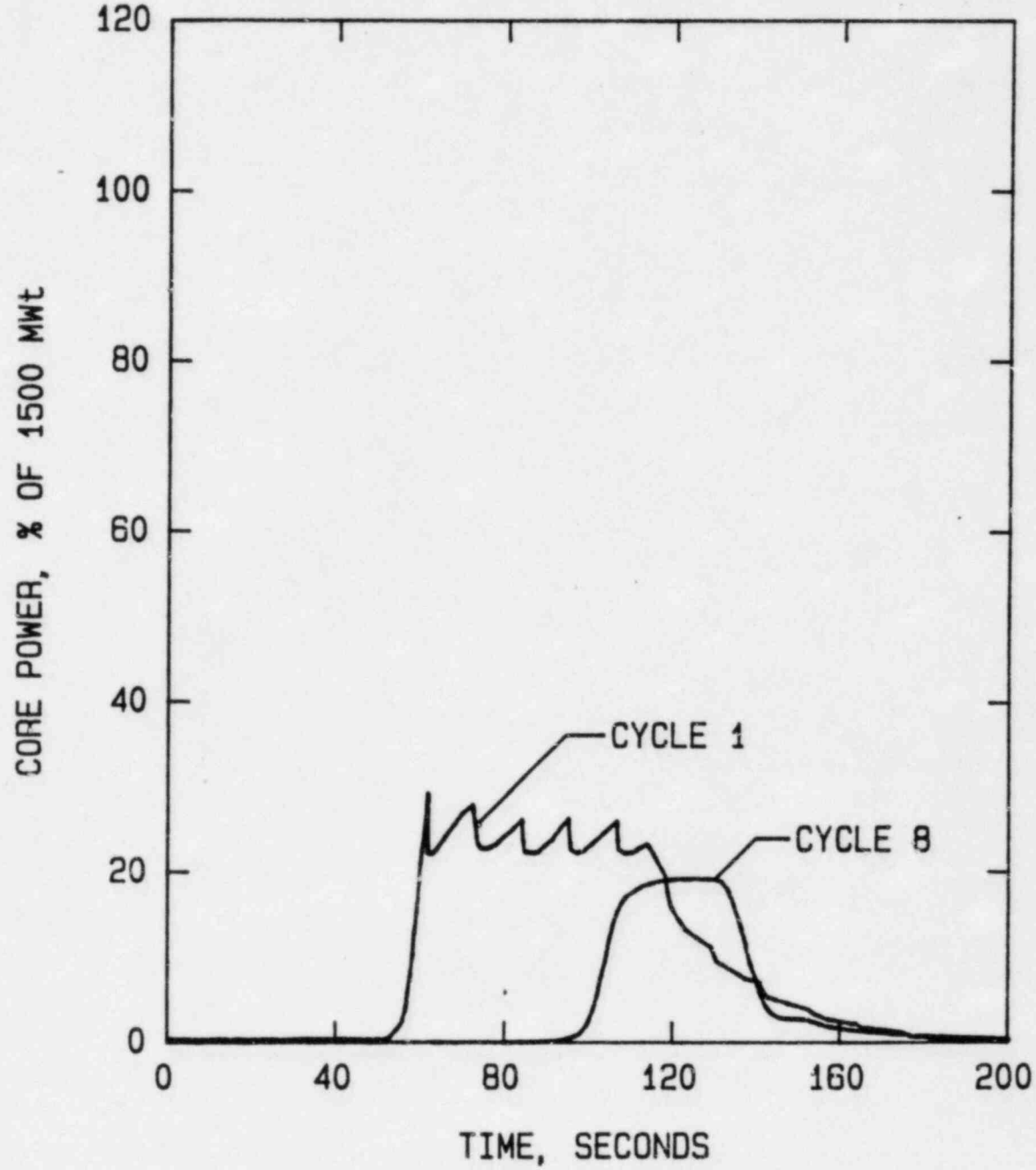

NOTE:
No Load Initial Condition
Two Loop Operation

Steam Line Break Incident Core Power vs Time	Omaha Public Power District Fort Calhoun Station-Unit No. 1	Figure 14.12-2

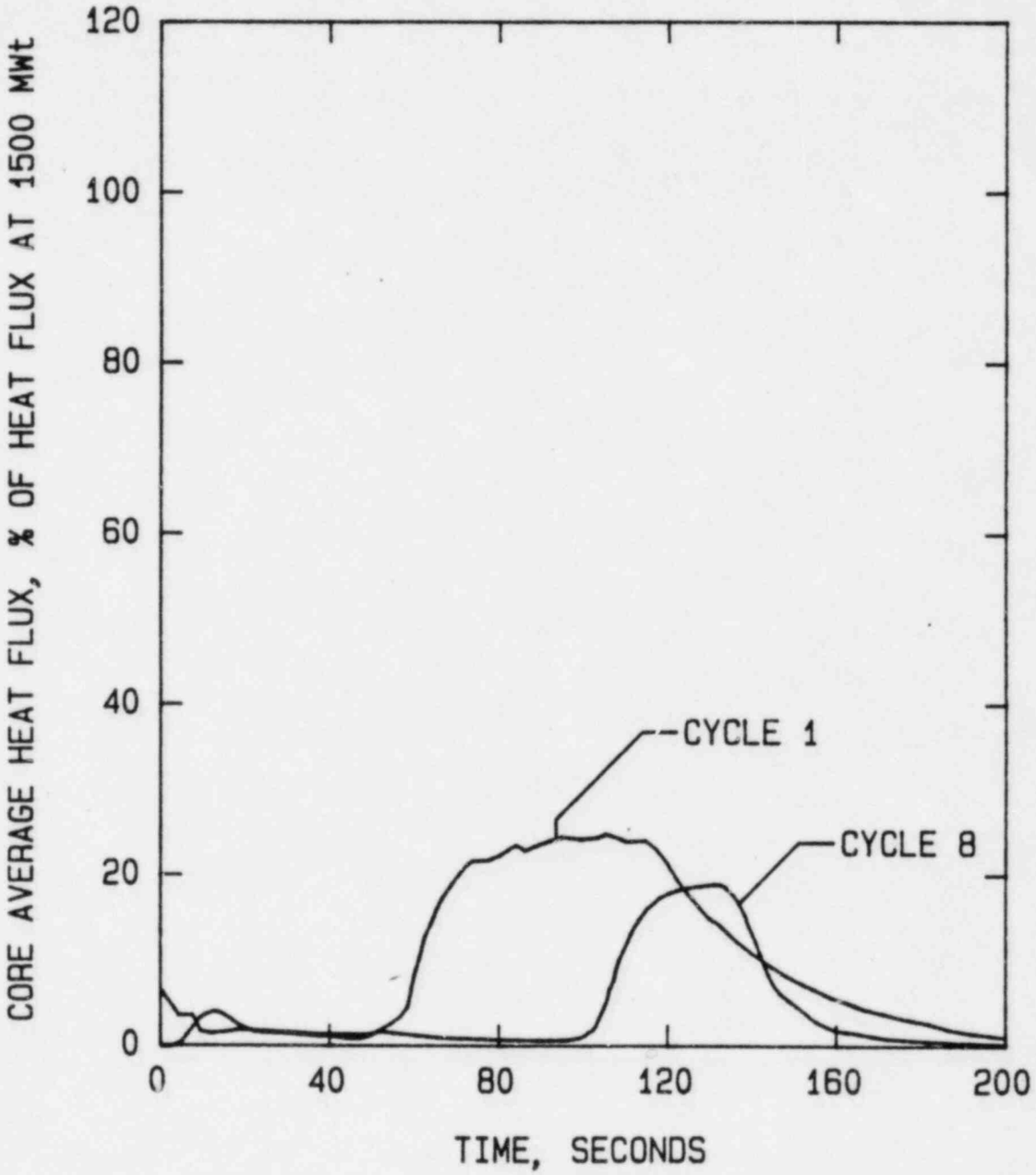

NOTE:
No Load Initial Condition
Two Loop Operation

Steam Line Break Incident Core Average Heat Flux vs Time	Omaha Public Power District Fort Calhoun Station-Unit No. 1	Figure 14.12-3

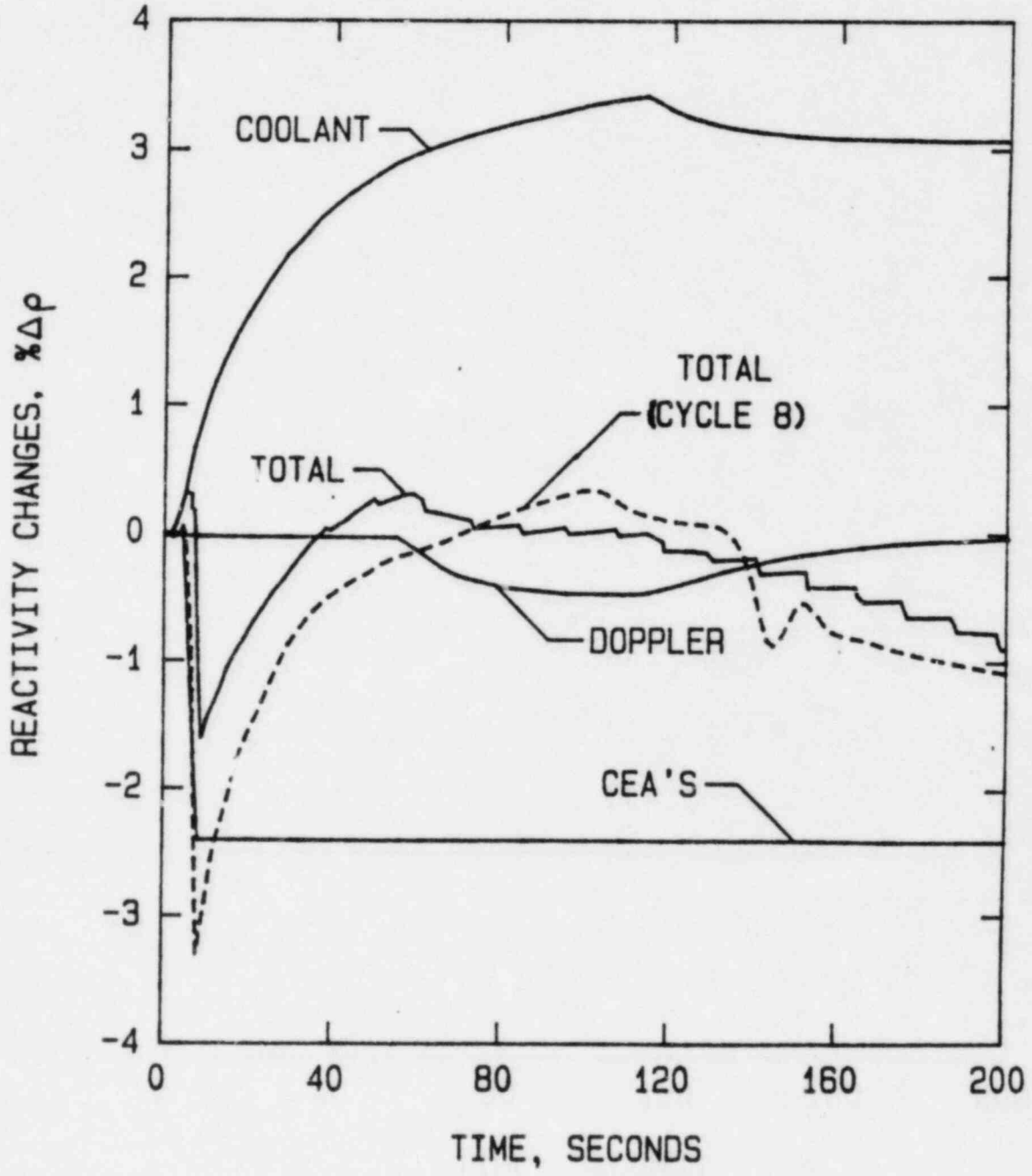

NOTE:

Limiting Cycle (Cycle 1) Unless Otherwise Noted
No Load Initial Condition - Two Loop Operation

Steam Line Break Incident Reactivity Changes vs Time	Omaha Public Power District Fort Calhoun Station-Unit No. 1	Figure 14.12-4

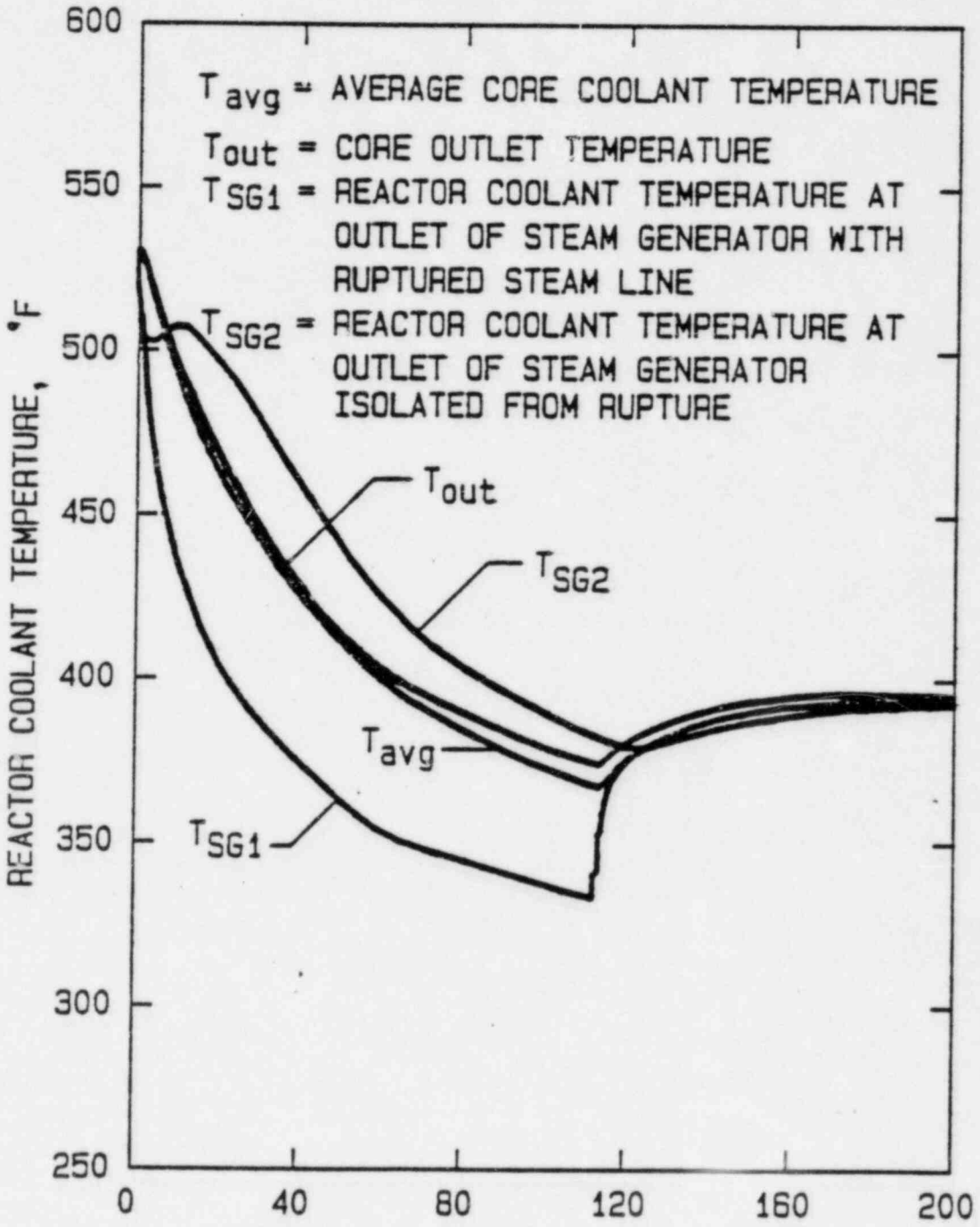

NOTE:

No Load Initial Condition - Two Loop Operation
Limiting Cycle (Cycle 1)

Steam Line Break Incident Reactor Coolant Temperatures vs Time	Omaha Public Power District Fort Calhoun Station-Unit No. 1	Figure 14.12-5

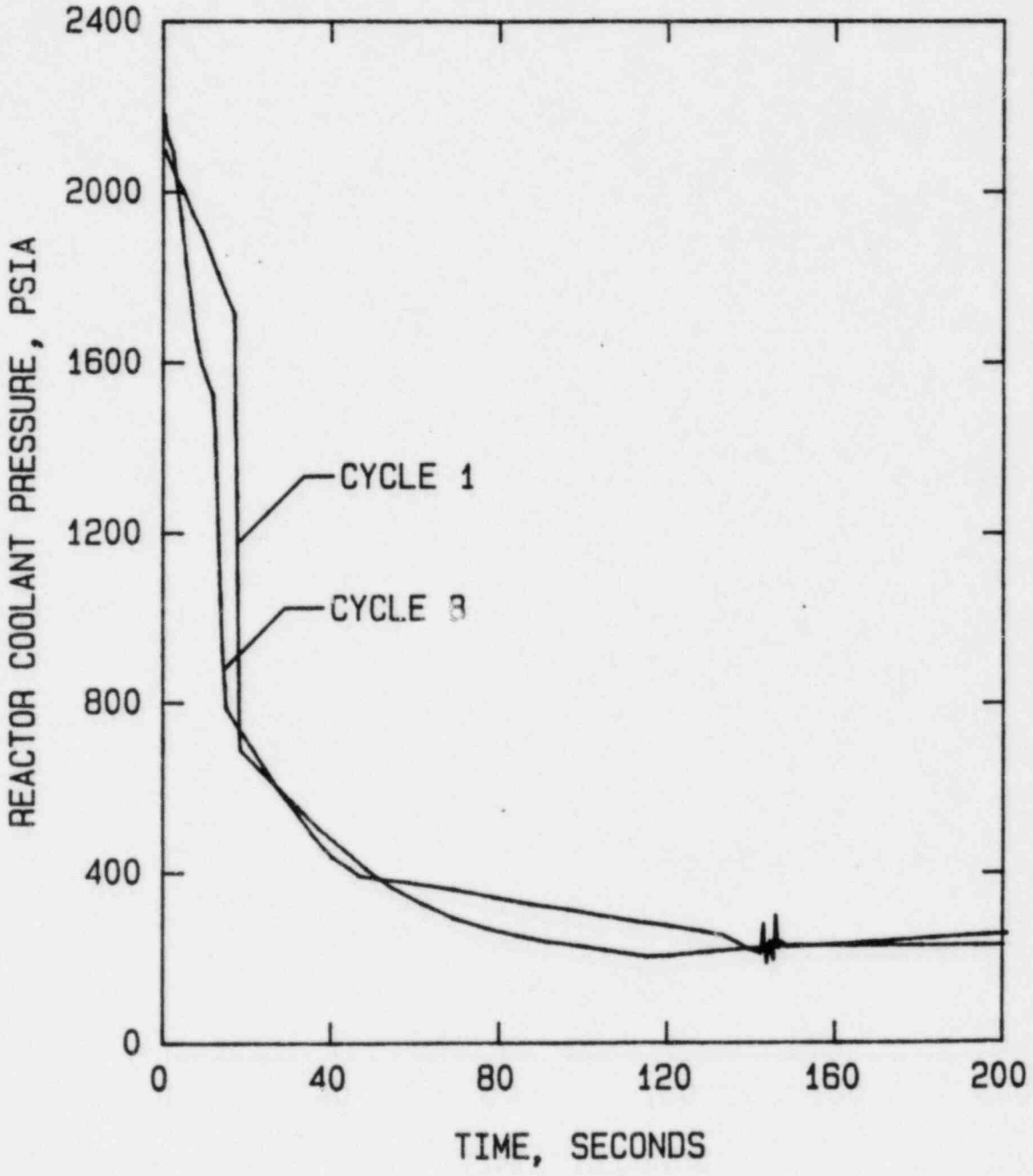

NOTE:
No Load Initial Condition
Two Loop Operation

Steam Line Break Incident Coolant System Pressure vs Time	Omaha Public Power District Fort Calhoun Station-Unit No. 1	Figure 14.12-6

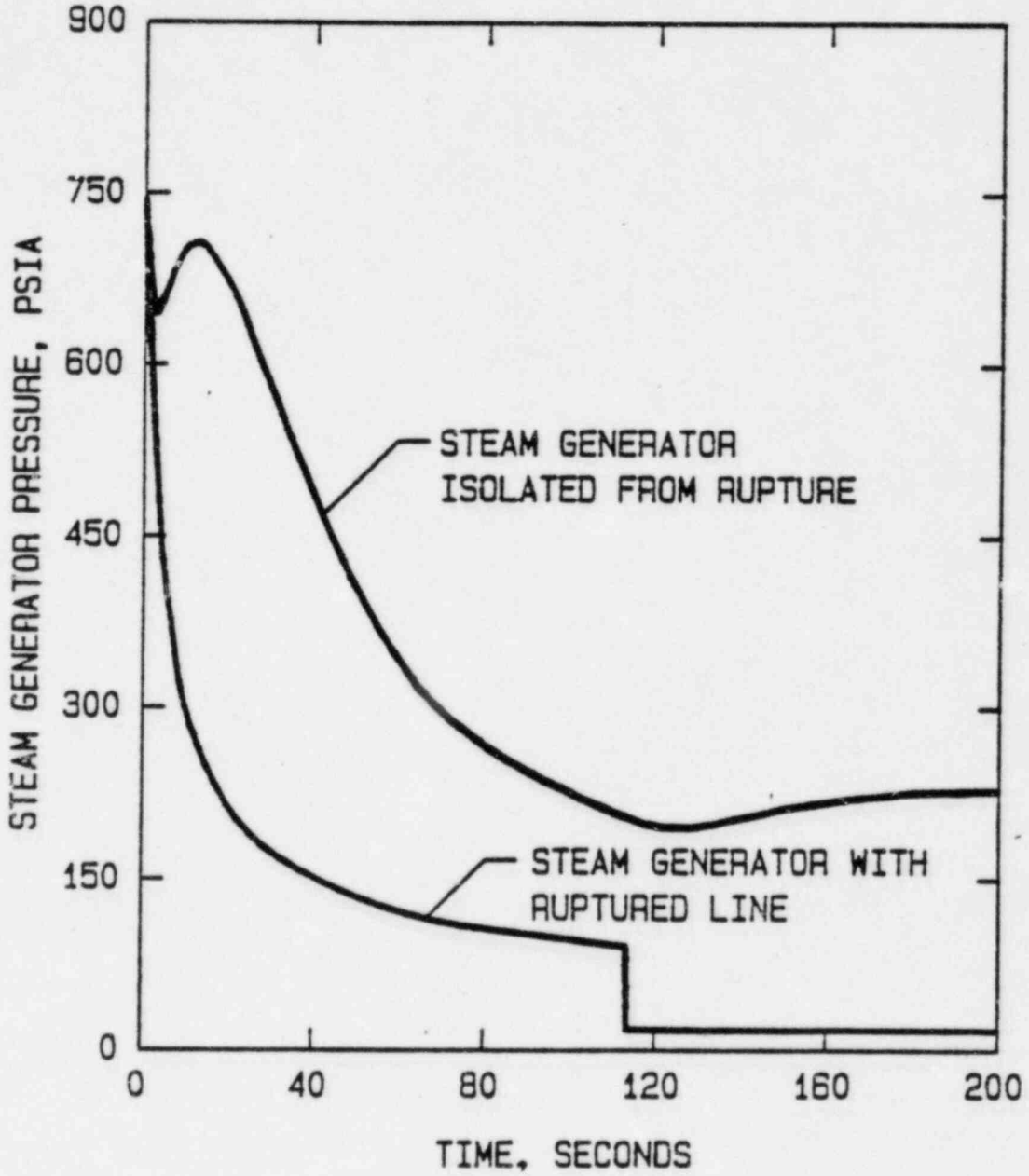

NOTE:

No Load Initial Condition
Two Loop Operation
Limiting Cycle (Cycle 1)

Steam Line Break Incident Steam Generator Pressure vs Time	Omaha Public Power District Fort Calhoun Station-Unit No. 1	Figure 14.12-7

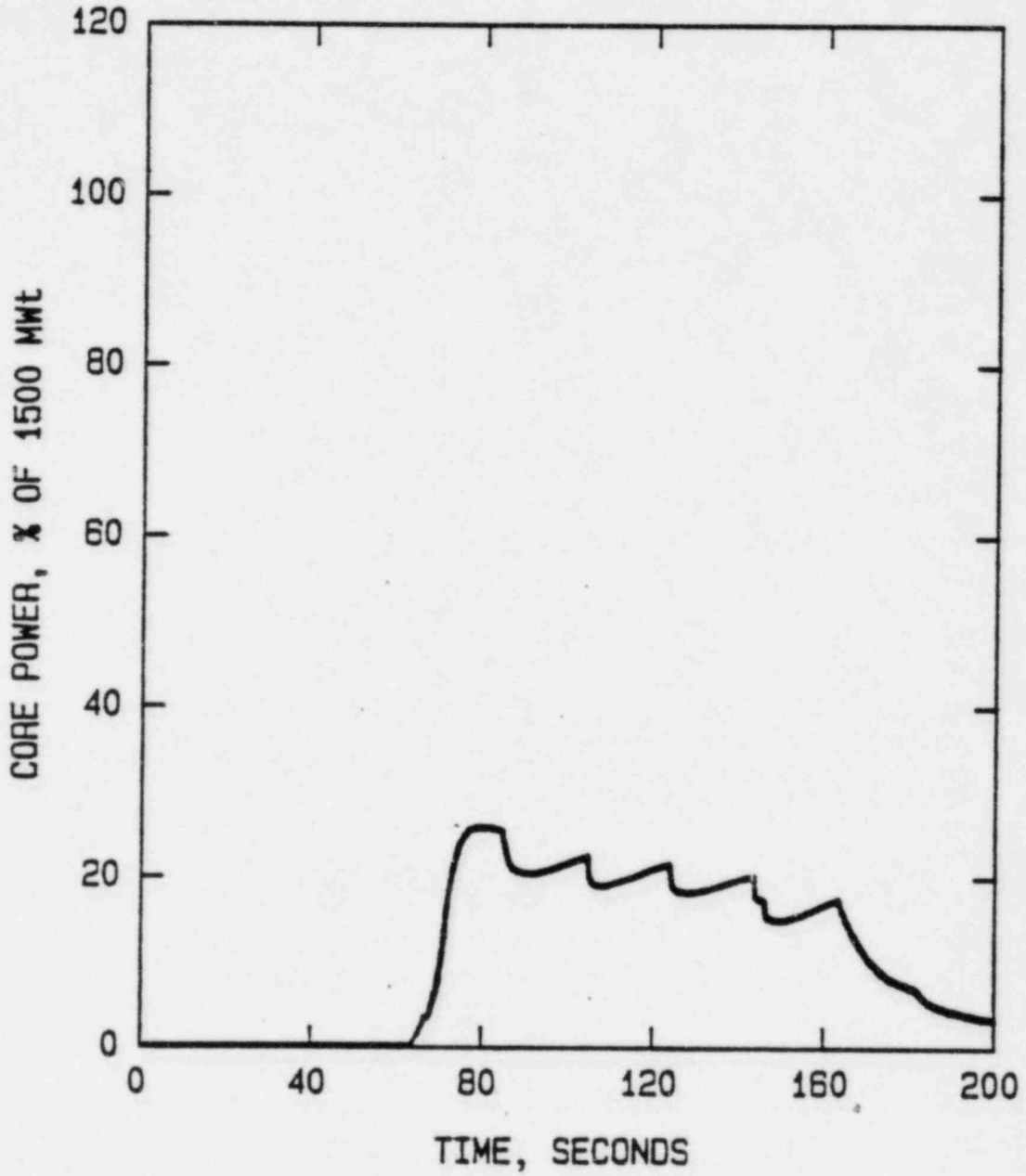

NOTE:
No Load Condition
One Loop Operation
Cycle 1

Steam Line Break Incident Core Power vs Time	Omaha Public Power District Fort Calhoun Station-Unit No. 1	Figure 14.12-8

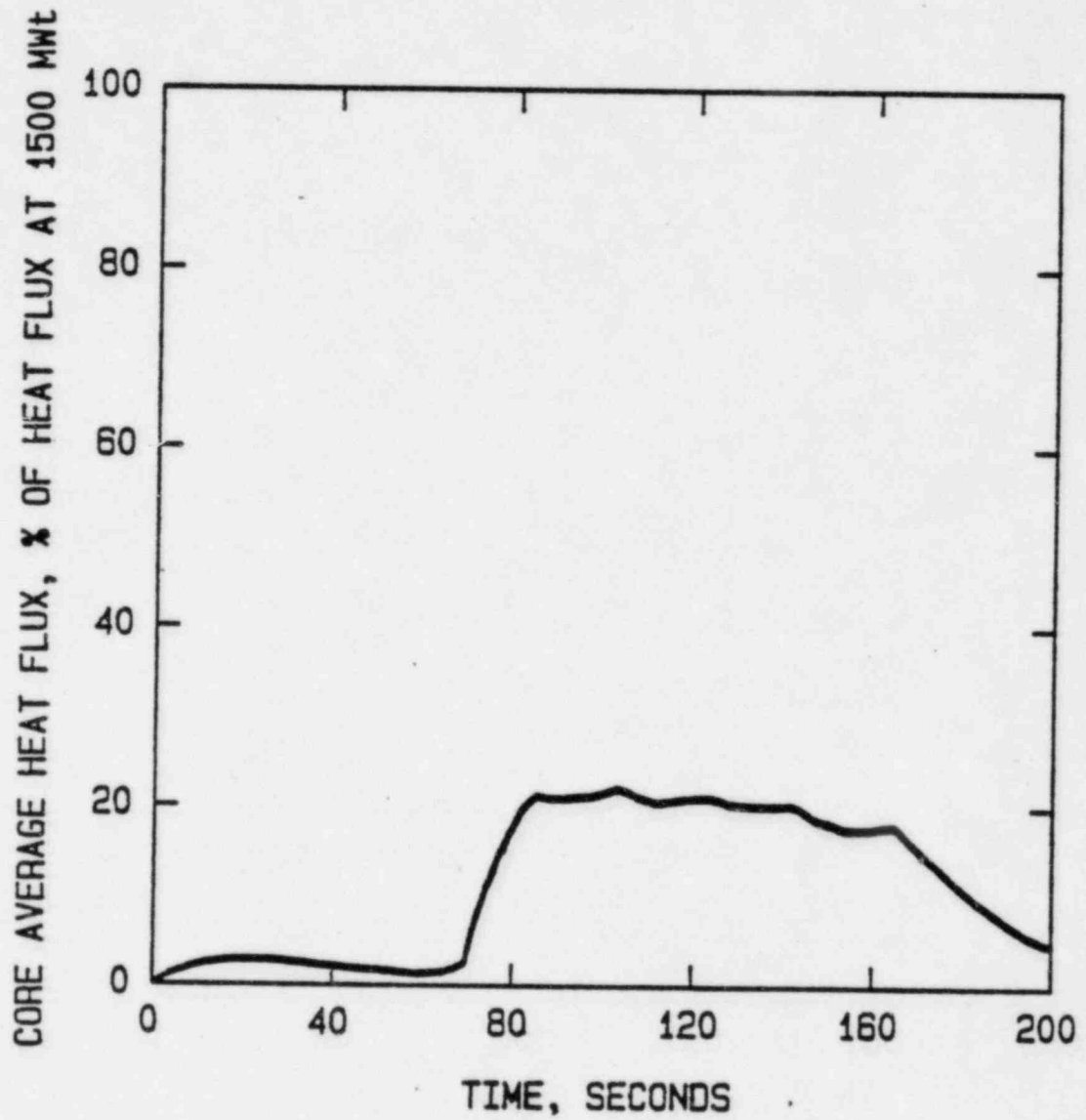

NOTE:
Cycle 1
No Load Initial Condition
One Loop Operation

Steam Line Break Incident Core Average Heat Flux vs Time	Omaha Public Power District Fort Calhoun Station-Unit No. 1	Figure 14.12-9

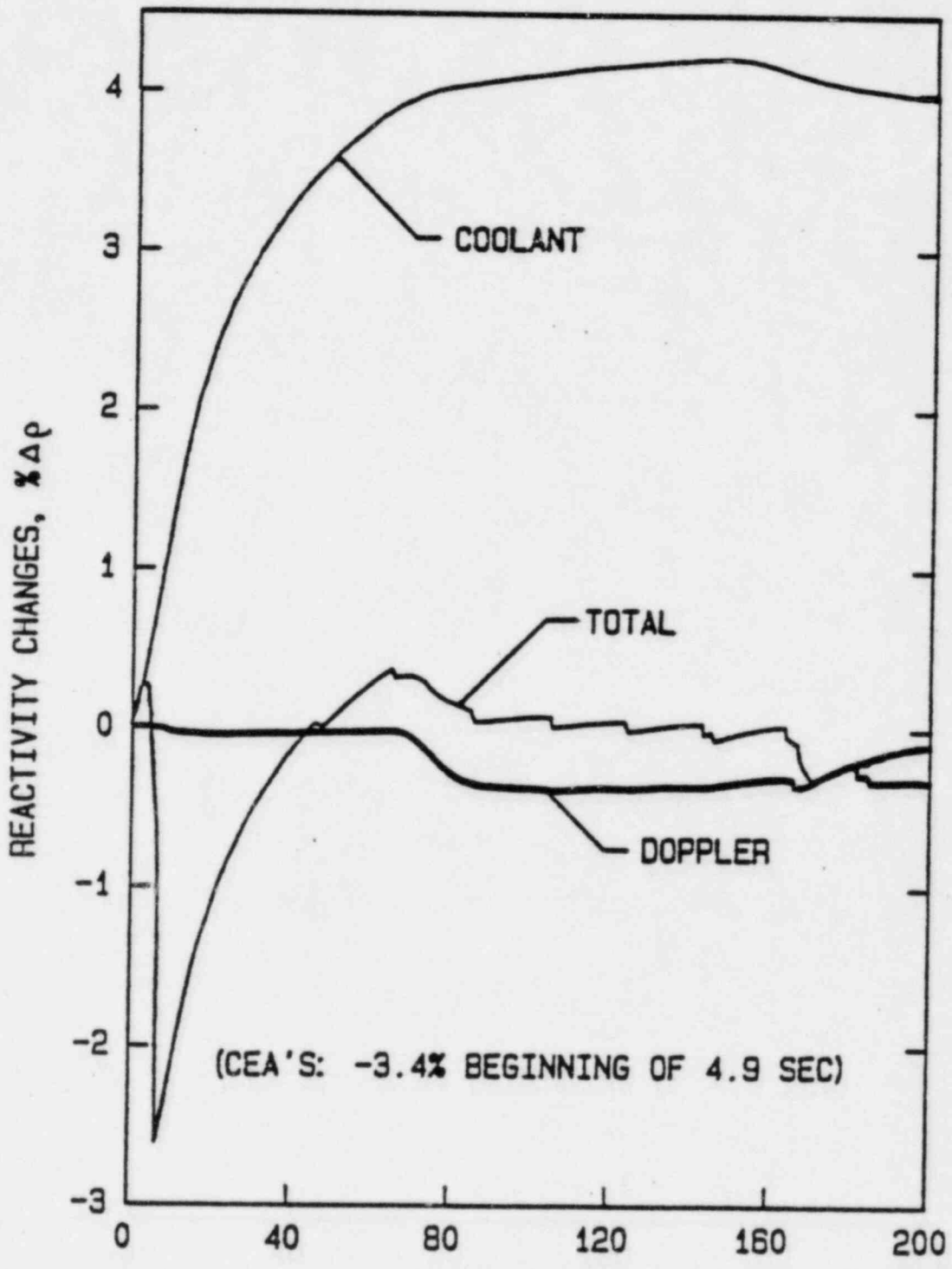

NOTE:
No Load Initial Condition
One Loop Operation - CYCLE 1 OPERATION

Steam Line Break Incident Reactivity Changes vs Time	Omaha Public Power District Fort Calhoun Station-Unit No. 1	Figure 14.12-10

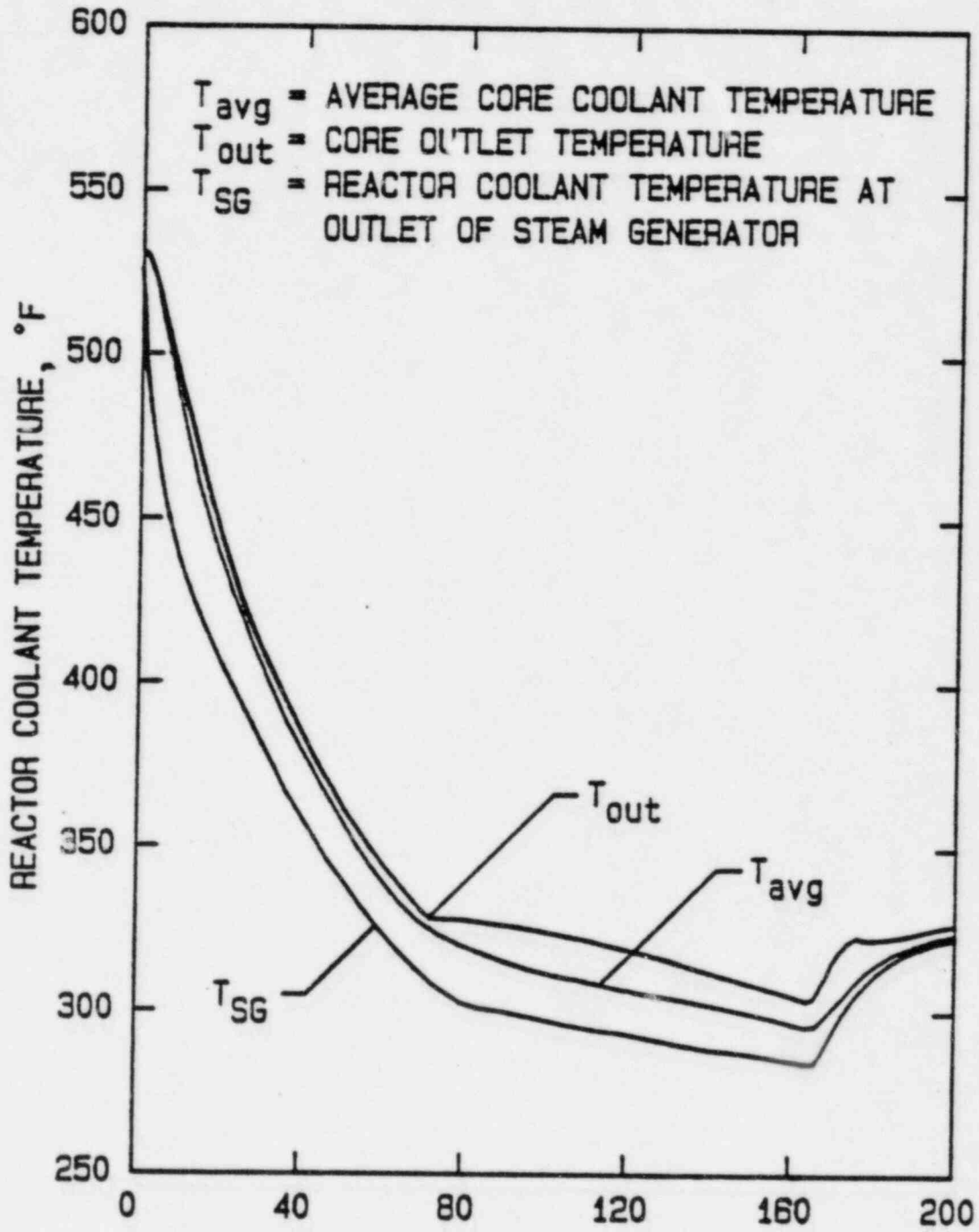

NOTE:
Cycle 1
No Load Initial Conditions - One Loop Operation

Steam Line Break Incident Reactor Coolant Temperatures vs Time	Omaha Public Power District Fort Calhoun Station-Unit No. 1	Figure 14.12-11

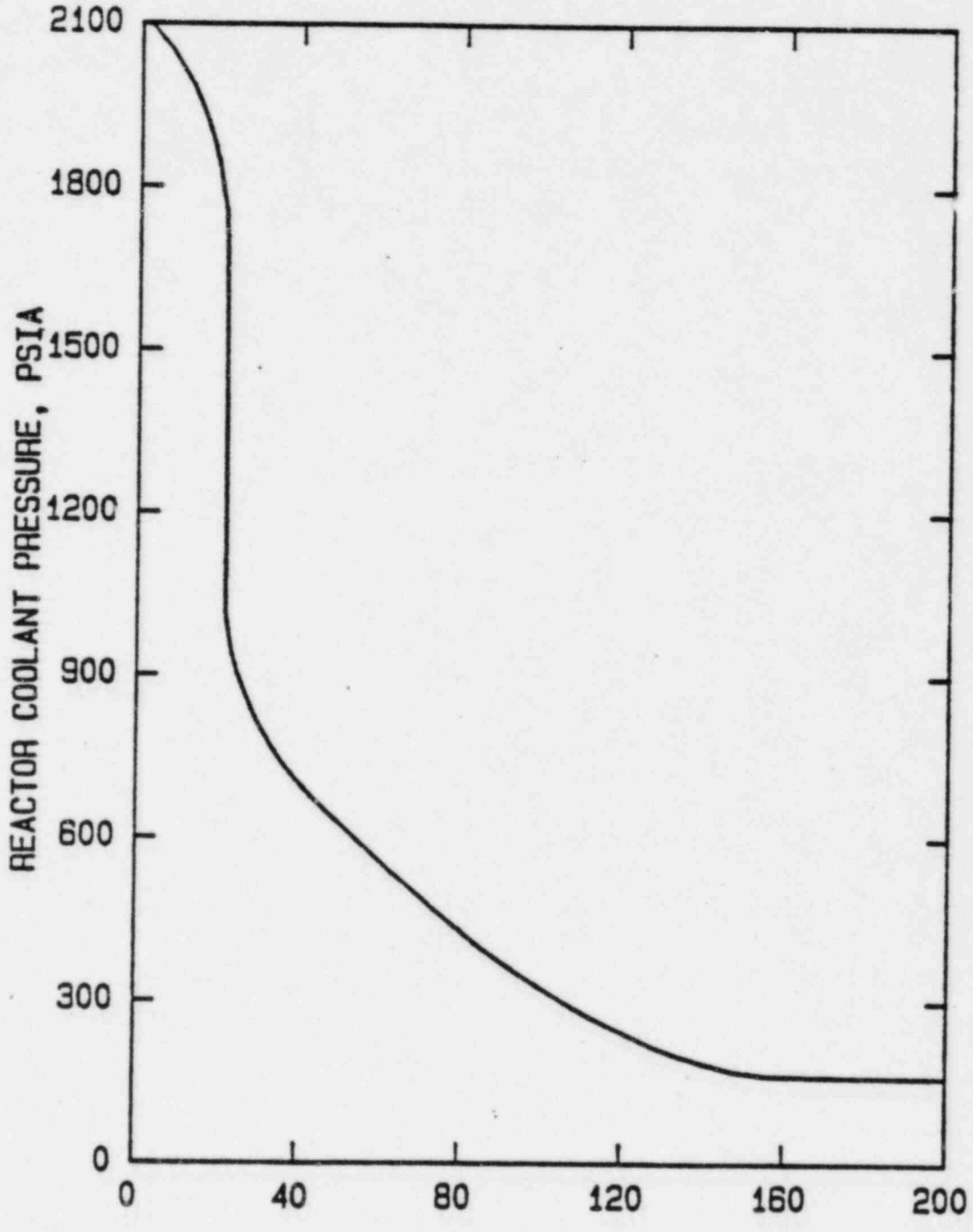

NOTE:
Cycle 1
No Load Initial Condition - One Loop Operation

Steam Line Break Incident Reactor Coolant Pressure vs Time	Omaha Public Power District Fort Calhoun Station-Unit No. 1	Figure 14.12-12

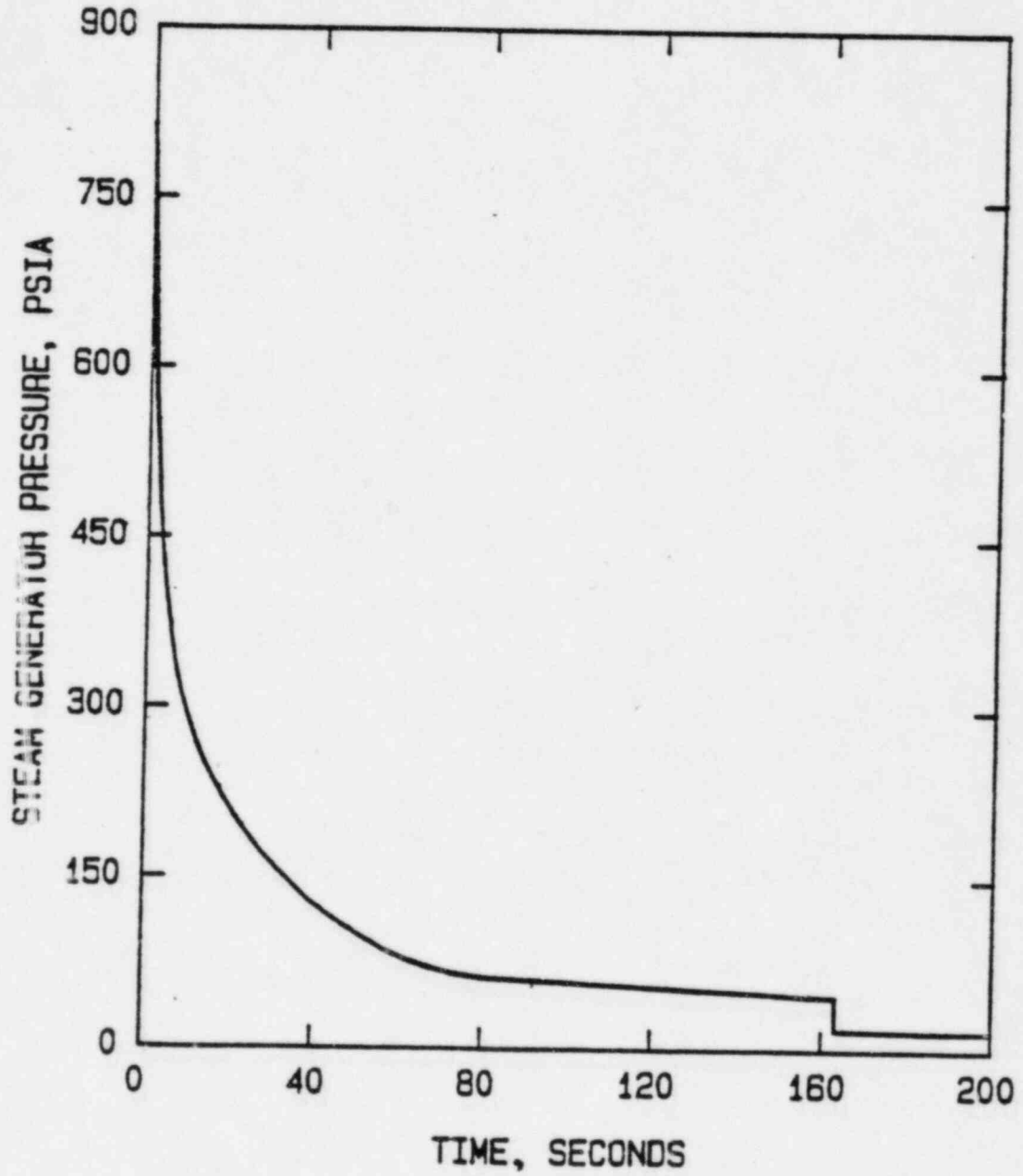

NOTE:

No Load Initial Condition
One Loop Operation
Cycle 1

Steam Line Break Incident Steam Generator Pressure vs Time	Omaha Public Power District Fort Calhoun Station-Unit No. 1	Figure 14.12-13

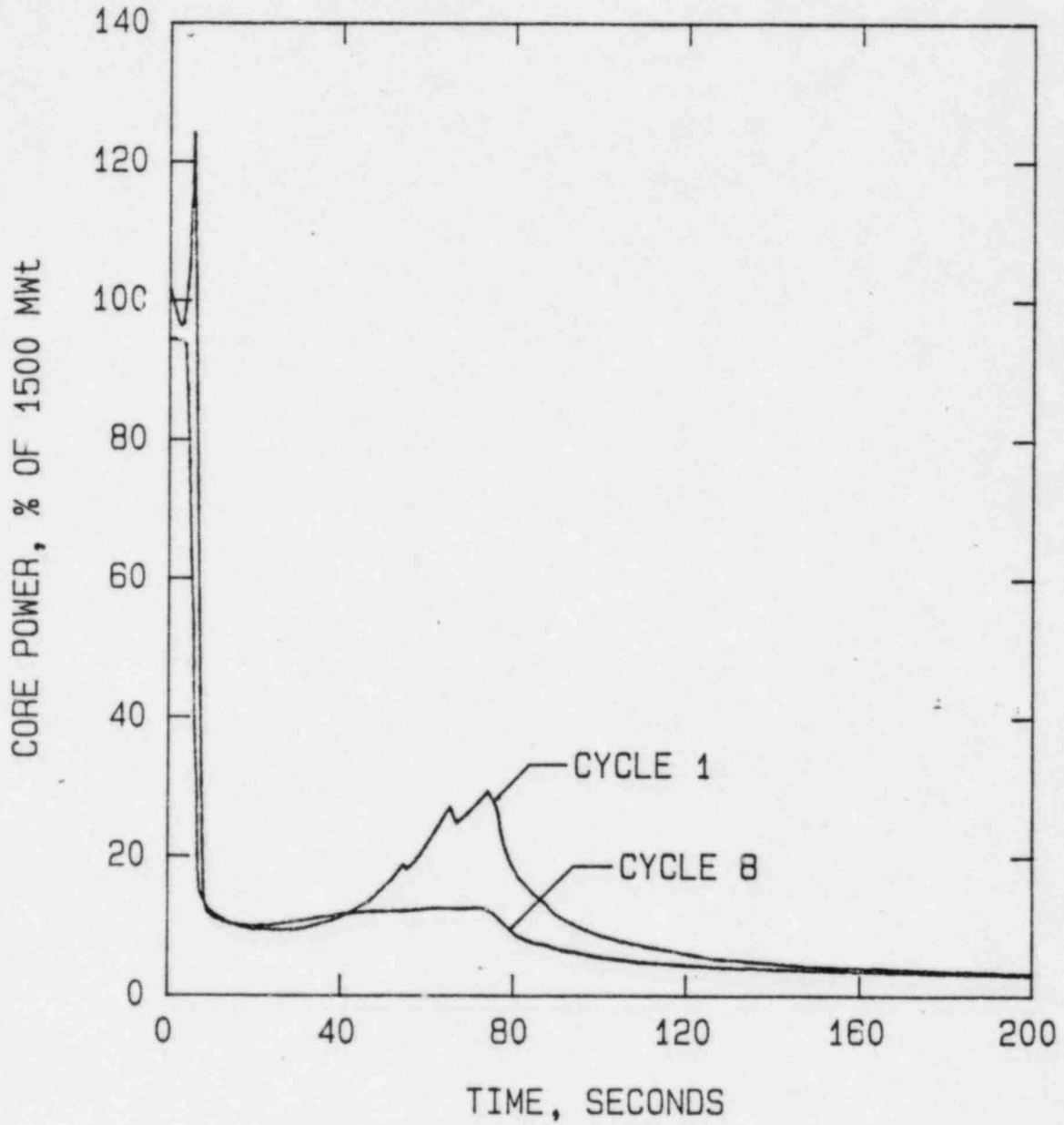

NOTE:
Full Load Initial Conditions

Steam Line Break Incident Core Power vs Time	Omaha Public Power District Fort Calhoun Station-Unit No. 1	Figure 14.12-14

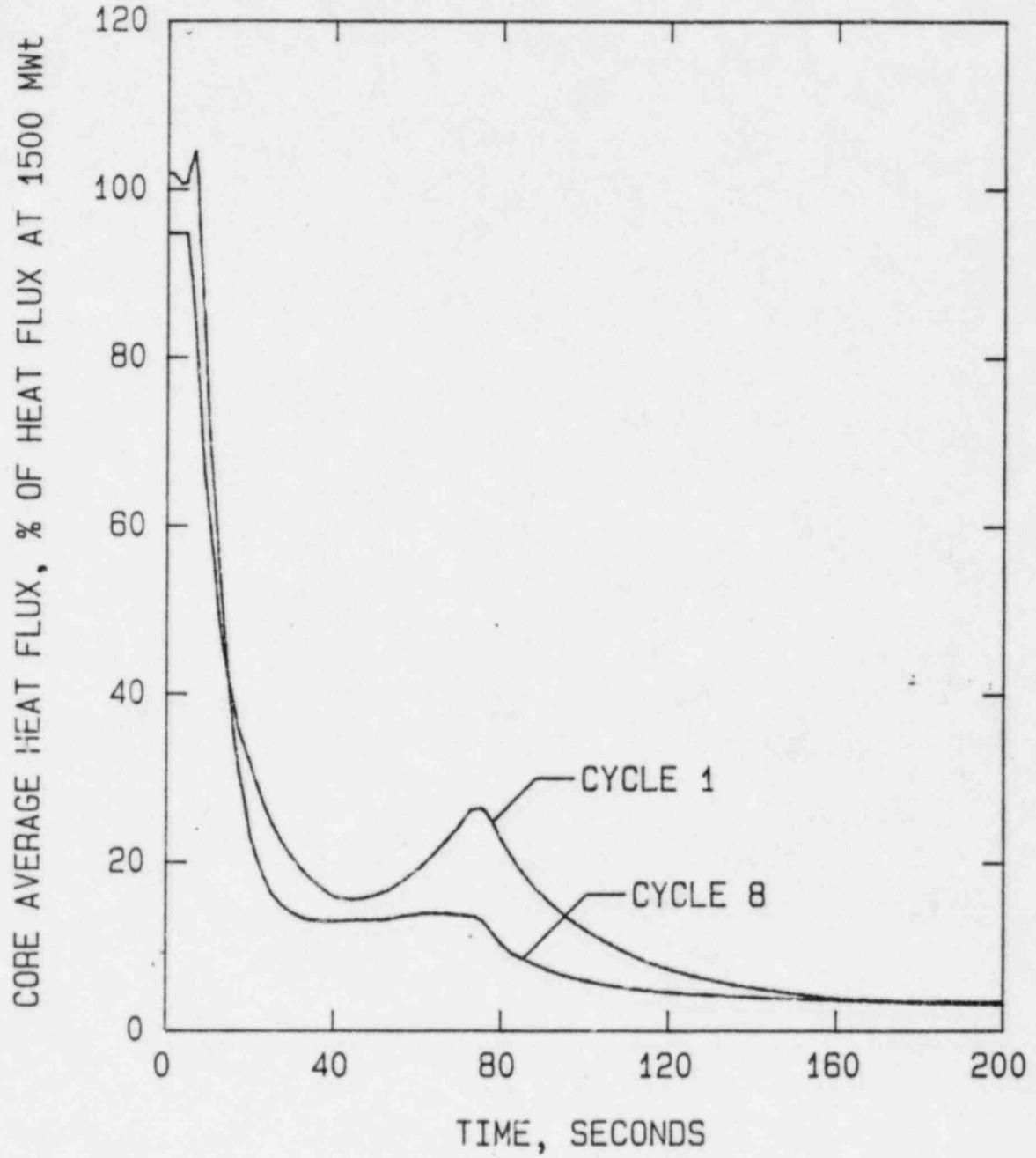

NOTE:
Full Load Initial Conditions

Steam Line Break Incident Core Average Heat Flux vs Time	Omaha Public Power District Fort Calhoun Station-Unit No. 1	Figure 14.12-15

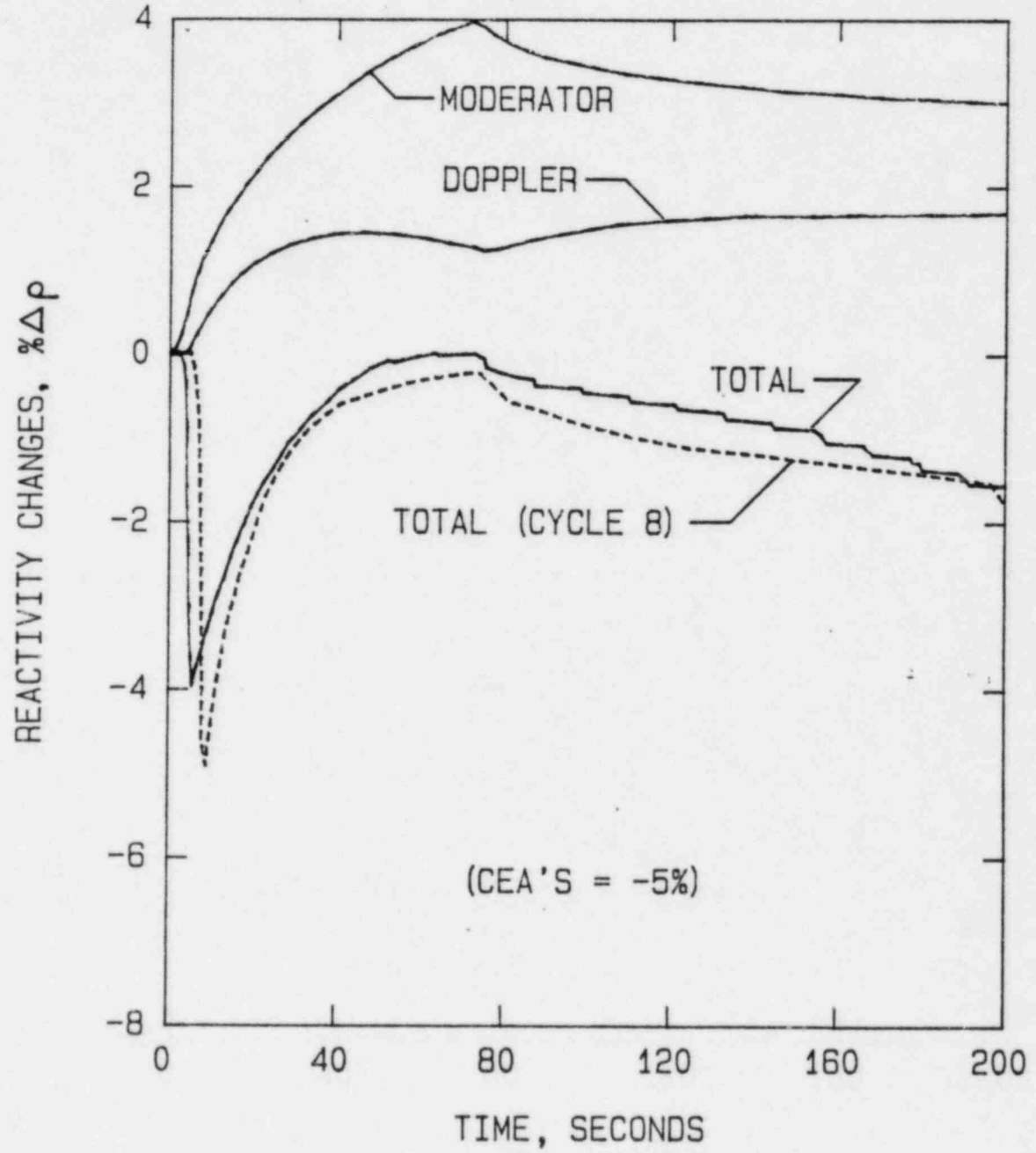

NOTE:

Limiting Cycle (Cycle 1) - Unless Otherwise Noted
Full Load Initial Conditions

Steam Line Break Incident Reactivity Changes vs Time	Omaha Public Power District Fort Calhoun Station-Unit No. 1	Figure 14.12-16

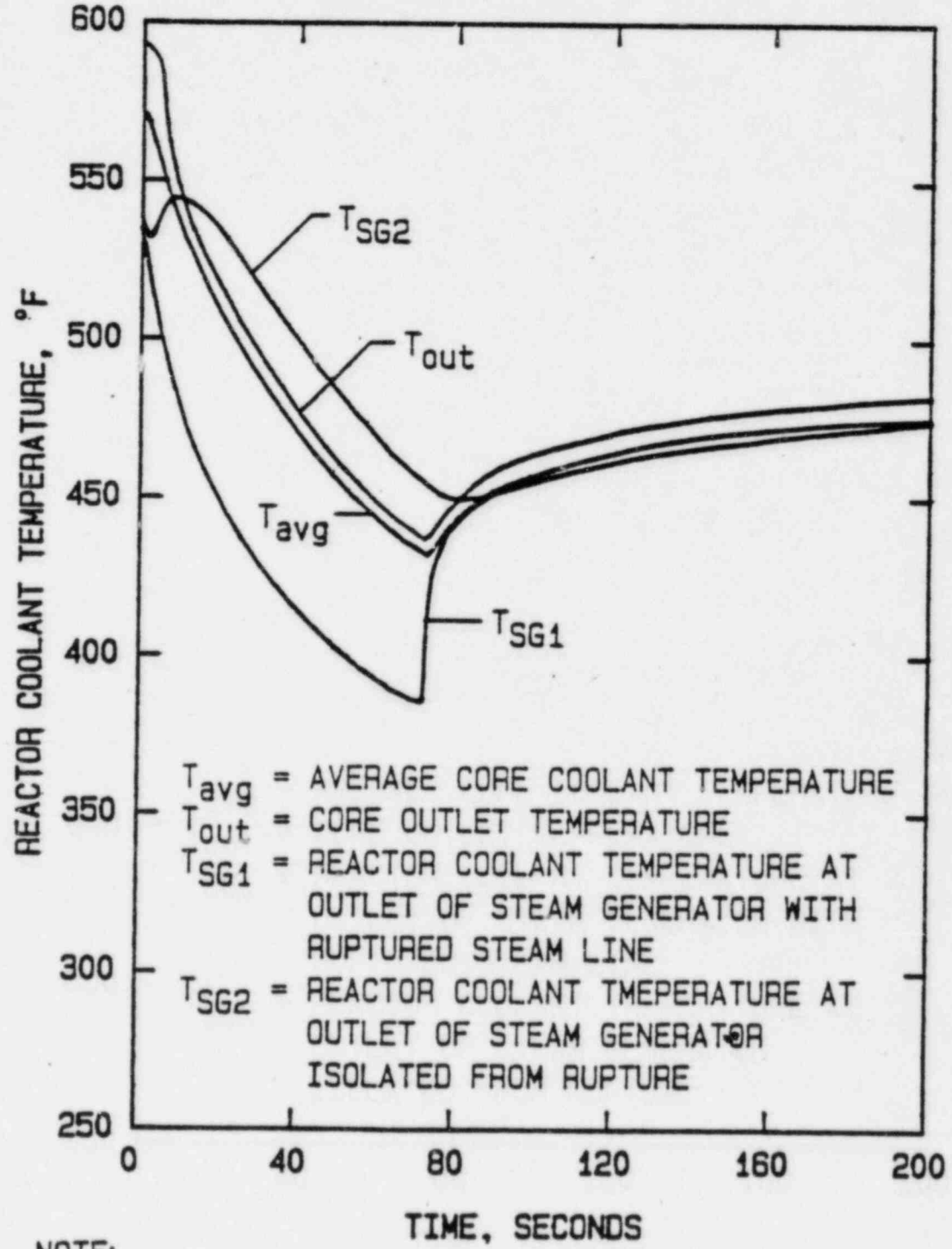

NOTE:
Limiting Cycle (Cycle 1) Full Load Initial Condition

Steam Line Break Incident Reactor Coolant Temperatures vs Time	Omaha Public Power District Fort Calhoun Station-Unit No. 1	Figure 14.12-17

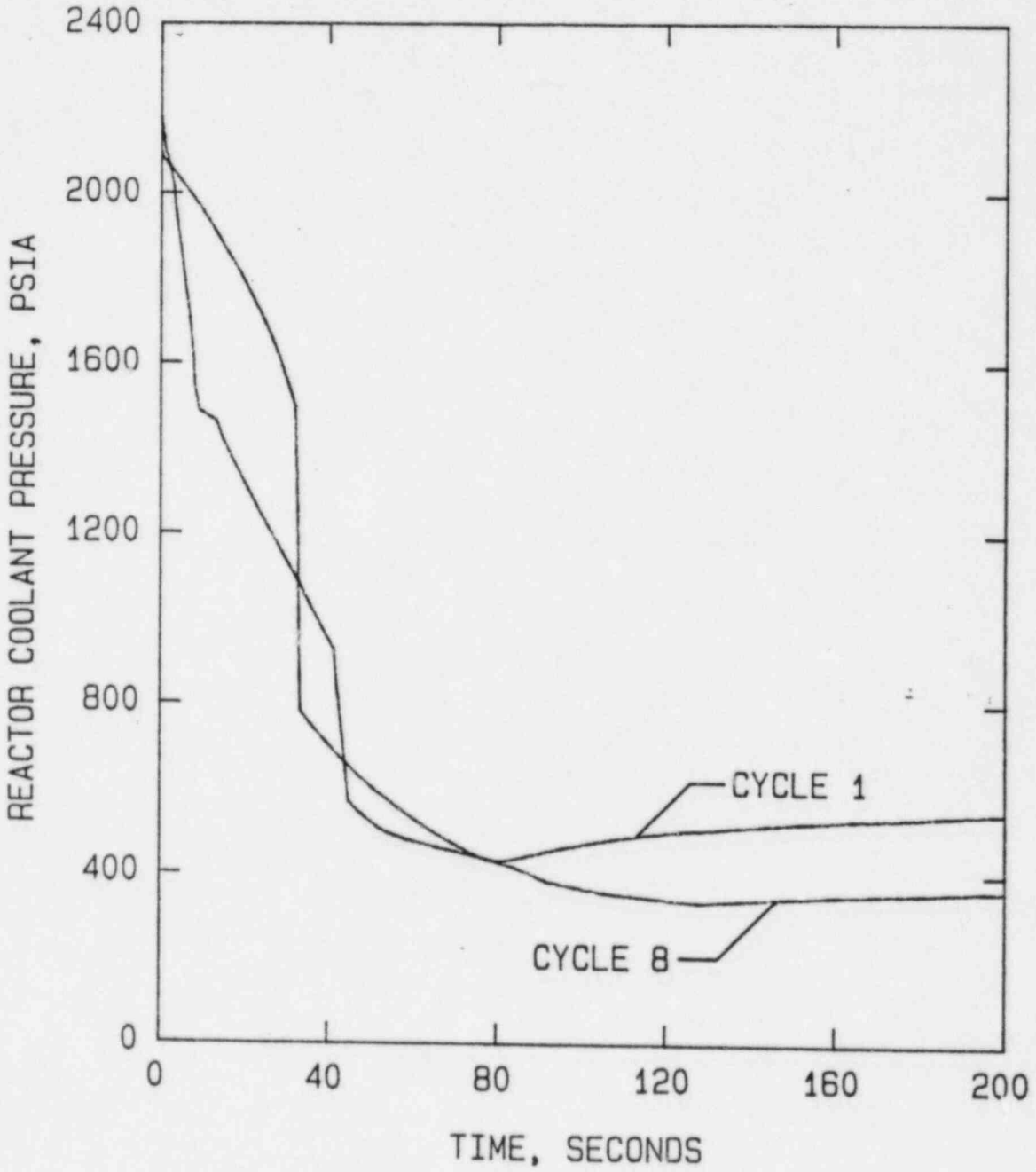

NOTE:
Full Load Initial Conditions

Steam Line Break Incident Coolant System Pressure vs Time	Omaha Public Power District Fort Calhoun Station-Unit No. 1	Figure 14.12-18

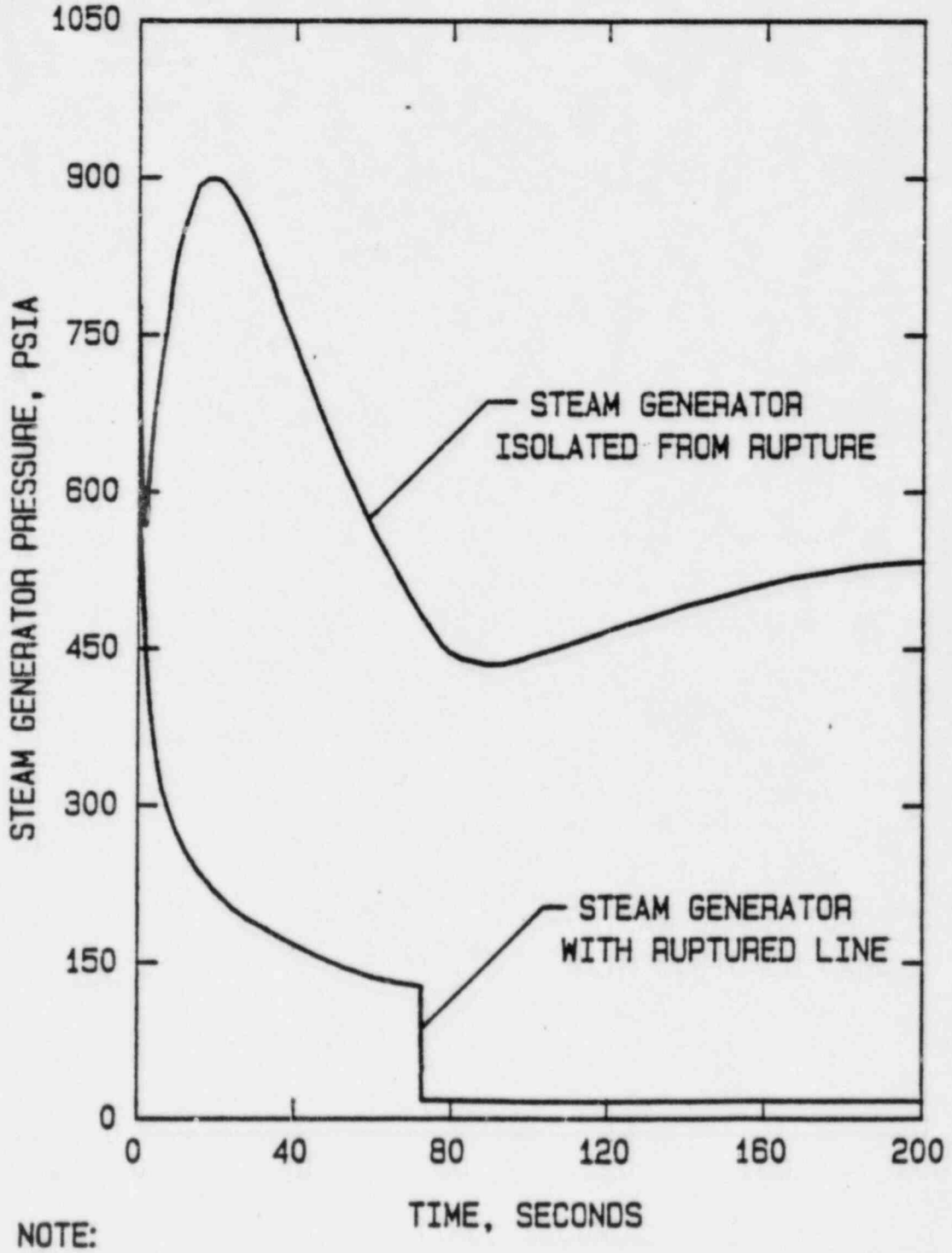

NOTE:
Limiting Cycle (Cycle 1) Full Load Initial Condition

Steam Line Break Incident Steam Generator Pressure vs Time	Omaha Public Power District Fort Calhoun Station-Unit No. 1	Figure 14.12-19

14.22 REACTOR COOLANT SYSTEM DEPRESSURIZATION INCIDENT

14.22.1 General

The RCS Depressurization event is characterized by a rapid decrease in the primary system pressure caused by either the inadvertent opening of both power operated relief valves (PORV's) or a single primary safety valve while operating at rated thermal power.

Following the initiation of the event, steam is discharged from the pressurizer steam space to the quench tank where it is condensed and stored. To compensate for the decreasing pressure, the water in the pressurizer flashes to steam and the proportional heaters increase the heat added to the water in the pressurizer in an attempt to maintain pressure. During this time, the pressurizer level also begins to decrease causing the letdown control valves to close and additional charging pumps to start so as to maintain level. As the pressure continues to drop, the backup heaters energize to further assist in maintaining the primary pressure. A reactor trip is initiated by the TM/LP trip to prevent exceeding the DNBR SAFDL.

In order to ensure that enough margin is built into the TM/LP trip, such that the DNBR SAFDL is not exceeded, a conservative pressure bias term for the TM/LP trip must be calculated. The pressure bias term accounts for the DNBR margin degradation, caused by the depressurization, between the time reactor trip conditions exist and the time of minimum DNBR. This time is primarily due to the signal processing delays in the TM/LP trip logic and the CEA clutch coil delay time.

14.22.2 Method of Analysis

The RCS Depressurization incident was analyzed using the CESEC computer code which models neutron kinetics with fuel and moderator temperature feedback, the reactor control system, the reactor coolant system, the steam generators, and the main steam and feedwater systems. The results of the transient simulation, the transient average core heat flux, average channel mass flow rate, reactor core inlet temperature, and reactor coolant system pressure serve as input to CETOP which performs open channel pressure balancing calculations. This code uses the CE-1 correlation to calculate the DNB ratio for the hot channel as a function of time and axial position (see Section 3.6).

The most negative moderator temperature coefficient (MTC) of reactivity was used to increase the coolant temperature feedback effects which result in higher heat fluxes and thus greater residual heat thereby minimizing DNBR. In order to maximize the negative reactivity feedback from the increasing fuel temperature a 1.15 multiplier was applied to the Doppler coefficient of reactivity. The initial pressurizer pressure was chosen to be 2172 psia which corresponds to the maximum allowed pressure plus uncertainties. The charging pumps, the pressurizer heaters and the pressurizer backup heaters were assumed to be inoperable. The higher initial pressure and the inoperability of the pressurizer heaters and charging pumps result in a faster rate of depressurization. These assumptions yield a lower transient minimum DNBR and a maximum pressure bias term.

Table 14.22-1 contains the list of initial conditions and assumptions including uncertainties for Cycle 8 used in the analysis of the RCS Depressurization event.

TABLE 14.22-1
CYCLE 8 KEY PARAMETERS FOR THE RCS DEPRESSURIZATION EVENT

Parameter	Units	Value
Initial Core Power Level	MWth	1530
Core Inlet Coolant Temperature	°F	547
Pressurizer Pressure	psia	2172
Moderator Temperature Coefficient	$10^{-4}\Delta\rho/°F$	-2.7
Doppler Coefficient Multiplier		1.15
Total Trip Delay Time (Processing plus CEA holding coil delay)	sec	1.4

14.22.2 Results

The RCS Depressurization event was reanalyzed for Cycle 8 to determine the pressure bias term input to the TM/LP trip. The trip setpoints incorporating this bias factor will provide adequate protection to prevent the DNBR SAFDL from being exceeded during the transient.

The analysis of this event shows that the pressure bias term is 23 psia. The sequence of events for the RCS Depressurization event is presented in Table 14.22-2. Figures 14.22-1 through 14.22-4 show the transient behavior of the core power, core average heat flux, reactor coolant system temperatures, and pressurizer pressure.

TABLE 14.22-2
CYCLE 8
SEQUENCE OF EVENTS FOR THE RCS DEPRESSURIZATION EVENT

Time	Event	Setpoint or Value
0.0	Inadvertent Opening of Both Pressurizer Relief Valves	-----
7.7412	Manual Trip Signal Generated	2072 psia
8.6412	Reactor Trip Breakers Open	----
9.1412	CEA's Begin to Drop Into Core	----
9.527	Time of Minimum DNBR	2049 psia

14.22.4 Conclusions

Since the RCS Depressurization event has a larger pressure bias term than the other events from which this term is generated, the calculated value of 23 psia will be incorporated into the TM/LP trip setpoints, thus preventing the DNBR SAFDL from being exceeded.

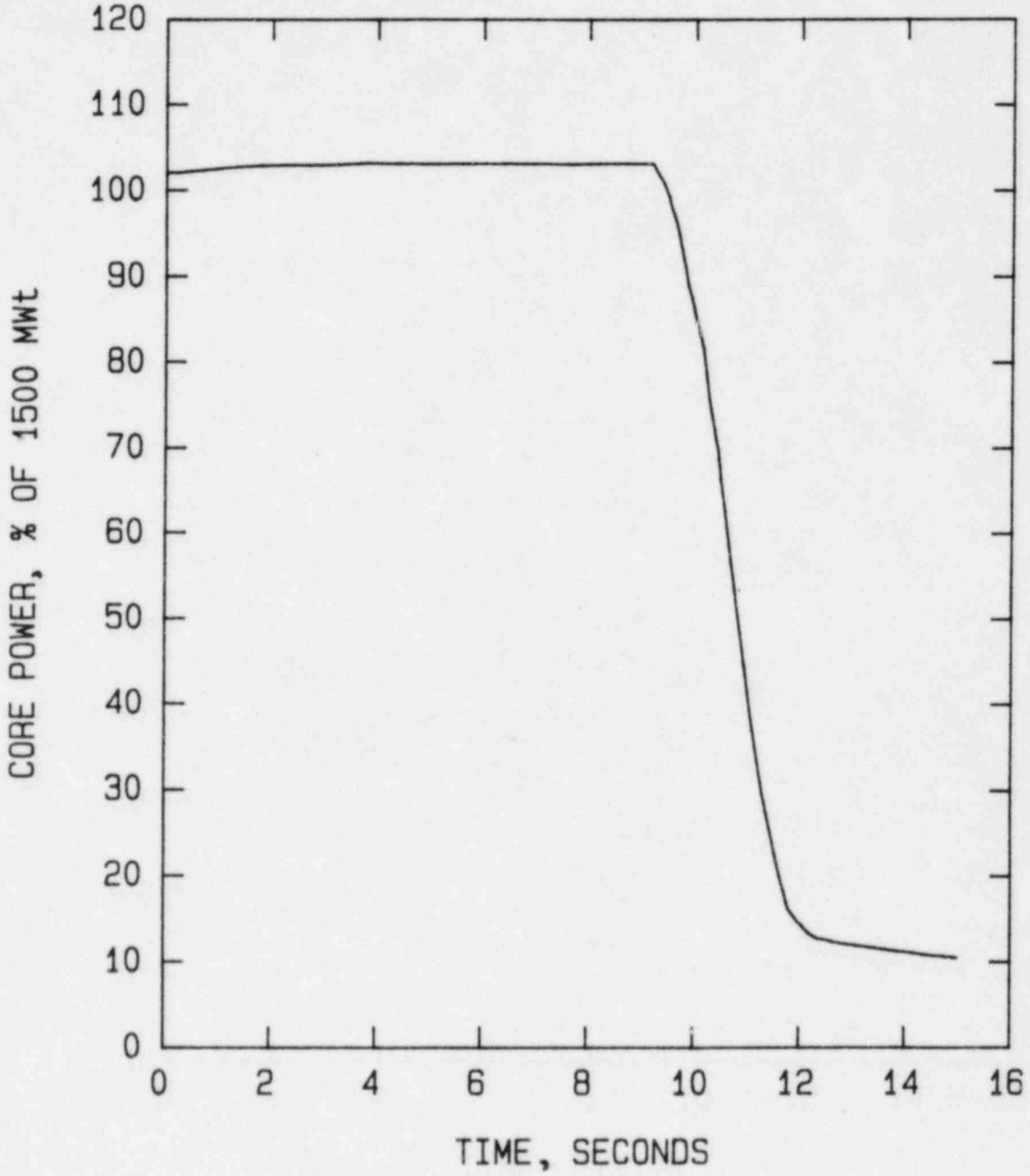

RCS Depressurization Incident Core Power vs Time	Omaha Public Power District Fort Calhoun Station-Unit No. 1	Figure 14.22-1

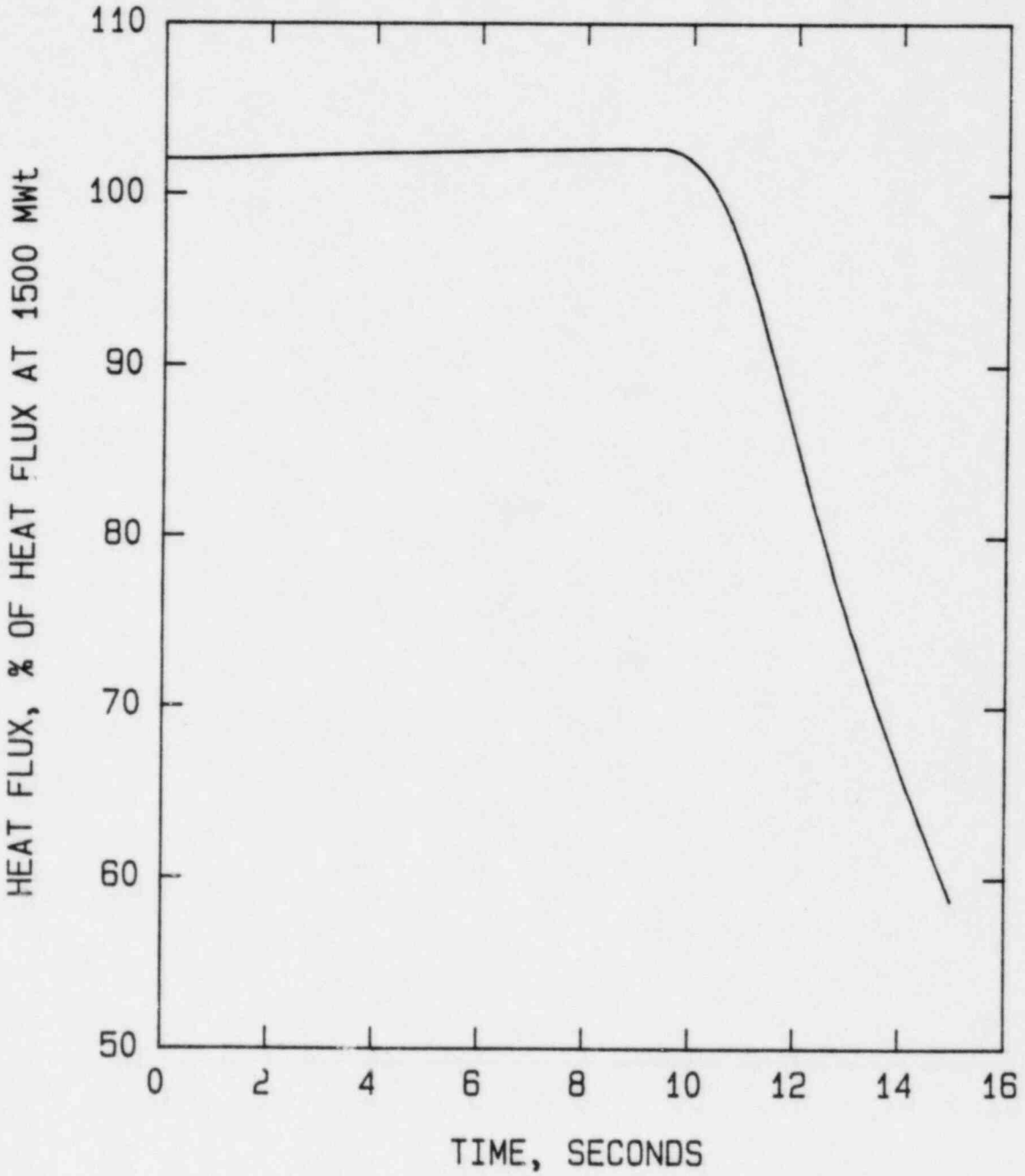

RCS Depressurization Incident Core Average Heat Flux vs Time	Omaha Public Power District Fort Calhoun Station-Unit No. 1	Figure 14.22-2

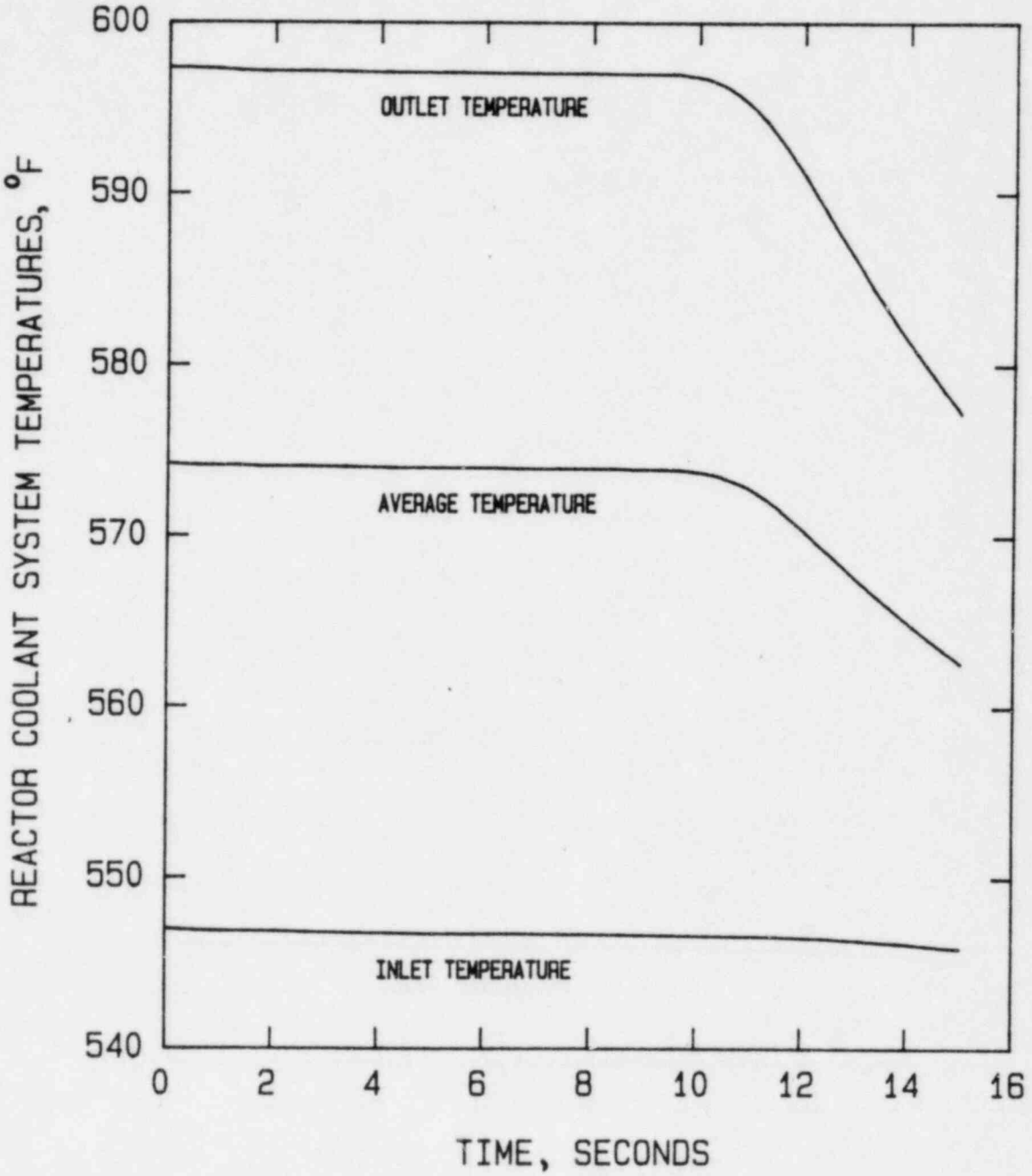

RCS Depressurization Incident Coolant Temperatures vs Time	Omaha Public Power District Fort Calhoun Station-Unit No. 1	Figure 14.22-3

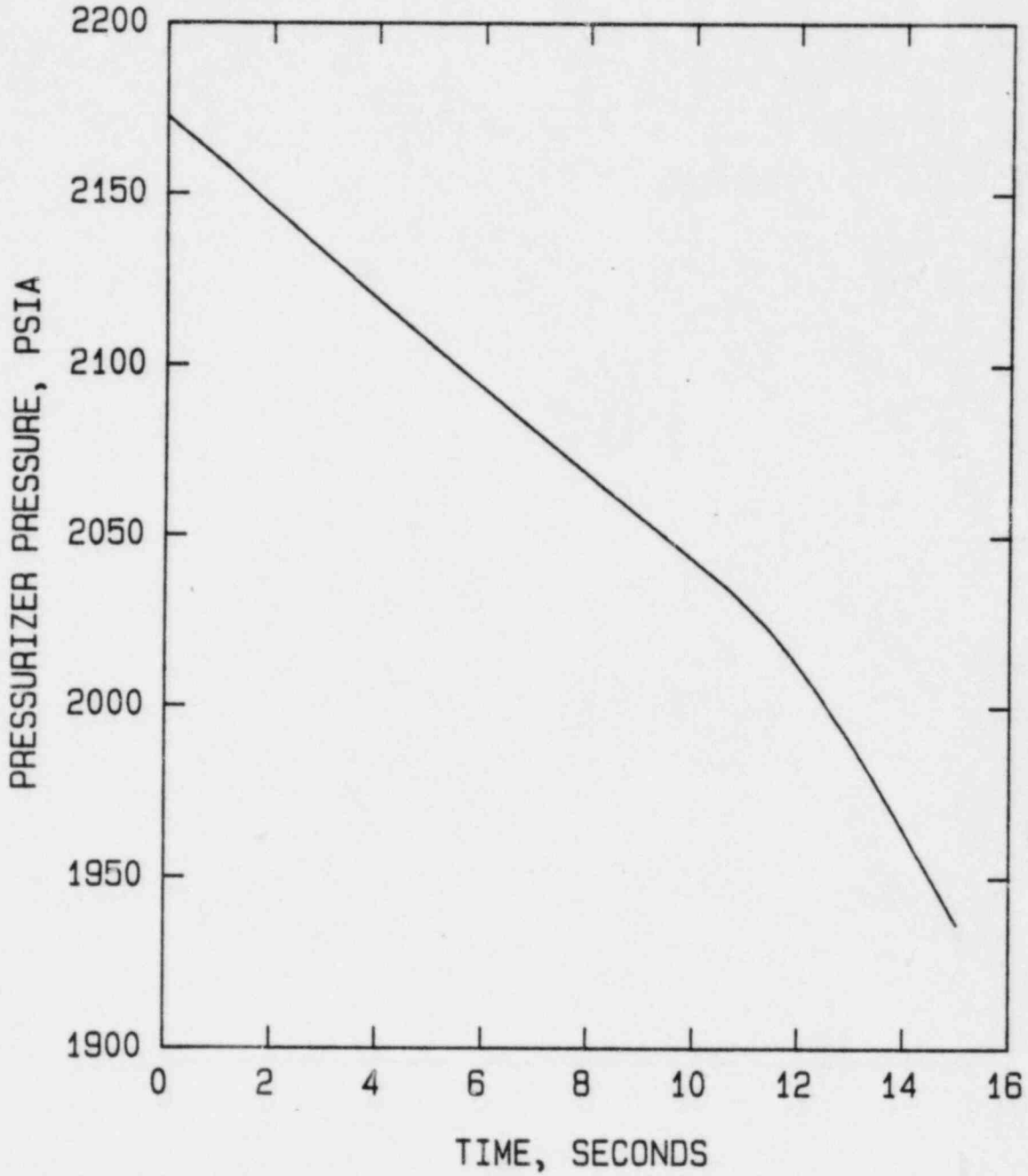

RCS Depressurization Incident Pressurizer Pressure vs Time	Omaha Public Power District Fort Calhoun Station-Unit No. 1	Figure 14.22-4

JUSTIFICATION FOR FEE CLASSIFICATION

The proposed amendment is deemed to be Class III, within the meaning of 10 CFR 170.22, in that it involves a single safety concern.

ATTACHMENT C